Role of DNA repair protein ERCC1 in skin cancer

Liang Song

Thesis presented for the degree of PhD

The University of Edinburgh

2009

Declaration

I hereby declare that this thesis has been composed by me and it has not been accepted in any previous applications for a degree at this time or at any other university. The work described has been performed by me, except where expressly indicated otherwise. All sources of information have been specifically acknowledged. The experiments were designed in collaboration with my supervisor Prof. David W. Melton.

Liang Song

Acknowledgements

I am very grateful to Prof. David Melton for his very kind support and guidance over the past years. I would like to thank my second supervisor Dr. Jim Selfridge for his kind help and advice with my daily lab work. Many thanks to those in the Melton group past and present, particularly Ann-Marie Ritchie, Dr. Ewan Brown, Jennifer Doig, Nicola Lawrence and Oliver Maddocks for their help. I am also grateful for the precious lab experiences with our new PhD students Weiling Li, Ewan McNeil and Yan Xu. I also have to give my thanks to those working in Prof. Kathryn Ball's and Prof. Ted Hupp's groups for their expertise and enthusiasm on cell signalling pathways and protein interactions, and people in Dr. Elizabeth Patton's group for their help with the cell proliferation assay. Finally, I am indebted to my family for their unwavering support.

~ 以女神之名 ~

n.a / Rui.

Table of contents

Abstract

Nucleotide excision repair (NER) is one of the major repair systems for removal of DNA lesions. The NER pathway has evolved mainly to repair UV-induced DNA damage and is also active against a broad range of endogenously generated oxidative lesions. Defects in NER result in the human inherited disorder xeroderma pigmentosum (XP), which is characterised by UV hypersensitivity and a 1000-fold increased risk of skin cancer. ERCC1 is essential for the NER pathway where it acts in a complex with the XPF protein to make the incision 5' to the DNA lesion. The normal 1.1kb Ercc1 transcript is expressed in all tissues. Our group has discovered a second larger 1.5 kb transcript, which initiates from an alternative promoter, and is the most abundant Ercc1 transcript in mouse skin.

The aims of this project were: 1, To investigate the role of ERCC1 and of the 1.5kb skin specific Ercc1 transcript in protecting the skin against UV-induced DNA damage. 2, To study the importance of ERCC1 in melanoma skin cancer and investigate ERCC1as a possible target for therapy against melanoma.

Using a panel of Ercc1 wild-type and deficient cells, we established a quantitative western blotting system to study the expression of ERCC1 in a range of mouse tissues and mouse and human cell types. Although the skin-specific Ercc1 transcript was found to be present at much higher levels in the skin of albino compared to pigmented mouse strains, this did not result in an elevated level of ERCC1 protein. We were also unable to demonstrate that UV-irradiation, or other stress-inducing treatments resulted in increased levels of ERCC1 protein in cultured mouse keratinocytes. We investigated the DNA methylation status of the normal Ercc1 promoter and that of two potential

upstream promoter regions that were candidates for the source of the 1.5kb skin-specific Ercc1 transcript. We found no evidence that they were the source and, instead, used 5' RACE analysis to locate the skin-specific promoter to a polymorphic region 500bp upstream of the normal initiation site. In albino strains this region contains a SINE element, which we hypothesize could be involved in the production of the skin-specific Ercc1 transcript.

We also investigated the protein level of ERCC1 and other DNA repair proteins, including XPF, MSH2, MSH6 and MLH1 in human melanoma cells and ovarian tumour cells. Significantly elevated protein levels of ERCC1 and XPF, as well as the mismatch repair protein MLH1 were found in melanoma cells. This could possibly contribute to the higher resistance to chemotherapy in melanoma, although the melanoma cell lines we tested did not show increased resistance to UV and cisplatin compared to the ovarian cancer cells tested. When Ercc1 proficient mouse melanoma cells were xenografted into nude mice the xenografts grew rapidly. Cisplatin treatment caused an initial shrinkage of the tumours, but re-growth rapidly followed. Cells re-isolated into culture from cisplatin treated xenografts had significantly higher levels of ERCC1 protein than either input cells, or cells re-isolated from untreated xenografts. An isogenic Ercc1 deficient derivative of the Ercc1 proficient mouse melanoma cell line grew as rapidly as the parent line in vitro, but grew much more slowly as xenografts. In addition, the xenografts shrank completely following cisplatin treatment and did not recover. This suggests that ERCC1 could be a drug target for melanoma therapy.

Abbreviations

6-4PP	6-4 photoproducts
A	adenosine
APS	ammonium persulphate
Bcl-2	B-cell leukaemia/lymphoma 2
BER	base excision repair
bp(s)	base pair(s)
BSA	bovine serum albumin
C	cytosine
CDK	Cyclin-dependent kinase
cDNA	complementary DNA
CO2	carbon dioxide
COFS	Cerebro-Oculo-Facio-Skeletal
CPD	cyclobutane–pyrimidine dimers
CS	Cockayne's syndrome
DDB	damage-specific DNA binding
DMBA	7,12-dimethylbenz-[a]anthracene
DMEM	Dulbecco's Modified Eagle Medium
DMF	dimethylformamide
DMSO	dimethyl sulphoxide
DR	direct reversal
DSB	double-strand break
DTIC	Dacarbazine
DTT	dithiothreitol
EDTA	ethylenediaminetetraacetic acid
ERCC1	excision repair cross-complementation group 1
ERK	Extracellular Signal-Regulated kinases

FANC	Fanconi anaemia
FCS	foetal calf serum
G	guanosine
GAPDH	glyceraldehyde-3-phosphate dehydrogenase
GGR	global genome repair
HR	homologous recombination
ICL	inter-strand cross-link
kb	kilobase
MAPK	mitogen-activated protein kinase 1
MEK	mitogen-activated protein kinase/ERK kinase
MOPS	3-(N-morpholino)propanesulfonic acid
MITF	Microphthalmia-associated transcription factor
MMR	mismatch repair
NCS	New-born calf serum
NEAA	non-essential amino acid
NER	nucleotide excision repair
NHEJ	non-homologous end joining
PBS	phosphate buffered saline
PCNA	Proliferating Cell Nuclear Antigen
PTEN	phosphate and tensin homologue
RACE	Rapid Amplification of cDNA Ends
RFC	Replication factor C
RGP	radial-growth-phase
RPA	replication protein A
RT-PCR	Reverse transcription polymerase chain reaction
SDS	sodium dodecyl sulphate
SRB	sulforhodamine B
T	thymidine
TCA	trichloroacetic acid

TCR	transcription-coupled repair
TE	transposable element
TEMED	tetramethylethylenediamine
TF	transcription factor
TLS	translesion synthesis
TPA	Tetradecanoylphorbol acetate
TTD	trichothiodystrophy
UV	ultraviolet
v/v	volume against volume
VGP	vertical-growth phase
WT	wild type
w/v	weight against volume
XP	xeroderma pigmentosum

Chapter 1:

Introduction

1.1 DNA damage and repair

Correct genetic and epigenetic information is essential for proper cellular functioning. However, DNA damage, which can result in the introductions of mutation into the genome, is an extremely common event in a cell's lifetime. Miscellaneous errors occur and accumulate in the genome during cell division as the machinery of DNA replication is not 100% efficient. On top of this, endogenous sources of DNA damage and exposures to environmental carcinogens, such as chemical contacts, tobacco smoke and ultraviolet (UV) radiation, can also result in various types of DNA lesions. The accumulation of DNA changes may eventually activate proto-oncogenes and inactivate tumour suppressor genes leading to an increased risk of tumourigenesis. Therefore, efficient repair of DNA damage and maintenance of genome integrity is fundamental to species survival.

To protect the information stored within the genome, cells have evolved various complex mechanisms to detect and repair DNA damage, and most of the time a cell repairs its damaged DNA properly. Depending upon the mutagenic agents involved, different DNA repair mechanisms are operative, including the direct reversal pathway (DR), mismatch repair (MMR), nucleotide excision repair (NER), base excision repair (BER), non-homologous end joining (NHEJ), homologous recombination repair (HR) and inter-strand cross-link (ICL) repair (Figure 1.1). DNA adducts, such as those created by alkylating agents, may be repaired by the direct reversal of the DNA alkylation (DR). The DNA lesions could also be excised and repaired before they are confronted by the replication machinery. This is achieved by BER (Sharma and Dianov 2007), which excises a single damaged DNA base, or a short strand containing the damaged base, or by NER, which excises a single-stranded DNA molecule of approximately 24-30 nucleotides containing the DNA lesion (Sugasawa et al. 2001). Direct double strand

Fig 1.1 DNA repair pathways

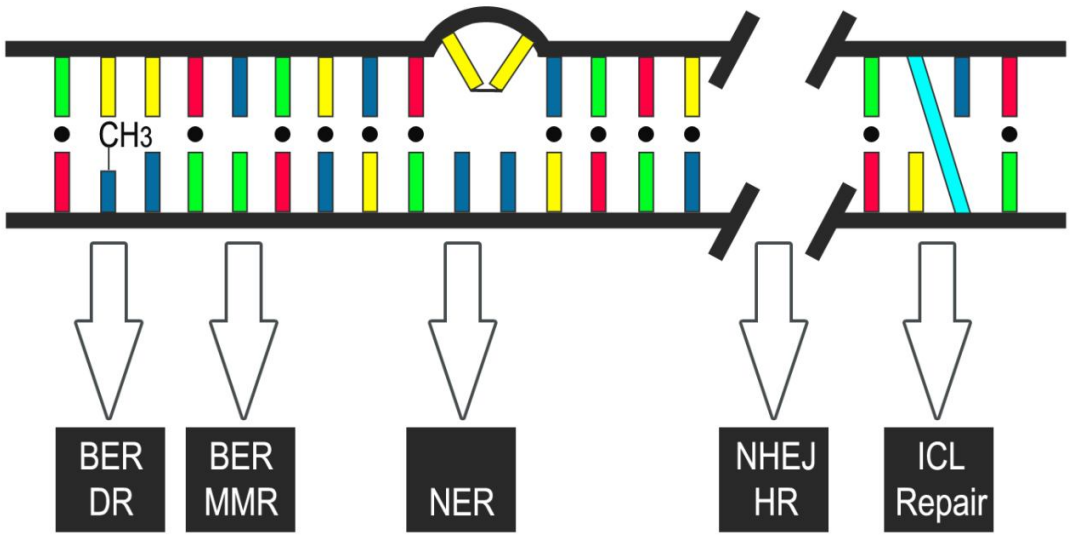

Several DNA repair pathways exist and deal with various types of DNA insults. These pathways include the direct reversal pathway, the MMR pathway, the NER pathway, the BER pathway, the NHEJ pathway, the HRR pathway, and the ICL pathway. DNA strands are shown in black lines and different nucleotides are shown as coloured squares. Correctly paired bases are shown by a connection using black dots.

breaks (DSB) are mainly repaired by NHEJ, whereas replication-associated DSBs are repaired by homologous recombination (HR) and related replication repair pathways (Sargent et al. 1997; Arnaudeau et al. 2001). Interstrand cross-links (ICLs), which are a complex lesion that covalently link duplex DNA molecules, can be repaired by a combination of NER, HR and lesion bypass mechanisms (Wang et al. 2001; Zheng et al. 2003).

Direct reversal of DNA damage is not a multistep process and does not involve multiple proteins (Sedgwick et al. 2007). Catalyzed by enzymes such as ABH2 (also known as ALKBH2), ABH3 (also known as ALKBH3) and O^6-methylguanine DNA methyl transferase (MGMT), DNA adducts are repaired in a process that directly reverses the DNA alkylation. MGMT, also known as AGT, removes the DNA adducts by transferring the alkyl group from the oxygen in the guanine ring to a cysteine residue in its active site (Lindahl et al. 1982). DNA dioxygenases ABH2 and ABH3 revert 1-methyladenine and 3-methylcytosine back to adenine or cytosine respectively (Duncan et al. 2002).

Mismatch repair, a system for recognizing and repairing erroneous insertion, deletion and mis-incorporation of bases during DNA replication and recombination, is a highly conserved process from prokaryotes to eukaryotes. MMR plays a key role in maintaining genomic integrity (Li 2008). Mismatch repair is strand-specific and has a number of cues which distinguish the newly synthesized strand from the template strand. Mismatches are recognized by the MutS homologue, which in conjunction with a MutL homologue initiates the repair. The incorporated base is replaced with the correct nucleotide on the newly synthesized strand by an excision repair mechanism. The consequences of defective MMR are associated with genome-wide instability, predisposition to certain types of cancer including hereditary non-polyposis colorectal

cancer, resistance to certain chemotherapeutic agents, and abnormalities in meiosis and infertility in mammalian systems (de la Chapelle 2004).

Base excision repair (BER) is a cellular mechanism that removes non-bulky adducts from the DNA throughout the cell cycle and is the primary mechanism for repair of oxidative base lesions (Sancar 1996; David et al. 2007). Other base modifications repaired by BER include uracil that results from cytosine deamination and 3-methyladenine caused by alkylating agents. The cut of the N-glycosyl bond between the sugar and the base is made by DNA glycosylase and an apurinic/apyrimidinic (AP) site is created, then the abasic sugar is released by AP lyase and endonucleases, before an undamaged nucleoside is inserted to fill the gap. Defects in human BER proteins can reduce cellular tolerance to oxidative DNA base damage caused by endogenous and exogenous sources, such as exposure to toxins and ionizing radiation, and increase the chance of cell dysfunction and mutagenesis, consequently leading to cancer, disease, and aging (Sokhansanj and Wilson 2006; Maynard et al. 2009).

The NER pathway is a multistep process that has evolved primarily to repair UV-induced DNA damage and is also active against a broad range of endogenously generated oxidative lesions (de Boer and Hoeijmakers 2000). NER consists of two subpathways in mammals, global genome repair (GGR) and transcription-coupled repair (TCR), which differ according to the initial recognition stage. GGR can remove DNA lesions throughout the genome while TCR mainly deals with lesions in the transcribed strand of actively transcribed genes (Leadon and Lawrence 1991; Lombard et al. 2005). Incisions are made in the damaged strand of DNA by endonucleases, upstream of the lesion by ERCC1/XPF complex and downstream by XPG, and then an oligonucleotide containing the DNA lesion is released before the section is replaced and ligated.

Double-strand breaks (DSBs), primarily caused by ionising radiation, certain chemicals and arrested replication, are repaired by homologous recombination (HR) and non-homologous end joining (NHEJ) (Pardo et al. 2009). The primary HR mechanism consists of two categories: the most important category is gene conversion, which requires that sequences surrounding the break can find their homology anywhere else in the genome. The non-damaged homologous sequence then acts as a template for repair synthesis. The second HR category is the non-conservative process of single-strand annealing (SSA), which utilizes direct repeats flanking the DSB. The secondary mechanism NHEJ, also called illegitimate recombination or non-homologous recombination, permits joining of ends even if there is no sequence similarity between them (Hefferin and Tomkinson 2005). NHEJ requires the broken ends to be physically closely aligned, before NHEJ proteins bind the broken ends together. This re-ligation process could simply restore the original sequence perfectly, or in an error-prone fashion by adding a few nucleotides or removing sequences ranging from 1 nucleotide up to a few Kb.

Inter-strand crosslinks (ICL), normally caused by cisplatin, mitomycin C, derivatives of nitrogen mustard, and other bifunctional alkylating agents, covalently join both DNA strands, preventing their separation and blocking DNA and RNA polymerases and therefore constituting and extremely toxic class of DNA damage. As most of the cross-linking agents are among the frequently used drugs in cancer chemotherapy the repair mechanisms of ICLs in cells are not just important to the maintenance of genome integrity, but can be also related to the resistance of tumour cells against chemotherapy. Although the repair of ICL is believed to be a complex process which recruits proteins from other DNA repair pathways as well as ICL repair specific enzymes, the detailed molecular mechanism of cross-link repair in humans is still not well characterized. It is reported that the ICL repair is initiated by FANC (Fanconi anaemia) gene products, then processed by multiple mechanisms including NER, HR and lesion bypass pathways

(Wang et al. 2001; Zheng et al. 2003). The cisplatin-induced DNA ICLs are reported to be recognized by replication protein A (RPA) (Patrick et al. 2008). The NER endonuclease-complex ERCC1/XPF is reported to be crucial for the repair of ICLs by making the incision at the DNA lesion (Chipchase and Melton 2002; Niedernhofer et al. 2004).

1.2 Nucleotide excision repair

1.2.1 Overview of NER

Nucleotide excision repair (NER) is one of the major repair systems for removal of DNA lesions. The NER pathway has evolved mainly to repair UV-induced DNA damage, and is also active against a broad range of endogenously generated oxidative lesions (Wood 1999; de Boer and Hoeijmakers 2000). UV radiation mainly induces two mutagenic and cytotoxic DNA lesions, cyclobutane–pyrimidine dimers (CPDs) and 6–4 photoproducts (6–4PPs), which both distort the DNA helix (Sinha and Hader 2002). The majority of proteins involved in the NER pathway are well characterised and are reviewed extensively (de Laat et al. 1999; Hoeijmakers 2001).

The NER pathway excises damaged nucleotides, along with adjacent undamaged DNA, in the form of oligomers that are 25-32 nucleotides long. Defects in NER will be discussed in more detail later in this chapter, but generally, they result in the human inherited disorder xeroderma pigmentosum (XP), which is characterized by UV

hypersensitivity, pigmentation abnormalities and a 1000-fold increased risk of skin cancer (Friedberg 2003). Sun exposure of XP patients can also lead to progressive degenerative alterations of the skin and eyes (Bootsma et al. 2002). Defects of components of the NER pathway are also associated with an increased incidence of internal tumours and neurological abnormalities. Additionally, some NER defects lead to premature ageing phenotypes.

1.2.2 The steps in NER

The NER pathway is biochemically complicated and involves about 30 distinct proteins in human cells, including ERCC1 (the excision repair cross complementing-group 1), ERCC2 (XPD), ERCC3 (XPB), ERCC4 (XPF), ERCC5 (XPG), ERCC6 (CSB), XPA, XPC, XPE, PCNA (proliferating cell nuclear antigen) and the TFIIH-complex (Wood 1999).

NER consists of two subpathways in mammals, global genome repair (GGR) and transcription-coupled repair (TCR), according to the initial recognition stage (Figure 1.2). GGR can remove DNA lesions throughout the genome (Lombard et al. 2005), while TCR deals with lesions in the transcribed strand of actively transcribed genes which lead to stalling of RNA polymerase II (Leadon and Lawrence 1991). Common NER factors are recruited in both GGR and TCR following recognition of the damaged DNA.

NER consists of the following 4 steps:

1) Recognition of DNA damage and binding of a multi-protein complex at the damaged site. As described before, the two sub-pathways, GGR and TCR, are different in this step only. In GGR, the proteins XPC and HHR23B are recruited to compose the first NER complex which recognizes and binds to the site of the DNA lesion. The binding to DNA lesions by the XPC/HHR23B complex is not only essential for the lesion recognition but is also essential for the recruitment of all subsequent NER components, including transcription factor TFIIH (Volker et al. 2001). XPC/HHR23B is a structure-specific DNA binding factor which preferentially recognizes and binds to double-stranded/single-stranded DNA lesions that induce a higher degree of DNA helix distortion (Sugasawa et al. 2002). XPC/HHR23B recognizes 6-4PPs efficiently but doesn't recognizes CPDs as competently (Sugasawa et al. 2002). The XPC-HHR23B complex is also reported to recognize DNA ICLs by interaction with another NER complex XPA-RPA (Thoma et al. 2005). The XPE protein is also involved with damage-specific DNA binding (DDB) activity, and is reported to recognize DNA lesions. The DDB complex consists a p48/p127 heterodimer which has high affinity for UV induced DNA lesions (Nichols et al. 2000). p48, also known as DDB2, is the XPE gene product and is involved in cell cycle checkpoints as well as NER (Rapic-Otrin et al. 2003; Kulaksiz et al. 2005). Furthermore, DDB2 has been recently reported to be linked with the modification of histone H2A by ubiquitination and the cause of a conformational change which enables DNA lesion binding by the NER machinery (Kapetanaki et al. 2006).

   By contrast, in the TCR subpathway, the stalled RNA polymerase II fulfills the DNA lesion binding function, facilitated by Cockayne syndrome proteins CSA and

Fig 1.2 Overview of NER mechanism

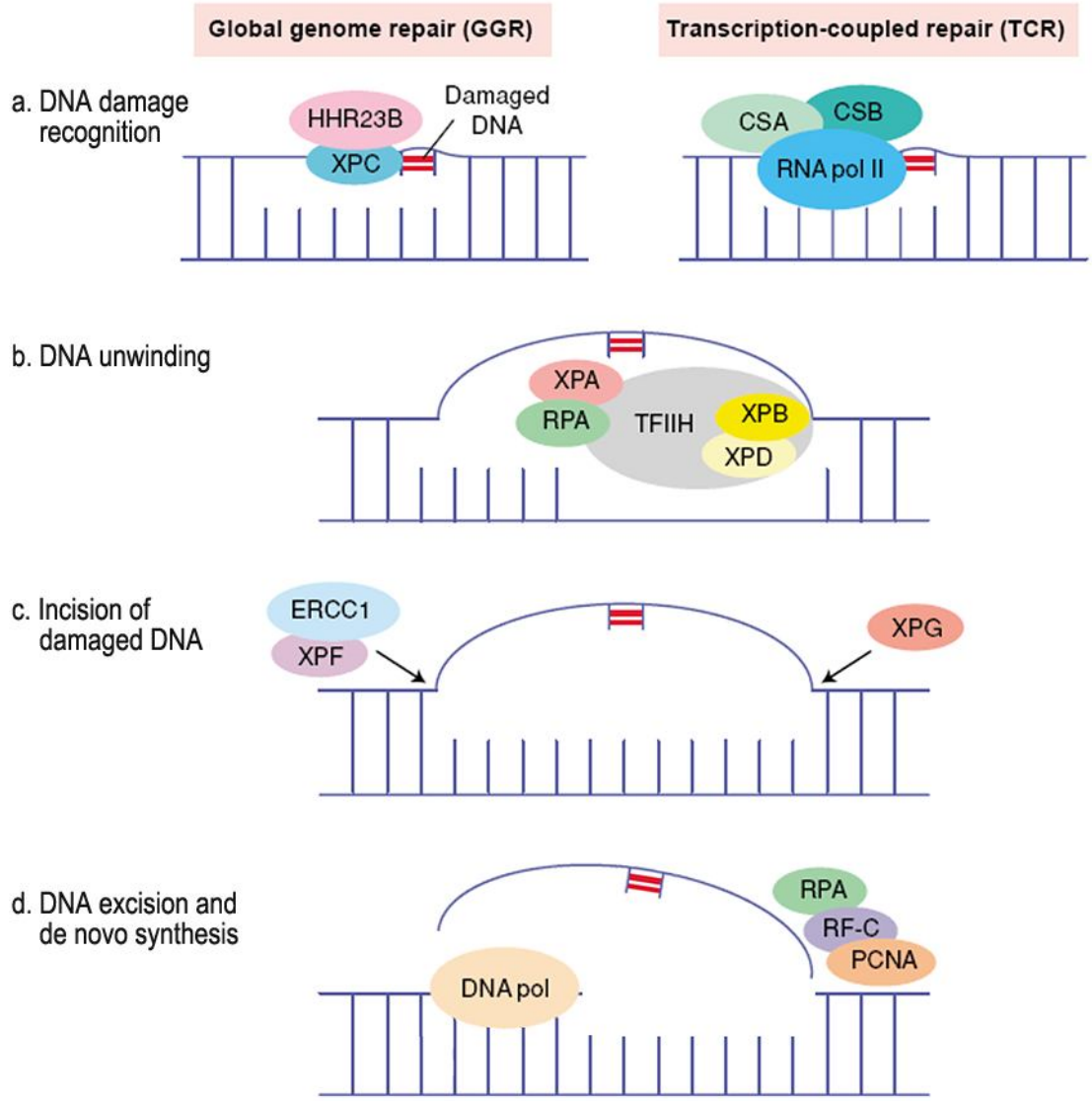

Model for mammalian nucleotide excision repair. Adapted from Matsumura and Ananthaswamy 2002.

CSB (Matsumura and Ananthaswamy 2002). The CSA protein contains a WD-40 repeat motif known to be involved in protein-protein interactions (Henning et al. 1995). It has been reported that CSA is part of an E3-ubiquitin ligase complex (Groisman et al. 2003; Fousteri et al. 2006). The CSB protein has nucleosome remodelling activity and binds to core histone proteins *in vitro* (Citterio et al. 2000). CSB does not remove the stalled polymerase but its ability to bind to repair proteins suggests that CSB protein plays a role in recruiting repair proteins to complexes formed at damage sites (Selby and Sancar 1997).

2) DNA helix unwinding. Once the DNA lesion is identified, GGR and TCR use a common mechanism to excise the damage. TFIIH is recruited to the damage site through interactions with XPC-HHR23B or CSB and CSA. TFIIH is a protein complex which has multiple enzymatic activities and is involved in initiation of RNA polymerase II transcription, NER and possibly in cell cycle regulation (de Laat et al. 1999). The multi-subunit TFIIH complex consists of ten polypeptides, including one recently identified trichothiodystrophy group A (TTDA)/ hTFB5 protein, which is not essential for cell viability but could potentially be an NER-specific factor. (Giglia-Mari et al. 2004; 2006). In NER, two essential subunits of TFIIH, known as XPB and XPD, exhibit DNA-dependent ATPase and helicase functions (Sancar 1996). XPB can unwind DNA in a 3' to 5' direction, and XPD in the opposite direction.

Once the damaged DNA-helix is unwound, the DNA lesion is exposed for the upcoming repair work. XPA and RPA are recruited to the site not only to stabilize this open repair intermediate but also to coordinate the following repair work. XPA is considered to verify NER lesions and to play a central role in positioning the repair machinery and recruiting other repair proteins such as the ERCC1/XPF

complex (de Laat et al. 1999). RPA also interacts with ERCC1-XPF, presumably via XPF, to position the nuclease at the DNA lesion (Matsunaga et al. 1996).

3) Incision of damaged DNA. During this step, two structure-specific endonucleases XPG and XPF/ERCC1 access the damaged site to make the dual incision. XPG, which is closely related to the flap structure-specific endonuclease 1 (FEN-1) that participates in base excision repair, has a cleavage polarity that always make incisions in one strand of duplex DNA at the 3' side of a junction with ssDNA. Consistent with this cleavage polarity, XPG makes the 3' incision during NER (O'Donovan et al. 1994). XPG is not only required for the 3' incision but also for full open-complex formation, indicating a structural role in the core NER reaction (Evans et al. 1997). ERCC1-XPF makes the 5' side incision in NER (Mu et al. 1996). However, unlike the XPG protein, ERCC1-XPF can be omitted for full open complex formation suggesting that they don't have an architectural function in the NER protein-DNA complex (Evans et al. 1997; Mu et al. 1997). It has been reported that the XPG-mediated 3' incision precedes the 5' incision made by ERCC1-XPF (Mu et al. 1996). The cut made by XPG is 2-8 nucleotides from the lesion, and the cut made by XPF/ERCC1 is 15-24 nucleotides away (Sancar 1996).

4) Lesion excision and de novo synthesis. The excised fragment is around 30 nucleotides in length. Part of the repair complex remains in the gap made by excision to protect the ssDNA. Once the lesion has been removed, the gap is filled by two DNA polymerases Polymerase δ and Polymerase ε. Both of the polymerases are proliferation cell nuclear antigen (PCNA) dependent, so that PCNA is also involved in this step, which adds nucleotides in a 5' to 3' direction. Replication factor-C (RF-C) and RPA are both involved as well. The final closure occurs with DNA ligase. This reaction is catalysed by DNA ligase I or DNA ligase III.

1.2.3 ERCC1 and ERCC1-XPF complex

As described in the previous section, the ERCC1-XPF complex is an essential component of the NER pathway for making incision to the 5' side of the lesions. The complex also has additional, NER-independent roles in the repair of interstrand DNA crosslinks (ICL) and homologous recombination (HR) (Busch et al. 1997; Kuraoka et al. 2000; Niedernhofer et al. 2004). Although the details of the ICL repair pathway are still not well-characterised, a suggested model indicates that the endonuclease function of ERCC1-XPF is essential to make the 5' end incision and remove the blocking ICL during repair (Niedernhofer et al. 2004). In the HR pathway, the ERCC1-XPF endonuclease was reported to be required for both gene conversion and SSA in mammalian cells (Al-Minawi et al. 2008).

Several structural studies have been done to better understand the ERCC1-XPF complex. In archaebacteria, the XPF homolog acts as a homodimer without the presence of ERCC1 (Nishino et al. 2003; Newman et al. 2005). However, in eukaryotic cells, formation of the ERCC1-XPF complex, by interaction of their C terminal regions is required for the stability of both components (de Laat et al. 1998) (Figure 1.3). Three-dimensional structural analysis of human ERCC1-XPF complex showed that the core of the complex, comprising residues 234–294 of ERCC1 and residues 836–895 of XPF, has a global pseudosymmetry with a very similar architecture of the associated partners (Tripsianes et al. 2005). In particular, a characteristic example of the double helix-hairpin-helix $(HhH)_2$ motif was detected in the ERCC1 protein fold, while a very similar fold was detected in XPF as well. This $(HhH)_2$ motif is present in a variety of protein families involved in non-sequence-specific DNA binding (Shao and Grishin 2000). This

Fig 1.3 Domain organization of the ERCC1/XPF complex

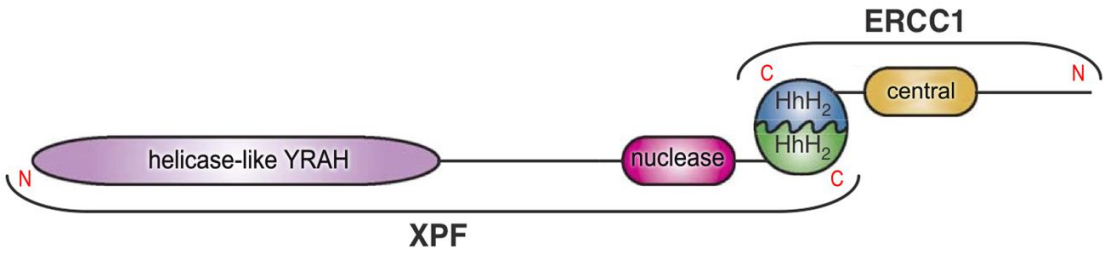

The heterodimeric $(HhH)_2$ motif interaction of the ERCC1-XPF complex is shown within a circle. Other main domains are shown in ellipse shapes. N and C terminus of each protein is indicated with red letters. Figure is adapted from Tripsianes et al. 2005.

heterodimeric $(HhH)_2$ motif from the ERCC1-XPF complex, containing two independent DNA-binding surfaces, was reported to be functional in ssDNA binding (Tripsianes et al. 2005; Tsodikov et al. 2005). The N-terminal helicase-like domain of XPF may contribute to the DNA binding and hydrolyzing activity (McCutchen-Maloney et al. 1999). The central domain of ERCC1 binds ssDNA/dsDNA junctions with a defined polarity, preferring a 5' single-stranded overhang (Tsodikov et al. 2005).

Functional domains of ERCC1 and XPF were initially investigated by deletional analyses. Deletion of the N-terminal 92 amino acids of ERCC1 had no major effect on ERCC1 in terms of DNA repair *in vivo*. However, disruption of the N-terminal 103 residues of ERCC1 completely destroyed the repair capacity (de Laat et al. 1998). The XPA binding domain was mapped to residues 93–120 in ERCC1. The ERCC1 C-terminus was directly linked with complex formation ability and repair capacity as a five amino acid deletion from the ERCC1 C-terminus completely destroyed both the XPF binding ability and the DNA repair capacity *in vivo* (Sijbers et al. 1996; de Laat et al. 1998). In XPF, residues 814–905 were mapped to be the region responsible for initial and stable complex formation between ERCC1 and XPF (de Laat et al. 1998).

1.2.4 ERCC1 gene expression

ERCC1 is highly conserved like many other DNA repair genes. It is homologous to RAD10 in Saccharomyces cerevisiae, SWI10 in Schizosaccharomyces pombe, and regions in the UvrA and UvrC genes in *E. coli* (van Duin et al. 1986; van Duin et al.

1987; Rodel et al. 1992). In both human and mouse, the normal 1.1kb Ercc1 transcript contains 10 exons and is believed to be driven by a promoter region lacking the "classical" promoter regulatory elements such as the TATA box and GC box immediately upstream of the transcription initiation site (van Duin et al. 1987). However, comparisons of the entire gene from mammalian species suggests that some potential regulatory regions may exist further upstream of the putative ERCC1 promoter region (Wilson et al. 2001). A conserved GC-rich region 5 kb upstream of ERCC1, which contains a conserved TATA box and a GC box, as well as some additional conserved segments such as LINE/L1 and LINE/L2 elements, indicate that the upstream region may also be involved in ERCC1 transcription (Wilson et al. 2001).

Comparative transcript analysis of human ERCC1 ESTs has revealed alternative splicing events involving exons 1, 2, 3, 7, 8 and 9 (reviewed by Wilson et al. 2001). A 5' variant containing a differentially spliced exon 1 has been reported that spans the entire region of the previously believed promoter (van Duin et al. 1987). Furthermore, a transcript with alternative polyadenylation, which reads through exon 9 and appears to utilize the polyadenylation signal on an adjacent Alu element was identified (Wilson et al. 2001).

A novel 1.5kb skin-specific Ercc1 transcript was characterized by our previous group work using a panel of tissues from an Ercc1 wild type mouse (Selfridge et al. 2001). According to the northern blotting using an Ercc1 probe, the normal 1.1kb Ercc1 transcript was evident in all tissues examined. In addition to the normal Ercc1 transcript, a second larger transcript of 1.5kb was evident in skin. The novel 1.5kb transcript presents as the major transcript in skin compared with the normal 1.1kb Ercc1 transcript.

An RT-PCR assay using primers in exon 2 and exon 10 of the Ercc1 cDNA indicated that the coding region from both novel and normal transcripts have the same size. Also 3' RACE analysis revealed the difference in size was not due to differential polyadenylation. As a result, the additional 400bp in the novel transcript should be due to initiation of transcription upstream of the normal transcription start site, driven by an alternative upstream promoter not utilized in other tissues. This hypothesis was supported using 5' RACE analysis. A 400bp larger product was obtained from skin than from embryonic stem cells (Jim Selfridge, unpublished observations). An investigation of the functional role of this skin-specific Ercc1 transcript was one of the aims of this thesis.

1.2.5 Human inherited NER deficiency syndromes

The phenotypic consequences caused by NER defects in humans are mainly three distinct diseases: xeroderma pigmentosum (XP), Cockayne syndrome (CS) and trichothiodystrophy (TTD).

Xeroderma pigmentosum (OMIM: 278700) is an autosomal recessive genetic disorder of DNA repair in which the ability to repair damage caused by ultraviolet (UV) radiation is deficient. This disorder in patients leads to extreme photosensitivity, excessive pigmentation in response to UV and a significant increased chance of UV induced skin cancer. Physically, the XP disease passes through 3 stages. The first stage typically appears after the age of 6 months and is characterized by diffuse erythema, scaling, and freckle-like areas of increased pigmentation. The second stage is characterized by poikiloderma, which consists of skin atrophy, telangiectasias, and mottled

hyperpigmentation and hypopigmentation. The third stage is heralded by the appearance of numerous malignancies, including squamous cell carcinomas, malignant melanoma, basal cell carcinoma, and fibrosarcoma. Two most common causes of death for XP victims are metastatic malignant melanoma and squamous cell carcinoma (Li 2007). XP patients get the initial development of skin cancer at the mean age of 8 compared with the age of 50 in the general population (Kraemer 1997). It has been identified through complementation studies that XP is caused by mutations in seven different NER genes, XPA to XPG, while an additional XP variant group, XPV, is caused by mutation in the lesion bypass DNA polymerase polη, which can contribute to DNA replication over the damage site and is needed when cells enter S-phase in the presence of unrepaired DNA damage. A small number of XP patients with more severe NER defects also develop neurological symptoms and cognitive dysfunction, which is believed to be due to the accumulation of oxidative lesions in neurons (Anttinen et al. 2008).

Cockayne syndrome, also known as Weber-Cockayne syndrome or Neill-Dingwall syndrome, is a rare autosomal recessive congenital disorder characterized by growth failure, impaired development of the nervous system, hypersensitivity to sunlight, and premature aging (Bertola et al. 2006). CS patients have hearing loss, eye abnormalities and some other common features like small head size, short stature and a prematurely aged appearance. However, problems with any or all of the internal organs are also possible (reviewed by de Boer and Hoeijmakers, 2000). Genetically, Type A CS (OMIM: 216400) is caused by mutations in the NER gene CSA and Type B CS (OMIM: 133540) is caused by the NER gene CSB, while the cause of Type C CS (OMIM: 216411) is still not clear. As described in the previous section, CSA and CSB proteins are involved in NER via the transcription-coupled repair mechanism. Compared to XP patients, CS patients are sensitive to sunshine but have a low risk of developing skin cancer. This is likely to be because the GGR pathway, which is still functional in CS patients, is essential for preventing skin cancer development.

Trichothiodystrophy (TTD) (OMIM: 601675) is a heterogeneous group of autosomal recessive disorders, characterised by brittle hair due to the lack of sulphur matrix rich proteins and accompanied by ichthyosis and other manifestations (Gillespie and Marshall 1983). In TTD patients, the hair appears dry, short and sparse. Existing hair is extremely fragile and splits longitudinally in to small fibres due to the poor viscoelastic parameters compared to controls. Physically, TTD patients generally have retarded overall growth and facial appearance with unusual protruding ears and receding chin. About half of the patients show abnormalities in NER of ultraviolet damaged DNA. Genetically, TTD is caused by mutations in one of the TFIIH subunits XPB, XPD or TTDA. Beyond deficiency in the NER pathway, it is hypothesized that basal transcription may also be altered leading to decreased transcription of specific genes (Itin et al. 2001; Nakamura et al. 2001).

Some other rare diseases are also linked with NER defects. For example, DeSanctis-Cacchione syndrome, which has been reported to be due to mutation in CSB, is an extremely rare disease with features of XP as well as a severe neurological phenotype (Colella et al. 2000). Another very rare disease combined xeroderma pigmentosum associated with Cockayne's syndrome (XP/CS), showing symptoms of both disorders has been identified to be linked with mutations in XPD (Lehmann 2001). The Cerebro-Oculo-Facio-Skeletal (COFS) (OMIM: 214150) syndrome, showing an autosomal, recessively inherited and rapidly progressive, neurologic disorder, also appears to be linked with mutations in CSB, XPG and XPD (Graham et al. 2001).

Different mutations in the same NER gene can lead to different syndromes. For instance, mutations in XPD or XPB can lead to XP, XP/CS, or TTD, while mutations in XPG can result in XP, or XP/CS. This has led to the idea that different mutations in NER genes

that function in both NER and transcription can result in either repair syndromes (such as NER), transcription syndromes (such as CS, or TTD) or a combination of the two (such as XP/CS).

ERCC1 defects have not seen associated with XP, CS or TTD. A case of human inherited ERCC1 deficiency was firstly reported to be associated with Cerebro-Oculo-Facio-Skeletal (COFS) syndrome with a mild defect in NER and severe developmental failure (Jaspers et al. 2007). The patient was born from nonconsanguineous Italian white parents and had microcephaly with premature closure of fontanels, bilateral microphthalmia, blepharophimosis, high nasal bridge, short filtrum, micrognathia, low-set and posterior-rotated ears. The patient didn't show spine abnormalities by X-ray scan, but a simplified gyral pattern and cerebellar hypoplasia were detected in the brain by nuclear magnetic resonance. These combined symptoms were compatible with a clinical diagnosis of a severe form of COFS syndrome. The patient failed to pass any developmental milestones and died at the age of 14 months due to respiratory failure from bilateral pneumonia. Sequencing analysis of both ERCC1 cDNA and genomic locus from cells from the patient and his parents revealed that a C to T transition in ERCC1 exon 5 on one allele inherited from the mother converted the amino acid glutamine codon to a translational stop signal (Q^{158}). This was predicted as the main cause of the patient's ERCC1 deficiency. The truncated ERCC1 protein encoded by this allele lacks the entire C-terminal $(HhH)_2$ domain, which is required for the interaction with ERCC1's partner XPF to form a stable complex as described before. A C to G transversion, which changes the Phe^{231} to a Leu, was detected on the other allele. This residue lies within the XPF binding domain of ERCC1 and is fully conserved among mammals and the transversion is likely to interrupt the binding activity. Comparative immunofluorescence showed a low level of ERCC1-XPF heterodimer in cells from this patient.

1.2.6 Mouse models of NER deficiency

Defective repair of various types of mutagenic DNA damage is a significant risk factor for diseases, especially cancer. However, difficulties such as limited access to tissues, lack of adequate clinical follow up, and failure to obtain complete autopsy information, complicate the use of human subjects for disease pathogenesis studies. Therefore, the availability of genetically-engineered mouse models becomes a powerful tool for understanding the molecular pathology of these diseases. Currently, several mouse mutants with defects in NER genes have been generated for further investigation of disease pathogenesis arising from NER deficiency.

XPA-deficient mice were generated using gene targeting in embryonic stem cells to study the function of the Xpa gene *in vivo* (de Vries et al. 1995; Nakane et al. 1995). The $Xpa^{-/-}$ mice appear normal, at least until the age of 13 months. $Xpa^{-/-}$ mice are highly susceptible to UVB-induced skin and eye tumours and to 7,12-dimethylbenz-[*a*]anthracene (DMBA)-induced skin tumours (de Vries et al. 1995). The skin cancer proneness displayed by XPA-deficient mice is highly comparable to that observed in human XP-A (Berg et al. 1997). Following treatment wih UVB radiation from a lower dose of $32J/m^2$/day to a higher dose of $80J/m^2$/day for up to 144 days, 100% of $Xpa^{-/-}$ mutants developed skin tumours. None of the UVB-exposed $Xpa^{+/+}$ or $Xpa^{+/-}$ mice developed tumors, nor did non-exposed $Xpa^{-/-}$ mice. Also, results indicate the development of different tumour types in Xpa-deficient mice is UVB dose dependent (Berg et al. 1997; de Vries et al. 1998). Histopathological observations of tumours show that irradiated hairless Xpa null mice developed papillomas, actinic keratosis (AK) and invasive squamous cell carcinomas (SCC) (de Vries et al. 1998).

A mouse homologue of the human gene for XP group C was isolated and XPC-deficient mice were generated by using embryonic stem cell technology to study the function of XPC in vivo (Sands et al. 1995). Mice homozygous for the Xpc mutant allele (xpc^{mut}/xpc^{mut}) were viable and do not exhibit an increased susceptibility to spontaneous tumour generation at one year of age. However, xpc^{mut}/xpc^{mut} mice were found to be highly susceptible to ultraviolet-induced carcinogenesis compared with mice heterozygous for the mutant allele ($xpc^{mut}/+$) and wild-type controls. Homozygous xpc^{mut} mutant mice also display a spectrum of ultraviolet-exposure-related pathological skin and eye changes consistent with the human disease xeroderma pigmentosum group C (Sands et al. 1995). Investigations showed cells from Xpc mutants are highly sensitive to UV radiation. Mouse embryonic fibroblasts (MEFs) isolated from Xpc mutant mice are severely defective in overall NER (Cheo et al. 1997; Reardon et al. 1997; Friedberg and Meira 1999). Studies show that Xpc mutant mice are highly predisposed to skin cancer (Sands et al. 1995). All $Xpc^{-/-}$ mutant mice develop skin cancer on shaved skin by 25 weeks after daily exposure to UVB radiation. Comparatively, no cancerous symptoms are observed in normal or $Xpc^{+/-}$ heterozygotes during this time. However, a significant increase in predisposition to skin cancer is observed in $Xpc^{+/-}$ mice compared to wild-type controls following more extended periods of UVB radiation, as 80% of $Xpc^{+/-}$ heterozygotes developed skin cancer compared to 40% in the wild type group. These observations suggest that loss of one Xpc allele predisposes to UV radiation-induced skin cancer because of a partial defect of NER (Cheo et al. 1997). Additionally, further study suggests that defective p53 function accelerates the progression of benign liver tumours in $Xpc^{-/-}$ mice (Cheo et al. 1999).

Xpd null mice are embryonic lethal (de Boer et al. 1998). A viable mouse model carrying the XPD^{R772W} allele mimicking a point mutation from a TTD patient showed a photosensitive phenotype and all the features of the TTD patient (de Boer et al. 1998).

Further investigations showed that this mouse was also susceptible to UV and chemical induced carcinogenesis, although not as much as Xpa mice (de Boer et al. 1999). Furthermore, the TTD mouse model has recently been determined to have a segmental progeroid or premature ageing phenotype, which is also evident in human TTD patients (Wijnhoven et al. 2005).

An Xpb mouse model for combined XP/CS has been reported very recently (Andressoo et al. 2009). Severe alterations in Xpb caused embryonic lethality while knock-in mice closely mimicking an XP/CS patient-derived XPB mutation were viable. Xpb mice showed XP features like UV sensitivity but no CS features unless the DNA repair capacity was further challenged by crossing to the NER-deficient Xpa background, which suggests that accumulation of DNA damage is an important determinant of clinical diversity in NER syndromes. Furthermore, Xpb and Xpd double mutant mice were healthy at birth but display neonatal lethality, indicating that transcription efficiency is sufficient to permit embryonal development even when both TFIIH helicases are deficient (Andressoo et al. 2009).

Xpe mice, also known as DDB mice, have been generated by deletion of exons 4 and 5. This mouse model showed a high susceptibility to internal tumours, particularly of the lymphoid tissue and UV induced skin cancers (Yoon et al. 2005).

An Xpf model mouse was created by modelling a point mutation from an XPF patient, which introduced a stop coden to exon 8 of the Xpf gene (Tian et al. 2004). Although the patient didn't suffer extremely severe symptoms, all Xpf mice died at three weeks similar to the Ercc1 null mice described below (McWhir et al. 1993).

Xpg mice were created by using a neo insertion into exon3 of the gene which abolished the *Xpg* mRNA (Harada et al. 1999). The Xpg mouse model showed features of impaired growth, dramatically reduced lifespan and cerebellar abnormalities, which was reminiscent of Xpf or Ercc1 deficiency (Harada et al. 1999; Sun et al. 2001).

Mouse models have also been generated to investigate the mutations in Csa and Csb. The Csa model was created by interrupting exon 2 of the Csa gene with a hygromycin insert, while the Csb model was generated by mimicking a gene truncation found in a CSB patient (van der Horst et al. 1997; 2002). These mice showed mild CS-like features such as photosensitivity and slightly retarded growth but the fertility and lifespan were found to be normal (van der Horst et al. 1997; 2002).

Investigation of ERCC1/XPF defective animals is still on-going. Our lab generated the first mouse with an Ercc1 knockout allele and has done several studies with the Ercc1 mutant animals (McWhir et al. 1993). The original knockout Ercc1 allele was generated by insertion of a Neo cassette into exon 5 of the wild type Ercc1 allele (Selfridge et al. 1992) (Figure 1.4).

Interestingly, the phenotype of $Ercc1^{-/-}$ mice is more severe and quite distinct from most other NER-deficient mice. Ercc1 knockout mice die before weaning, around three weeks of age, because of the extensive physiological abnormalities (McWhir et al. 1993). These animals were severely runted with a weight around only 20% of their control littermates. Investigations showed that Ercc1 null mice with the original *Ercc1* knockout allele suffer from severe liver failure, which was supposed to be the main cause of the premature death (Selfridge et al. 2001). Highly polyploid cells were found in animals' liver through histological examination. Liver polyploidy is a characteristic

Fig 1.4 Schematic diagram of Ercc1 KO allele

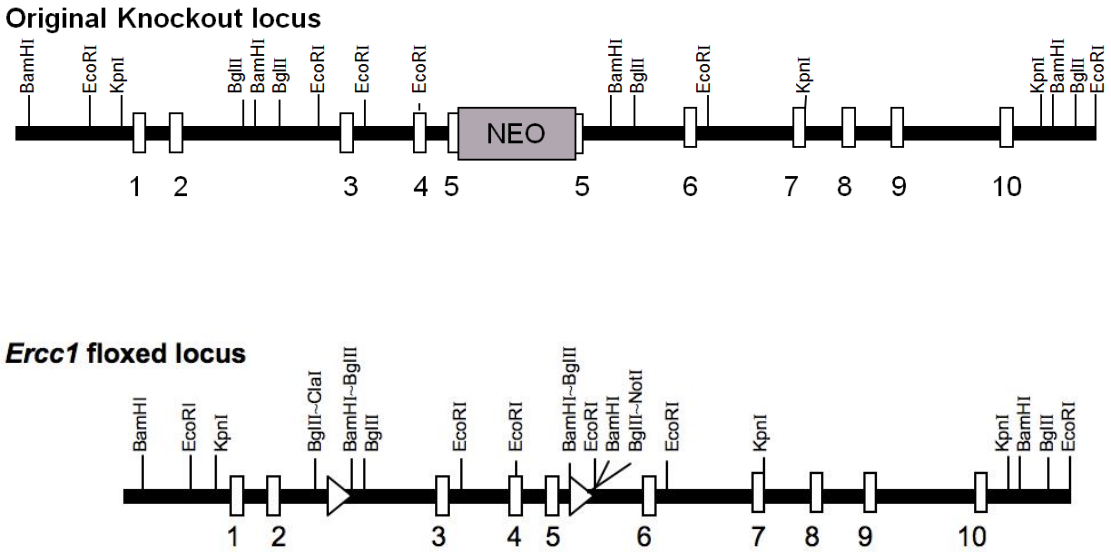

Schematic diagram of targeted Ercc1 alleles. White boxes show exons. Horizontal black boxes show introns. White triangles show LoxP sites.

feature of ageing. The Ercc1 null mice showed ploidy levels at about twenty days of age that were reminiscent of two years old mice. The p53 level was also found to be elevated in our Ercc1 null mice. In addition, an independent Ercc1 mutant mouse exhibited an absence of subcutaneous fat, early onset of ferritin deposition in the spleen and compromised NER and cross-link repair (Weeda et al. 1997). Unlike cells from mice with only an NER defect, ERCC1 mutant cells undergo premature replicative senescence, which may contribute to the premature ageing phenotype (Weeda et al. 1997).

Because the premature mortality of our Ercc1 null mice has effectively precluded studies on the role of Ercc1 in older mice, another Ercc1 knockout mouse model was created with an Ercc1 proficient liver using an Ercc1 transgene under the control of a liver-specific promoter (Selfridge et al. 2001). The Ercc1 null mice expressing the liver transgene had a weight around 60% of their littermates and a lifespan ranging from 9 to 12 weeks. Although the liver function was corrected, it didn't revert these mice to a normal wild type phenotype. Some kidney abnormalities including slightly increased plasma creatinine level, increased 8-oxo-guanine DNA adducts, some histopathology and an increasd level of ploidy arose in the transgene-positive Ercc1 knockout mice. Polyploid nuclei of kidney proximal tubule cells were revealed by FACS from 10-week-old transgene-positive nulls, similar to the polyploidy seen in the liver of 3-week-old Ercc1 nulls. These abnormalities finally led to the death of the liver corrected Ercc1 knockout animals (Selfridge et al. 2001). Further study revealed that the Ercc1 liver-corrected null mice suffered from proteinuria from a young age and had brain abnormalities and swollen brains consistent with uraemic disease (Lawrence et al. 2008).

Many of these features of the Ercc1 null mouse phenotype were reminiscent of a premature ageing syndrome (McWhir et al. 1993; Weeda et al. 1997). This progeroid

syndrome was suggested to be a consequence of genotoxic stress suppressing the somatotroph axis, which is one of the major hormonal systems regulating postnatal growth in mammals, and has now been characterised more extensively in Ercc1-deficient mice and has also been found in a patient with a severe XPF mutation (Niedernhofer et al. 2006). Close parallels were also found between the clinical course in the ERCC1 deficient patient, which was reported to be associated with COFS syndrome, as described in the section 1.2.5 (Jaspers et al. 2007) and the phenotype of Ercc1-deficient mice.

The lifespan of the liver-corrected animals with the Ercc1 transgene was still not ideal for some long-term investigations such as sensitivity to UV radiation. Therefore, an Ercc1 floxed allele has been engineered using the *Cre-lox* system, which enables us to inactivate Ercc1 in specific tissues (Figure 1.4). In the *Cre-lox* system, bacterial *Cre* recombinase is controlled by a tissue-specific or development-specific promoter sequence. With the expression of *Cre* recombinase, two *loxP* sites in the engineered Ercc1 gene are recognised and then the sequence between these two *loxP* sites is excised by recombination. A transgenic mouse line expressing *Cre* recombinase under the control the keratin *K5* promoter was used in our group to generate the epidermal specific Ercc1 knockout (Ramirez et al. 2004). Hairless mice with *Ercc1*-deficient skin were hypersensitive to the short-term effects of UV irradiation, showing a very low minimal erythemal dose and a dramatic hyperproliferative response. Ultraviolet-irradiated mice with Ercc1-deficient skin developed epidermal skin tumours much more rapidly than controls (Doig et al. 2006).

The minimal erythemal dose (MED) for Ercc1 skin-specific knockouts was lower and the 20-fold difference from control mice was greater than reported for other NER knockouts (Berg et al. 1997; Berg et al. 2000). Ercc1 skin-specific knockouts were > 7-

fold more sensitive than controls to UV-induced skin cancer, while Xpa mice were only 4-fold more sensitive than controls and Csb mice only 2-fold more sensitive (Berg et al. 1997; Berg et al. 2000). Thus, Ercc1 skin-specific knockouts appear more sensitive to UV irradiation than other NER knockouts and the resulting tumours also showed more raped actinic progression than controls. This has not been reported previously for other NER knockouts.

1.3 Melanoma

1.3.1 General introduction to melanoma

Melanoma is one of the rarer types of skin cancer but causes the majority of skin cancer related deaths. It is a malignant tumour of melanocytes which are cells of neural-crest lineage that are evenly distributed in the basal epidermal layer of human skin.

There are about 160,000 new cases of melanoma diagnosed worldwide each year, and it is more frequent in males and Caucasians (Tsao et al. 2004). Cutaneous melanoma is the eighth most common cancer in the UK and the second commonest in young people aged from 20 to 39. In Scotland the incidence of melanoma is rising rapidly, from 1979 to 1998 it increased 300% for men and 180% for women (MacKie et al. 2002). A further 73% rise is predicted over the next 10 to 15 years in terms of melanoma cases in Scotland. Melanoma is commonest on the legs in female and on the trunk in male.

A family history of melanoma will greatly increase the risk of an individual developing this disease. Chromosome 9p21 was identified as the site of a familial melanoma gene (Tsao 2000). About 8% to 12% of all melanoma cases are familial and 25% to 40% of inherited cases of melanoma carry mutations in the CDKN2A (which encodes p16 and ARF proteins and is located at 9p21) or CDK4 loci (Kamb et al. 1994). This will be addressed in more detail in section 1.3.2. Melanoma risk is highest in those with fair skin and inability to tan, particularly in those with red hair (Marrett et al. 1992). Freckling and blue eyes are also associated with modest increase in melanoma risk (Bliss et al. 1995). The melanocortin-1 receptor (MC1R) gene plays an important role in determining if a person has red hair, fair skin, and sensitivity to UV radiation. An increased UV sensitivity and a 2-4 fold elevation in melanoma risk is linked with some inherited variants of the MC1R gene (Hayward 2003). The presence of multiple naevi in an individual is a strong marker for melanoma risk irrespective of family history (Berwick and Halpern 1997). Coinheritance of variants of the MC1R gene seen in red-haired patients, along with CDKN2A mutations, further increases the risk of melanoma in melanoma-prone families (Goldstein et al. 2005).

There are several phase in the development of melanoma (reviewed by Gray-Schopfer et al. 2007). In the skin, melanocytes reside in the basal layer of the epidermis (Fig. 1.5.a) and in the hair follicles. In response to ultraviolet (UV) radiation, epidermal keratinocytes regulate the homeostasis of melanocytes by secreting factors that regulate melanocyte survival, differentiation, proliferation and motility, also stimulating melanocytes to produce melanin and resulting in the tanning response. Thereby, melanocytes are essential in protecting the skin from the UV radiation induced damaging effects and in preventing skin cancer. Melanin production occurs mainly in a lysosome-like structure known as the melanosome. Generally, there are two types of melanin and both derive from a common tyrosinase-dependent pathway with the same precursor tyrosine. The brown black eumelanin is produced mainly in the dark skin and

hair, while the red-yellow pheomelanin is mainly found in red hair and freckled individuals. The production of melanin in the hair and skin is tightly regulated by the MC1R. Binding of melanocyte stimulating hormone to a functional MC1R leads to an increase in intracellular cAMP levels. This stimulates the conversion of red/yellow pheomelanin to black/brown eumelanin. This conversion does not occur in individuals homozygous for "red hair" mutations in the MC1R gene (Cone et al. 1996).

Mutations in critical growth regulatory genes disrupt the intracellular signalling in melanocytes and allow them to escape their tight regulation by keratinocytes (Haass et al. 2004). Consequently, melanocytes can proliferate and spread, leading to the formation of a naevus or common mole (Figure 1.5.b). Although the majority of naevi are benign, a small number can progress to radial-growth-phase (RGP) melanoma, which is an intra-epidermal lesion and can involve some local microinvasion of the dermis (Figure 1.5.c). The RGP cells can then progress to the vertical-growth phase (VGP) which is a more dangerous stage due to its metastatic potential, with nodules or nests of cells invading the dermis (Figure 1.5.d). Not all melanomas pass through each of these individual phases. RGP or VGP can both develop directly from isolated melanocytes or naevi and progress directly to metastatic malignant melanoma (Miller and Mihm 2006).

Many melanomas metastasize because of their propensity for vertical growth with deep invasion. The majority of patients with early-stage melanoma following simple surgical resection could have a long-term survival (5 year survival rate > 90%) but patients with metastatic case would normally have a dismal prognosis (5 year survival rate < 30%). This emphasises the importance of early diagonosis. Most melanoma can be identified by clinical examination with several features, including Asymmetry of a lesion, Border

Fig 1.5 Progression of melanocyte transformation

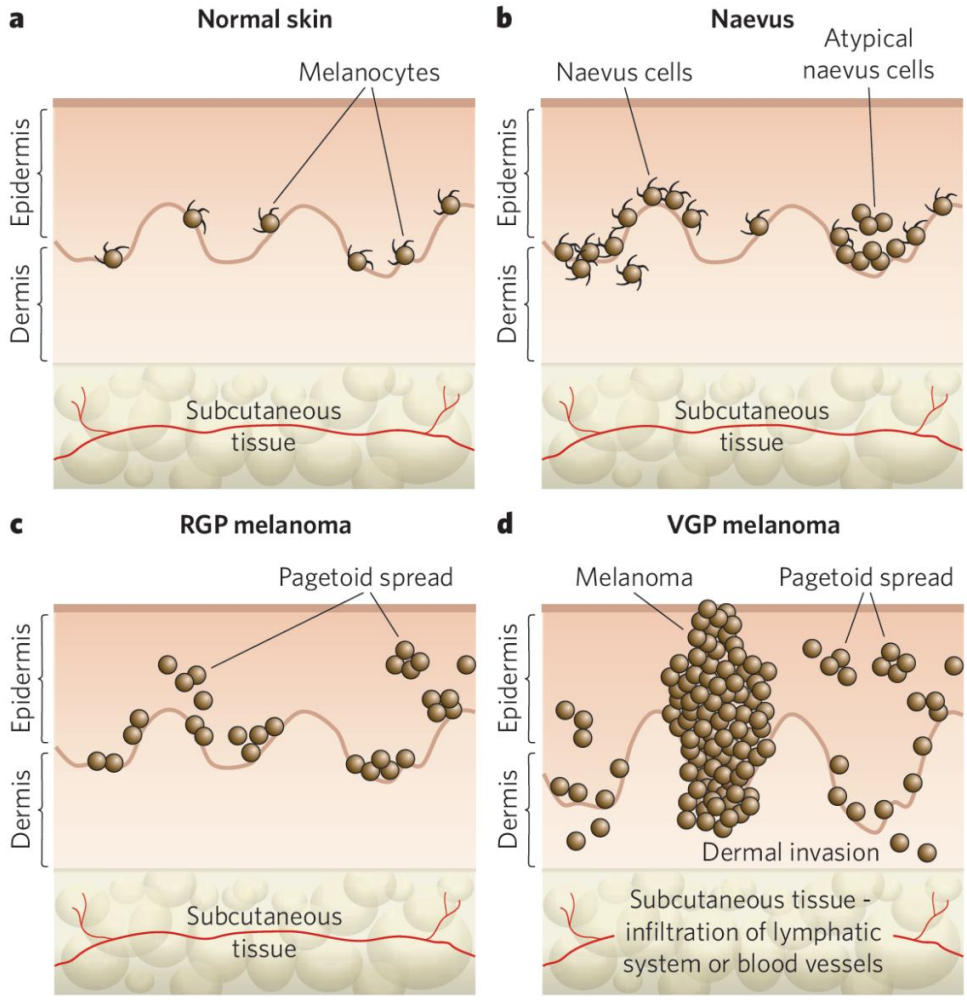

Various stages of melanocytic lesion. a, Normal skin. Evenly distributed dendritic melanocytes are shown within the basal layer of the epidermis. b, Naevus. Naevus cells are shown. Naevi are termed either junctional, dermal or compound according to their localization. c, Radial-growth-phase (RGP) melanoma, which is considered to be the primary malignant stage. d, Vertical-growth-phase (VGP) melanoma, which is the first stage that is considered to have malignant potential and leads directly to metastatic malignant melanoma and the most deadly stage. Figure is adapted from Gray-Schopfer et al. 2007.

irregularity, colour Change and Diameter greater than 6mm, an ABCD system of diagnosis (Friedman et al. 1985). Clinical suspicion should also be aroused by any significant change in an existing nevus or skin lesion.

Melanoma is a disease with high metastatic potential and is highly resistant to chemotherapy. This is likely to be explained by melanocytes originating from highly motile cells that have enhanced survival properties. Melanoma cells have low levels of spontaneous apoptosis *in vivo* compared with other tumour cell types, and are relatively resistant to drug-induced apoptosis *in vitro* (Soengas and Lowe 2003). Currently there is no effective therapeutic regime to improve the survival of patients with advanced melanoma in randomized trials.

Patients with intermediate or high risk of recurrence could potentially benefit from eradication of micrometastatic disease through the use of effective systemic adjuvant therapy. Currently high dose intravenous interferon-alpha is the only drug that has been shown reproducibly to have some impact on patients according to large randomised trials (Hersey 2003). A pooled analysis of trials in median follow-up times of 2.1 to 12.6 years showed that high dose intravenous interferon-alpha treatment was linked with a significant improvement of about 10% at 5 years in relapse-free survival for patients but no obvious benefit in terms of overall survival (Kirkwood et al. 2004).

For patients with metastatic melanoma, there is no evidence to show a significant survival advantage with use of any specific drug or combination of drugs (Brown and Kirkwood 2003). Dacarbazine (DTIC) is one approved chemotherapeutic agent for the treatment of advanced melanoma. DTIC produces a response rate in 15-20% with a median duration of response of 4 months (Eggermont and Kirkwood 2004). Regimens

using a combination of DTIC and other cytotoxic agents such as tamoxifen or interferon-alpha have shown promising response rates in single-institution phase 2 trials but no survival advantage in randomised phase 3 studies (Tsao et al. 2004). The cytokine interleukin 2 has approval for use in the US for treating metastatic melanoma but its overall response rate is low (16%) and systemic toxicity is high.

1.3.2 Melanoma and its cell signalling pathways

As melanoma is a complex and refractory genetic disease, a clear understanding of the biology underlying its initiation and progression is required to contribute to the refining of the classification system, the design of better therapeutic agents and approaches. Therefore, a number of cell signalling pathways related to melanoma pathogenesis and development of effective drugs to treat melanoma have been investigated, which are described below (Figure 1.6).

Inactivation of the $p16^{INK4a}$/cyclin dependent kinases 4 and 6/retinoblastoma protein ($p16^{INK4a}$/CDK4,6/pRb) and $p14^{ARF}$/human double minute 2/p53 ($p14^{ARF}$/HDM2/p53) tumor suppressor pathways has been shown to be strongly associated with melanoma development. These pathways are involved in the control of the G_1/S phase transition of the cell cycle and are most often inhibited via mutations or deletion in the *cyclin-dependent kinase inhibitor 2A* (CDKN2A) locus on chromosome 9p21, which encodes 2 tumour suppressors, $p16^{INK4a}$ and $p14^{ARF}$ (Chin 2003; Sharpless et al. 2003). $p16^{INK4}$ is a CDK inhibitor that binds to and inhibits CDK4 and CDK6, which otherwise phosphorylates pRb and induces G_1-S phase progression (Serrano et al. 1993), while

Fig 1.6 Cell signalling pathways in melanoma

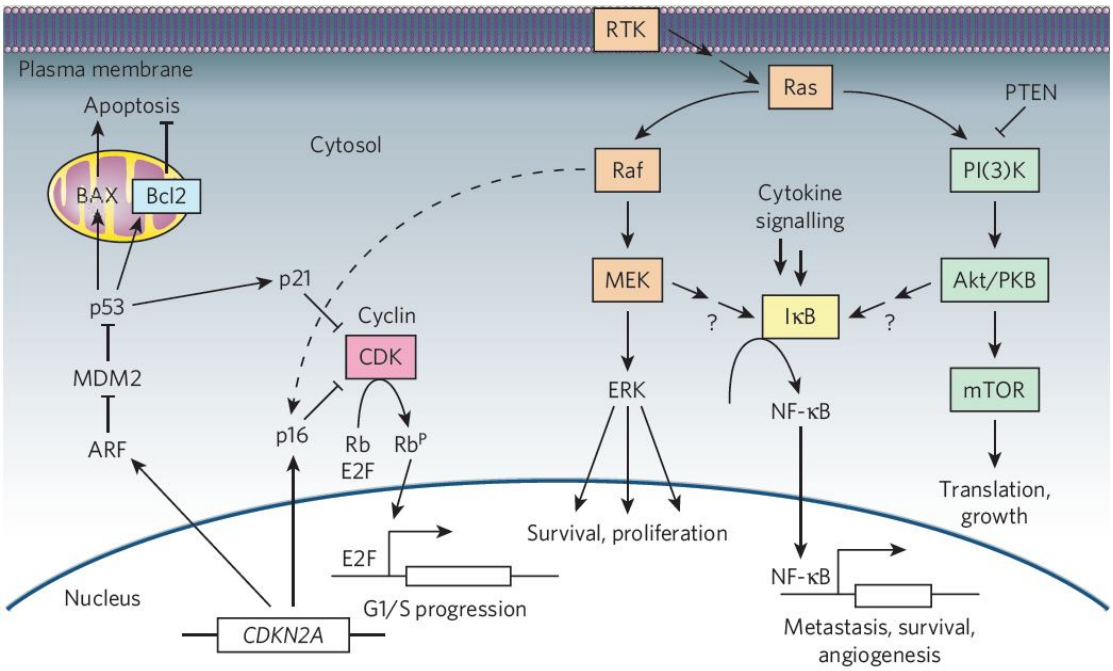

Several of the main pathways involved in melanoma initiation, progression and maintenance are indicated by different colours. Figure is adapted from Gray-Schopfer et al. 2007.

$p14^{ARF}$ acts through a distinct pathway which stabilizes p53 by preventing murine double minute-2 (MDM2) induced p53 degradation (Pomerantz et al. 1998). The importance of the CDKN2A gene in melanoma susceptibility was confirmed by studies showing that the penetrance of CDKN2A mutations varies with melanoma population incidence rates (Bishop et al. 2002) and that CDKN2A mutation carriers have increased total nevus number and total nevus density, both known as risk factors for melanoma, compared with noncarriers within the same family (Florell et al. 2004).

The Ras/Raf/MEK(mitogen-activated protein kinase/ERK kinase)/ERK(extracellular-signal-regulated kinase) pathway regulates proliferation, differentiation and cell survival. In this pathway, the small G protein Ras works upstream of a core module consisting of three kinases: the MAPK (mitogen-activated protein kinase) kinase kinase (MAPKKK) Raf that phosphorylates and activates the MAPK kinase (MAPKK) MEK, which in turn activates the MAPK ERK (Kolch 2000). The Ras/Raf/MEK/ERK pathway is a key regulator of melanoma cell proliferation. ERK is hyperactivated in up to 90% of human melanoma. NRAS, one of the three Ras genes in human, is mutated at the rate of 15% to 30%. BRAF, which together with ARAF and CRAF are the three human RAF genes, is the most commonly mutated component in this pathway with a mutation rate from 50% to 70% (Gray-Schopfer et al. 2007). 80% to 90% of the BRAF mutations involve a glutamic acid for valine substitution at position 600 (V600E) (Davies et al. 2002). This V600E BRAF has a 10 times greater kinase activity compared to wild-type BRAF and constitutively stimulates ERK activity *in vivo* independent of Ras (Karasarides et al. 2004). Does UV-irradiation induce the BRAF mutation? The GTG to GAG change in the V600E is not a typical UVB-damaged DNA signature as the most characteristic signature mutation by UV is CC to TT or C to T (Davies et al. 2002). It is possible that the V600E mutation is not induced by UV irradiation directly but is a secondary consequence of exposure, arising from error prone translesion synthesis (Thomas et al. 2006).

The phosphoinositide-3-OH kinase (PI3K) pathway, which regulates cell survival, proliferation, growth and motility, is another important pathway in melanoma and is often hyperactivated in melanoma. PI3K mutations occur in 3% of metastatic melanomas. One component in the PI3K pathway PTEN (phosphate and tensin homologue) is also found to have loss of function rates from 5% to 20% in late-stage melanomas (Gray-Schopfer et al. 2007), and the PI3K effector protein kinase B (PKB) is overexpressed in up to 60% of melanomas (Figure 1.6). Both ERK and PI3K signalling pathways must be inhibited to suppress cell growth in melanomas indicating that both pathways are important targets for drug development (Smalley et al. 2006).

Microphthalmia-associated transcription factor (MITF) is considered to be the master regulator of melanocyte biology because of its regulation of the expression of melanogenic proteins (Levy et al. 2006). It also plays a key role in melanoma through its regulation of melanoblast survival and melanocyte lineage commitment. Continued MITF expression is essential for melanoma cell proliferation and survival (Levy et al. 2006). MITF is expressed in most human melanomas and its target genes have already been used as diagnostic markers (Levy et al. 2006). However, the protein level of MITF must be carefully controlled. There is a significantly lower level of MITF in melanoma cells compared to the level in melanocytes. Increased MITF levels could reduce melanoma proliferation even in the presence of oncogenic BRAF, while critically low levels lead to cell cycle arrest and apoptosis (Wellbrock and Marais 2005). Although MITF alone cannot immortalize human melanocytes, it can achieve this by cooperating with the V600E BRAF to transform immortalized melanocytes (Garraway et al. 2005).

Other signalling pathways involved in human melanoma development include the overexpression of B-cell leukaemia/lymphoma 2 (Bcl-2), nuclear factor-κB (NF- κB)

and Akt3. It is common in melanoma that mutations in these pathways contribute to reduce apoptosis and promote growth (Figure 1.6). Furthermore, as described before, it has been reported that many inherited cases of melanoma carry inactivating mutations in the CDKN2A gene, which encodes p16INK4A and p14ARF, or activating mutations in CDK4.

1.3.3 Melanoma and DNA repair

1.3.3.1 DNA repair and melanoma susceptibility

As described in the previous section, exposure to the ultraviolet component in sunlight is a key environmental risk factor for the incidence of cutaneous melanoma by inducing mutations in important genes involved in cell proliferation and apoptosis. UVB radiation at wavelengths of 290–320 nm causes damage in the form of cyclobutane pyrimidine dimers and pyrimidine 6-4 photoproducts, while UVA radiation at wavelengths of 320-400nm normally induces single-stranded breaks, DNA-protein crosslinking, and generates free-radicals that cause oxidative damage. Multiple pathways are involved in repairing UV-DNA damage including the NER pathway, the BER pathway, the MMR pathway and the homologous double-stranded DNA repair pathways.

The NER pathway plays the main role in the repair of UVB-induced DNA lesions. Thereby, polymorphisms in nucleotide excision repair genes that affect function are likely to constitute genetic susceptibility factors for melanoma. Defects in the NER

pathway lead to accumulation of photoproducts, which is associated with melanoma risk. This is exemplified by the NER deficiency disease XP. Based on a study with 596 Scottish melanoma patients and 441 population-based controls, significant associations were found for the NER genes ERCC1 and XPF, with the strongest associations for melanoma cases aged 50 and under (ERCC1 OR 1.59, P = 0.008; XPF OR 1.69, P = 0.003) (Povey et al. 2007).

For other NER genes, there was no association found between the XPG exon 15 Asp 1104 His polymorphism (rs17655) and melanoma. For the XPC gene, there was no association for three XPC polymorphisms, G1580A, T1601C and G2166A (Blankenburg et al. 2005), but association was found for three other XPC markers, intron 9 PAT, Intron 11-6A and Lys 939 Gln (Blankenburg et al. 2005). However, no association was found for XPC Lys 939 Gln, nor for two SNPs (Arg 1213 Gly, Arg 1230 Pro) in CSB and one SNP (Ala 249 Val) in HR23B (Millikan et al. 2006). For XPD, no association was found between the XPD exon 23 Lys 751 Gln polymorphism and melanoma (Povey et al. 2007). In other studies of the XPD gene, Baccarelli et al. reported an association between the Gln 751 allele and melanoma in older patients (OR 2.3, 95% CI 1.1-4.9, P = 0.03) (Baccarelli et al. 2004). However, Han et al. reported an inverse association between the Gln 751 allele and melanoma (OR 0.63, 95% CI 0.38-1.05, P= 0.09) (Han et al. 2005). The genes environment and melanoma study found an association between the XPD 751 Gln/Gln genotype and melanoma (OR 1.4, 95% CI 1.1-1.7, P = 0.004) (Millikan et al. 2006).

It is also possible that genes involved in other pathways for the repair of DNA damage may also contribute to the susceptibility to melanoma as not all melanomas arise on sun-exposed sites.

The XRCC3 gene encodes a member of the RecA/Rad51-related protein family that participates in homologous recombination to maintain chromosome stability and repair DNA damage. It has been reported that the XRCC3 gene is significantly associated with melanoma development based on a study with 125 individuals with malignant melanoma and 211 individuals in the control group. (P = 0.004; odds ratio, 2.36; relative risk, 1.74) (Winsey et al. 2000). However, our study didn't find any evidence to support that XRCC3 exon 7 Thr 241 Met (rs861539) polymorphism is associated with melanoma (Povey et al. 2007).

Our previous study was also particularly interested in the possibility that genes in the BER pathway, which is responsible for the repair of UVA-induced oxidative DNA damage, might be genetic susceptibility factors for melanoma. However, no association was found for XRCC1 exon 10 Arg 339 Gln (rs25487), nor for OGG1 exon 7 Ser 326 Lys (rs1052133), which has not been investigated before for a role in melanoma (Povey et al. 2007).

1.3.3.2 DNA repair and melanoma metastasis

Analysis of differential gene expression at the level of whole biological pathways, rather than individual genes was carried out using microarray to identify the gene-profile signature for human primary malignant melanoma associated with metastasis (Kauffmann et al. 2008). 48 DNA repair genes, among a list of 234 genes, were found to be associated with metastatic progression, in which 44 genes are overexpressed (Figure 1.7). These genes typically showed low expression in non-recurrent primaries and a 2.5-

Fig 1.7 DNA repair genes and melanoma metastasis

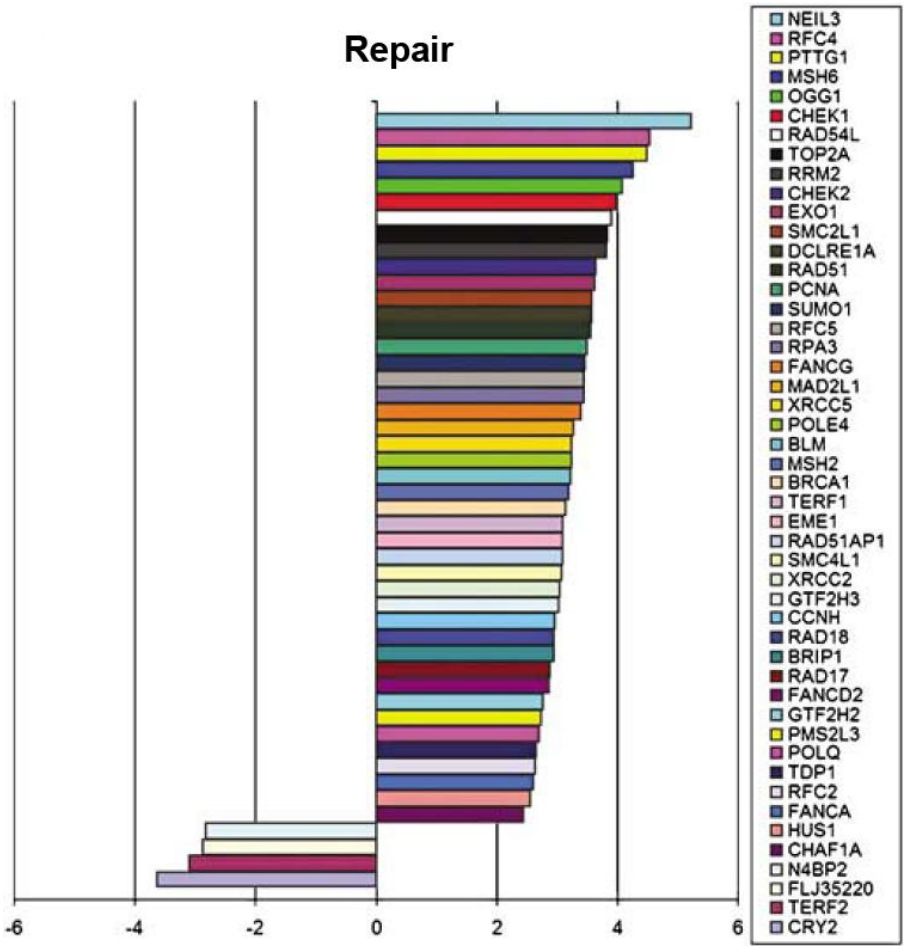

Standardized mean differences of log (ratio) for genes involved in DNA repair between non-recurrent primary melanomas and primaries that recurred within 4 years. A positive mean difference indicates overexpression in primary melanoma tumours that will metastasize within 4 years compared to those that will not. Figure is adapted from Kauffmann et al. 2008.

to 5-fold elevated expression in recurrent primary tumours. From the microarray investigation, only four NER genes including two TFIIH factors, GTF2H2 and GTF2H3, as well as the replication pathway proteins RFC and RPA are overexpressed in metastatic melanomas. Since the TFIIH factor is also involved in RNA transcription initiation, this result suggests that the NER pathway is not strongly implicated in metastasis induction (Kauffmann et al. 2008).

In the BER pathway, two interesting genes were found to be overexpressed in recurrent primary melanomas. One is the hOGG1 gene, which encodes the main glycosylase involved in the repair of oxidized guanines, while another one is the NEIL3 gene which also codes for a DNA glycosylase which is able to repair oxidized purines (Kauffmann et al. 2008).

Two MMR proteins, MSH6 and MSH2, are overexpressed in metastatic melanomas (Figure 1.7). These two proteins deal with DNA mismatches produced during normal DNA replication but also have the potential function of detecting bases mispaired with unrepaired DNA lesions to avoid mutagenesis during translesion synthesis (TLS) (Kauffmann et al. 2008).

However, surprisingly the majority of the genes overexpressed in recurrent primaries were not key players in the NER, BER, or DSB repair pathways. Instead, many belonged to repair pathways allowing recovery of stalled replication forks as a result of spontaneous or DNA lesion-induced blockage, or correction of replication errors, while others were involved in more general pathways acting to preserve genome stability. This increased expression would allow metastatic melanoma cells to replicate their genomes

rapidly and accurately and could also contribute to their extreme resistance toconventional DNA-damaging therapeutics (Kauffmann et al. 2008).

Chapter 2

Materials and Methods

2.1 Materials

2.1.1 General reagents and equipment

Amersham: ECL fluorescence kit, Hyperfilm™ MP high performance autoradiography film, Storm 840 phosphorimager.

Bioline: DNA Hyperladder I.

Biometra: Thermocycler.

BioRad: Gel Doc 2000 System with Quantity One 4.6 software, Mini-PROTEAN Electrophoresis System, Mini Trans-Blot Cell.

DAKO: Secondary HRP-conjugated forms of goat anti-rabbit, swine anti-rabbit, rabbit anti-goat and rabbit anti-mouse antibodies.

Fisher Scientific: 3M blotting paper, absolute alcohol, chloroform, Na_2EDTA, filter paper haematoxylin, isoamyl alcohol, isopropanol (propan-2-ol), methanol, potassium acetate, sodium hydroxide, trichloroacetic acid, xylene.

Invitrogen: agarose, Benchmark™ prestained protein ladder, NuPAGE™ 4-12% Bis-Tris gel, NuPAGE™ 10% Bis-Tris gel, NuPAGE™ transfer buffer, Subcloning Efficiency DH5α™ Competent Cells.

Millipore (UK) Ltd: disposable sterile filter. Immobilon P PVDF membrane.

New England Biolabs: restriction endonucleases and relevant buffers.

Pierce Biotechnology: Bicinchoninic acid (BCA) protein assay kit.

Promega: 25mM magnesium chloride, 10x PCR buffer, 5x PCR buffer, Taq DNA polymerase, Oligo dT, RNasin, pGEM-T Easy® Vector Systems.

Qiagen Ltd: QIAprep Spin Miniprep Kit. QIAGEN Plasmid Maxi Kit.

Roche: Protease Inhibitor cocktail tablets, Protein G Immunoprecipitation Kit, 3'/5' RACE kit (2nd Generation), High Pure PCR Product Purification Kit.

Santa Cruz Biotechnology: bovine anti-goat IgG-HRP antibody, ERCC1 (D-16) goat polyclonal IgG antibody, goat anti-rabbit IgG-HRP antibody.

Sigma-Aldrich: ammonium persulphate (APS), DMSO, DTT, Na_2EDTA, glycerol, herring sperm DNA, MOPS, parafilm M, PBS tablets, propidium iodide, ribonuclease inhibitor, sodium chloride, sodium deoxycholate, sodium hydroxide, oligonucleotides, trypsin, trypsin inhibitor, Triton X-100, Tween 20.

2.1.2 DNA manipulation reagents

Loading dye: 20% glycerol, 100mM Na_2EDTA, 0.1% bromophenol blue or orange G.

CA: 24 parts chloroform, 1part isoamyl alcohol.

DNA isolation buffer: 10mM Tris HCl pH8.0, 400mM NaCl, 3mM Na_2EDTA, 1% (w/v) SDS. Stored at 4°C.

PCA: 25 parts redistilled phenol, 24 parts chloroform, 1 part isoamyl alcohol.

Proteinase K: 2% proteinase K w/v in sterile distilled water.

10X RT buffer: 500mM Tris-HCl pH8.3, 60mM $MgCl_2$, 400mM KCl, 10mM DTT.

TAE electrophoresis buffer: 40mM Tris-acetate, 1mM Na_2EDTA.

TBE electrophoresis buffer: 90mM Tris-HCl, 90mM boric acid, 2mM Na_2EDTA, pH 8.3.

2.1.3 RNA manipulation reagents

Denaturation buffer: 0.5M NaOH, 1.5M NaCl.

Formamide sample buffer (RNA sample buffer): 2.3X MOPS, 50% de-ionised formamide, 11% formaldehyde.

Labelling buffer: 50ul solution A, 125ul solution B, 75ul solution C.

10X MOPS: 200mM 3-(N-morpholino) propane-sulphonic acid (MOPS), 50mM sodium acetate, 10mM Na_2EDTA, pH7.0.

Northern blot stripping buffer: 0.01% (wt/v) SDS, 0.01X SSC.

RNA loading buffer: 50% (v/v) glycerol, 1mM Na_2EDTA pH 8.0, 0.4% (wt/v) bromophenol blue, 1mg/ml ethidium bromide. Stored at -20°C.

RNAzol^{TM}B: RNA isolation solvent.

5X sample buffer: 20% (v/v) glycerol, 100mM Na_2EDTA, 0.1% (wt/v) bromophenol blue

Solution A: 1.25M Tris-HCl pH8.0, 0.125M $MgCl_2$, 25mM beta-mercaptoethanol, 0.5mM each of dGTP, dATP and dTTP.

Solution B: 2M HEPES buffer adjusted to pH6.6 with NaOH.

Solution C: Random hexadeoxyribonucleotides OD_{260nm}=90units/ml in TE

SSC (20X): 3M NaCl, 300mM tri-sodium citrate dihydrate pH 7.0.

TE buffer: 10mM Tris-HCl, 1mM EDTA, pH8.0.

2.1.4 Protein manipulation reagents

Immunoprecipitation washing buffer 1: 50mM Tris-HCl pH 7.5, 150mM NaCl, 1% Nonidet P40, 0.5% sodium deoxycholate, 1 protease inhibitor cocktail tablet (Roche Complete) / 25-50ml.

Immunoprecipitation washing buffer 2: 50mM Tris-HCl pH 7.5, 500mM NaCl, 0.1% Nonidet P40, 0.05% sodium deoxycholate.

Immunoprecipitation washing buffer 3: 10mM Tris-HCl pH 7.5, 0.1% Nonidet P40, 0.05% sodium deoxycholate.

Modified RIPA buffer: 50mM Tris-HCl pH 7.2, 1% (v/v) Triton X-100, 0.2% (w/v) sodium deoxycholate, 0.2% (wt/v) sodium dodecyl sulphate, 1 protease inhibitor cocktail tablet (Roche Complete) / 25-50ml.

RIPA buffer: 25mM Tris-HCl, pH 7.2, 150mM NaCl, 1% Triton X-100, 0.1% SDS, 1% deoxycholate, 1mM Na_2EDTA, 20mM NaF, 100uM orthovanadate, 1 protease inhibitor cocktail tablet (Roche Complete) / 25-50ml.

Stripping buffer: 20ml of 10% SDS, 12.5ml 0.5M Tris HCl pH 6.8, 67.5 ml ultra pure water and 0.8 ml ß-mercaptoethanol.

TBS: 5mM Tris-HCl, 75mM NaCl, pH 7.4.

TBS-T: 5mM Tris-HCl, 75mM NaCl, 0.05-0.1% Tween-20 v/v, pH 7.4.

Transfer buffer: 192mM Glycine, 25 mM Tris, pH 8.3.

2.1.5 Oligonucleotides

Table 2.1 General PCR primers

Code	Sequence (5' →3')	Description
Skin A forward	TCATCACTGAGCCGGATCTGGAG TCTGG	214 bp 5' of mouse Ercc1 exon1
Skin B reverse	GTTCCCCGCTCTAACTCCTC	57 bp 5' of mouse Ercc1 exon1
Skin C reverse	GAAGTGAGTCTAGCAGGAGTTG TG	Within mouse Ercc1 exon1
Exon 2 reverse	ATGGACCCTGGGAAGGACGAGG	Within mouse Ercc1 exon2
Exon 2b reverse	ACCACCCACCAGGAGGAAGT	Within mouse Ercc1 exon2

Exon 3a reverse	AGAACCCCAGCCAGACCCT	Within mouse Ercc1 exon3
M13 Forward	GTAAAACGACGGCCAGT	Forward sequencing primer
M13 Reverse	CATGGTCATAGCTGTTTCC	Reverse sequencing primer

Table 2.2 RT-PCR primers

Code	**Sequence (5' →3')**	**Description**
Novel promo	GCTGAGTCGTCGCTGCCTTA	For 11kb putative promoter
Novel promo b	GGAAGCGCTGAGTCGTCG	For 11kb putative promoter
Novel promo rev	TTGTGAGGGGCTCAGACGAG	For 11kb putative promoter
Novel promo rev b	ACGAGCAGCCATTGGAGATG	For 11kb putative promoter
ERC1 NP + 57	ACCGCGGCTAAGTTTAGAGG	For 2.5kb putative promoter
ERC1 NP + 65	TAAGTTTAGAGGCGGGTGGGG	For 2.5kb putative promoter

Table 2.3 5'RACE primers

Code	**Sequence (5' →3')**	**Description**
Oligo dT anchor	GACCACGCGTATCGATGTCGACTT TTTTTTTTTTTTTTV (V= A,C or G)	Anchor primer
PCR anchor	GACCACGCGTATCGATGTCGA	Internal anchor primer

Control primer neo1/rev	CAGGCATCGCCATGGGTCAC	Neo control primer
Control primer neo2/rev	GCTGCCTCGTCCTGCAGTTC	Neo control primer
Control primer neo3/for	GATTGCACGCAGGTTCTCCG	Neo control primer

Table 2.4 Bisulfite sequencing primers

Code	**Sequence (5' →3')**	**Description**
BIS CpG#1 FWD	CCCAGTGGACACATTGAGGTGCAGTAGTAG	CGI#1 forward primer
BIS CPG#1 RVS	TTGATACAGGAGGAAGAAAC	CGI#1 reverse primer
Bis CpG#1 FWD ABi8429	CACATTGAGGTGCAGTAGTAGAAGAGGTGTC	CGI#1 internal forward primer
Bis CpG#1 RVS ABi8429	TCTGGAGTGCAGAGGGGAACAGAAC	CGI#1 internal reverse primer
BIS CGI#2 FWD	ACAGAAAGCAAACTTGGGGATGCTG	CGI#2 forward primer
BIS CGI#2 RVS	GATACCTTTGCCCTGTGGGAGAA	CGI#2 reverse primer
BIS CGI#3 FWD	GCCTTGGAACACAACTACTTGAAGTCAAAG	CGI#3 forward primer
BIS CGI#3 RVS	GAAAGACCAGGTGAGTTTTGGCAGT	CGI#3 reverse primer

2.1.6 Antibodies

2.1.6.1 Primary antibodies

Table 2.5 List of primary antibodies used in this study

Code	Target *	kDa	Supplier	Dilution
SC-10157	ERCC1 (m)	33	Santa Cruz	1:1000
SC-17809	ERCC1 (m/h)	33/35	Santa Cruz	1:1000
FL-297	ERCC1 (h)	35	Santa Cruz	1:1000
ab2356	ERCC1 (m/h)	33/35	Abcam	1:300
AB-5 (51)	XPF (m)	102	Lab Vision	1:1000
NA27	MSH2 (h)	105	Calbiochem	1:500
SC-10789	MSH6 (h)	160	Santa Cruz	1:200
51-1327GR	MLH1 (h)	84	BD Biosciences	1:500
ab6046-200	Beta-tubulin (m/h)	50	Abcam	1:6000
015K-4821	Beta-actin (m/h)	42	Sigma	1:5000
MAB375	GAPDH (m/h)	36	CHEMICON	1:10000
SC-7907	PCNA (m/h)	36	Santa Cruz	1:3000

*m:mouse protein; h:human protein

2.1.6.2 Secondary antibodies

Secondary antibodies were sourced from Dako and Santa Cruz. HRP-conjugated forms of goat anti-rabbit (P0448 1:3000), swine anti-rabbit (P0217 1:1000), rabbit anti-goat

(P0449 1:4000) and rabbit anti-mouse (P0260 1:2000) antibodies were from Dako. A HRP-conjugated form of bovine anti-goat (SC-2305 1:3000) antibody was from Santa Cruz.

2.1.7 Cell culture reagents

Autogen Bioclear: Stem cell factor.

Beckman-Coulter: Coulter counter, FACScan machine, Isoton®II diluents.

BioRad: Chelex® 100 resin.

Greiner Bio One: Cellstar® cell culture flasks, cell culture dishes, cell culture plates, pipettes, cell scrapers.

Invitrogen: GIBCO® Dulbecco's Modified Eagle's Medium without calcium (No calcium DMEM, Cat. 21068-028), Dulbecco's Modified Eagle's Medium (DMEM, Cat. 10938-025), RPMI-1640 (Cat. 21875), Glasgow's Modified Eagle's Medium (GMEM, Cat. 21710), 400mM L-glutamine, 100X non-essential amino acids (NEAA), 100 mM sodium pyruvate (NaPy).

LONZA: Fetal calf serum (FCS).

New Biowest: New-born calf serum (NCS).

Sigma: beta-mercaptoethanol, Tetradecanoylphorbol acetate (TPA), cholera toxin, DMSO, endothelin, epidermal growth factor, penicillin G, streptomycin.

PBS: 140mM NaCl, 3mM KCl, 2mM KH_2PO_4, 10mM Na_2HPO_4

Trypsin-EDTA**:** 10× trypsin (Cambrex) diluted in PBS to 0.25% (w/v) trypsin, 1mM EDTA. Stored at -20°C.

2.1.8 Mammalian cells and culture media

Table 2.6 List of mammalian cell lines used in this study

Human cell lines:

Cells	**Source**	**Description**
HERMES 1	Prof. D. Bennett. St. Georges' Hospital Medical School, London	Human melanocytes immortalised with a telomerase expressing retrovirus

HERMES 4a	Prof. D. Bennett. St. Georges' Hospital Medical School, London	Human melanocytes immortalised with a telomerase expressing retrovirus
A375	The European Collection of Cell Cultures (ECACC)	Human malignant melanoma
C32	ECACC	Human malignant melanoma
EDMEL_3	Melton group	Human malignant melanoma
G361	ECACC	Human malignant melanoma
HBL	Gentaur. Brussels, Belgium	Human malignant melanoma
WM115	ECACC	Human malignant melanoma
PEA1	Dr. G. Sellar. Cancer Research Centre, The University of Edinburgh	Human ovarian tumour cell line
PEA2	Dr. G. Sellar. Cancer Research Centre, The University of Edinburgh	Cisplatin-resistant derivative line of PEA1
PEO1	Dr. G. Sellar. Cancer Research Centre, The University of Edinburgh	Human ovarian tumour cell line
PEO4	Dr. G. Sellar. Cancer Research Centre, The University of Edinburgh	Cisplatin-resistant derivative line of PEO1
PEO6	Dr. G. Sellar. Cancer Research Centre, The University of Edinburgh	Cisplatin-resistant derivative line of PEO1
PEO14	Dr. G. Sellar. Cancer Research Centre, The University of Edinburgh	Human ovarian tumour cell line
PEO23	Dr. G. Sellar. Cancer Research Centre, The University of Edinburgh	Cisplatin-resistant derivative line of PEO14

Mouse cell lines:

Cells	Source	Description
Keratinocyte ERCC1 WT	Melton group	Spontaneously immortalised mouse keratinocytes
Keratinocyte ERCC1 NULL	Melton group	Spontaneously immortalised Ercc1 deficient mouse keratinocytes
PAM212	Dr. John Mee. King's College, London	Spontaneously immortalised mouse keratinocytes
PF20	Melton group	Spontaneously immortalised Ercc1 wild-type mouse embryonic fibroblasts
PF24	Melton group	Spontaneously immortalised Ercc1-deficient mouse embryonic fibroblasts
3-1-1 T1a	Melton group	Spontaneously immortalized mouse melanocyte cell line containing a non-recombined Ercc1 floxed allele
3-1-1 T1a #5	Melton group	Ercc1 deficient derivative of 3-1-1 T1a mouse melanocytes by deletion of the Ercc1 exon 3-5 region
HM1	Melton group	Mouse ES cell line
DNMT3^{-}	Nick Gilbert. Cancer Research Centre, The University of Edinburgh	DNA methyltransferase 3 deficient mouse ES cell line

Our undifferentiated Ercc1 wild-type and deficient keratinocyte cultures were maintained in DMEM with a low calcium concentration to prevent the cells from

becoming differentiated (Lawrence et al. 2009). Differentiated keratinocyte cultures were maintained in normal DMEM. Medium was supplemented with 8% (v/v) chelex treated FCS (to minimize Ca^{2+}) for undifferentiated keratinocytes or 8% (v/v) normal FCS for differentiated keratinocytes, 10ng/ml epidermal growth factor or 10ng/ml keratinocyte growth factor, 4mM L-glutamine, 25U/ml penicillin and 25ug/ml streptomycin.

PAM212 keratinocyte cells were maintained in RPMI media with 10% FCS, 25U/ml penicillin and 25ug/ml streptomycin (Tani et al. 1992).

Immortalised Ercc1 wild type mouse embryonic fibroblast (PF20) and Ercc1 deficient mouse embryonic fibroblast (PF24) cultures were maintained in GMEM media supplied with 10% (v/v) FCS, 1mM NaPy, 25U/ml penicillin and 25ug/ml streptomycin (Melton et al. 1998).

Immortalised Ercc1 wild type and deficient mouse melanocyte cell lines were maintained in RPMI-1640 with 10% FCS, 200nM TPA, 25U/ml penicillin and 25ug/ml streptomycin (unpublished).

Mouse wild type ES cell line HM1 was isolated directly from HPRT-deficient strain 129 mice by previous group work (Magin et al. 1992). HM1 and $DNMT3^{-}$ cultures were grown in GMEM supplemented with 5% FCS, 5% New-born calf serum (NCS), 1X NEAA, 1mM NaPy, 0.1mM beta-mercaptoethanol, leukaemia inhibitory factor, 25U/ml penicillin and 25ug/ml streptomycin.

Human melanocytes, Hermes 1 and Hermes 4 cultures were grown in RPMI-1640 supplemented with 10% FCS, 4mM L-glutamine, 10ng/ml SCF, 200nM TPA, 200pM cholera toxin, 10nM endothelin and 25U/ml penicillin and 25ug/ml streptomycin (Gray-Schopfer et al. 2006).

Human melanoma cell cultures were maintained in RPMI media with 10% FCS, 25U/ml penicillin and 25ug/ml streptomycin.

Human ovarian tumour cell cultures were maintained in RPMI-1640 media with 10% FCS, 25U/ml penicillin and 25ug/ml streptomycin.

2.1.9 Bacterial strains

Sub-cloning Efficiency™ DH5α™ Competent Cells were sourced from Invitrogen, and were grown on/in LB medium at 37°C.

2.1.10 Bacterial culture media and related reagents

Ampicillin stock solution: 50mg/ml ampicillin in dH2O. 0.2µm filter sterilised and stored at -20°C. Optimal working concentration in LB was 100µg/ml.

Blue/white lacZ screen LB agar plates: For DH5α 20µl of 40mg/ml X-gal was spread over LB agar plates containing the antibiotic ampicillin. The plates were dried at room temperature before being used.

X-gal stock solution: 40mg/ml X-gal in dimethylformamide (DMF). Stored at -20°C and protected from light.

2.2 Methods

2.2.1 Cell Culture

2.2.1.1 Mammalian cell culture

All cells were cultured using appropriate media in an incubator at 37°C with 5% CO_2. Flasks were medium changed at least every second day, using aseptic technique inside a category II biological safety hood. When required, medium was aspirated (along with dead, floating cells), cells were passaged using trypsin-EDTA solution and counted using a Coulter cell counter.

2.2.1.2 Liquid nitrogen frozen stock

For long term storage, cells were frozen in liquid nitrogen using the appropriate culture medium supplemented with 10% DMSO and 20% FCS.

2.2.1.3 Counting of cells

Cells were diluted 1:100 in isoton and counted using the Coulter Counter Z series (Beckman Coulter).

2.2.1.4 Ultraviolet-C irradiation of cells

Ultraviolet-C (UVC) irradiation was carried out using a UV lamp (Mineralight Lamp UVGL-58, UV Products.), emitting $0.5Jm^{-2}s^{-1}$ from a fixed position. Cells were plated out 24 hours before irradiation in 100mm Petri dishes with 10ml of medium, or in 35mm Petri dishes with 2ml of medium before UVC irradiation. For irradiation, the medium was aspirated from dishes and a small amount of sterile PBS was applied (0.1ml/35mm dish) to prevent the cells from drying out. After the UVC irradiation, medium was replaced and cells were then put back into the incubator and cultured as stated previously.

2.2.1.5 Drug treatments of cells

Drug (Cisplatin, MG132 or cycloheximide) was directly added to the cell culture 24-hours post plating to give a designed final concentration. Treated cells were then incubated under standard conditions before being harvested at appropriate time points.

2.2.1.6 Colony forming assay

An optimal number of cells were plated in 6ml of complete media in 60mm Petri dishes. Duplicates or triplicates were set up in each assay. 24 hours later cultures were UV-irradiated or cisplatin treated as described above. Cultures were then incubated and were monitored for growth using an inverted microscope. At the time of good primary colony formation (7 to 30 days in culture), dishes were fixed with Carnoy fixative (3:1 methanol: glacial acetic acid) and stained with 0.25% (wt/v) Crystal Violet. Stained dishes were imaged using the Gel-Doc 2000 (Bio-Rad) system and colonies were counted using the Quantity One software (Bio-Rad).

2.2.1.7 Cytotoxicity screening by Sulforhodamine B assay

Cells were plated in a 96-well plate with 150ul of medium per well at the appropriate seeding density and incubated under normal conditions (DAY 0). 50ul of medium with cisplatin was added to the cell culture 24 hours following the plating to give the designed final cisplatin concentration (DAY 1). Plates were assayed at 72-hour (DAY4),

96-hour (DAY 5), 120-hour (DAY6) and 144-hour (DAY 7) following the drug treatment. For the assay, the medium was replaced with 50ul of 10% (wt/v) TCA, and incubated at 4°C for 1h fixation. Plates were washed with slow-running tap water for four times and air-dried at 40°C in an oven. 100ul of 0.057% (wt/v) SRB solution was added, incubated at room temperature for 30 min and quickly rinsed four times with 1% (vol/vol) acetic acid to remove unbound dye. 100ul of 10mM Tris-base solution (pH 10.5) was added to each well after the plates were air-dried, and then incubated at room temperature for 30min with agitation to solubilise the protein-bound dye. The O.D value at 510nm was measured using a plate reader.

2.2.1.8 Preparation of genomic DNA from mammalian cell lines

Cells were harvested by trypsinisation and pelleted by centrifugation at 1,300 rpm for 5 minutes. The pellet was resuspended in PBS and digested overnight at 37^{o}C in 750µl DNA isolation buffer supplemented with proteinase K to a final concentration of 280µg/ml. The supernatant was extracted twice with 750µl PCA and vigorous shaking and subsequently with 750µl CA to remove traces of phenol. The DNA was precipitated for 10 minutes at room temperature by addition of 750µl of isopropanol. Following 10 minutes centrifugation, the nucleic acid pellet was washed twice with 70% ethanol, dried, resuspended in 200µl sterile distilled water and stored either at 4^{o}C in the short term or -20^{o}C for longer periods.

2.2.1.9 Protein extraction from mammalian cell lines

Cells were washed with cold PBS, scraped into 1ml of cold PBS in a 1.5ml microcentrifuge tube and centrifuged at 3000rpm for 3min. PBS was removed and the cell pellet was resuspended in 100 to 200ul of RIPA lysis buffer. The cell lysates were then incubated on ice for 15 minutes before being centrifuged at 13000rpm for 15 minutes. The supernatant was recovered as cleared cell lysate and stored at -70°C.

2.2.1.10 Protein extraction from tissues

Fresh tissues were wrapped with foil and snap-frozen in liquid nitrogen. The frozen tissues were smashed into small pieces and then homogenised in 2ml of ice-cold modified-RIPA buffer for 1min, and then incubated on ice for 30 minutes before being centrifuged at 13000 rpm for 15 minutes. The supernatant was recovered as cleared cell lysate and stored at -70°C.

2.2.1.11 Generation of xenografts

Cells were grown in standard culture dishes and then trypsinised and counted. 10^7 cells were resuspended in 0.1ml DMEM media with 0.1ml of matrigel and injected subcutaneously into the flanks of nude mice. 5 mice were used for each cell line and

each mouse had an injection on either flank. Xenograft growth was monitored over a 16 week period.

2.2.2 Molecular Biology Methods

2.2.2.1 DNA ligation of PCR products into pGEM®-T Easy Vector Systems

DNA ligation reactions were performed in a 10ul volume using reagents from the pGEM®-T Easy Vector Systems. The ligation reactions contained 5ul of 2X Rapid Ligation Buffer, 1ul of T4 DNA ligase (3 Weiss units/µl) and 50ng vector DNA. A 3:1 molar ratio of insert DNA to vector DNA was present in each reaction. DNA ligation reactions were incubated for either 1h at room temperature or at 4°C overnight to ligate the T-tailed pGEM®-T Easy vector with the Taq polymerase generated A-tailed PCR products.

2.2.2.2 Transformation of bacteria by heat shock

50µl of DH5α competent bacterial cells were thawed on ice. 10-100ng of plasmid DNA, or 5µl of a ligation reaction, was added to a tube of competent bacterial cells, and mixed gently. A positive control consisting of pUC19 plasmid DNA (250pg), and a negative control consisting of dH_2O alone, was also included in each group of bacterial

transformations. The mixture of cells and DNA was incubated on ice for 30min, before being heat shocked in a 42°C water bath for 20s. Following 2min incubation on ice, 1ml LB broth was added and the transformations were incubated at 37°C for 1h with shaking (225rpm). After that, 100µl of the transformations were then plated out onto warm LB agar plates containing the antibiotic ampicillin. The plates were inverted and incubated at 37°C overnight.

2.2.2.3 Amplification of plasmid DNA using DH5α

A single colony of transformed DH5α bacteria was used to inoculate 5 ml of LB medium containing ampicillin, and then incubated at 37°C at 225 rpm for 6-8 hours to amplify the plasmid DNA containing bacteria.

2.2.2.4 Purification of plasmid DNA

Plasmid DNA was isolated from DH5α bacteria using Qiagen® plasmid DNA Mini or Maxi Kits. For Miniprep, the starter culture was used directly according to the manufacturer's instructions. For Maxiprep, the starter culture was diluted 1:500 in 250 ml of LB medium with antibiotic and then incubated overnight at 37°C at 225 rpm. Cells were centrifuged at 6000 rpm for 10 minutes at 4°C and plasmid DNA was isolated according to the manufacturer's instruction. In brief, the protocol is based on a modified alkaline lysis procedure, followed by binding of plasmid DNA to resin columns under appropriate low-salt and pH conditions. Impurities are removed by a medium-salt wash.

Plasmid DNA is eluted in a high-salt buffer and then concentrated and desalted by isopropanol precipitation. Isolated plasmid DNA was resuspended in nuclease-free dH_2O and stored at -20°C.

2.2.2.5 Quantification of DNA/RNA

The concentration of plasmid DNA/RNA was determined by spectrophotometry at 260nm using the Nanodrop Spectrophotometer (ND-1000, Medrano Lab). After blanking, 1.5µl of samples was loaded for quantification by measuring absorbance at 260nm, and for an estimate of purity by measuring the 260:280 absorbance ratios. Pure preparations of DNA and RNA have 260:280 ratios of 1.8 – 2.0. Concentrations were calculated on the basis that 50mg/ml of double-strand DNA or 40mg/ml of RNA give an OD260nm of 1.0.

2.2.2.6 Restriction digestion

Restriction digests contained 4U restriction enzyme (New England BioLabs)/µg DNA and the appropriate reaction buffer, and were supplemented with 100µg/ml bovine serum albumin (BSA) if required. Restriction digests were incubated at the appropriate temperature for the restriction enzyme (usually 37°C) for a minimum of 1h.

2.2.2.7 Polymerase chain reaction

Amplification of specific DNA molecules from a DNA template was performed by the polymerase chain reaction (PCR). Routine PCRs reactions contained Taq PCR buffer (Promega), 2.5mM $MgCl_2$, 1U Taq DNA polymerase (Promega), 0.5μM forward and reverse primers, 0.25mM dNTPs and 100ng genomic DNA template and dH_2O in a total volume of 25ul mix. A no template DNA negative control was also prepared. The PCR cycling conditions were as follows: initial DNA denaturation at 94°C for 3 min, then 30-38 cycles of DNA denaturation at 95°C for 60s, primer annealing at 50-65°C for 60s, and DNA polymerase extension at 72°C for 1min/kb PCR product. The primer annealing temperature was based on primer-specific recommendations from the oligonucleotide supplier and empirical observations. After PCR cycling, the PCRs were incubated at 72°C for 10min to extend any remaining incomplete PCR products. PCR products were stored at 4°C before analysis.

2.2.2.8 DNA sequencing

All sequence analysis was performed by the Sequencing Unit at the MRC Human Genetics Unit, Edinburgh and using the BigDye Terminator v3.1 Cycle Sequencing kit (ABI). DNA sequencing reactions contained 2ul BigDye Terminator v3.1, 3.2pmol primer and 50-300ng DNA template in a 10ul volume. The sequencing reactions were performed using the following conditions: initial DNA denaturation at 96°C for 1min, then 25 cycles of DNA denaturation at 96°C for 10s, primer annealing at 50°C for 5s, and extension at 60°C for 4min. The sequenced DNA was then precipitated at room

temperature for 15 minutes by mixing the reaction with 2.5ul of 125mM Na_2EDTA and 30ul of 100 % (v/v) ethanol. After that, DNA fragments were centrifuged at 13000rpm at 4°C for 20 minutes, the solution was removed and precipitated DNA was washed again with 70 % (v/v) ethanol. The ethanol was removed following centrifugation at 7500rpm for 15min and the precipitated DNA was air-dried in the dark at room temperature, and stored at -20°C before sequence analysis.

2.2.2.9 Separation of DNA fragments by electrophoresis

DNA fragments were separated by gel electrophoresis using 1-2% (w/v) agarose in TBE with 0.5mg/ml ethidium bromide for visualization. Loading dye was added to the DNA samples to a final concentration of 20%. DNA Hyperladder I was used to provide size markers with which to compare the band sizes. Electrophoresis was carried out in a horizontal tank, with a TBE buffered system, with a voltage of 75-150V run through the system. UV irradiation was used to visualize the DNA fragments and the gel image captured using Gel Doc EQ software.

2.2.2.10 Purification of DNA from agarose gels

DNA fragments required for cloning were resolved by agarose gel electrophoresis and were purified using the QIAquick gel extraction kit (QIAGEN) according to the manufacturer's instructions. In brief, an agarose gel piece containing the DNA fragment was cut out and dissolved. After that the DNA fragment was bound to resin. Impurities

were removed by a medium-salt wash and the DNA fragment was eluted in a high-salt buffer.

2.2.2.11 5' RACE assay

Characterisation of the 5' end of the Ercc1 cDNA was performed using the 2nd Generation 5'/3' RACE Kit (Roche) following the manufacturer's protocol (Figure 2.1). Ercc1 specific primers were used in the procedure with all other reagents supplied by the manufacturer. The NEO RNA from the kit was used as a control for the assay. The first strand of cDNA was synthesised from total RNA using an Ercc1-specific primer Ex2b rev with reverse transcriptase and deoxynucleotides. The resultant cDNA was then purified using High Pure PCR Product Purification Kit (Roche) to remove the unincorporated primers and deoxynucleotides. A homopolymeric A-tail was added to the 3' end of the cDNA using terminal transferase. The tailed cDNA was then amplified by PCR using a second Ercc1-specific primer Skin RT rev C and oligo dT-anchor primer. Thic cDNA was amplified with a further round of nested PCR using internal primers Skin RT rev B and PCR-anchor and then cloned into the p-GEM T-EASY vector for sequencing analysis.

Figure 2.1 Flowchart of 5' RACE analysis

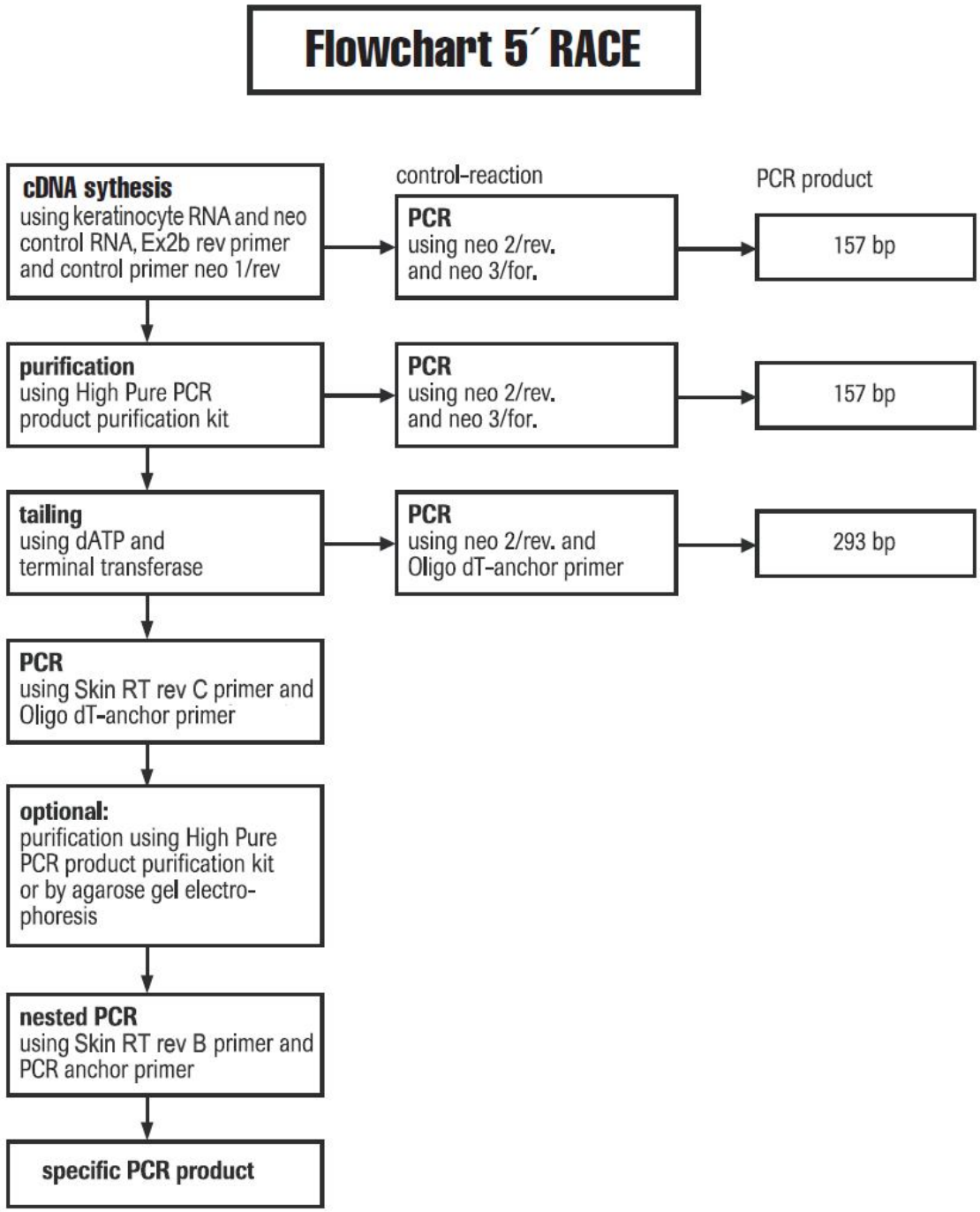

2.2.2.12 Preparation of RNA

Total RNA was extracted from cultured mammalian cells using RNAzol^{TM}B. Cultured cells in 100mm culture dishes were lysed directly by the addition of 5ml of RNAzol^{TM}B. The RNA was solubilised by pipetting the lysate several times and extracted by the addition of 1ml of chloroform followed by vigorous shaking of the mixture for 30 seconds. The mixture was then centrifuged at 12000g for 15 minutes at 4^{o}C and the aqueous phase was transferred to a fresh tube and an equal volume of isopropanol was added. RNA was allowed to precipitate at room temperature for 10 minutes and then pelleted by centrifugation at 12000g for 5 minutes, then washed in 70% ethanol and centrifuged at 7500g for 5 minutes. The pellet was air-dried at room temperature before being resuspended in 50µl of RNase-free dH_2O for storage at -70^{o}C.

2.2.2.13 Electrophoresis of RNA in agarose gels

The separation of RNA on the basis of molecular weight was achieved by the electrophoresis of RNA denatured in a formaldehyde-formamide sample buffer in denaturing agarose gels. RNA samples were electrophoresed on denaturing 1.4% (w/v) agarose gels containing 0.5µg/ml ethidium bromide, 1X MOPS and 0.66M formaldehyde. 20µg of total RNA in 20µl of sterile distilled water was added to an equal volume of formamide sample buffer and ¼ volume of 5X sample buffer. Samples were heated for 5 minutes at 65^{o}C and snap chilled on ice immediately prior to loading. Electrophoresis was carried out in a 1X MOPS buffer system at 100V for 3-4 hours.

2.2.2.14 Randomly primed labelling method (Northern Blotting)

The mouse Ercc1 mRNA was detected by northern blot using an Ercc1 cDNA probe (Selfridge et al. 2001). Radioactively labelled DNA was obtained using a randomly primed DNA labelling method, which is based on the hybridisation of a mixture of many different nonamer nucleotides to the DNA which allows small amounts of DNA to be labelled to high specific activities. The complementary strand is synthesised from the 3'OH termini of the primer using Klenow polymerase, simultaneously incorporating radiolabelled dCTP into the newly synthesised DNA strand. Approximately 10ng of DNA was dissolved in 28µl of dH_2O and denatured by boiling for 5 minutes. 10µl of labelling buffer, 50µCi of α-^{32}PdCTP and 2 units of Klenow polymerase were then added and incubated at 37^{o}C for 15 minutes.

2.2.2.15 Separation of unincorporated radionucleotides (Northern Blotting)

Unincorporated nucleotides were separated from the labelled DNA by chromatography on a NICK R Column (Pharmacia). The labelling reaction was added to TE equilibrated column, then 400µl of TE was added and the labelled DNA was eluted by the addition of a further 400µl TE.

2.2.2.16 Hybridisation (Northern Blotting)

Membranes onto which RNA had been transferred were blocked by prehybridising in 30ml of 6X SSC, 1% (wt/v) SDS and 10% (wt/v) dextran sulphate with 3.5mg of denatured sonicated herring sperm DNA for two hours at 60°C in a hybridisation bottle. Hybridisation was then performed by addition of denatured radiolabelled probe to the prehybridisation mixture, and further incubated at 60°C for 12 to 24 hours. After the hybridisation, non-specifically RNA bound molecules were removed by immersing the membrane in 2X SSC at room temperature for 5min with agitation, and then twice in 2X SSC, 1% (wt/v) SDS for 30min at 60°C. Finally the membrane was rinsed in 0.1X SSC for 10min before being sealed in a plastic bag, and then visualised by phosphorimager (Molecular Dynamics). Signals were analysed with ImageQuant TL software (GE Healthcare Life Science).

2.2.2.17 Reverse transcription of RNA

Total RNA samples were treated with DNase 1 to ensure removal of contaminating DNA using a DNA-free Kit (Ambion) prior to reverse transcription. cDNA was prepared from RNA using the Retroscript Kit (Ambion) following manufacturer's instructions. In brief, 2µg of total RNA was mixed with 2µl of random decamers, mixed and then denatured at 70^{o}C for 3 minutes. 2µl 10 x RT buffer, 4µl dNTPs, 1µl RNase inhibitor, and 1µl reverse transcriptase enzyme were then added, incubated at 42^{o}C for 1 hour and then heated to 92^{o}C for 10 minutes to inactivate the RT.

2.2.3 Protein Detection

2.2.3.1 Protein quantification

Protein concentrations were determined using the BCA™ Assay Kit (Pierce) in a 96-well plate. Protein samples were diluted 10-fold in dH_2O to a total volume of 25ul. dH_2O was used as a blank control. After 200ul of working reagent was added to each sample and incubated at 37°C for 30min, the protein concentration was determined at 562 nm using a plate Spectrophotometer (MRX, Dynatech). Concentrations of samples were calculated using the standard curve generated from the known BSA standards and were adjusted by the dilution factor.

2.2.3.2 Immunoprecipitation

Immunoprecipitation of protein was performed using the Protein G Immunoprecipitation Kit (Roche Applied Science). 50ul of the homogeneous protein G-agarose beads (25ul bed volume) was add to 1ml of protein samples and incubated for at least 3 h or overnight at 4°C on a rocking platform prior to the immunoprecipitation to reduce background caused by non-specific adsorption of irrelevant cellular proteins. Beads were pelleted by centrifugation at 12,000 × g for 20 s in a microfuge. Supernatants were transferred to fresh tubes and incubated with an appropriate amount of the specific antibody for 1 h at 4°C with gently rocking. After that 50ul of the homogeneous protein G-beads were added to the mixture and incubated for at least 3 h or overnight at 4°C on a rocking platform. Beads were collected by centrifugation at 12,000 × g for 20 s and washed with 1 ml of wash buffer according to the manufacturer's instructions. Following

the removal of the wash buffer, the immunoprecipitated proteins were heated at 95-100°C for 5 minutes in sample buffer to denature the protein and separate it from the protein G beads before analysis by western blotting.

2.2.3.3 SDS polyacrylamide gel electrophoresis (SDS-PAGE)

The separation of proteins on the basis of their molecular weight was achieved by discontinuous SDS-PAGE. SDS-PAGE at appropriate polyacrylamide concentrations was prepared using a Mini-PROTEAN3 electrophoresis system (Bio-Rad). Concentration of polyacrylamide in the resolving gel was determined by the molecular weight of the protein tested. Proteins with molecular weight from 30kDa to 200kDa were separated by 10% to 12% resolving gel (10% - 12% Acrylamide, 390 mM Tris-HCl pH 8.8, 0.1 % SDS, 0.1 % APS, polymerisation was initiated by adding 0.08 % TEMED). The resolving gel was overlaid with isopropanol to remove air bubbles and flatten the top surface before being left to polymerise at room temperature. After that isopropanol was removed and the stacking gel (5 % Acrylamide, 123 mM Tris-HCl pH6.8, 0.1 % SDS, 0.1 % APS, 0.1 % TEMED) was added with either a 10-well or 15-well comb. After the stacking gel was set, the comb was removed and the gel cassette was assembled with the Mini-PROTEAN3^{TM} electrophoresis module and immersed in running buffer (192mM Glycine, 25 mM Tris, 0.1 % (w/v) SDS). Appropriate amounts of protein samples were prepared with 5X SDS sample buffer and were heated at 95°C for 5 minutes before loading onto the gel with 12ul of the Prestained Protein Ladder (Invitrogen). Protein samples were separated by electrophoresis in running buffer at 80V for the stacking gel and 150 V for the resolving gel.

2.2.3.4 Western immunoblotting

Following the SDS-PAGE, the resolved proteins were transferred electrophoretically to a methanol rinsed Immobilon-P PVDF transfer membrane (Millipore, Billerica, Massachusetts) with transfer buffer according to the method of Towbin (Towbin et al. 1979). The transfer was completed by using a Mini Trans-Blot system (Biorad) at 100V, constant voltage at 4^{o}C with an ice block for 1 hour, or at 20mA, constant current at 4^{o}C overnight. After the transfer, the membrane was rinsed in TBS/T for 5 minutes before the filter was blocked with 5 % (w/v) dried skimmed milk diluted in TBS/T for 1 hour. The membrane was then incubated with the primary antibody diluted in 5 % (w/v) milk-TBS/T for 1 hour at room temperature or overnight at 4°C, washed with TBS/T three times 10 minutes each at room temperature, and incubated with the appropriate diluted secondary antibody diluted in 5 % (w/v) milk-TBS/T for 1 hour at room temperature. Unbound antibodies were removed with three 10 minutes washes in TBS/T. The membrane was then overlaid with enhanced chemiluminescence solution (ECL) or ECL-Plus (Amersham Biosciences, Buckinghamshire, UK) for 1 minute. Excess ECL solution was drained before membranes were exposed to Hyperfilm™ ECL (Amersham Biosciences).

2.2.3.5 Fluorescent ECL plus western blot detection with Storm image analysis system

For accurate quantitative analysis of western blotting results, fluorescent ECL plus western blot detection with the Storm 840 phosphorimager (Molecular Dynamics) was performed. Following SDS-PAGE and protein transfer, the PVDF membrane was

incubated in ECL Plus detection reagent for 5 min. Excess reagent was drained and the wet membrane was placed in an open, low-fluorescence plastic hybridization bag. The membrane was covered slowly to avoid trapping air bubbles. The membrane was scanned using the Blue Fluorescence/Chemifluorescence scan mode of Storm model 840 with a PMT voltage setting of between 650 and 800 V. The intensities of bands on the western blot were measured and analysed using the ImageQuant TL software (GE healthcare life science).

2.2.3.6 Stripping nitrocellulose membranes

Membranes were stripped to remove primary and secondary antibodies from the membrane before they were re-probed with additional antibodies. The membrane was incubated with pre-warmed 100ml of stripping buffer in a tightly sealed plastic box for up to 45 minutes at 50°C. The membrane was then rinsed under a running water tap for 1-2 hours and treated for 1min of methanol rehydration before the blocking stage.

2.2.3.7 Coomassie Brilliant Blue staining

Resolving gels were washed 3 times in water, for 5 minutes each time with agitation. After that, water was replaced with EZblue stain reagent. Gels were incubated in the stain reagent for 1 hour with agitation, and then washed with water for 1 hour or overnight until the protein bands became visible and the gel background was clear. Stained gels were dried onto a 3 mm Whatman paper using a gel-dryer.

Chapter 3:

Characterization of ERCC1 protein expression in mouse cells and tissues

3.1 Introduction

This chapter addresses the investigation of ERCC1 protein expression in mouse keratinocytes and tissues.

The nucleotide excision repair (NER) pathway has evolved primarily to repair UV-induced DNA damage and is also active against a broad range of endogenously generated oxidative lesions (de Boer and Hoeijmakers 2000). NER consists of two subpathways in mammals, global genome repair (GGR) and transcription-coupled repair (TCR), according to the initial recognition stage. GGR can remove DNA lesions throughout the genome, while TCR mainly deals with lesions in the transcribed strand of actively transcribed genes (Leadon and Lawrence 1991; Lombard et al. 2005). The NER pathway involves about 30 distinct proteins. ERCC1 is essential for NER where it acts in a complex with XPF protein to make the incision 5' to the DNA lesion (Newman et al. 2005). In the NER pathway, the TFIIH complex, including XPB and XPD is recruited to the damage site to unwind the DNA helix (de Laat et al. 1999). After that, XPG and XPF/ERCC1 access the damaged site to make the dual incision. XPG cuts on the 3' side while XPF-ERCC1 makes the 5' side incision (Mu et al. 1996; de Laat et al. 1999). Once the oligonucleotide containing the lesion has been removed, the gap is filled by two polymerases, using the intact strand as a template. The ends are then joined by DNA ligase.

Because skin receives the greatest exposure to UV it is reasonable to expect that the expression of NER proteins may display different properties in the skin in an attempt to deal with a more demanding role in that tissue. As described in the Introduction chapter, we have identified the skin-specific 1.5kb Ercc1 mRNA as the major transcript in skin in terms of abundance. This novel Ercc1 transcript was found at much higher levels in albino mouse strains than in pigmented strains leading to the hypothesis that this may be

a mechanism to enhance the level of repair in albino mouse skin which would not be protected against UV-induced DNA damage by melanin pigment. One of the main aims of this chapter was to investigate this hypothesis.

3.2 Optimization of western blotting and selection of appropriate antibodies for ERCC1 and loading controls in cells and tissues

Before investigating the level of ERCC1, we first tested several anti-ERCC1 antibodies against mouse and human ERCC1 protein. The commercial antibodies SC-17809, SC-10157 and FL-297 were obtained from Santa Cruz biotech. The R540 is an "in house" ERCC1 antibody used previously for ERCC1 detection on mouse tissues by our group. According to the manufacturer's datasheet, antibodies SC-17809 and FL-297 could detect the ERCC1 protein in both mouse and human species while SC-10157 could only react against the mouse ERCC1.

The western blotting results using the optimal primary and secondary antibody dilutions are shown in Figure 3.1. We first tested all antibodies using a cell panel of ERCC1 wild-type and deficient mouse embryonic fibroblasts, named PF20 and PF24 respectively. SC-17809, SC-10157 and R540 all detected a band at the expected position of 33kDa in the PF20 lane that was missing in the PF24 lane (Figure 3.1.A). All three antibodies picked up one or more cross-reacting bands in both PF20 and PF24 lanes in western blotting analysis. Antibody SC-17809 mainly cross-reacted with a protein at the molecular weight of 30kDa, while antibody SC-10157 only cross-reacted with one protein at about 40kDa. The home-made antibody R540 cross-reacted with several

proteins and generated a dirty background in western blotting. The crossing-reacting band detected by SC-17809 was very close to the target band of ERCC1 and was much stronger than the ERCC1 band in terms of abundance. Thus, the antibody SC-10157 was chosen for western blotting of mouse samples.

An investigation of the cross-reacting band generated by SC-10157 was performed to identify whether the cross-reactivity was specific (ie. ERCC1-related) or not. This is described later in this chapter.

For ERCC1 detection in human samples, similar antibody selection was performed. Three human melanoma cell lines G361, WM115 and A375 were used in this investigation. Figure 3.1.B showed that the antibody SC-17809 could detect the target ERCC1 protein (35kDa) but also detected a cross-reacting protein underneath the main ERCC1 band. Because the molecular weight of human ERCC1 is 2kDa larger than mouse ERCC1, the separation between human ERCC1 and this cross-reacting band was much better. Whole cell protein lysate of mouse ERCC1 deficient keratinocyte cells was used in this western blotting as a negative control because no human ERCC1 deficient cells were available in the lab. The membrane was then probed with anti-beta-tubulin as a loading control. FL-297 also gave a clean result in western blotting of human samples. FL-297 normally generated a higher background compared to SC-17809. However after a higher dilution of the primary antibody plus extensive washing with TBS-T, the dirty background could be removed. Figure 3.1.C shows a western blotting result using optimized conditions for FL-297. Only the target human ERCC1 protein was detected at the expected position of 35kDa. Note that in Figure 3.1.C the loading may not be matched as neither the BCA assay nor a loading control re-probing was performed in this western blot. The SC-17809 antibody was selected for routine western blotting

Figure 3.1: Tests of different ERCC1 antibodies for detection of mouse and human ERCC1 by western blotting.

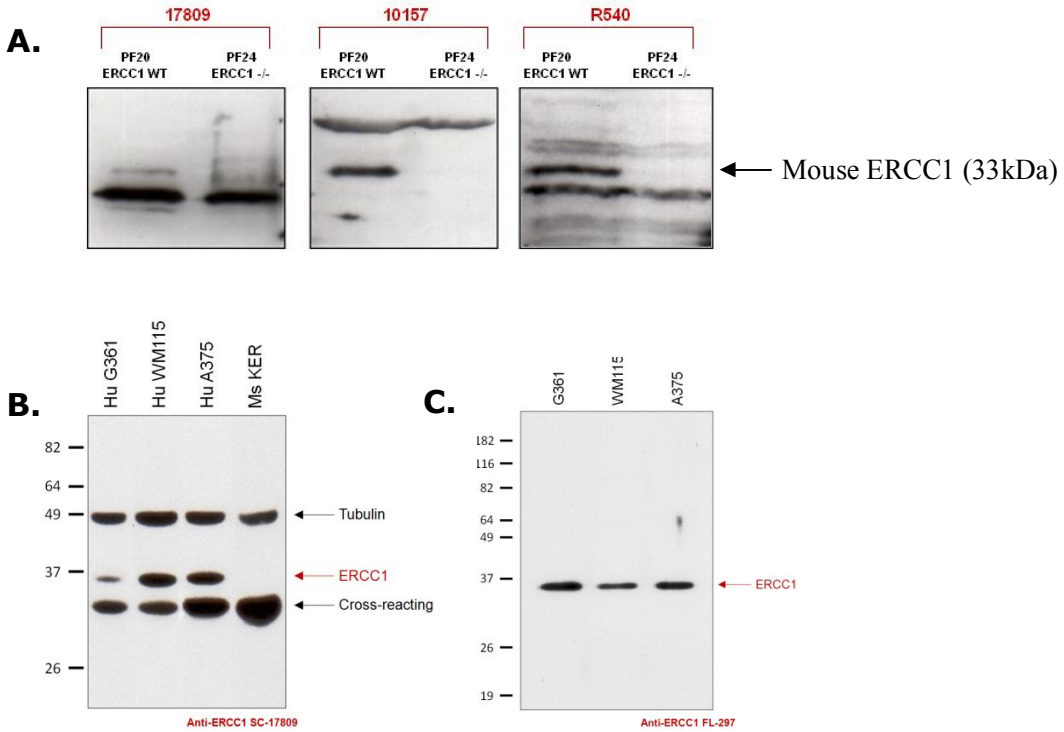

A. Western blotting on mouse embryonic fibroblast cell lines PF20 (ERCC1 wild-type) and PF24 (ERCC1 deficient) using different antibodies against ERCC1. SC-17809 and SC-10157 are the commercial antibodies from Santa Cruz biotech, R540 is the "in house" antibody used for previous investigations.

B. Western blotting using anti-ERCC1 antibody SC-10789 on human melanoma cell lines G361, WM115 and A375. Human ERCC1 bands at the position of 35kDa are indicated with red arrows. Cross-reacting bands and loading control band of beta-tubulin are indicated with black arrows. Mouse ERCC1 deficient keratinocyte cell line was used as a negative control in this panel. Protein ladders are labelled to the left of the membrane.

C. Western blotting using anti-ERCC1 antibody FL-297 on human melanoma cells lines G361, WM115 and A375. The identical ERCC1 bands are indicated with red arrows. Protein ladders are labelled to the left of the membrane.

analysis of human samples. The FL-297 could be ideal for immunohistochemistry applications.

To measure the ERCC1 protein level quantitatively, good loading controls are essential to make sure the samples are equally loaded. Several loading control antibodies were tested for quantitative western blotting analysis. There were three important points for selecting a good loading control in this investigation. First, the loading control antibody should be specific and able to produce a clean western blotting result. Thus, most of the popular loading control antibodies raised in mouse cannot be used for western blotting on mouse samples, especially on mouse tissues due to secondary antibody cross-reactivity with mouse immunoglobulins. Second, the band generated by the loading control antibodies should be as far as possible from the target ERCC1 band and cross-reacting bands. Good separation is required to measure the intensity of different bands using the phosphorimager. Finally, levels of the ideal loading control protein should be independent of the biological status of the cell or tissue. For example, changing the culture conditions could potentially induce proliferation. As a result, a commonly used loading control such as PCNA would not be suitable for such an investigation.

Beta-actin, beta-tubulin, TBP-like protein, GAPDH and PCNA were tested in western blotting using mouse cells and tissue and human cells. Beta-actin was not suitable for western blotting on mouse samples because most beta-actin antibodies were raised in mouse. However the beta-actin antibody could be used for loading control determination on human samples.

Anti-GAPDH is a mouse antibody which detects a band at the position of 37kDa. It was not ideal to use the GAPDH on mouse and human samples in conjunction with ERCC1

detection because the GAPDH band would be too close to the ERCC1 band at 33kDa to 35kDa. With human samples, GAPDH detected only one band of GAPDH specifically, thus it was reasonable to use the GAPDH loading control for quantitative detections of proteins of different molecular weight. For example, GAPDH could be used for XPF, MSH2, MSH6 and MLH1 quantitative measurements, which were part of our investigation of DNA repair in human melanoma and ovarian tumour cells in Chapter 5.

The loading control antibody beta-tubulin from abcam was finally selected for the quantitative measurement of ERCC1 protein by western blotting. Firstly, this antibody detected a single clean band at 50kDa representing beta-tubulin with very low background. Secondly, because it was a rabbit polyclonal antibody, there was no problem of cross-reacting with mouse or human immunoglobulin. Thirdly, the position of the band at 50kDa was far away from the ERCC1 band and cross-reacting bands. It was also well-separated from other DNA repair proteins in our investigation. Figure 3.2 shows the result of using the beta-tubulin loading control in different investigations. In the Figure 3.2.A, B and C, whole protein lysate of two mouse keratinocyte cell lines, two mouse melanocyte cell lines and two mouse skin samples were separated by SDS-PAGE and then probed with the antibody SC-10157 against mouse ERCC1. After that the filters were re-probed with the loading control beta-tubulin antibody. The three bands, beta-tubulin, cross-reacting and mouse ERCC1 from the top to the bottom as indicated on the membrane were separated well enough for the next step of phosphorimager scanning. In the Figure 3.2.D, whole cell protein lysate of two human melanoma cell lines, A375 and WM115, were probed with the antibody SC-17809 against human ERCC1. As indicated on the figure, human ERCC1 and a cross-reacting band were detected at their expected position. Then the membrane was probed with beta-tubulin. The clear band detected by beta-tubulin was specific and identical in both lanes and also well separated from other bands.

Figure 3.2: Tests of loading control antibody anti-beta-tubulin in different applications by western blotting analysis

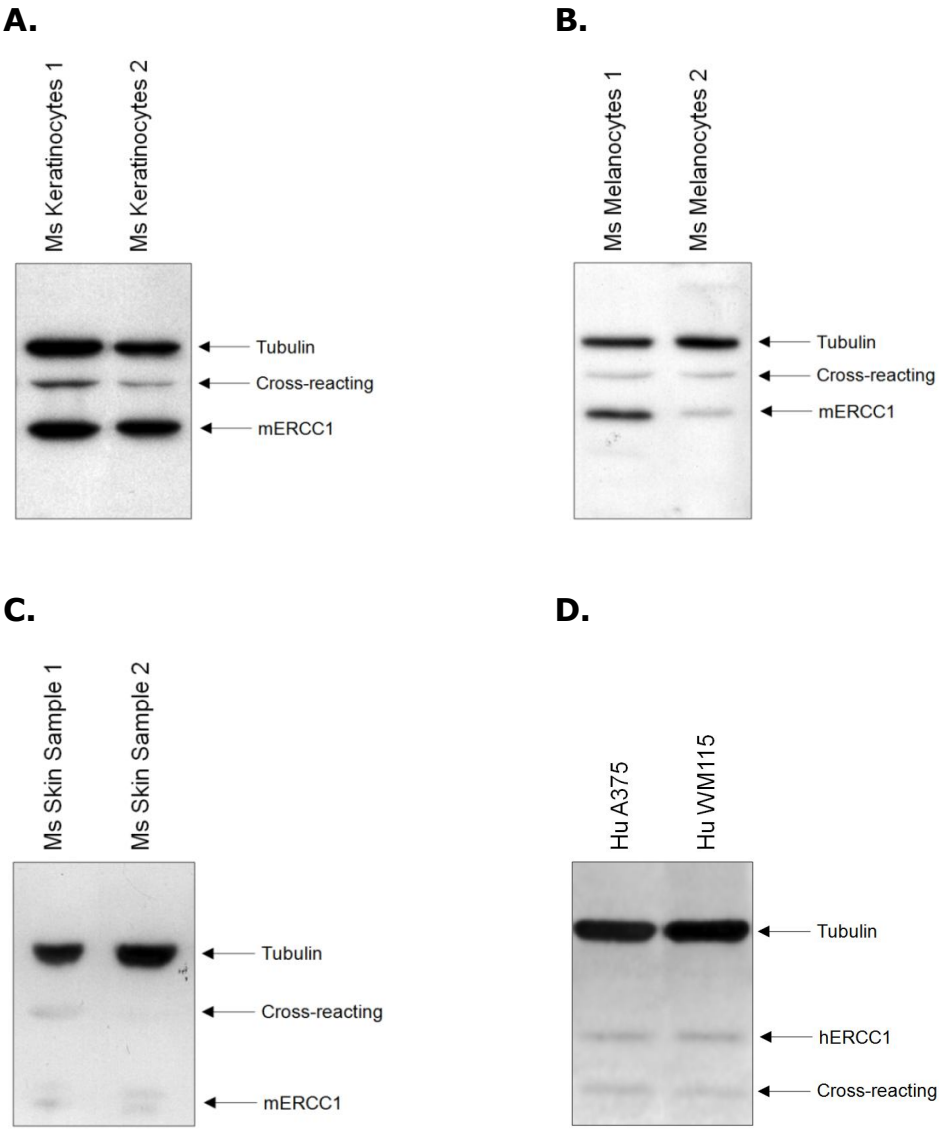

Whole cell protein lysates were separated by SDS-PAGE and transferred to PVDF membranes for probing. Membranes were blocked and then probed with anti-ERCC1 antibody SC-10157 (mouse) or SC-17809 (human). After that membranes were reprobed with the loading control antibody against beta-tubulin.

A. Western blotting of mouse keratinocytes. **B.** Western blotting of mouse melanocytes. **C.** Western blotting of mouse skin samples. **D.** Western blotting of human melanoma cells A375 and WM115.

To determine if the cross-reacting band detected by the anti-ERCC1 antibody SC-10157 in mouse samples was specific or not, an immunizing peptide blocking experiment was performed. The primary antibody SC-10157 was neutralized by pre-incubation with its blocking peptide at different concentrations for 1 hour before being applied to the membrane for detection. By doing this neutralization, the antibody that was bound to the blocking peptide should no longer bind to the epitope present in the target protein on the western blotting analysis. The neutralized SC-10157 antibody was then used side-by-side with the normal untreated SC-10157 antibody, and the results were compared. By comparing bands from the blocked antibody versus the untreated antibody, the specificity of the antibody recognition could be determined: specifically-recognized bands would be absent from the western blot performed with the neutralized antibody.

Without neutralization by the blocking peptide, the SC-10157 antibody detected both ERCC1 and the cross-reacting protein. The cross-reacting bands were slightly stronger compared to ERCC1 bands in terms of the intensity. Once the SC-10157 antibody was neutralized by 0.0001ng/ml of blocking peptide, ERCC1 bands were only barely detectable. The intensity of cross-reacting bands was only slightly reduced by SC-10157 antibody neutralization. The membrane strips were then probed with the loading control beta-tubulin to make sure the loading was matched (Figure 3.3). The neutralization of SC-10157 prevented recognition of ERCC1 more efficiently than it prevented recognition of the cross-reacting protein, supporting the conclusion that the detection of the cross-reacting protein with anti-ERCC1 SC-10157 resulted from a non-specific interaction.

Figure 3.3 Investigation of the specificity of binding of the SC-10157 antibody to the cross-reacting band by western blotting using mouse samples

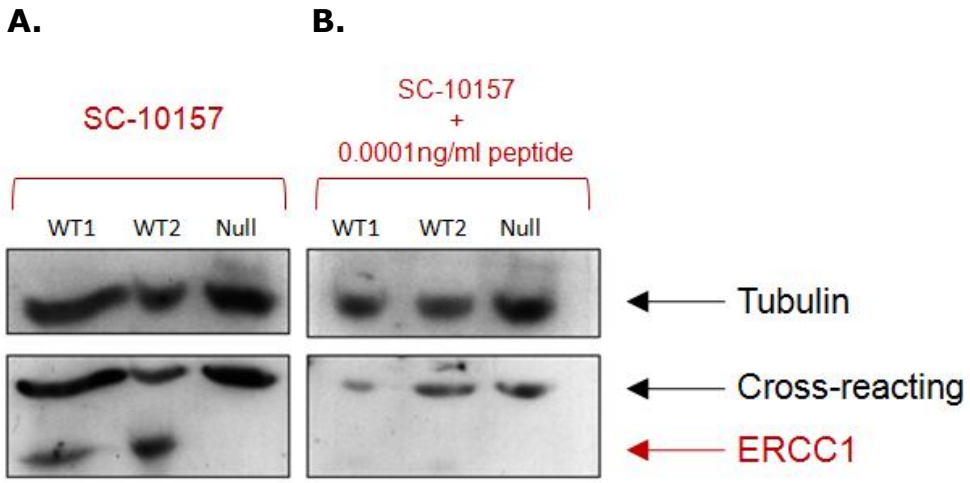

Mouse skin protein lysates were separated by SDS-PAGE and transferred to the membrane, then blocked with 5% milk in TBS-T buffer. Duplicates of the blocked membrane strips were then probed with untreated anti-ERCC1 antibody SC-10157 on its own or anti-ERCC1 SC-10157 neutralized by blocking peptide. Membrane strips were then probed with secondary antibody and protein bands were visualized by ECL-PLUS on film. After that, strips were washed and then re-probed with loading control beta-tubulin.

A. Western blotting using anti-ERCC1 SC-10157 alone.

B. Western blotting using neutralized anti-ERCC1 SC-10157 by pre-incubation with 0.0001ng/ml blocking peptide.

3.3 Western blotting of ERCC1 WT and knockout samples of mouse embryonic fibroblasts, keratinocytes, melanocytes and skin tissues

Having optimized conditions for western blotting analysis, we then tested all of our stock cells and animals. As shown in the Figure 3.4, a panel of whole protein lysates of ERCC1 wild-type and deficient mouse keratinocyte cells (KER WT and NULL), embryonic fibroblast cells (PF20 and PF24), skin samples (SKIN WT and SKIN NULL) and mouse melanocyte cells (Melanocyte ERCC1 WT and Melanocyte ERCC1 NULL), and also a human melanoma cell line A375 were separated by SDS-PAGE and then transferred to the PVDF membrane for ERCC1 detection.

The anti-ERCC1 antibody SC-10157 detected the expected mouse ERCC1 bands in the ERCC1 wild-type tracks at the position of 33kDa. A single clear band was detected by the SC-10157 in the human melanoma cell line A375 track as well at the position of 35kDa. In lanes of ERCC1 deficient samples, there was no ERCC1 band detected. A cross-reacting band at about 40kDa was detected in every mouse sample lane. There was a second higher cross-reacting band at about 80kDa in the ERCC1 deficient mouse melanocyte lane. This band had appeared randomly before in mouse samples by western blotting detection using anti-ERCC1 SC-10157, but the frequency was very low. Loading control GAPDH indicated that the loading was equally matched.

The western blotting demonstrated that we could detect ERCC1 protein expression in wild-type mouse keratinocytes, embryonic fibroblasts, melanocytes and mouse skin and confirmed the expected ERCC1 deficiencies in the corresponding ERCC1 knockout samples.

Figure 3.4 ERCC1 protein expression pattern in our ERCC1 wild-type and deficient cells and animals by western blotting

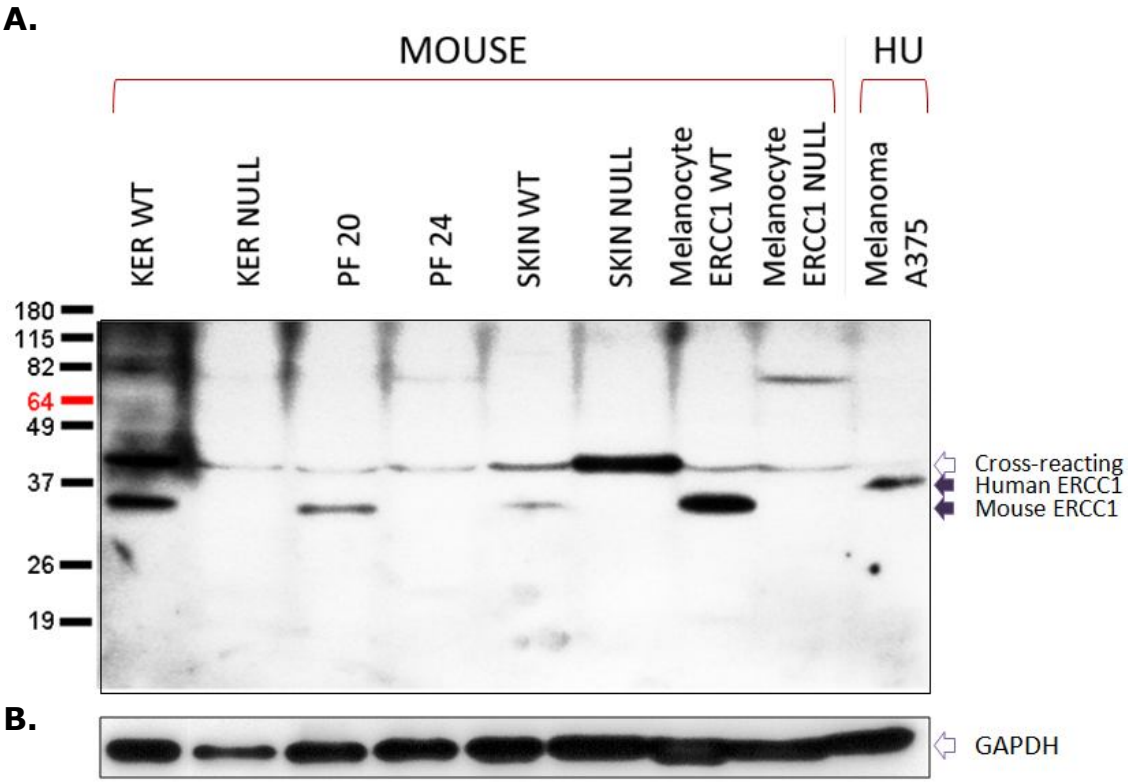

A. Western blotting assay using panel of ERCC1 wild-type and ERCC1 null mouse keratinocytes, fibroblasts, skin samples, melanocytes and ERCC1 wild-type human melanoma cell line A375. The anti-ERCC1 antibody SC-10157 detected bands, indicated as Mouse ERCC1, at the expected molecular weight of 33kDa in ERCC1 wild-type samples but not in ERCC1 deficient samples. An expected band at 35kDa in human melanoma cell line A375 is labelled as Human ERCC1. Cross-reacting bands at 42kDa in all tested protein samples are labelled as Cross-reacting.

B. Filter re-probed with loading control GAPDH to show the total protein loaded in each lane.

3.4 ERCC1 protein levels were consistent with Ercc1 mRNA levels in various mouse tissues except skin

A panel of tissues from a wild-type Balb/C adult male mouse was analysed previously by northern blot using an Ercc1 cDNA probe by Dr. Jim Selfridge (unpublished observations). The normal 1.1 kb Ercc1 transcript as identified in human, was evident in all tissues examined (Figure 3.5.A). The level of expression of this transcript was lowest in the liver and generally low in all other tissues except for the testis, where the level of expression of this transcript was much higher than elsewhere. The pattern of expression seen in the skin was clearly different from any other tissue. In addition to the normal Ercc1 transcript, a second larger transcript of 1.5kb was evident. In terms of abundance the novel Ercc1 transcript was the major transcript in skin. Since skin receives the greatest exposure to UV, it might require more DNA repair capability. Thus we hypothesized that the skin-specific 1.5kb Ercc1 transcript might have a special biological function to help skin deal with the increased DNA lesions and the expression of NER proteins may display different properties in the skin to deal with a more demanding repair role.

Based on the northern blotting result, we performed a western blotting using the same panel of tissues, but from 4 different mouse strains. The Balb/C and CD1 strains were albino while the 129/Ola and C57BL/6 strains were pigmented.

Because this western blotting involved several different tissues, it was difficult to use a loading control antibody to check the matched loading because we found that protein expression levels of loading controls varied significantly between different tissues from the same mouse. Instead of using a loading control antibody, we stained the transferred

membrane with ink as a control to check the general loading levels. As shown in the Figure 3.5.C, the ink control indicated that the loading of each lane was generally matched, despite the presence of some highly-expressed and tissue-specific bands. Beside the ink control, a duplicate of the SDS-PAGE gel with the same loading of protein samples was stained with coomassie blue. The coomassie blue staining results were the same as the ink control (data not shown). The expression of ERCC1 protein was detected by anti-ERCC1 antibody SC-10157 (Figure 3.5.B).

First, it is evident that the size of the ERCC1 protein is the same in skin as in other tissues examined (33kDa). This suggests that differential transcription in skin has no effect on the size of the ERCC1 protein product. This result agrees with a previous western blotting analysis using a Balb/C tissue panel probed with a different home-made R540 anti-ERCC1 antibody for ERCC1 detection (Andrew Winter, unpublished). The result is also in agreement with a previous RT-PCR assay using primers in exon2 to exon10, which suggested that the coding region of the skin-specific Ercc1 transcript was no different to that in the normal Ercc1 transcript (Andrew Winter, unpublished).

Second, all strains examined showed a similar tissue pattern of ERCC1 protein level, which matched the tissue pattern of Ercc1 transcript. The level of ERCC1 was highest in testis, followed by brain. Skin and kidney showed a lower level than testis and brain. Liver had the lowest level of ERCC1. The duplicated ERCC1 bands in the 129 strain panel might be due to some degradation of protein samples. The protein level of ERCC1 was not elevated in skin compared to other tissues, suggesting that the novel 1.5kb skin-specific Ercc1 transcript was not acting to boost the protein expression under normal conditions.

Figure 3.5 Ercc1 mRNA and ERCC1 protein expression pattern in different mouse tissues.

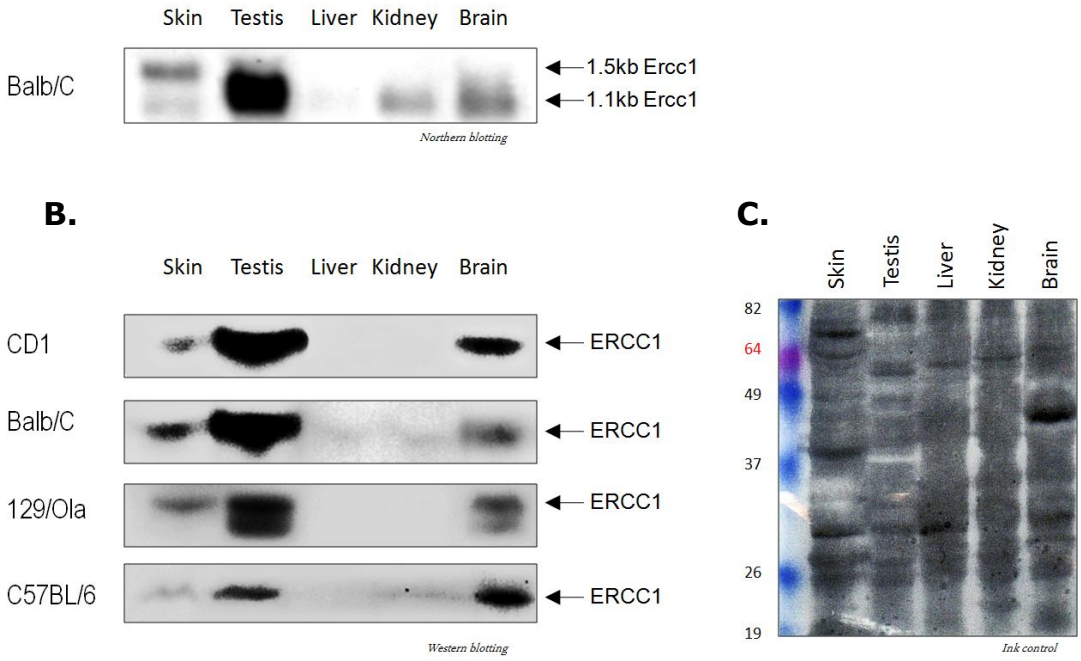

A. Northern blotting analysis using a panel of wild-type mouse tissues from strain Balb/C. The normal 1.1kb Ercc1 transcript and novel 1.5kb skin-specific Ercc1 transcript are indicated by arrows on the right side.

B. Western blotting using the same mouse tissue panel. The ERCC1 protein expression in different tissues was also tested in 3 other mouse strains CD1, 129/Ola and C57BL/6 as indicated on the left.

C. Due to the difficulty of using a loading control for different tissues, the western blotting filters were inked before probing to determine whether the loading was matched. The ink control of the C57BL/6 western blotting filter stain indicated that the loading was generally well-matched. The ink control of other western blotting filters showed the same results.

Northern blotting for Ercc1 was carried out by a previous group study on RNA extracted from the skin of adult mice of inbred albino strains Balb/c, FVB, MF1, the outbred albino strains, MF1 and CD1, and the inbred pigmented strains C57Bl/6, DBA/2, CBA/Ca and 129/Ola (Figure 3.6.A) (Andrew Winter, unpublished). These results show that every pigmented strain had barely detectable levels of the novel transcript originally observed in BALB/c mice. However, the novel transcript was seen in two other strains of albino mice, CD1 and MF1. The albino strain FVB was the only albino strain to have the same expression pattern as pigmented mice. Because the albino strains did not have pigment in their skin, they are at great risk of UV-induced DNA damage, so we hypothesized that the 1.5kb novel Ercc1 transcript may help the albino strains to deal with the DNA damage in skin.

To investigate whether this novel transcript could indeed induce a different protein expression of ERCC1 in skin, a western blotting using different skin samples from albino and pigmented strains was performed. CD1 and Balb/C strains were chosen from the albino strains while C57Bl/6 and 129/Ola strains were chosen from the pigmented strains. Two to three pieces of back skin samples were cut from each animal. Four mice were used for CD1 and C57Bl/6 strains while three mice were used for Balb/C and 129/Ola. The protein level in ERCC1 of all samples was detected by western blotting using antibody SC-10157 using the phosphorimager system. Membranes were re-probed with loading control beta-tubulin and scanned by the phosphorimager system as well. The quantified protein level of ERCC1 was then standardized by the level of loading control beta-tubulin (Figure 3.6.B).

The Balb/C strain showed the lowest level of ERCC1 protein in skin. The CD1 and C57 strains had a similar level of ERCC1, which was slightly higher compared to Balb/C. The 129 strain showed the highest level of ERCC1, double that in Balb/C (Figure 3.6.C).

When the results for CD1 and Balb/C strains were plotted together (albino group) and compared to C57BL/6 and 129/Ola strains plotted together (pigmented group) the ERCC1 protein levels were much more similar. The level of ERCC1 was slightly lower in the albino group, but the difference was not statistically significant ($p=0.085$ by Mann-Whitney U test). Thus, we found no support for our hypothesis that the 1.5kb skin-specific Ercc1 transcript might result in increased ERCC1 protein level in the skin of albino strains.

3.5 Stress treatment induced changes in levels of ERCC1 in mouse keratinocytes

Previous group work had found no increase in levels of the 1.5kb skin-specific Ercc1 mRNA in mouse skin after UV irradiation (Andrew Winter, unpublished observation). Although we had found no evidence that ERCC1 protein levels were affected by the level of the 1.5kb skin-specific Ercc1 transcript under normal conditions, we wished to explore the possibility that ERCC1 protein levels may change in skin in response to UV-irradiation or other stresses. These experiments were most conveniently carried out in cultured keratinocytes, rather than in mouse skin.

As another NER protein, XPC, was reported be modified by SUMO-1 and ubiquitin following UV irradiation (Wang et al. 2005), we investigated whether the level of ERCC1 protein might be post-translationally regulated. Initially a simple preliminary experiment was carried out on mouse keratinocyte cells following treatment with the proteasome inhibitor MG132. Proteasomes are large protein complexes that degrade unneeded or damaged proteins in cells. MG-132 is a potent, cell permeable, and

Figure 3.6 The Ercc1 mRNA and ERCC1 protein expression pattern between albino and pigmented mouse strains

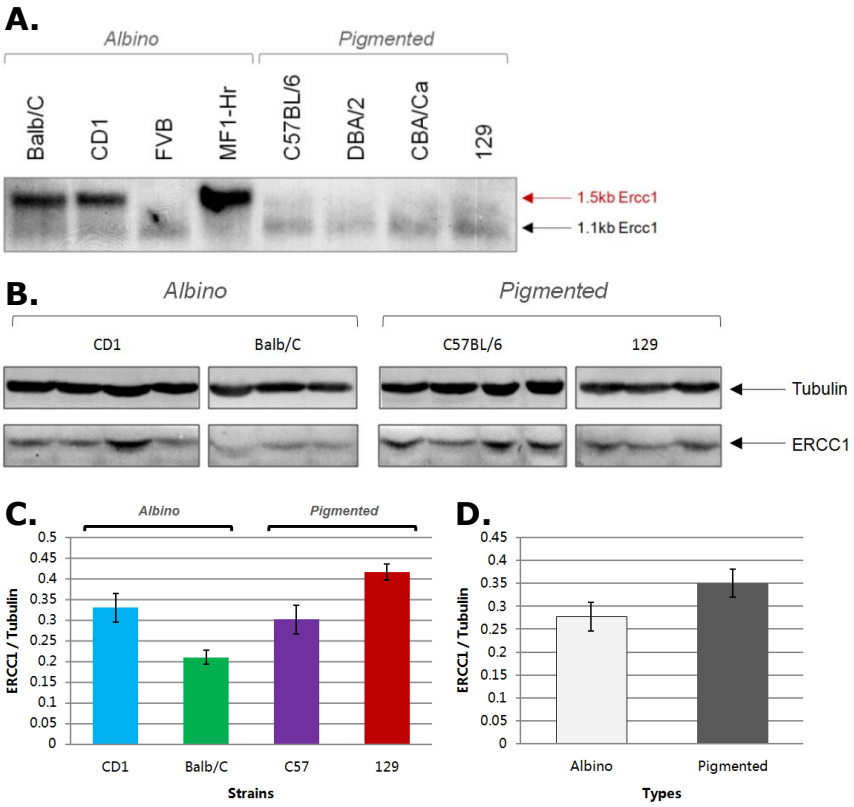

A. Northern blotting for Ercc1 was carried out on RNA extracted from the skin of adult mice of inbred albino strains BALB/c, FVB, the outbred albino strains, CD1 and MF1, and the inbred pigmented strains C57Bl/6, DBA/2, CBA/Ca and 129/Ola. The 1.5kb and 1.1kb Ercc1 transcripts are indicated with arrows.

B. Whole protein lysates of independent mouse skin samples from CD1, Balb/C, C57BL/6 and 129/Ola strains were separated by SDS-PAGE and then probed with anti-ERCC1 SC-10157 and detected by the phosphorimager system. After that, the membranes were re-probed with loading control beta-tubulin. Top panel shows the beta-tubulin bands and bottom panel shows the ERCC1 bands.

C. Histogram shows mean level of ERCC1 protein in skin ±SEM standardized against beta-tubulin for individual albino and pigmented mouse strains.

D. Histogram shows mean level of ERCC1 protein in skin ±SEM standardized against beta-tubulin for pooled albino and pigmented mouse strains.

selective proteasome inhibitor (Ki=4nM), which inhibits NFkappaB activation by preventing IkappaB degradation. MG132 can be used to block degradation of short-lived proteins.

Surprisingly, given that the published half-life of ERCC1 is not particularly short (a half-life of about 7 hours was reported in human tumour cells by McGurk, et al. 2006), MG132 induced a significant accumulation of ERCC1 in our keratinocyte cells. ERCC1 wild-type and deficient keratinocyte cell lines were treated with MG132. Cells were harvested 6 hours following the treatment, lysed and analyzed by western blotting. As shown in the Figure 3.7.A, the protein level of ERCC1 was barely detectable in the ERCC1 wild-type keratinocyte cells without the proteasome inhibitor MG132. However, when treated with MG132, the level of ERCC1 was boosted dramatically. In the negative control ERCC1 deficient keratinocyte cells, no ERCC1 protein was detected. The cross-reacting bands detected by the anti-ERCC1 SC-10157 could be used as a loading control in the western blotting to show the loading was well-matched. This result was very interesting as it revealed that there might be a potential post-translational pathway to regulate the protein level of ERCC1 in keratinocytes.

In addition to the proteosome inhibitor MG132 treatment, UV-irradiation was then performed on keratinocytes (Figure 3.7.B). ERCC1 was barely detectable in non-irradiated cells and cells following $5Jm^{-2}$ UVC-irradiation. Following $50Jm^{-2}$ UVC-irradiation, the level of ERCC1 protein had increased by 6 hours and was highest at 24 hours post UV. UVC radiation induces two of the most abundant mutagenic and cytotoxic DNA lesions cyclobutane pyrimidine dimers (CPDs) and 6-4 photoproducts (6-4PPs). This damage is repaired mainly by the NER pathway in cells (Sinha and Hader 2002). As ERCC1 plays an essential role in the NER pathway, this result indicated a potential up-regulation of ERCC1 and of NER following UV-induced DNA damage.

Figure 3.7 ERCC1 protein levels in mouse keratinocytes following various treatments by western blotting

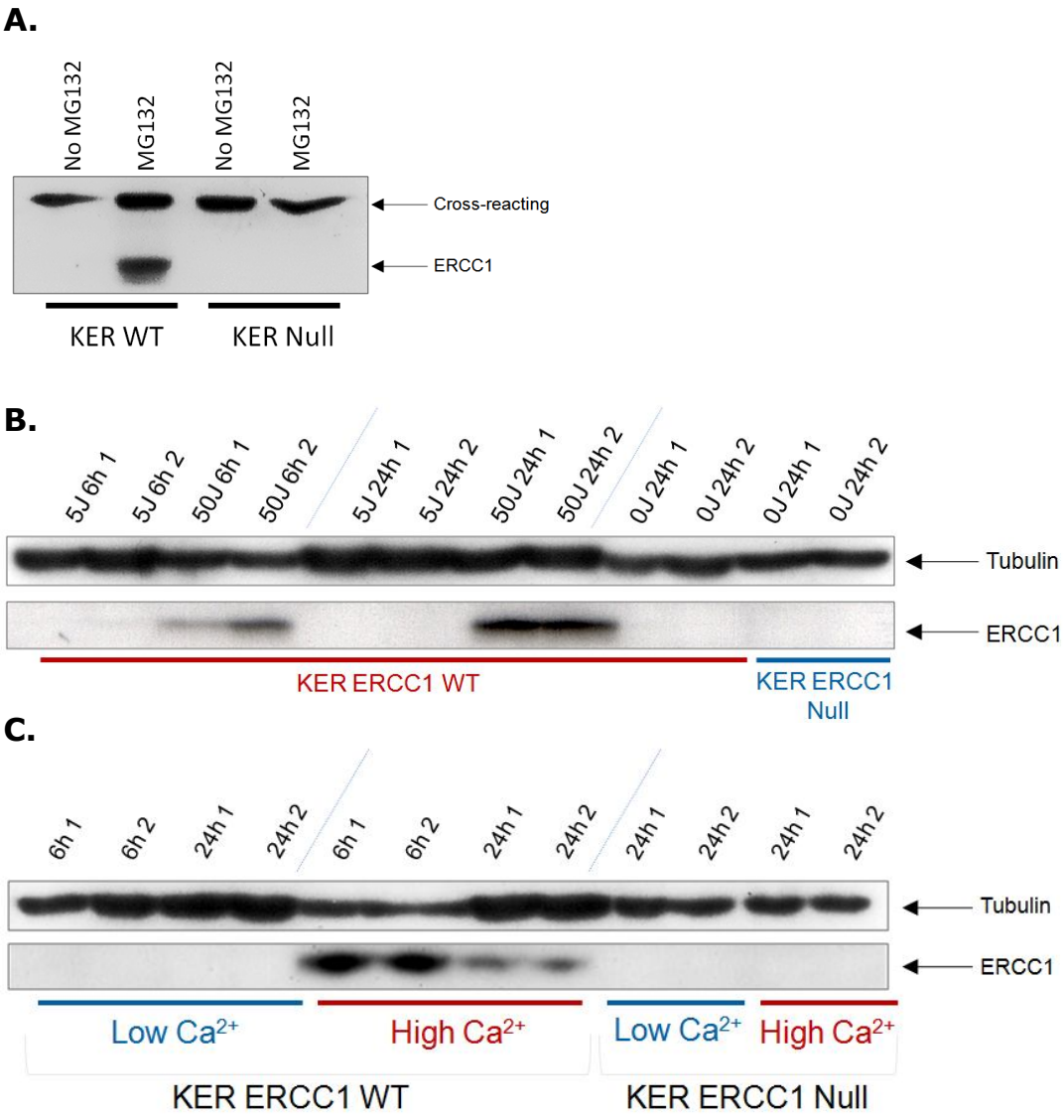

A. Proteasome inhibitor treatment. Elevated protein level of ERCC1 was seen in mouse keratinocytes 6 hours following proteasome inhibitor MG132 treatment. ERCC1 wild-type and deficient keratinocytes are labelled as KER WT and KER Null, respectively.

B. UV-irradiation. ERCC1 wild-type keratinocytes were labelled as KER ERCC1 WT in red and deficient keratinocytes were labelled as KER Null in blue. Cells were treated with $5Jm^{-2}$, $50Jm^{-2}$ and no UV ($0Jm^{-2}$) as indicated on the top of the gel. The different harvest time points following UV-irradiation are labelled on the top as well. Number 1 and 2 indicates duplicate samples. Top panel of gel shows bands of the loading control beta-tubulin and bottom panel shows bands of ERCC1, as indicated by the arrows on the right.

C. Treatment with high Ca^{2+} containing medium. The high Ca^{2+} culture condition could also elevate the level of ERCC1. Normal low Ca^{2+} culture condition is labelled in blue under the gel. High Ca^{2+} culture condition is labelled in red. Cells were harvested at 6 hour and 24 hour following the medium change. The time points are labelled on the top of the gel. Number 1 and 2 indicates duplicate samples. Top panel of gel shows bands of the loading control beta-tubulin and bottom panel shows bands of ERCC1, as indicated by the arrows on the right.

We also investigated whether the concentration of calcium in the culture medium could affect the level of ERCC1 protein (Figure 3.7.C). The differentiation programme of cultured keratinocytes is regulated by the Ca^{2+} concentration of the culture medium (Hennings et al. 1980). In low-calcium medium keratinocytes remain undifferentiated. Increasing the calcium concentration triggers the differentiation of keratinocytes (Darmstadt et al. 1998). With Ca^{2+} below 0.1mM, keratinocytes form a monolayer of basal epithelial-like cells, with a characteristic "crazy paving" appearance under the microscope. When Ca^{2+} rises above 0.1 mM, the cells begin to stratify and mature to fully differentiated squames.

Our western blotting results showed that the level of ERCC1 increased significantly 6h following transition from low (concentration<0.1mM) to high (concentration=1.8mM) calcium. The ERCC1 level decreased 24h after the transition and returned to normal 72h after the high Ca^{2+} treatment started.

In all the above experiments in section 3.5 with our ERCC1 wild-type mouse keratinocytes there was an unexpectedly low level of ERCC1 protein under normal culture conditions without any treatment. At the beginning of the year 2007, this situation changed. The ERCC1 protein level in untreated keratinocyte cultures increased such that we could no longer detect an increase following any of the treatments used. The keratinocyte samples analysed in earlier sections of this Chapter (shown in Figure 3.2 and Figure 3.4) were prepared after this change had occurred. While we were investigating the reason for this change to our ERCC1 wild-type keratinocyte cultures we investigated our ERCC1 wild-type mouse embryonic fibroblast line and an independent mouse keratinocyte cell line to see if they showed treatment-related changes in ERCC1 protein levels.

The same elevation of ERCC1 protein level was not seen in mouse embryonic fibroblasts. As shown in the Figure 3.8.A, the ERCC1 level was already high in the wild-type fibroblast line (PF20) without any treatment. After 6 hours of treatment with proteasome inhibitor MG132, the ERCC1 level remained the same as in untreated cells. The ERCC1 deficient fibroblasts (PF24) were a negative control for this experiment. As expected there was no ERCC1 band detectable in the PF24 lanes, no matter whether treated with MG132 or not. The loading control of beta-tubulin showed the loading was well-matched.

We then tested the level of ERCC1 in the PAM212 cell line following changing culture conditions. The PAM212 cell line was another mouse keratinocyte cell line which had different culture conditions from the ones used by our group. PAM212 was normally cultured in high Ca^{2+} RPMI medium where the cells had the appearance of differentiated keratinocytes under the microscope. When changed to low Ca^{2+} culture conditions, the growth of PAM212 cultures slowed down significantly. A few cells died in the low Ca^{2+} condition but the majority cells remained alive.

PAM212 cells were transferred to the low Ca^{2+} condition for 6 hours and 24 hours, then cells were harvested and ERCC1 protein was detected by western blotting along with controls cultured in normal high Ca^{2+} medium. The whole cell protein concentrations were measured by the BCA assay and equal amounts of protein were loaded on the gel and separated by SDS-PAGE. ERCC1 was detected by anti-ERCC1 SC-10157 and the cross-reacting band was used as loading control (Figure 3.8.B). The level of ERCC1 increased slightly in PAM212 cells cultured for 6 hours in low Ca^{2+} medium. The band intensities were then measured by the Quantity One densitometry system (BIO-RAD). The level of ERCC1 was standardized against the cross-reacting band. The mean standardized ERCC1 levels were plotted on a histogram (Figure 3.8.C).

Figure 3.8 ERCC1 protein levels in mouse embryonic fibroblasts and mouse PAM 212 keratinocytes following various treatments.

A.

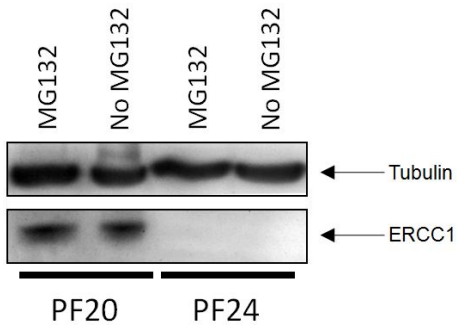

B.

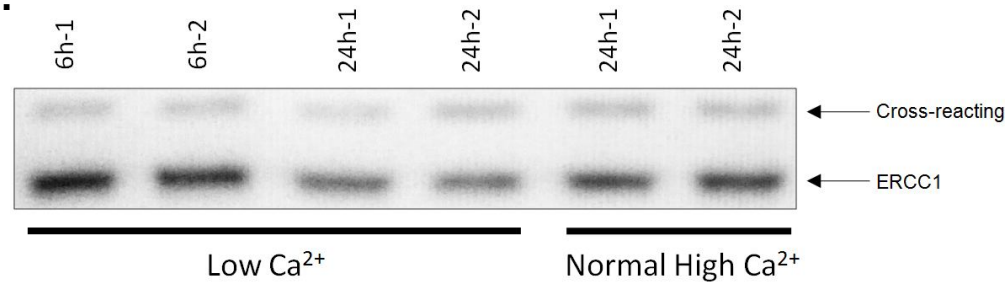

C.

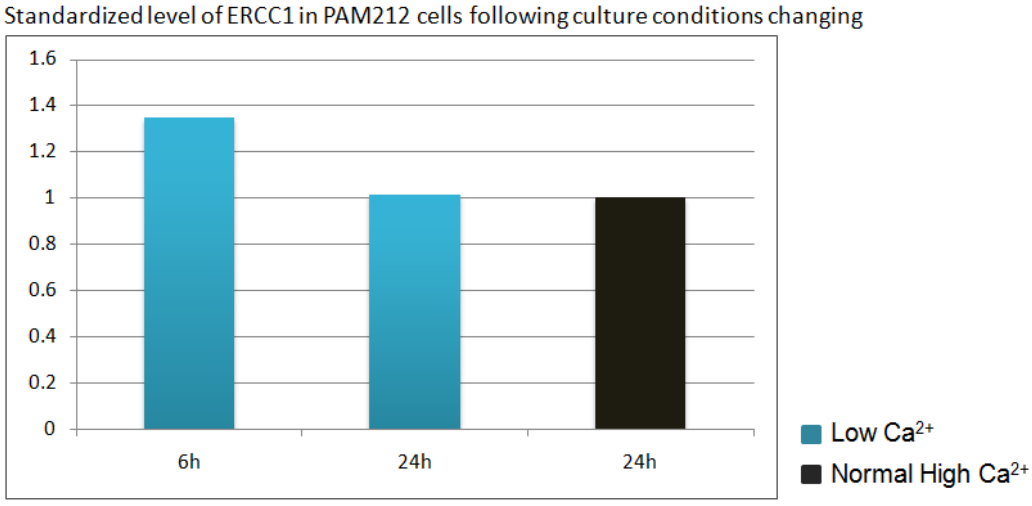

A. Proteasome inhibitor MG132 treatment of mouse embryonic fibroblasts. Protein lysates from ERCC1 WT mouse fibroblasts (PF20) and deficient mouse fibroblasts (PF24) either untreated or treated for 6h with MG132 were separated by SDS-PAGE, transferred to the PVDF membrane and then probed with anti-ERCC1 SC-10157 and the loading control of beta-tubulin. The top panel shows bands of beta-tubulin while the bottom panel shows bands of ERCC1.

B. Effects of different culture conditions on PAM212 cells. PAM212 cells were transferred to low Ca^{2+} medium and harvested after 6 hours and 24 hours. PAM212 cells cultured under normal high Ca^{2+} conditions were used as control in the western blotting. Number 1 and 2 indicates duplicates of samples above the gel. Cross-reacting bands and ERCC1 bands are indicated by arrows on the right.

C. Histogram showing mean level of ERCC1 protein in PAM212 standardized against the cross-reacting band. Mean level of ERCC1 in PAM212 cultured in low Ca^{2+} medium is plotted in blue columns. Mean level of ERCC1 of PAM212 cultured in normal high Ca^{2+} medium is plotted in the black column. Time points are labelled under their relevant columns. Y-axis shows the mean ratio of ERCC1 against cross-reacting band, relative to the ratio in high Ca^{2+} medium.

The ERCC1 level was slightly elevated 6 hours following the change to low Ca^{2+} medium, but had returned to normal (high Ca^{2+}) levels after 24 hours in low Ca^{2+} medium. This difference was not considered large enough compared to the difference seen in our own keratinocyte cell line to justify further experiments with this cell line.

3.6 Investigation of the reason for the loss of stress treatment induced changes in ERCC1 levels in keratinocytes

As described in Section 3.5, an uncontrolled change in the ERCC1 expression levels in our keratinocytes occurred at the beginning of the year 2007. The level of ERCC1 protein in untreated cultures increased from the very low level seen in our initial experiments to a higher level more equivalent to that observed in untreated embryonic fibroblast and PAM 212 keratinocyte cultures. Going back to the freezer for fresh stocks did not solve this problem. To investigate what had happened to our keratinocytes, a series of experiments were carried out.

At the beginning we thought that the change of the ERCC1 protein level might be related to different cell densities. When keratinocytes are cultured at low density the appearance of cells changes and they look similar to differentiated keratinocytes. Thus we compared the level of ERCC1 protein in keratinocytes between low density and high density following different stress treatments. As shown in Figure 3.9.A, when keratinocytes were cultured at high density, which means nearly 100% confluence in dishes, control cells without any treatments showed the same high level of ERCC1 as cells treated with either MG132 for 6 hours or grown in a high concentration of $Ca^{2+}$for

Figure 3.9 Investigation of the reason for the loss of stress treatment induced changes in ERCC1 levels in keratinocytes.

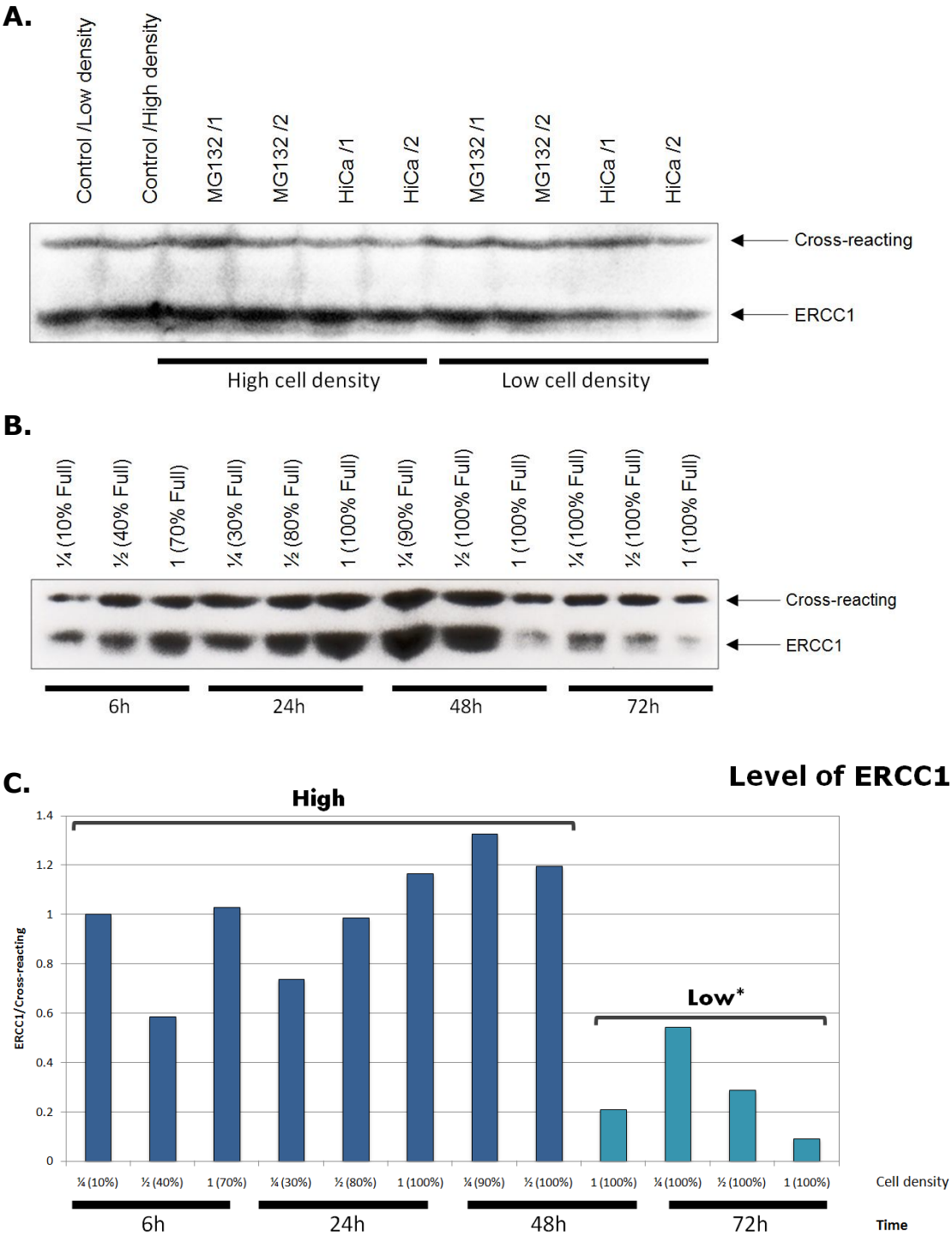

D.

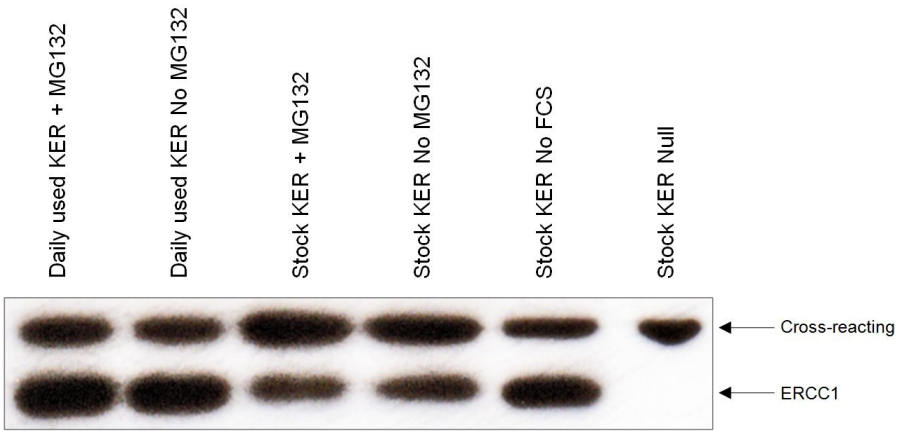

A. ERCC1 protein levels in mouse keratinocytes grown to a high density (100% confluence) or to a much lower density (50% confluence) as indicated below the gel. Cultures were either untreated (control), treated with MG132 for 6 hours, or treated with high Ca^{2+} medium for 6 hours as indicated at the top of the gel. Cross-reacting bands and ERCC1 bands are indicated on the right.

B. ERCC1 protein levels in mouse keratinocytes harvested at different cell density and different time points following passage. The four different harvest time points of 6 hours, 24 hours, 48 hours and 72 hours are indicated below the gel. Different starting cell numbers used to set up the cultures and the different cell densities reached at the harvest time point are indicated at the top of the gel. Cross-reacting bands and ERCC1 bands are indicated on the right.

C. Histogram showing level of ERCC1 protein in mouse keratinocytes harvested at different cell density. The different harvest time points, starting cell numbers used to set up the cultures and cell densities reached at the harvest time point are indicated below the gel. In terms of the level of ERCC1, data are divided into two groups, namely high and low expression, as indicated above the histograms. Asterisk indicates a significant difference ($p=0.007$) between these two groups by Mann–Whitney U test.

D. ERCC1 protein levels in stock and daily used keratinocyte cultures. Cultures were either untreated, or treated with MG132 for 6 hours, or cultured without fetal calf serum (FCS) for 24 hours as indicated at the top of the gel. ERCC1 deficient keratinocytes were used as a negative control. Cross-reacting bands and ERCC1 bands are indicated on the right.

6 hours. Previously control cultures had shown a very low level of ERCC1. When cells were cultured at low density, which means about 50% confluence in dishes, the levels of ERCC1 were again similar between control cultures and cultures treated with MG132, or a high concentration of Ca^{2+}. There was now no clear difference in ERCC1 level between control and treated keratinocytes at either cell density.

We then set up another experiment to detect the level of ERCC1 in cells at different density and time points following passage (Figure 3.9.B). When passaging keratinocytes, four groups of dishes were set up. Each group contained three dishes, one with the normal number of cells, one with half the normal number of cells and one with a quarter the normal number of cells. These four groups of dishes were harvested 6 hours, 24 hours, 48 hours and 72 hours following the passage and the levels of ERCC1 were detected by western blotting using anti-ERCC1 SC-10157. Before harvest, the cell densities were estimated under the microscope and recorded.

The groups of keratinocytes harvested at 6-hour and 24-hour time points showed the same high level of ERCC1 irrespective of the cell density. In the group of keratinocytes harvested at the 48-hour time point, the two dishes which were set up using quarter and half the normal number of cells showed high levels of ERCC1. At this time point the dish set up using half the normal number of cells had reached 100% confluence. At the 48-hour time point, the dish containing the normal number of cells plated showed a decreased level of ERCC1. In the last group, at the 72-hour time point, all the three dishes of keratinocytes were 100% confluent and all showed a low level of ERCC1 protein in the western blotting analysis. Even allowing for the reduced levels of the cross-reacting protein in the 72-hour samples, there was a clear reduction in ERCC1 protein levels in cultures that had grown to and been maintained at high densities. Of

course this does not explain the sudden change in the ERCC1 protein levels in our control cultures which were not maintained at confluent cell densities.

The level of ERCC1 proteins were then standardized against the cross-reacting proteins and plotted on a histogram (Figure 3.9.C). The data were clearly divided into two groups in terms of ratio of ERCC1. Samples harvested at 6h and 24h, as well as the two samples harvested at 48h with lower starting cell numbers (1/4 and 1/2) had a high level of ERCC1. The sample harvested at 48h with high normal starting cell numbers and samples harvested at 72h showed a 3.3-fold lower level of ERCC1. Statistical analysis using Mann Whitney U test showed the level of ERCC1 in the group with longer culture time and higher cell confluence was significantly lower ($P=0.007$).

We also compared the level of ERCC1 protein between our in use cultures and a new culture obtained by going back to the early passage frozen sotck. As shown in Figure 3.9.D, the stock keratinocytes from liquid nitrogen showed a slightly lower level of ERCC1 compared to the daily used keratinocyte culture, but the ERCC1 levels in both untreated cultures were much higher than we had seen previously. The level of ERCC1 didn't change in either keratinocyte culture following MG132 treatment. We also starved our stock culture by removing the fetal calf serum from the medium for 24 hours to stop the cell growth. By analogy with the experiments described above (Figure 3.9.B), we expected that the ERCC1 protein level would be decreased by serum starvation, but the effect was the opposite and a slight increase was seen. ERCC1 deficient keratinocytes were used as a negative control in this western blotting.

In summary, neither changing the keratinocyte cultures, nor manipulating the growth conditions enabled us to reproduce the stress-related increase in ERCC1 protein levels

that we observed in our initial experiments. Consequently we were forced to terminate this series of experiments.

3.7 Discussion

The expression of a gene is largely determined by the biological function and demand on the protein that the gene encodes. The NER pathway mainly deals with UV-induced DNA lesions and is also active against a broad range of other DNA damage. In wild type mouse, Ercc1 transcripts could be detected in all organs (van Duin et al. 1988). The level of Ercc1 expression was lowest in the liver and generally low in all other tissues except for the testis, where the level of expression of this transcript was much higher than elsewhere (Selfridge et al. 2001). In addition ERCC1 expression is also relevant to cancer; a low level of ERCC1 expression correlated with better response to chemotherapies and longer survival. For example, in gastric cancer, survival for patients with low ERCC1 levels was significantly longer than in those with high levels (15.8 vs 6.2 months; $P<0.0001$) (Lord et al. 2002; Wei et al. 2008). The same correlation was found in some other cancer types, such as non-small cell lung cancer (Olaussen et al. 2006; Wang et al. 2008), colorectal cancer (Shirota et al. 2001) and ovarian cancer (Selvakumaran et al. 2003).

In skin, the NER pathway removes the majority of the DNA adducts induced by UVB-irradiation. It has been reported that the mRNA level of ERCC1 was elevated in human keratinocytes at 6 hours post UV-irradiation (Murakami et al. 2001). However, previous group work had found no increase in levels of the 1.5kb skin-specific Ercc1 transcript in mouse skin after UV irradiation (Andrew Winter, unpublished observation). We first

considered that the elevated level of the 1.5kb skin-specific Ercc1 transcript in albino strains could lead to an increased level of protein to protect the skin against UV-induced DNA damage.

To investigate this hypothesis, we first tested the ERCC1 protein expression pattern in different tissues using a panel of mouse tissues from wild-type Balb/C, CD1, 129/Ola and C57BL/6 strains. All strains showed similar tissue patterns and levels of ERCC1 protein, which matched the tissue pattern of Ercc1 transcripts apart from skin. In skin although the larger 1.5kb transcript predominated over the normal 1.1kb transcript found in other tissues, the size of the ERCC1 protein was the same in skin as in other tissues examined. This result agrees with our previous RT-PCR assay using primers in exon2 to exon10, which suggested that the skin-specific Ercc1 transcript had the same ERCC1 protein coding region as the normal transcript. We further tested the ERCC1 protein levels in skin between albino and pigmented strains. Although the Ercc1 mRNA expression pattern was entirely different, there was no significant difference in terms of the ERCC1 protein level in skin between albino and pigmented strains.

In addition, we had previously identified that the Ercc1 expression pattern in mouse skin was determined by the Ercc1 gene sequence and not by the coat colour (Andrew Winter, unpublished observations). A cross between BALB/c and C57BL/6 mice was performed to segregate the Ercc1 gene from those determining coat colours. F2 mice were genotyped for the strain of origin of the Ercc1 gene using a polymorphism in the 5' UTR. Northern analysis revealed that skin from recombinant white mice which are homozygous for the C57BL/6 Ercc1 gene have the expression pattern found in C57BL/6 mice, and recombinant black mice which are homozygous for the BALB/c Ercc1 gene have the expression pattern found in BALB/c mice. As expected, non-recombinant F2 mice of both colours have their original expression patterns.

Combining these results together, we found no support for our hypothesis that the 1.5kb skin-specific Ercc1 transcript might result in increased ERCC1 protein level in the skin of albino strains. However, we found an interesting different sequence pattern between albino and pigmented strains in the region 1kb 5' of the known Ercc1 promoter. The regulatory elements in this region might be linked with the altered Ercc1 expression observed. This will be discussed in more detail in Chapter 4.

The rapid change in ERCC1 protein levels that we observed in our cultured mouse keratinocytes in the absence of changing Ercc1 transcript levels suggested to us that there may be post-translational regulation of ERCC1. Protein modification by ubiquitin and SUMOylation has been observed for a number of DNA repair proteins, which has been reviewed recently (Bergink and Jentsch 2009). For example, the NER protein XPC is reported to be modified by ubiquitin and SUMO-1 following UV irradiation (Wang et al. 2005). DNA damage usually activates the DNA repair or damage-avoidance pathways, and often induces a checkpoint response that triggers cell-cycle arrest for the repair of DNA lesions, referred to as the DNA-damage response (DDR) (Harrison and Haber 2006; Branzei and Foiani 2008). Some repairs need to assemble large protein assemblies, which needs to be disassembled when the repair is completed. Therefore, the reversible modification of proteins by conjugation of ubiquitin, or its relative SUMOylation is ideally suited for regulatory purposes.

Compared to our other mouse cell lines, untreated cultures of our Ercc1 wild type mouse keratinocytes showed a very low level of ERCC1 from 2005 to 2007. This level increased rapidly following exposure to UV, or to a proteasome inhibitor, or by moving cells from their normal low Ca^{2+} medium to a high Ca^{2+} medium which induced differentiation. However, in 2007 the ERCC1 protein level in our untreated mouse

keratinocyte cultures increased so that the previous treatments were now ineffective at stimulating responses. After the ERCC1 protein changed from a low level to a high level in our keratinocyte cultures, we did a series experiments to investigate the cause of the change. We confirmed that the high level of ERCC1 protein in untreated cultures was due to the culture conditions as going back to the liquid nitrogen stock cells had no effect. The epidermal growth factor (EGF) used in the culture medium was considered to be a candidate to affect ERCC1 protein levels as EGF-mediated induction of ERCC1 expression through the ERK2 and MAPK pathway in human carcinoma cells has been reported (Adly Yacoub 2003; Andrieux et al. 2007). However, changing the EGF concentration in culture medium had no effect. We further tried using keratinocyte growth factor (KGF) instead of EGF but the level of ERCC1 protein remained at the same high level in our cultures. Other conditions like cell density and confluence, calcium concentration, trypsinization and possible UV-irradiation were investigated but no cause of the elevated ERCC1 protein could be found. It is important to stress that after the change in our keratinocyte cultures, the level of ERCC1 was similar to that in our mouse embryonic fibroblast and another widely used keratinocyte cell line PAM212. Thus, this increase in ERCC1 protein level could be regarded as a kind of "recovery" in our keratinocytes. From 2005 to 2007 it might be that an undefined different culture condition was acting to reduce ERCC1 expression. We lost this culture condition and then the ERCC1 protein level was returned back to its normal level. During the course of our investigation into the reason for the changing ERCC1 levels in untreated keratinocyte cultures we did see clear evidence that the level of ERCC1 protein dropped in cultures maintained at high density. Presumably there is less requirement for DNA repair in non proliferating cells. In retrospect we should have passaged these high density cultures to confirm that their reduced levels of ERCC1 were reversed by a return to proliferation.

Chapter 4:

Are upstream CpG islands the source of the novel *Ercc1* skin-specific transcript?

4.1 Investigations of the novel 1.5kb mouse *Ercc1* skin-specific transcript and potential upstream *Ercc1* promoters.

Previous group work has identified a novel 1.5kb skin-specific mRNA transcript for Ercc1 in mice. It was shown by RT-PCR and RACE that this transcription of Ercc1 in skin was driven by an alternative upstream promoter not utilised in other tissues. However, the accurate position of the promoter region was still unclear.

Based on the previous results, a further investigation was carried out in an attempt to identify the promoter for the 1.5kb skin-specific Ercc1 transcript. A series of computer-based promoter prediction programmes were used to identify candidate promoter regions.

As shown in the Figure 4.1, the *Ensembl Genscan* program, a joint project to develop a software system which produces and maintains automatic annotation on selected eukaryotic genomes, reported one potential transcript in mouse (labelled as TSS No.2). This transcript could possibly contain two potential exons about 11kb upstream of the known Ercc1 transcript spliced onto Ercc1 exon 2 to exon 10.

Another potential Ercc1 transcript (labelled as TSS No.1) is predicted in both human and mouse by several computer prediction programs, and has been reported in the literature (Wilson et al. 2001). The putative promoter regions containing regulatory elements, located 2.5kb upstream of the Ercc1 gene in mouse and 5kb upstream of ERCC1 in human, were analyzed by several promoter-predicting programs including PROMOTER SCAN II (Prestridge 1995), McPromoter (http://tools.genome.duke.edu/generegulation/

McPromoter/), and Tfsitescan (www.ifti.org/). A conserved GC-rich region with 77% GC content was found in this promoter region to share 81% identity with the mouse and human. Within this promoter region, an 112bp gap-free region with a sequence identity of 93% between species contains a conserved TATA box and a GC box. Other classical elements and putative regulatory elements were found as well. A computer predicted gene, located very close to the 2.5kb upstream Ercc1 putative promoter and generating a putative transcript in the opposite direction to the Ercc1 transcript, was noticed in mouse by NCBI BLAST search (Gene: D830036C21, Figure 4.1). There was no known protein product of this putative gene and a BLAST search in human did not show this gene. Thus, this putative promoter region, conserved in mouse and human, was a strong candidate to be the source of the 1.5kb skin-specific Ercc1 transcript.

4.2 RT-PCR showed no positive evidence that the two potential upstream Ercc1 promoter regions were active.

As described before, there were two potential upstream promoter regions for Ercc1. We first investigated the 11kb upstream promoter which was an *Ensembl Genscan* predicted Ercc1 transcript (Genscan ID: GENSCAN00000061823). The *Ensembl Genscan* program predicted this Ercc1 transcript with two putative exons at its 5' end. According to the *Ensembl Genscan* result, the putative exon 1 was 166bp and putative exon 2 was 208bp with a 1.5kb intron between them. The putative exon 2 spliced into the middle of known Ercc1 exon 2 and skipped the known exon 1. The known Ercc1 exon 3 to exon 10 remains the same and the size of this putative Ercc1 transcript is 1278bp. Although this transcript is about 200bp smaller, it was considered a reasonable match to the 1.5kb novel Ercc1 transcript, the size of which was estimated by northern blotting

Figure 4.1: A schematic diagram of the investigation of potential promoter regions of the novel 1.5kb Ercc1 transcript.

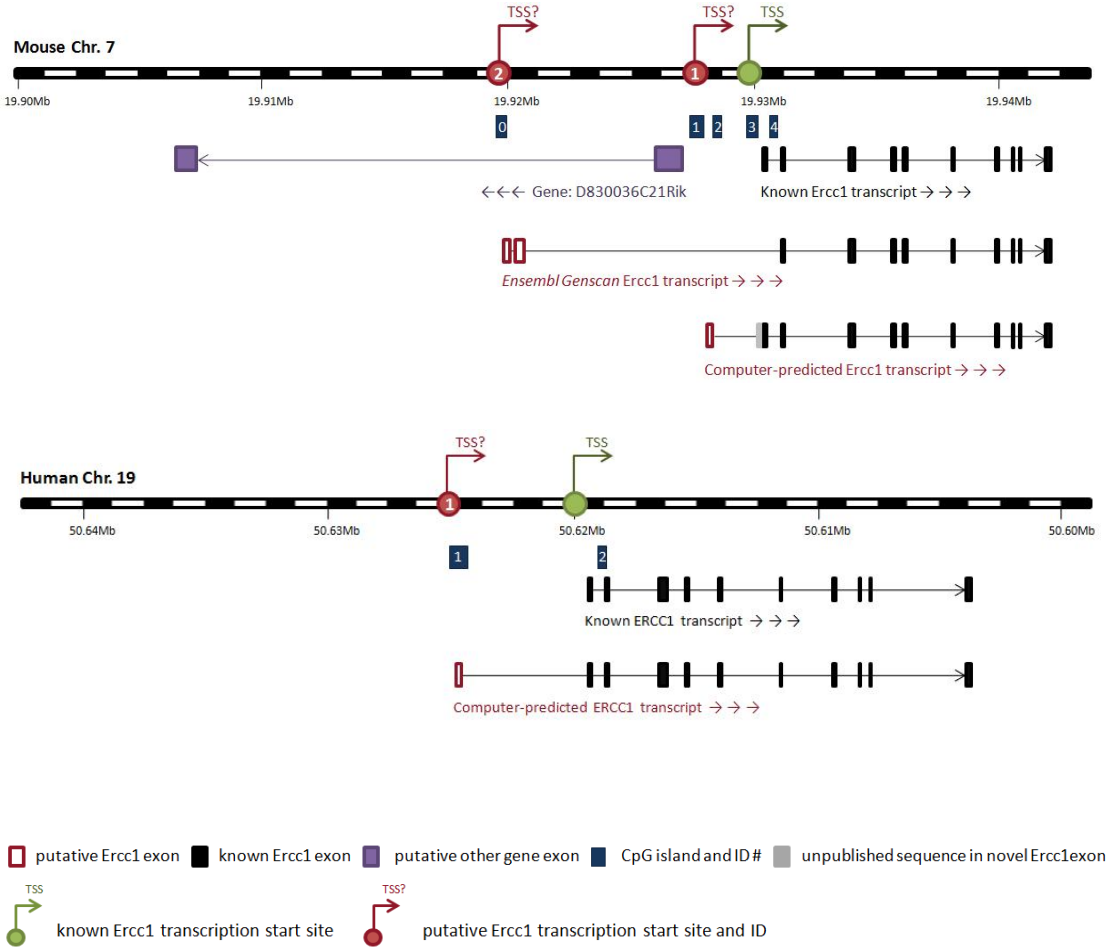

Mouse chromosome 7 and human chromosome 19 are shown as a black and white line. Red rectangles show putative Ercc1 exons predicted by *Ensembl Genscan* and other computer programmes. Black rectangles show known Ercc1 exons recorded in the database. Purple rectangles show putative exons of other genes. Dark blue rectangles show CpG islands around promoter regions. The grey rectangle shows unpublished sequence in the novel Ercc1 exon. Known and putative Ercc1 transcription start sites are labeled in green and red respectively. Directions of transcription of the genes are indicated by arrows.

(Figure 4.2.A). However, this transcript was not compatible with the previous RACE and RT-PCR work, which had shown that the 1.5kb Ercc1 transcript contained sequence immediately upstream of the normal Ercc1 exon1.

Analysis of the DNA sequence of the 11kb upstream region revealed a CpG island and a possible transcriptional start site. The presence of these promoter elements gave support to this prediction. To investigate the possibility that this 11kb upstream Ercc1 promoter was functional, RT-PCR analysis was performed on mouse embryonic fibroblasts and keratinocytes.

Novel primers were designed located in these putative exons, as shown in the Figure 4.2.A. These primers should generate 1.6kb (approximately) PCR products on keratinocyte DNA, and 237bp to 257bp PCR products on keratinocyte cDNA (Figure 4.2.B).

Total RNA from mouse keratinocyte cells was reverse transcribed using an oligo-dT primer to generate a pool of cDNA. Skin A forward primer in combination with Ex2b reverse primer, which we had tested before and which generated 382bp PCR products on keratinocyte cDNA and 791bp products on keratinocyte DNA, were used as a control reaction for Ercc1 cDNA synthesis (Figure 4.2.B). PCR using Skin A and Ex2b rev on the pooled mouse keratinocyte cDNA generated a single clear band at the expected position of 382bp, indicating that the Ercc1 cDNA quality was good and that there was no DNA contamination (Figure 4.2.C). PCRs using different combinations of novel primers were then performed on the wild type fibroblast DNA, keratinocyte DNA and pooled keratinocyte cDNA to amplify the sequence between putative upstream Ercc1 exon 1 and exon 2. The PCR products were electrophoresed on a 1.2% agarose gel and

Figure 4.2 No evidence by RT-PCR assay for activity from the 11kb upstream promoter (No.2) detected by the *Ensembl Genscan* program.

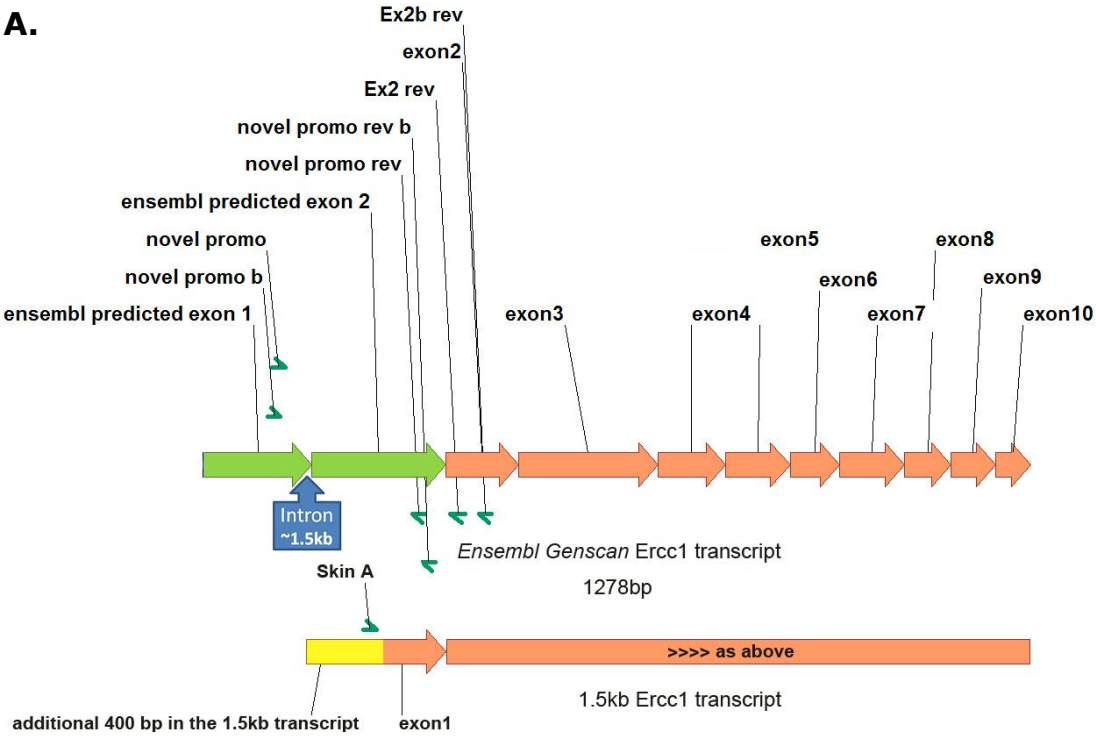

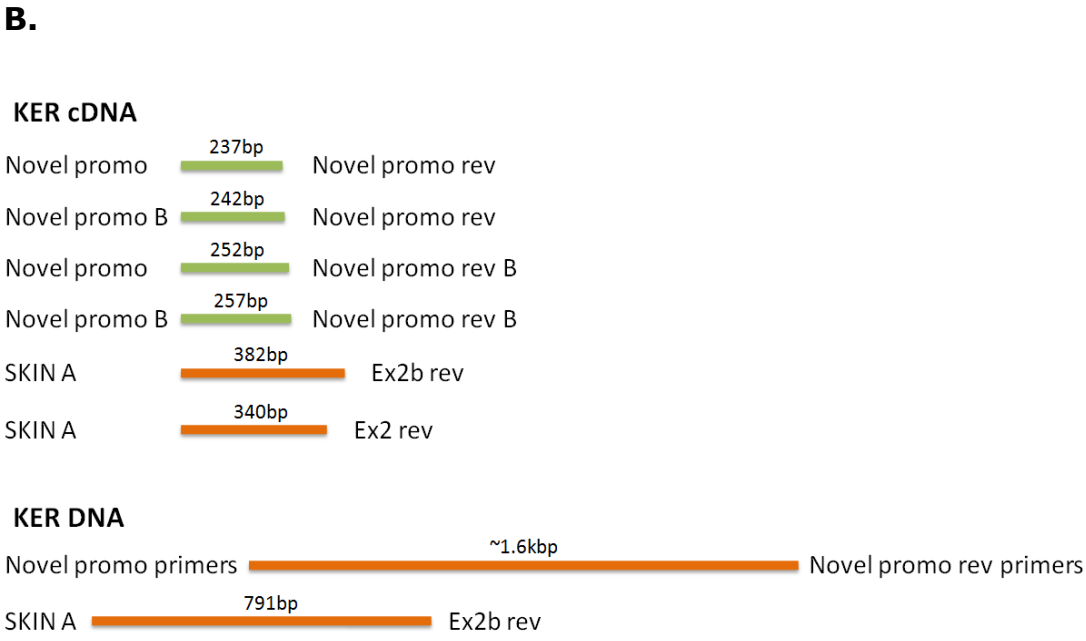

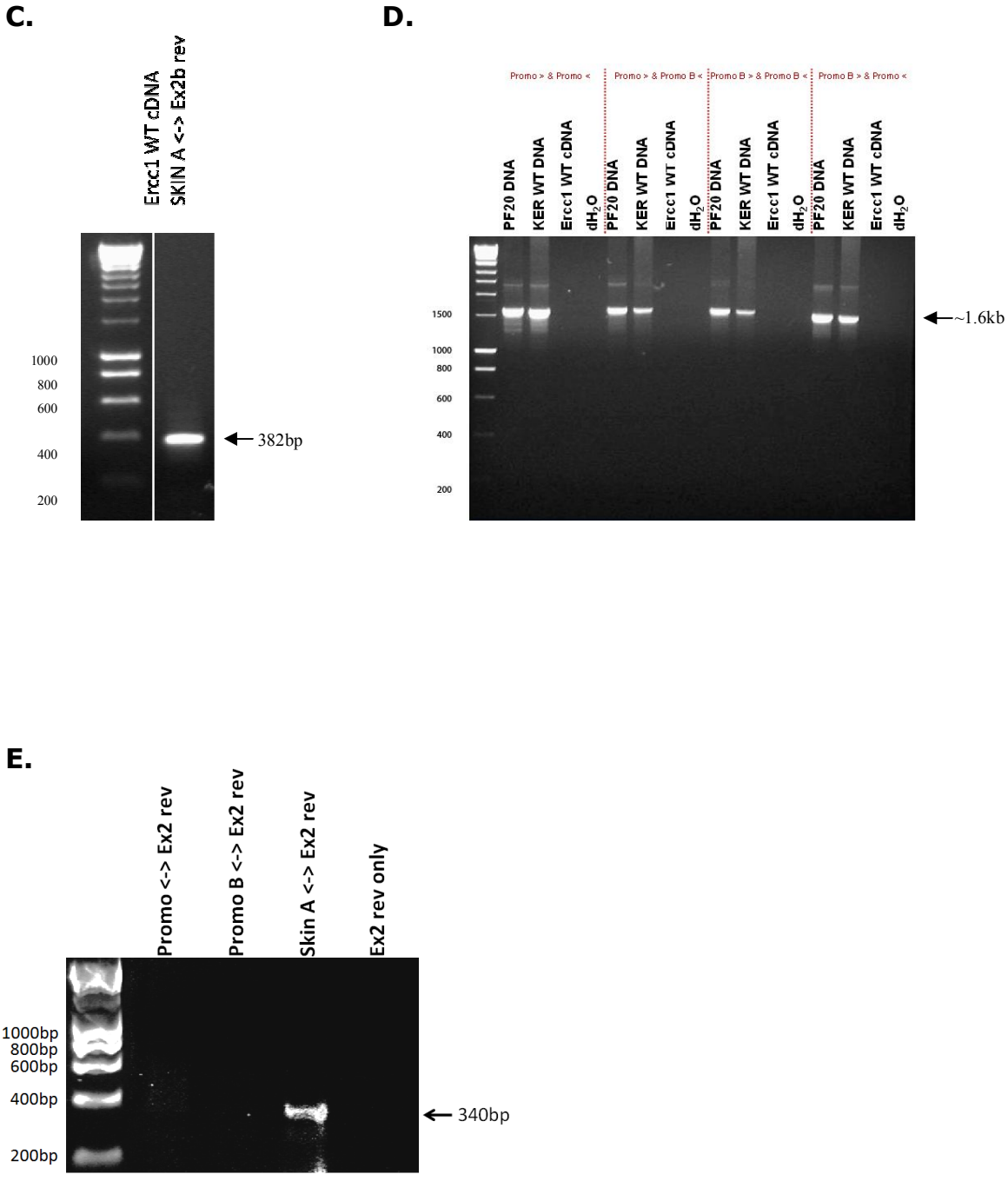
C.
Ercc1 WT cDNA
SKIN A <-> Ex2b rev
1000
800
600
400
200
382bp
D.
Promo > & Promo <
Promo > & Promo B <
Promo B > & Promo B <
Promo B > & Promo <
PF20 DNA
KER WT DNA
Ercc1 WT cDNA
dH2O
1500
1000
800
600
400
200
~1.6kb
E.
Promo <-> Ex2 rev
Promo B <-> Ex2 rev
Skin A <-> Ex2 rev
Ex2 rev only
1000bp
800bp
600bp
400bp
200bp
340bp

A. A schematic diagram of RT-PCR investigation. Potential exons predicted by *Ensembl Genscan* are showed in green. Known Ercc1 exons are shown in orange. Additional sequence present in the 1.5kb transcript upstream of exon 1 is shown in yellow. Primers used in the RT-PCR are labelled along exons in light green. Intron between potential exons is labelled in blue.

B. Predicted sizes of RT-PCR products on mouse keratinocyte cDNA and DNA.

C. PCR using primers SKIN A and Ex2b rev on mouse keratinocyte cDNA. A product at the size of 382bp indicates the cDNA is working well in this RT-PCR.

D. PCR using primers for the predicted upstream exons. The RT-PCR showed no positive evidence to support this *Ensembl Genscan* predicted promoter. The positive controls on mouse DNA showed the predicted bands at the size of 1.6kb. No product could be detected from RT-PCR using mouse cDNA.

E. PCR using primers for the predicted upstream exon together with Ercc1 exon 2. The positive controls using Skin A with Ex2 rev on mouse cDNA showed the predicted bands at the size of 340bp. No product could be detected from RT-PCR using novel primers for the *Ensembl Genscan* predicted exon together with Ex2Rev.

visualized by ethidium bromide staining. As shown in the Figure 4.2.D, clear bands at the predicted 1.6kb size were detected in both fibroblast and keratinocyte DNA lanes, no matter which combination of novel primers were used in the PCR. This result indicated that the novel primers were working well in this analysis. However, no PCR product could be detected in Ercc1 cDNA lanes, suggesting that the *Ensembl Genscan* Ercc1 transcript may not be real (Figure 4.2.D).

As these novel primers were all located in the putative exons, the above RT-PCR assay had no connections between the putative exons and known Ercc1 exons. Moreover, it was possible that there were mistakes in the *Ensembl Genscan* prediction. For example, the length, position and numbers of the putative exons could be different in reality. Thus it was possible that the negative RT-PCR result may be due to prediction mistakes rather than to lack of promoter activity. Therefore, another RT-PCR was performed using the novel forward primers with a reverse primer Ex2 rev which is located in the known Ercc1 exon2 and 42bp upstream of the Ex2b rev primer (Figure 4.2.E). Forward Skin A primer and the Ex2 rev primer were used in this RT-PCR as a control for Ercc1 cDNA. Because the Ex2 rev primer had not been tested before, a RT-PCR using Ex2 rev only was performed as another control to test for spurious PCR amplification. The two novel primers paired with Ex2 rev didn't show any band in the RT-PCR. Skin A primer and the Ex2 rev primer produced a band at the expected size of 340bp indicating good cDNA quality. No band was detected by Ex2 rev on its own.

From these two RT-PCRs results we did not find any evidence that the skin-specific transcript initiates from this *Ensembl Genscan* promoter region 11kb upstream of the normal Ercc1 transcript.

The second putative promoter region we investigated was predicted by several computer programs. This putative promoter region was located 2.5kb upstream of Ercc1 in mouse and 5kb upstream of ERCC1 in human. The Figure 4.3.A shows the sequence of this putative promoter region in mouse (C57BL/6 strain). The sequence labelled as "Potential Novel Promoter" shared 81% identity in the mouse and human. Classical promoter elements, such as a GC box and a TATA box were detected in this region. The potential transcriptional start site was predicted to be 23bp downstream of the TATA box. Furthermore, two CpG islands were detected around the putative promoter. The CpG Island 1 covered the whole promoter region while the CpG Island 2 was located about 400bp downstream of the putative promoter.

Two forward primers (ERC1 NP+57 and ERC1 NP+65), located 57bp and 65bp downstream of the potential transcriptional start site, were designed for RT-PCR assay with the Ex2b reverse primer. Skin A with Ex2b rev was used as positive control for Ercc1 cDNA. For PCR product size prediction (Figure 4.3.B), Skin A and Ex2b rev should generate 382bp PCR products on keratinocyte cDNA and 791bp products on keratinocyte DNA. ERC1 NP+57 and ERC1 NP+65 should generate 3358bp and 3350bp PCR products, respectively, with the Ex2b reverse primer on keratinocyte DNA. For PCR products using the novel forward primers with Ex2 rev on Ercc1 cDNA, firstly, there was 29bp from the start of Ercc1 exon 2 to the Ex2 reverse primer and 479bp from the end point of Dr. Selfridge's old 5'RACE result to the end of Ercc1 exon 1, thus the minimum size of RT-PCR product should be 508bp. Secondly, as it was 382bp from the 5'RACE end point to the start of Ercc1 exon 1, and the skin-specific 1.5kb transcript was about 400bp larger than the normal 1.1kb transcript, the 5'RACE end point identified by Dr. Selfridge should be very close to the real end of the Ercc1 cDNA. Therefore the RT-PCR product should not be much larger than 508bp. Using the same argument, genuine PCR products by novel forward primers with Ex2b reverse primer on Ercc1 cDNA

Figure 4.3 No evidence by RT-PCR that the skin-specific transcript initiates from another computer-predicted promoter region 2.5kb upstream of the normal Ercc1 transcript.

A.

B.

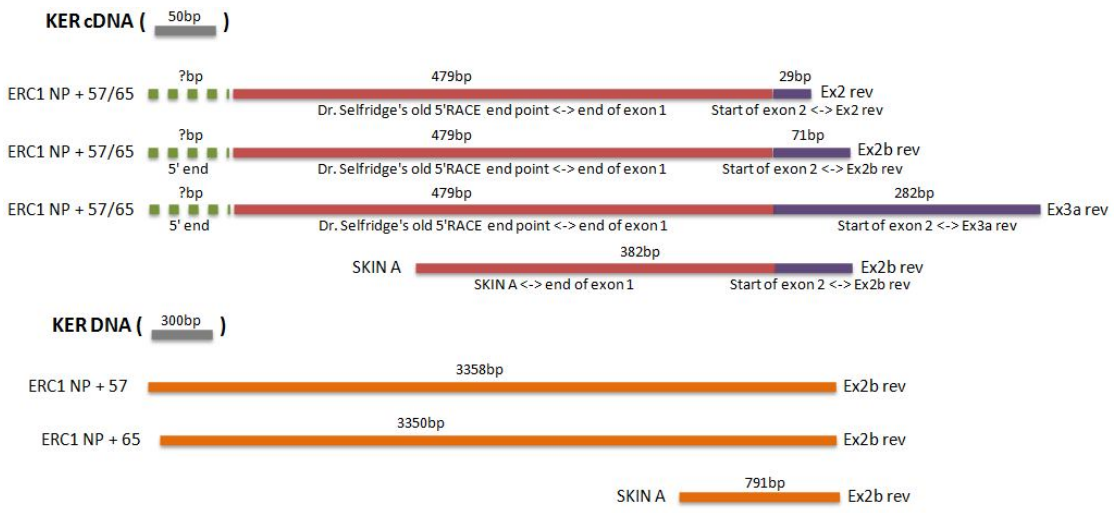

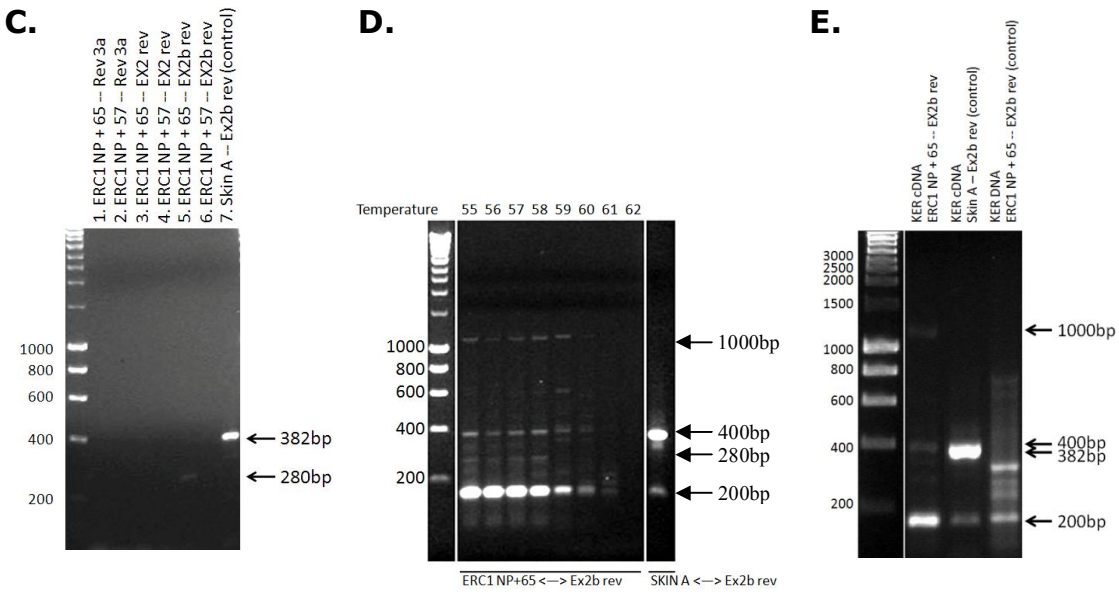

A. Computer program predicted 2.5kb upstream ERCC1 promoter region (**TSS No.1**) in mouse. The computer-predicted promoter region is labelled as "Potential Novel Promoter". Classical TATA box and GC box are marked in red boxes. The putative transcription start site is indicated with a black star shape. Novel forward primers ERC1 NP+57 and ERC1 NP+65 used in RT-PCR and two computer-detected CpG islands (CGI #1 and CGI #2) are labelled above the sequence.

B. A schematic diagram showing the minimum size of genuine Ercc1 RT-PCR products using different primer combinations. Predicted products' sizes are labelled on the top. The 5' end, exon 1 and exon 2 sequences are illustrated in green dash-line, red line and purple line respectively. The PCR size predictions on DNA are illustrated in orange lines. Primers are labelled at the relevant end of sequence. The different scales used for cDNA and DNA are indicated.

C. RT-PCR using various combinations of primers to investigate the possible activity of the 2.5kb upstream potential promoter region. The primers Skin A and Ex2b rev were used as a positive control to show cDNA quality. A weak band at the position of about 280bp could be detected using primer pair ERC NP+65 and Ex2b rev.

D. Gradient RT-PCR performed on keratinocyte cDNA using ERC NP+65 with Ex2b rev. Forward primer Skin A and reverse primer Ex2b rev were used as control for quality of cDNA. Three main products detected, sized 200bp, 400bp and 1kb are indicated by arrows on the right. The product at 280bp seen in Figure 4.3.C was also present at a low level. Primer pairs used in reactions are labelled.

E. Final round of RT-PCR performed on keratinocyte cDNA and DNA using annealing temperature at 57°C according to the result of gradient PCR. As previous result, three main products sized 200bp, 400bp and 1kb were detected. An expected 382bp product was detected in cDNA control lane. Primers and template type are labelled on the top. Sizes of the PCR products are indicated on the right.

should be only slightly bigger than 550bp, and only slightly bigger than 760bp by novel forward primers with Ex3a reverse primer.

The PCR was performed under normal conditions with an annealing temperature at 62°C. PCR products were electrophoresed on 1.2% agarose (Figure 4.3.C). The novel forward primers with Ex3a and Ex2 reverse primers didn't generate any product. There was no product generated by ERC1 NP+57 with Ex2b rev either. The PCR using ERC1 NP+65 with Ex2b rev showed a very faint band at the size of 280bp. The positive control using Skin A with Ex2b rev generated a clear single band at 382bp indicating that the cDNA quality was good and there was no DNA contamination.

Though this 280bp band generated by primers ERC1 NP+65 with Ex2b was too small to be the expected PCR product related to the 1.5kb Ercc1 transcript, it suggested that this primer pair could work on the Ercc1 cDNA. A gradient PCR with lower annealing temperatures to 55°C was then performed using ERC1 NP+65 and Ex2b rev on the Ercc1 cDNA to investigate this possibility further (Figure 4.3.D). Beside the very faint band at the size of 280bp detected previously, other major bands at about 200bp, 400bp and 1000bp were detected. The same PCR was repeated using the annealing temperature at 57°C to produce the 400bp and 1000bp products as well as to control the background non-specific bands to the minimum (Figure 4.3.E). The 400bp product was potentially interesting because of its size though it was slightly smaller than the 550bp PCR product size prediction. However, as the size of 1.5kb skin-specific transcript was measured by northern blotting before, the size might not be accurate. The control reaction using Skin A and Ex2b rev primers on keratinocyte cDNA generated a band at 382bp indicating good Ercc1 cDNA quality. Another control reaction using NP+65 and Ex2b rev on the keratinocyte DNA didn't generate the expected band at 3350bp, possibly due to the synthesis time used in the PCR not being long enough to generate this large fragment.

There were some non-specific bands detected in the DNA control reaction in which the two main bands were at 200bp and 360bp. This indicates that the 200bp product in the RT-PCR reaction was probably due to the contamination of genomic DNA in the keratinocyte cDNA preparation.

The 400bp and 1kb products were cloned into the p-GEM T-EASY vector using the lacZ blue white screen. 5 positive clones of each fragment were sequenced. However, the sequencing showed that neither 400bp nor 1kb products were Ercc1 related.

To sum up, no evidence was found by RT-PCR that the skin-specific transcript initiates from computer-predicted promoters 2.5kb and 11kb upstream of the normal mouse Ercc1 transcript.

4.3 Investigation of the methylation status of CpG islands around putative and normal Ercc1 promoters.

Because the methylation status of CpG islands can have a major impact on gene expression, we studied the methylation status of the CpG islands detected around the putative and normal Ercc1 promoters for any possible evidence to support the activity of the putative promoters in the production of the Ercc1 skin-specific transcript. We mainly focused on the 2.5kb upstream promoter region in mouse as it had more classical promoter elements than the 11kb upstream promoter and was conserved in human. There were 4 CpG islands detected from 3kb upstream to the normal Ercc1 promoter region

(Figure 4.4.A). These CpG islands were named CGI #1 to CGI #4. Normally, the CpG island around the active promoter region of the gene is unmethylated. Therefore our hypothesis was: In mouse skin cells, if the larger 1.5kb skin-specific transcript was driven by this upstream promoter, then CpG islands CGI #1 and CGI #2 that are located around the putative 2.5kb upstream promoter should be unmethylated, while CpG islands CGI #3 and CGI #4 that are around the normal Ercc1 promoter should be methylated. In contrast, in other tissues where the normal 1.1kb Ercc1 transcript was transcribed, the methylation status of these CpG islands around the 2.5kb upstream region and normal promoter region should be the opposite of the situation in skin.

Besides the mouse keratinocytes and fibroblasts, where the 1.5kb transcript is the major Ercc1 transcript, two different mouse ES cell lines, HM1 and DMNT3^{-}, were used to investigate the methylation patterns. HM1 was a wild-type ES cell line, while DNMT3^{-} was a DNA methyltransferase 3 deficient ES cell line. The skin-specific Ercc1 transcript was not detected by northern analysis in HM1 cells by previous group study. According to the hypothesis, the methylation patterns of the putative and normal Ercc1 promoters should be opposite between mouse HM1 ES cells and skin cells.

DNA from the different cell lines was freshly extracted before the bisulphite treatment. The bisulphite conversion was carried out using the kit from Cambridge Bioscience. Optimal amounts of DNA were converted according to the manufacturer's protocol to avoid incomplete conversion. After that, the converted DNAs were amplified by PCR using specially designed bisulphite sequencing primers for individual CpG islands. After the first round PCRs, samples of CGI #2 and CGI #3 generated the expected products at the positions of 272bp and 283bp, respectively, along with a heterogeneous smear of DNA (Figure 4.4.B). The sample of CGI #1 only generated a smear of DNA encompassing the expected size of its PCR product with no major band.

Figure 4.4 PCR amplification of bisulphite treated CpG islands around the putative and normal Ercc1 promoters in mouse keratinocytes, fibroblasts and ES cells.

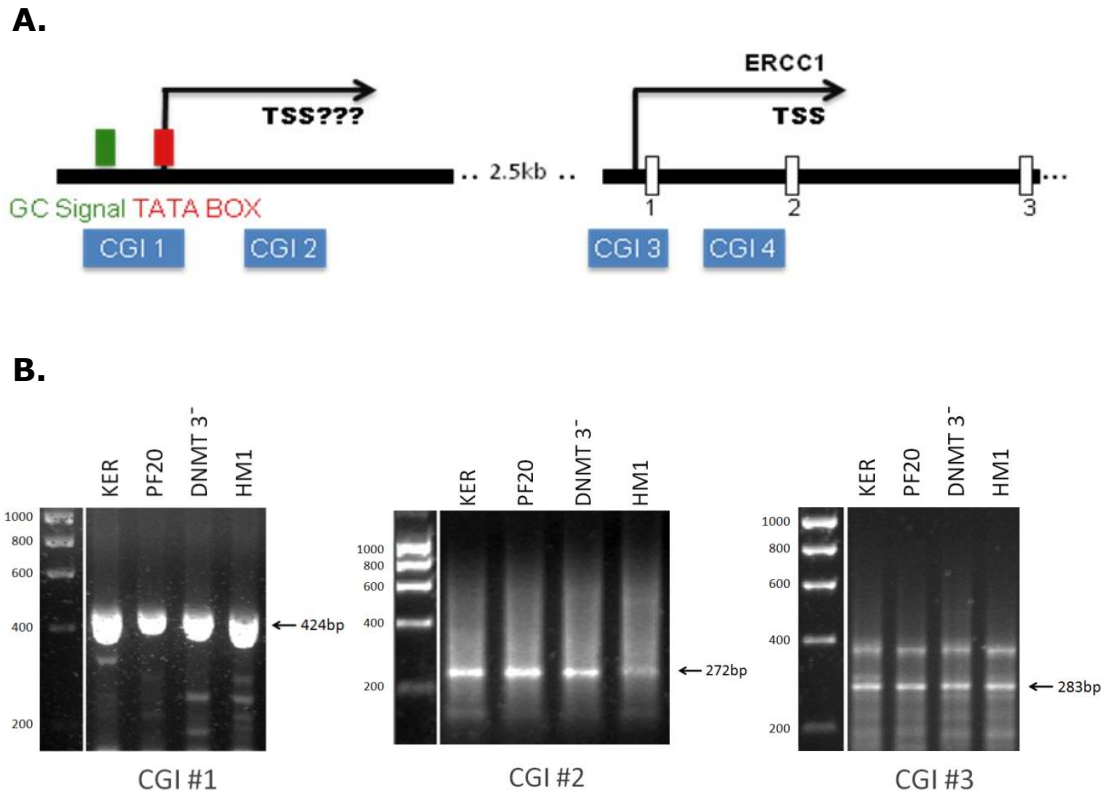

A. A schematic diagram showing the potential 2.5kb upstream promoter region and normal promoter region in mouse. Blue boxes show CpG islands with CpG/GpC contents greater than or equal to 60%. White boxes show known Ercc1 exons. Classic promoter elements are indicated: TATA box (red) and GC signal (green). The transcriptional start sites are labeled as TSS with an arrow.

B. The bisulphite treated DNA from keratinocytes (KER), mouse embryo fibroblasts (PF20), DNA methyltransferase deficient mouse ES cells (DNMT3^{-}) and mouse ES cells (HM1) was amplified with bisulphite sequencing primers specific for individual CpG islands. PCR products were visualized after gel electrophoresis.

To improve the quality of the bisulphite sequencing PCR product of CGI #1, the smear regions were cut out, gel purified, and a second round of nested PCRs using internal primers were then performed on DNA fragments retrieved from the first round PCRs (Figure 4.4.B). The second round of nested PCR generated a much better quality of bands in all samples. Strong bands corresponding to the converted CGI #1 region were detected at the expected position of 424bp. The band sizes varied slightly among these four cell lines because of the sequence difference between the different mouse strains (described later in Section 4.5).

At this stage all unmethylated cytosine residues should be converted to uracil residues by bisulphite treatment and then changed to thymine residues in the PCR step. The 5-methycytosine residues of the dinucleotide CpG would be unaffected by the bisulphite treatment and then changed to cytosine in the PCR step.

The expected PCR products for CGI #1, CGI #2 and CGI #3 for all four cell lines were then carefully cut out, gel purified and then cloned into p-GEM T-EASY vector using the lacZ blue white screen. At least 10 clones of each converted CpG island fragment were sequenced for analysis.

The methylation status of CpG islands was analyzed by BiQ analyzer software, which worked out the methylation status by the following three steps: (a) align the CT converted sequence with the genomic sequence, (b), remove erroneous sequence, such as poor quality sequencing results and wrong sequence according to the input genomic sequence etc, and (c) compile information of the sequence identities relative to the genomic sequence, the sequences' conversion rates, methylation statistics and representation of methylation data. The conversion rates that reflected the bisulphite

treatment efficiency were determined by calculating the C to T conversion rate for cytosine bases not in CpG dinucleotides.

All three CpG islands in the four different cell lines we tested showed very good sequence conversion rates. The substantial majority of clones we sequenced had a conversion rate of 100%, while a few clones had slightly lower rates from 97% to 99%, according to the BiQ analyzer software. More than 90% of the clones were genuine products containing the target CpG island fragment. Therefore there was no negative effect from the bisulfite conversion and cloning procedure in this investigation. The methylation rates of individual CpG sites from different clones were calculated and aggregated representations of methylation data for the whole CpG islands are shown in the Figure 4.5.

As predicted by our hypothesis, CpG island 2, located about 400bp downstream of the putative promoter was fully unmethylated in keratinocytes. There were 17 CpG sites in this island in the mouse keratinocytes and fibroblasts. The CpG sites 8, 16 and 17 were missing in the HM1 and DNMT3^{-} cells because both ES cell lines were derived from a different mouse strain that lacked these sites. In the mouse fibroblasts, where the skin-specific transcript is expressed, CGI #2 showed a very low level of methylation, at the overall rate of less than 4%. Three mouse fibroblast CGI#2 clones didn't have the CpG sites 8, 16 and 17 due to the heterozygosity of the Ercc1 allele. In contrast, the mouse ES cell line HM1 showed a much heavier methylation of the whole CGI #2 region at the overall rate of 52%. The CpG sites 15 and 14 were heavily methylated at the rate of 73%. The methyltransferase deficient ES cell line DNMT3^{-} was fully unmethylated as expected (Figure 4.5.A).

However, the CpG island 1, which had 35 CpG sites and was probably more important than CGI #2 as it covered the whole region of the 2.5kb upstream putative promoter region, showed an increased level of methylation at the beginning (CpG sites 1 to 7) and the middle (CpG sites 20 to 26) in keratinocytes (KER) compared to the other three cell lines. The CpG site 20 was 43bp downstream of the putative TATA box and 20bp downstream of the potential transcription start site. The CpG sites 22, 24 and 25 were 73%, 67% and 64% methylated respectively. At the CpG sites 9, 27 and 29, one clone in fifteen was methylated. In mouse embryonic fibroblasts (PF20), the CGI #1 was predominantly unmethylated while some CpG sites showed a very low methylation rate around 10%. In HM1 mouse ES cells the CGI #1 was generally unmethylated. The CpG sites 7, 14, 17, 19, 30, 31 and 35 showed a weak methylation rate from 23% to 40%. Another two CpG sites 10 and 33 were methylated in one clone of the thirteen. As expected, the CGI #1 of the DNMT3^{-} cell line was also largely unmethylated. However, unexpectedly there were still 4 CpG sites methylated in one or two clones of the eleven sequenced (Figure 4.5.B).

The CpG island 3 located around the normal Ercc1 promoter had 15 CpG sites. The CpG site 10 was missing in mouse keratinocyte and fibroblast cells due to the different sequence between strains (Figure 4.5.C). This island was predominantly unmethylated in all four cell lines tested. There were 2 CpG sites in keratinocytes and one in fibroblasts that showed a very low methylation rate of less than 10%. One clone of the DNMT3- cell line showed a methylation at CpG site 1 as well.

In summary, the methylation status of CpG island 2 fitted our hypothesis with a very low level of methylation in both cell lines (keratinocytes and fibroblasts) showing high levels of the 1.5kb transcript and heavy methylation in the ES cell line (HM1) that expresses predominantly the 1.1kb transcript. However, the hypothesis was not

Figure 4.5 DNA methylation data for CpG islands around the 2.5kb upstream and normal Ercc1 promoter regions.

A. Methylation data for CpG Island 2

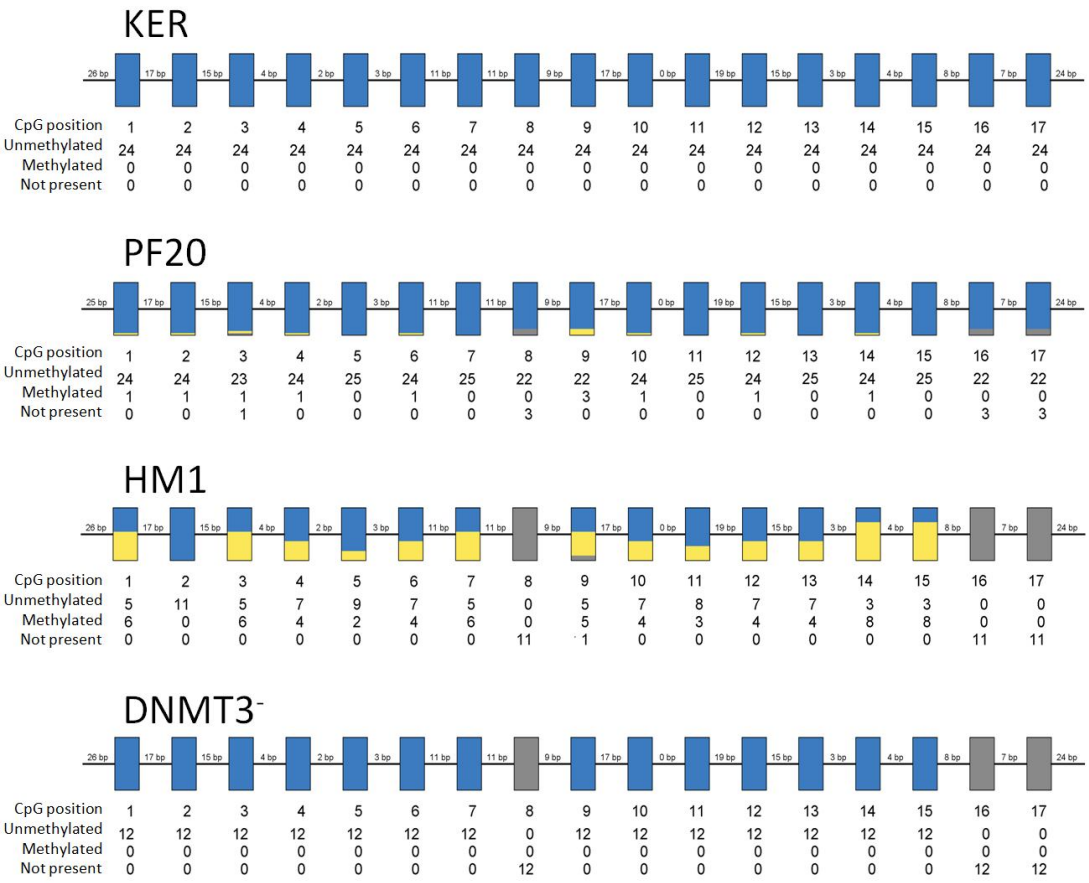

B. Methylation data for CpG Island 1

KER

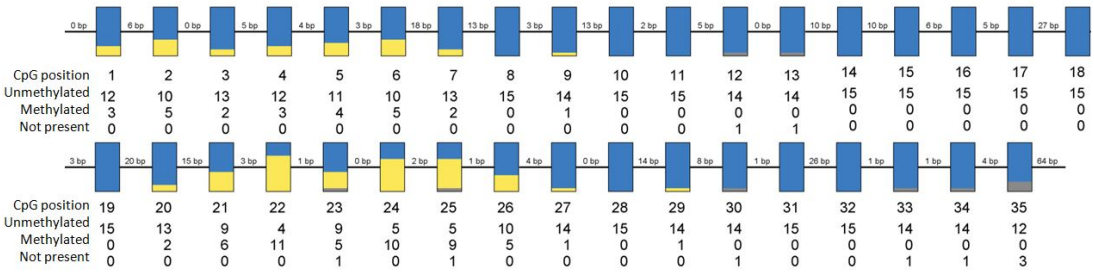

PF20

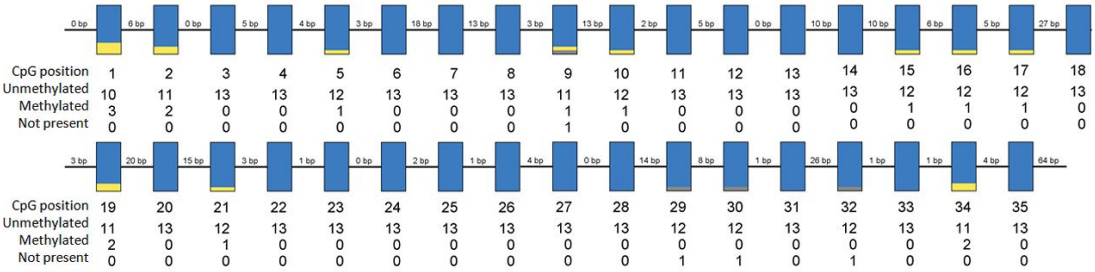

HM1

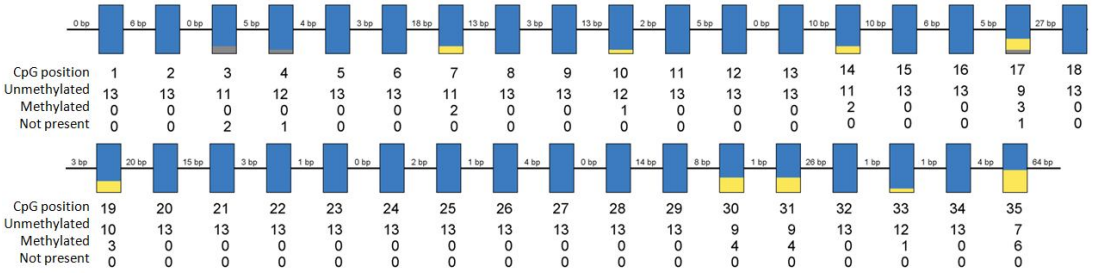

DMNT3-

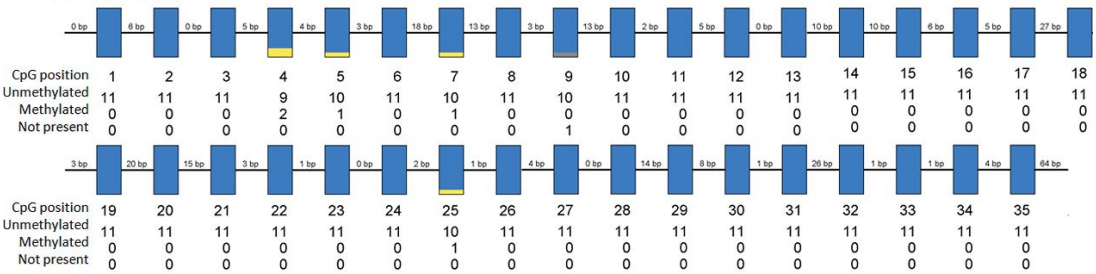

C. Methylation data for CpG Island 3

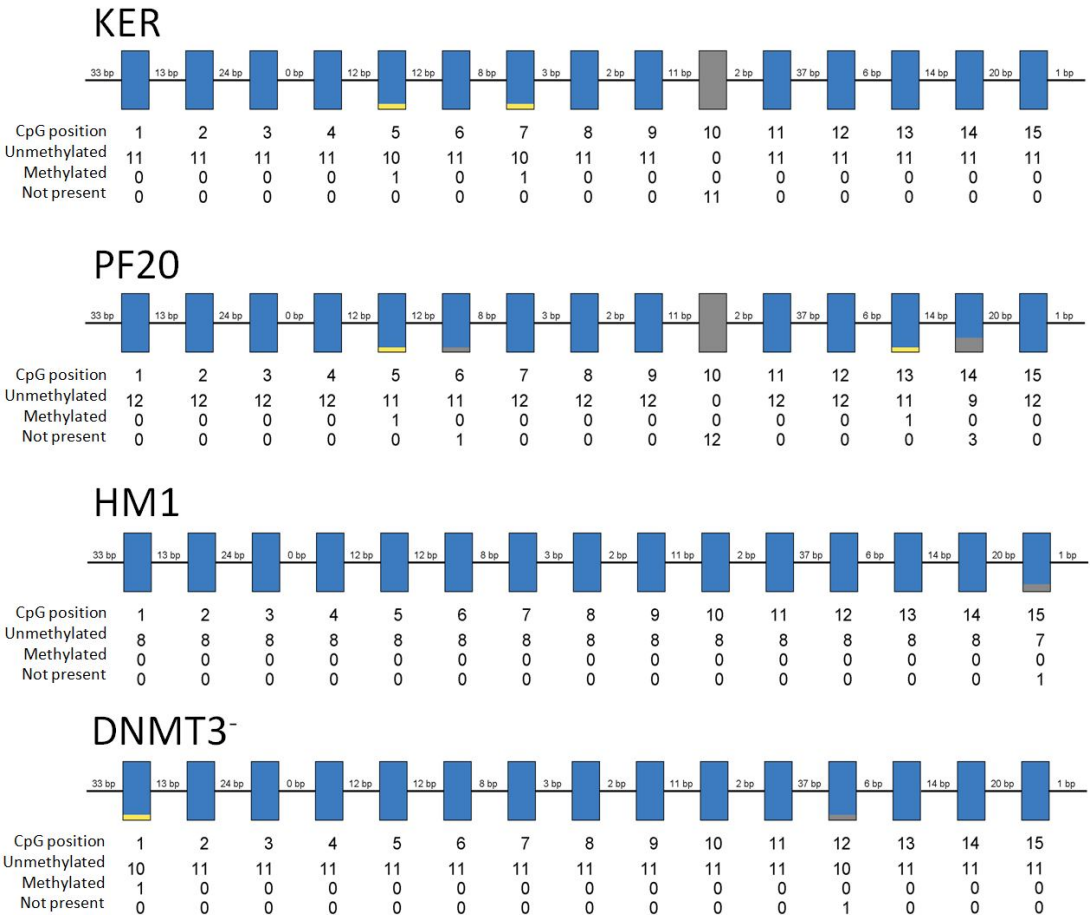

Aggregated representation of methylation data obtained by bisulphite sequencing. Unmethylated CpG positions are indicated in blue. Methylated CpG positions are indicated in yellow. A grey box indicates a CpG position that is not present in a particular cell line. For all cell lines, occasional failure of sequencing of a specific clone to detect a particular CpG position was registered as not present.

supported by the methylation status of CpG island 1, which actually spanned the putative 2.5kb upstream promoter. This, correlated with the failure to find any significant levels of methylation around the normal promoter (CGI #3) in any of the cell lines tested, meant that we had no evidence from the methylation status that the 2.5kb upstream promoter was the source of the 1.5kb Ercc1 transcript.

4.4 Northern blotting to investigate whether the 1.5kb Ercc1 transcript is expressed in DNA methyltransferase 3 deficient ES cells

As described in the previous section, CpG island 2, located about 400bp downstream of the 2.5kb upstream promoter, showed a different methylation pattern between the mouse ES cell line HM1 and keratinocytes. It was heavily methylated in HM1 but fully unmethylated in keratinocytes. Although this island did not span the putative promoter, it could still be involved in regulating expression of the skin-specific Ercc1 transcript. To investigate this possibility, a northern blotting analysis was performed on a panel of cell lines. The aim of the northern was to look at whether the skin-specific transcript could be detected in the methyltransferase deficient mouse ES cell line DNMT3^{-}. As identified by the bisulphite sequencing, the CGI #2 was fully unmethylated in DNMT3^{-}. This was the same pattern as keratinocytes. Therefore if CGI #2 is involved in the regulation of the putative promoter, the larger 1.5kb Ercc1 transcript may be detected in DNMT3^{-} as well as the 1.1kb transcript seen in HM1 cells.

A panel of Ercc1 wild-type and deficient mouse keratinocytes and fibroblasts, ES cell line HM1, methyltransferase deficient ES cell line DNMT3$^-$ and mouse melanocyte cell line Melan A were screened by northern blotting for the 1.5kb Ercc1 transcript (Figure 4.6). Total RNA was freshly isolated from cells, separated by electrophoresis, transferred on to a nylon membrane and the Ercc1 transcript was detected by hybridisation to a mouse Ercc1 cDNA probe.

The ethidium bromide staining of the gel indicates that the loading of RNA was generally well matched. As expected, the skin-specific 1.5kb Ercc1 transcript was present in both Ercc1 wild-type mouse keratinocyte and fibroblast lanes. No bands were detected in the Ercc1 deficient cells. The normal 1.1kb transcript was present in HM1, DNMT3$^-$ and Melan A lanes. No hint of the 1.5kb transcript was detected in the DNMT3$^-$ lane.

Thus, there was no correlation between non-methylation of CpG island 2 and expression of the 1.5kb Ercc1 transcript.

4.5 5' RACE to reinvestigate the origin of the skin-specific Ercc1 transcript

We performed the 5'RACE analysis on mouse keratinocytes to re-investigate and characterise the 5' end of the skin-specific 1.5kb Ercc1 transcript. Previous 5'RACE analysis performed by Dr. Selfridge in 1999 mapped a putative transcriptional start site

Figure 4.6 No evidence for the presence of the 1.5kb novel Ercc1 transcript in the DNA methyltransferase 3 deficient mouse ES cells by northern blotting.

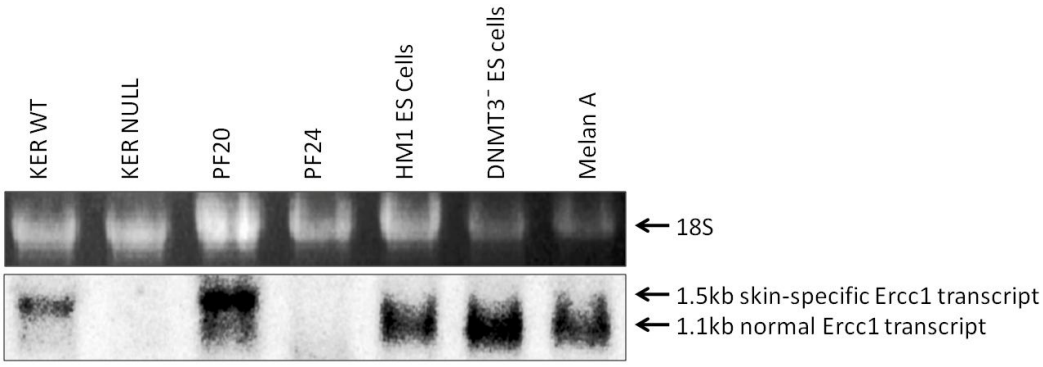

Northern analysis of mouse cell lines with an Ercc1 cDNA probe. Ercc1 wild type and deficient keratinocytes are labelled as KER WT and KER NULL. Ercc1 wild type and deficient mouse embryo fibroblasts are labelled as PF20 and PF24. HM1 is a mouse ES cell line. DNMT3^{-} is the DNA methyltransferase 3 deficient mouse ES cells. Melan A, mouse melanocyte cell line. Upper panel, ethidium bromide staining of the gel with 18S rRNA band indicated. Lower panel, Ercc1 mRNA detection with the 1.5kb and 1.1kb Ercc1 transcripts indicated.

to a position 389nt upstream of the normal start site of mouse Ercc1 (unpublished observations). We repeated the 5'RACE using improved RACE technology to investigate whether this position really corresponded to the beginning of the transcript.

Figure 4.6.A shows a schematic representation of the 5'RACE analysis. The Neo RNA came from the 5'RACE kit and was used as control according to the manufacturer's protocol. PCR product size prediction is shown in Figure 4.6.B. Total RNA was freshly isolated from Balb/C mouse keratinocytes for the 5'RACE.

The first strand cDNA synthesis was carried out using gene specific primers, neo/rev1 for NEO and Ex2b rev for Ercc1 respectively. The synthesised Neo cDNA was amplified using neo3/for in combination with neo2/rev and Ercc1 cDNA was amplified using primers Skin A in combination with Ex2b rev (Figure 4.6.C). PCR products were electrophoresed on a 1.5% agarose gel. Strong bands at the expected position of 157bp in the NEO lane and at 382bp in the keratinocyte lane indicated that the efficiency of first strand cDNA synthesis was good and that there was no contamination from DNA.

The cDNA was then purified using the high pure PCR product purification kit, a homopolymeric A-tail was added to the 3' end and then it was PCR amplified using Oligo-DT anchor primer in combination with gene specific reverse primers: Neo2 for the NEO and Skin RT rev C for Ercc1. The PCR products were then separated by electrophoresis on a 1.5% agarose gel and visualised by ethidium bromide staining (Figure 4.6.D). The NEO control showed a single band at 293bp indicating that the quality of the cDNA synthesis and efficiency of the dA-tailing reaction of the purified cDNA was good. In the Ercc1 cDNA lane, a diffuse band at the position of 600bp and a second weaker band, slightly bigger than 400bp, were detected. The 600bp band in the

Figure 4.6 Re-investigation of the origin of the 1.5kb skin-specific Ercc1 transcript in mouse keratinocytes by 5'RACE.

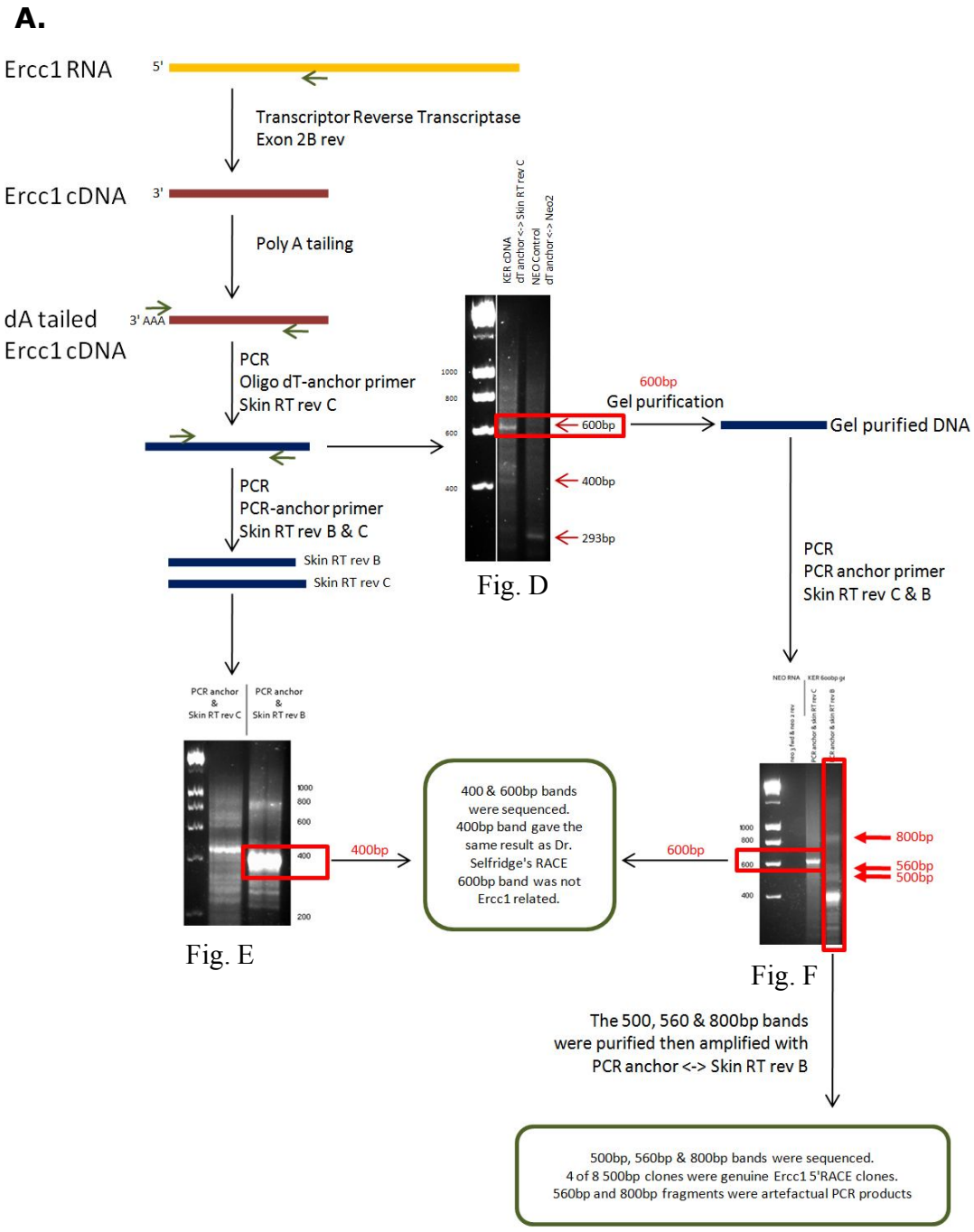

B.

Control of cDNA synthesis

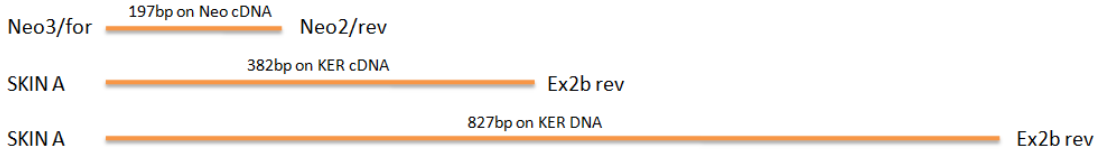

Amplification of dA-tailed cDNA

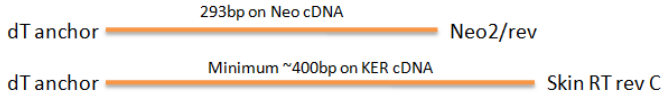

Nested PCRs

C.

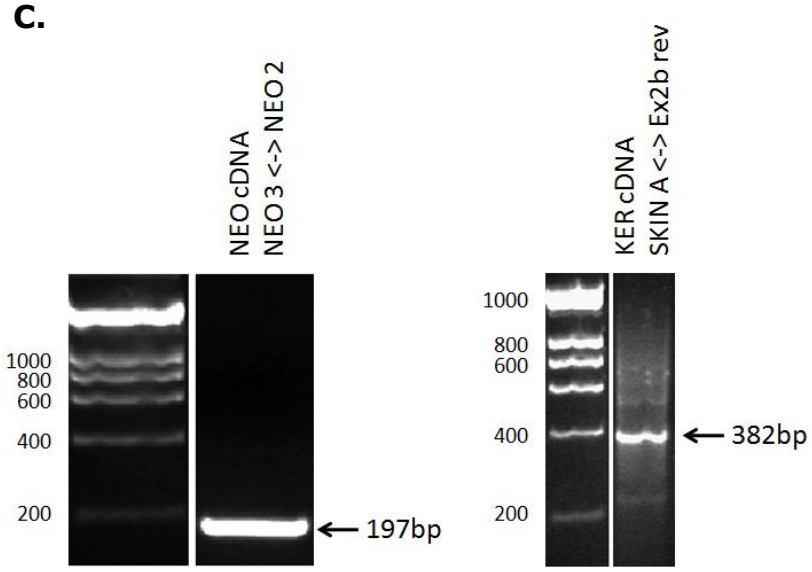

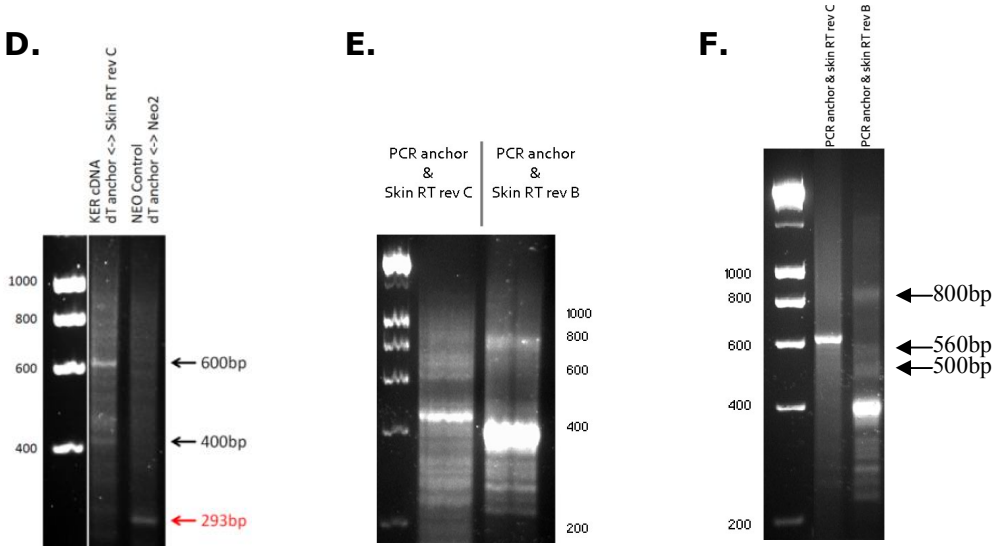
D.
KER cDNA
dT anchor <-> Skin RT rev C
NEO Control
dT anchor <-> Neo2
1000
800
600
400
600bp
400bp
293bp
E.
PCR anchor
&
Skin RT rev C
PCR anchor
&
Skin RT rev B
1000
800
600
400
200
F.
PCR anchor & skin RT rev C
PCR anchor & skin RT rev B
1000
800
600
400
200
800bp
560bp
500bp

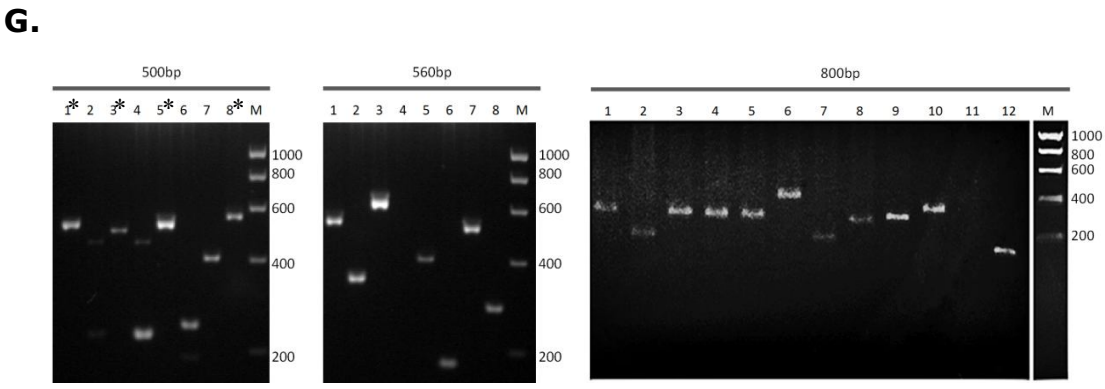
G.
500bp
1* 2 3* 4 5* 6 7 8* M
1000
800
600
400
200
560bp
1 2 3 4 5 6 7 8 M
1000
800
600
400
200
800bp
1 2 3 4 5 6 7 8 9 10 11 12 M
1000
800
600
400
200

A. A schematic representation of the investigation of the potential upstream Ercc1 promoter using 5' RACE.

B. Predicted sizes of different PCR products on control Neo cDNA, mouse keratinocyte cDNA and DNA.

C. After reverse transcription using exon 2B rev primer and addition of a homopolymeric poly(A)-tail, PCR was performed on the first strand cDNA. The Ercc1 cDNA was amplified by forward primer SKIN A and reverse primer Ex2b rev. The control NEO cDNA was amplified by NEO3 and NEO2 according to the manufacturer's protocol. An expected PCR product at the size of 382bp was detected in Ercc1 the cDNA lane. The PCR on control NEO cDNA produced an expected product at the size of 197bp.

D. The tailed Ercc1 cDNA was amplified using OligodT-anchor forward primer and skin RT rev C reverse primer. The PCR product was visualized and the positions of bands at 400bp and 600bp in the mouse keratinocyte track are indicated in black. The expected band generated by dT-Oligo anchor and NEO2 primers at 293bp in the positive control Neo cDNA track is indicated in red.

E. A further round of nested PCR was performed using PCR anchor forward primer and either skin RT rev B or skin RT rev C reverse primers showing two bands of 400bp and 460bp respectively.

F. A further round of nested PCR was performed on the gel purified 600bp PCR product in Fig C. Bands of 600bp were detected from PCR using reverse skin RT rev C. Bands of 400bp, 500bp, 560bp and 800bp were detected from PCR using an internal reverse primer skin RT rev B.

G. Digestion with restriction enzyme EcoR1 on the sequenced plasmids retrieved from purified 500bp, 560bp and 800bp PCR products showing various size inserts. Asterisks indicate clones containing the genuine Ercc1 products from the 500bp PCR product.

keratinocyte lane was cut out, gel purified and analyzed later. Meanwhile, a further round of PCR was carried out using primers PCR-anchor in combination with Skin RT rev C and another internal primer Skin RT rev B. PCR products at about 460bp using Skin RT rev C and 400bp using Skin RT rev B were detected by electrophoresis (Figure 4.6.E). This was unexpected because if Oligo dT-anchor primer with Skin RT rev C generated a product at about 600bp then using primers PCR-anchor with Skin RT rev C should have generated a product only slightly shorter. We gel purified the 400bp fragment produced. Fragments were cloned into p-GEM T-EASY vector by the lacZ blue white screen. 10 positive clones from each fragment were sequenced in order to map the end point of the Ercc1 mRNA in mouse skin. The sequencing analysis of 400bp fragments showed the same result as Dr. Selfridge's previous 5'RACE (Figure 4.8). When the sequence was numbered with the A of the translational start (ATG) being +1, a homopolymeric A-tail added by terminal transferase to the end of the Ercc1 cDNA was detected at nt position around -500. The 5' end sequence was dominated by 150bp of CT repeats. The new 5'RACE result from the 400bp fragment didn't extend any further 5' compared to the old 5'RACE result.

The 600bp fragment from the first round of PCR using Oligo dT-anchor primer in combination with Skin RT rev C was then amplified by a further round of PCR using forward primer PCR-anchor with reverse primers Skin RT rev C and Skin RT rev B. A single clear band at slightly bigger than 600bp was detected in the PCR-anchor with Skin RT rev C lane (Figure 4.6.F). This product should be the same fragment as the 600bp one detected in the first round of PCR as the same primers were used in each reaction. The 600bp band was then gel purified and cloned into p-GEM T-EASY vector using the lacZ blue white screen. 8 positive clones were sequenced and analyzed. The sequencing results showed that this 600bp band was not Ercc1 related. It was just an artificial product containing several fragments from different mouse chromosomes.

The second round of PCR on the gel purified 600bp fragment using PCR-anchor with Skin RT rev B showed several bands. One main abundant band was detected at 400bp. This 400bp product was considered to be the same as the one described before in Figure 4.6.E. Besides the 400bp band, 3 other bigger bands were detected at 500bp, 560bp and 800bp respectively. All these bands were cut out, gel purified and cloned for sequence analysis as described in this section before. The results showed that the 560bp and 800bp fragments were artificial products which contained fragments from other mouse chromosomes fused to Ercc1 sequence. The sequencing results of the 500bp fragments showed that 4 clones of the 8 were genuine Ercc1 5'RACE clones. Sequence analysis of these clones is explained later.

The DNA plasmids expected to contain the 500bp, 560bp and 800bp fragments that we used in sequencing were investigated by restriction enzyme digest to determine the actual inserts sizes (Figure 4.6.G). The digest result showed that most of the inserts were not of the expected size, especially for the 800bp group which contained no fragment at the expected size. We conclude that many of these low abundance PCR products that we were trying to clone were artefactual products generated by multiple rounds of PCR rather than true Ercc1 RACE products.

10 genuine sequences of 5'RACE clones from 400bp, 460bp and 500bp fragments were mapped along with Dr. Selfridge's old RACE result to the 5' flanking sequence of keratinocyte Ercc1 DNA. In the Figure 4.8.A, the longest 5'RACE clone is labelled as "New RACE". All end points from other genuine RACE clones are indicated by a black arrow above this sequence. The translational start site (ATG) is numbered as +1. It was evident that five of the 10 new RACE clones had an end point which was very close to Dr. Selfridge's old RACE end point at -502 nt, within a region of 30nt. Four new RACE clones were 140bp to 240bp shorter compared to Dr. Selfridge's old RACE end point.

Figure 4.8: Sequence analysis of 5'RACE results aligned with Balb/C keratinocyte DNA

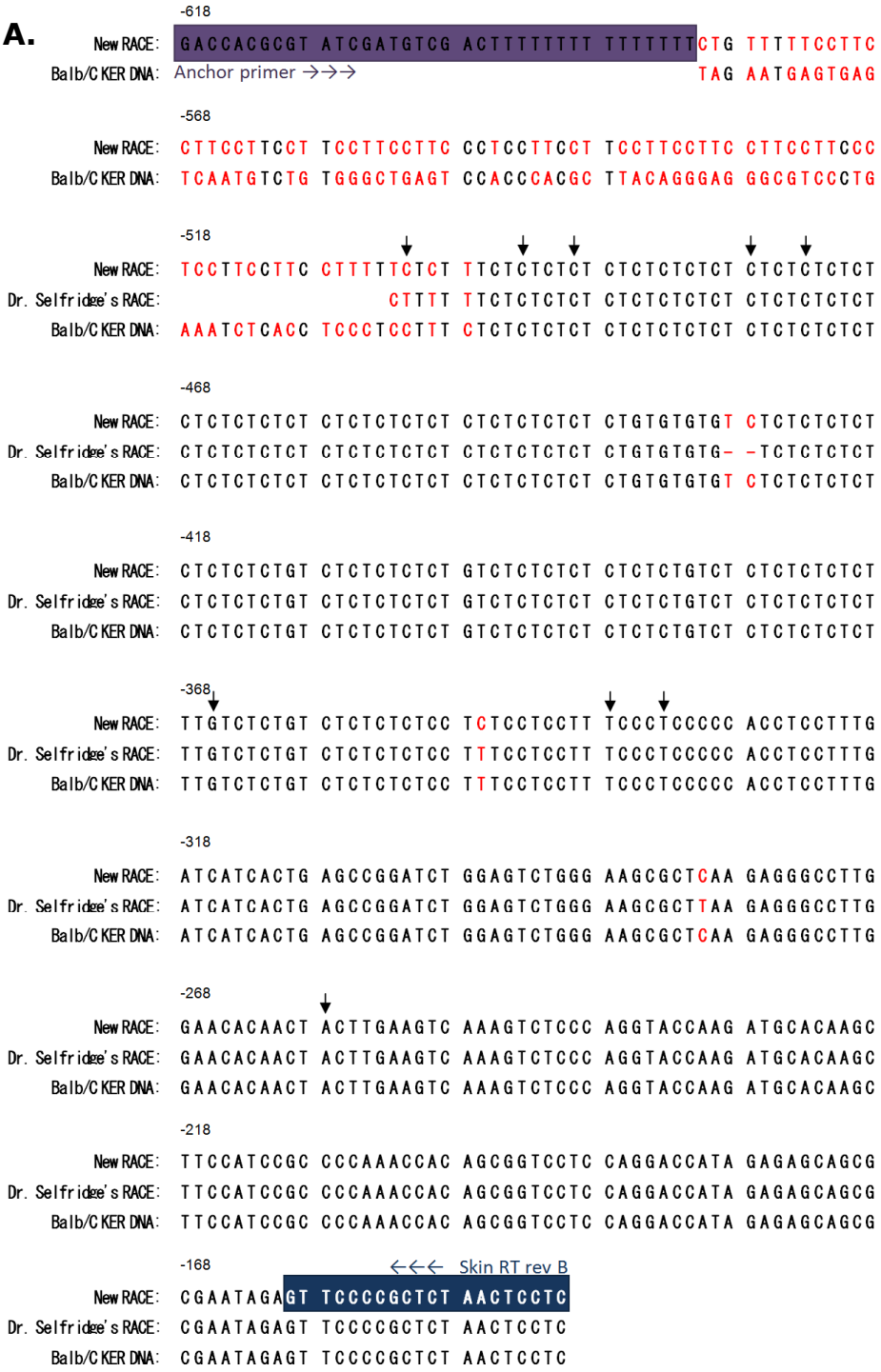

B.

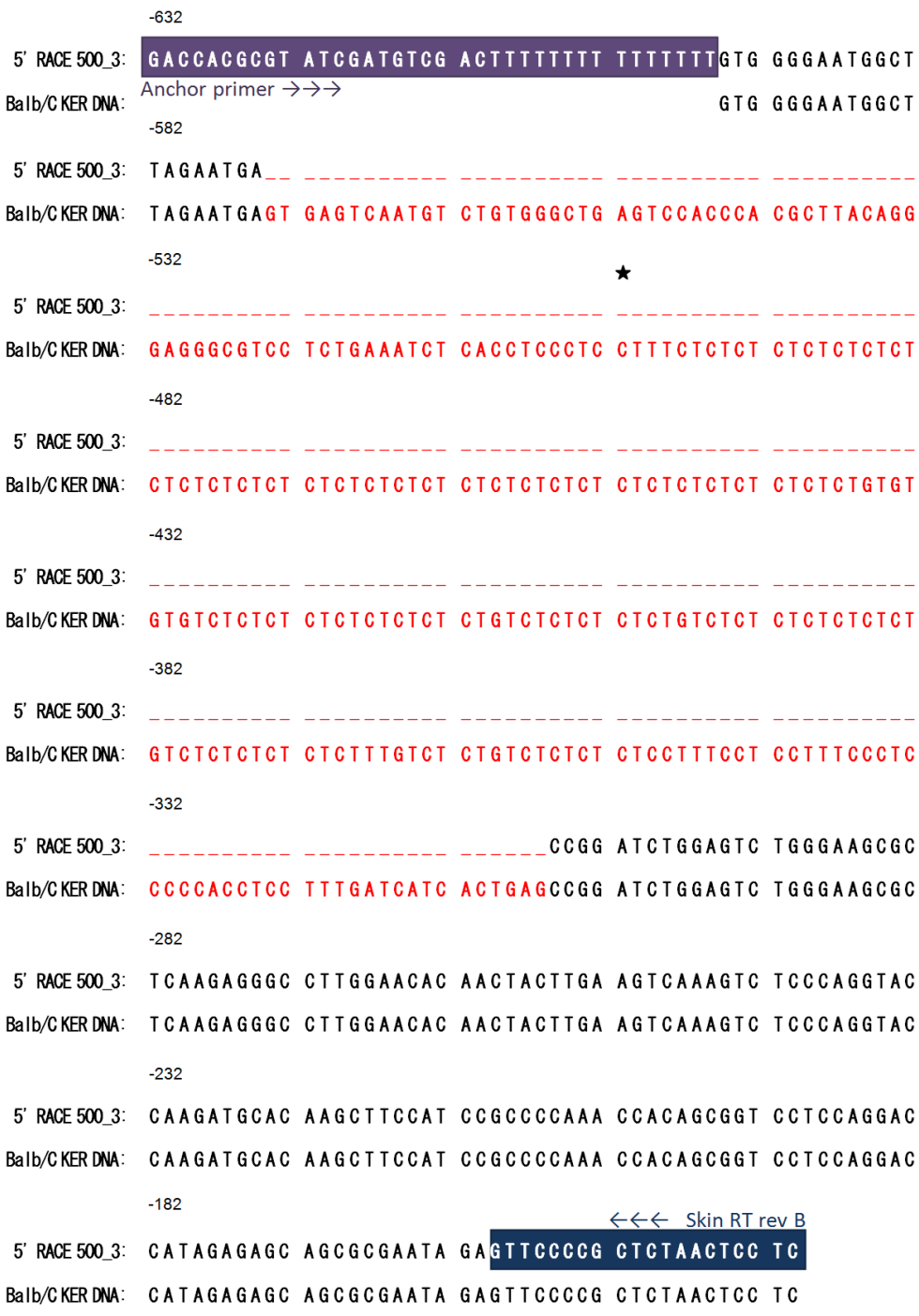
-632
5' RACE 500_3: GACCACGCGT ATCGATGTCG ACTTTTTTTT TTTTTTGTG GGGAATGGCT
Anchor primer →→→
Balb/C KER DNA: GTG GGGAATGGCT
-582
5' RACE 500_3: TAGAATGA__ _____ _____ _____ _____
Balb/C KER DNA: TAGAATGAGT GAGTCAATGT CTGTGGGCTG AGTCCACCCA CGCTTACAGG
-532
5' RACE 500_3: _____ _____ _____ _____ _____
Balb/C KER DNA: GAGGGCGTCC TCTGAAATCT CACCTCCCTC CTTTCTCTCT CTCTCTCTCT
-482
5' RACE 500_3: _____ _____ _____ _____ _____
Balb/C KER DNA: CTCTCTCTCT CTCTCTCTCT CTCTCTCTCT CTCTCTCTCT CTCTCTGTGT
-432
5' RACE 500_3: _____ _____ _____ _____ _____
Balb/C KER DNA: GTGTCTCTCT CTCTCTCTCT CTGTCTCTCT CTCTGTCTCT CTCTCTCTCT
-382
5' RACE 500_3: _____ _____ _____ _____ _____
Balb/C KER DNA: GTCTCTCTCT CTCTTTGTCT CTGTCTCTCT CTCCTTTCCT CCTTTCCCTC
-332
5' RACE 500_3: _____ _____ _____CCGG ATCTGGAGTC TGGGAAGCGC
Balb/C KER DNA: CCCCACCTCC TTTGATCATC ACTGAGCCGG ATCTGGAGTC TGGGAAGCGC
-282
5' RACE 500_3: TCAAGAGGGC CTTGGAACAC AACTACTTGA AGTCAAAGTC TCCCAGGTAC
Balb/C KER DNA: TCAAGAGGGC CTTGGAACAC AACTACTTGA AGTCAAAGTC TCCCAGGTAC
-232
5' RACE 500_3: CAAGATGCAC AAGCTTCCAT CCGCCCCAAA CCACAGCGGT CCTCCAGGAC
Balb/C KER DNA: CAAGATGCAC AAGCTTCCAT CCGCCCCAAA CCACAGCGGT CCTCCAGGAC
-182
←←← Skin RT rev B
5' RACE 500_3: CATAGAGAGC AGCGCGAATA GAGTTCCCCG CTCTAACTCC TC
Balb/C KER DNA: CATAGAGAGC AGCGCGAATA GAGTTCCCCG CTCTAACTCC TC

A. The sequence of the longest new 5'RACE clone determined using mouse keratinocyte RNA, Dr. Selfridge's old Skin 5'RACE result and unpublished keratinocyte DNA sequence from Balb/C mouse strain are aligned using the Invitrogen AlignX software. Identical sequence is indicated in black. Mismatched sequence is indicated in red. The PCR anchor primer and Skin RT rev B primer used in the 5'RACE are labeled with purple and blue boxes respectively. All other end points of shorter genuine new 5'RACE clones are mapped above the "New RACE" sequence by black arrows. The translational start site of mouse Ercc1 is considered as the "+1" base pair.

B. A different 5'RACE result from the 500_3 clone showed a small new exon 482bp upstream of known Ercc1 exon1 and then spliced to 203bp upstream of Ercc1 exon1. Dr. Selfridge's previous 5'RACE end point is indicated with a black asterisk in the figure. The PCR anchor primer and Skin RT rev B primer used in the 5'RACE are labeled with purple and blue boxes respectively. The translational start site of mouse Ercc1 is considered as the "+1" base pair.

The longest 5'RACE clone contained 79bp upstream of the old RACE result. However, this additional sequence did not align with the corresponding Ercc1 DNA sequence, nor did it align with any sequence up to 10kb upstream of the Ercc1 gene. Blast search using National Center for Biotechnology Information (NCBI) BLAST programme reported that there was no significant similarity found in the mouse genome to this additional sequence (Ye et al. 2006). There was no evidence for an acceptor splice site at the junction between the genuine 5' Ercc1 sequence and the extra sequence either.

Therefore, we considered the longest RACE clone to be another spurious artefactual PCR product. Thus, the new RACE result confirmed our old 5'RACE results and identified that the 5' end of the Ercc1 mDNA in mouse skin was at nt position 502, 382 nt upstream of the normal transcriptional start site. The alignment between the RACE result and 5' flanking sequence of Ercc1 in keratinocytes was perfectly matched, except for a single base mismatch at nt position -347. In the new RACE clone the nt at this position was a C, compared with a T in the keratinocyte DNA sequence.

There was another 5'RACE clone from the 500bp fragment that showed a very interesting result (Figure 4.8.B). This clone was labelled as "500_3" and aligned with keratinocyte DNA. A new short 21nt exon was detected in this clone from nt position -595 to -574 and 47bp upstream of the previous RACE end point. The sequence was then spliced into nt position -307 and continued to the known exon 1. Note that although this clone had a more 5' start point than the other RACE clones, the presence of the intron meant that it would only contain 217 nt upstream of the normal transcriptional start site, compared to 382 nt for the consensus RACE end point. There was only one clone detected to have this variant splice pattern in all tested 5'RACE clones.

Figure 4.9 Sequence alignment of the region 5' of the normal Ercc1 promoter region among Balb/C, 129/Ola and C57BL/6 strains.

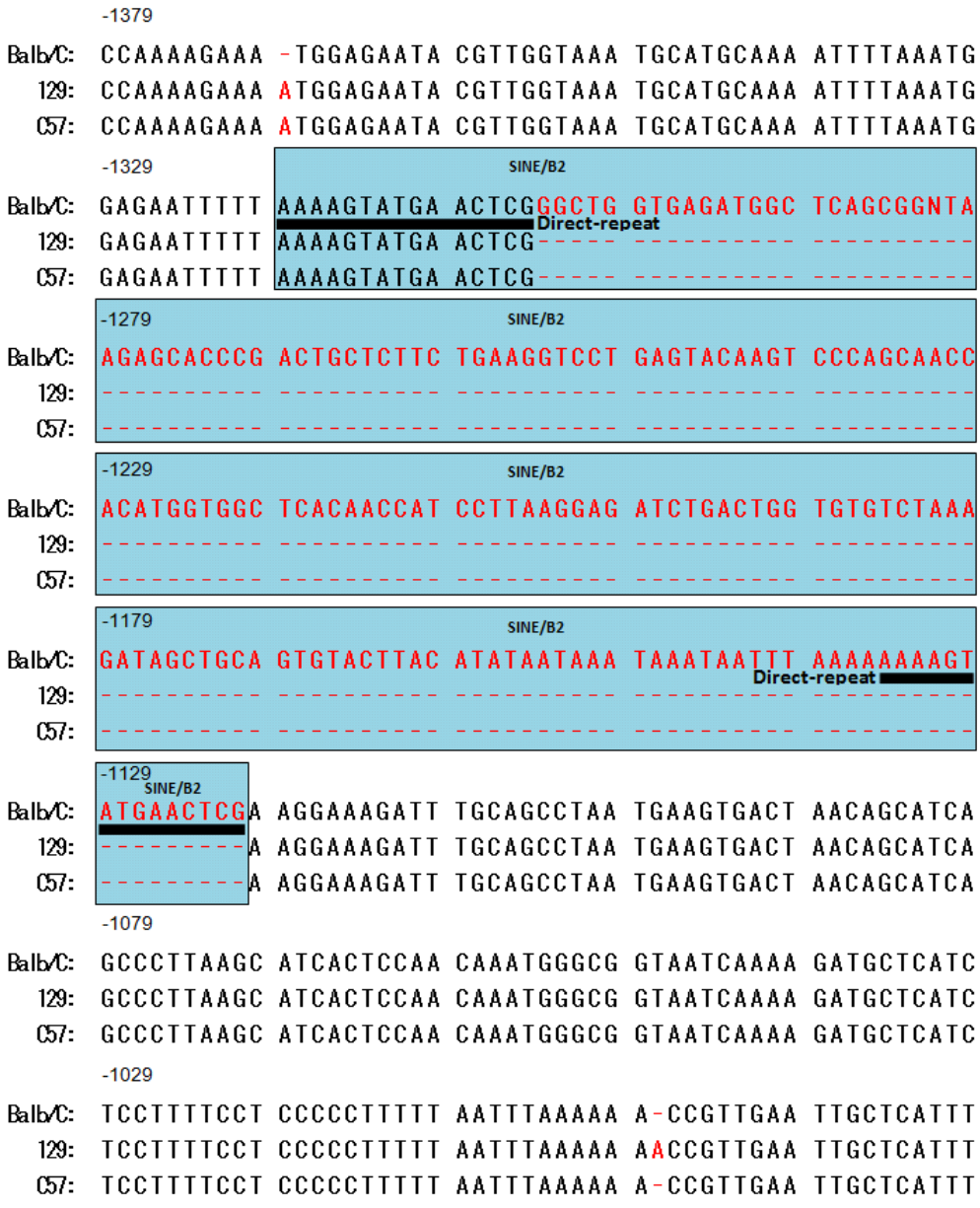

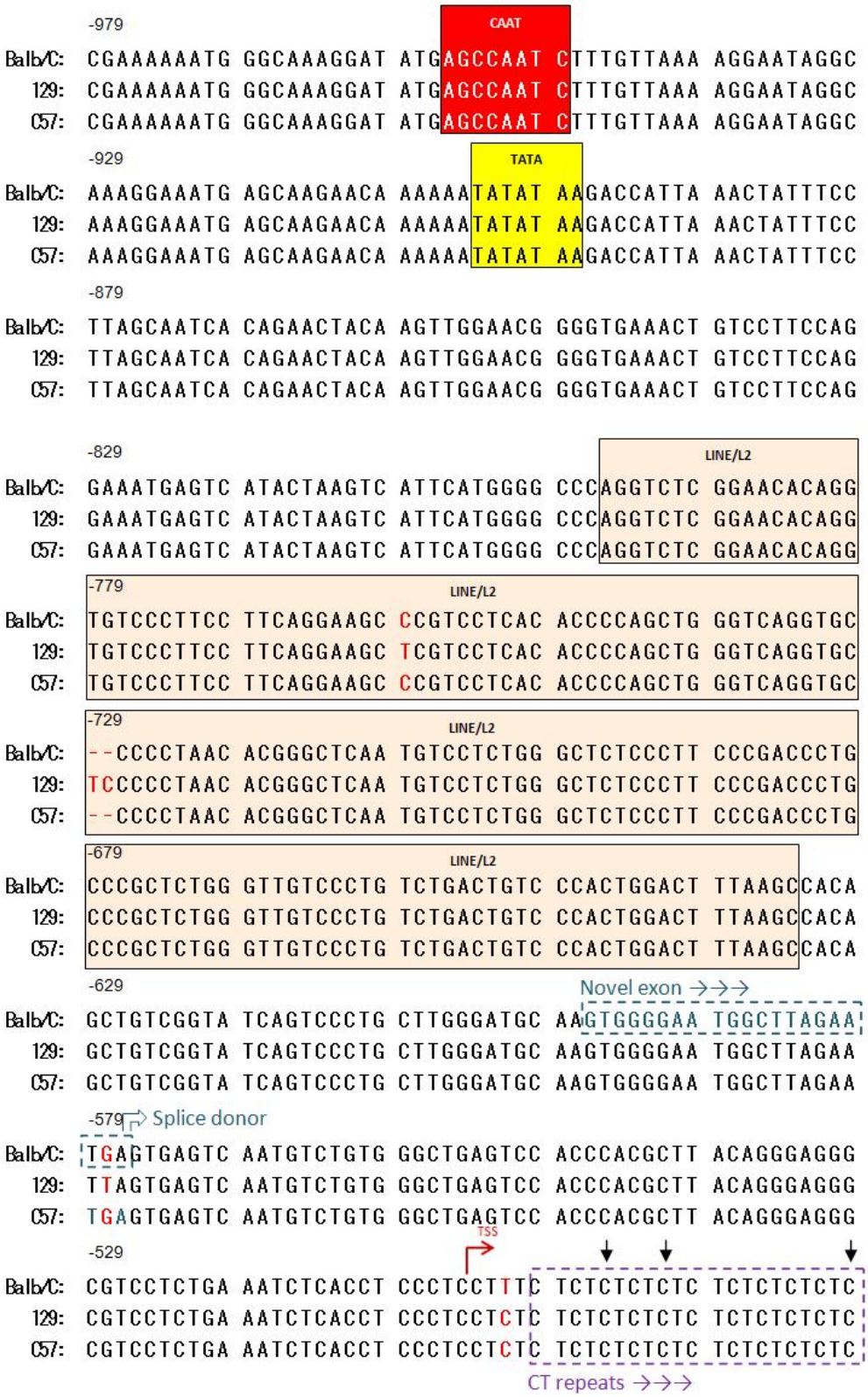
-979
CAAT
Balb⁄C: CGAAAAAATG GGCAAAGGAT ATGAGCCAAT CTTTGTTAAA AGGAATAGGC
129: CGAAAAAATG GGCAAAGGAT ATGAGCCAAT CTTTGTTAAA AGGAATAGGC
C57: CGAAAAAATG GGCAAAGGAT ATGAGCCAAT CTTTGTTAAA AGGAATAGGC
-929
TATA
Balb⁄C: AAAGGAAATG AGCAAGAACA AAAAATATAT AAGACCATTA AACTATTTCC
129: AAAGGAAATG AGCAAGAACA AAAAATATAT AAGACCATTA AACTATTTCC
C57: AAAGGAAATG AGCAAGAACA AAAAATATAT AAGACCATTA AACTATTTCC
-879
Balb⁄C: TTAGCAATCA CAGAACTACA AGTTGGAACG GGGTGAAACT GTCCTTCCAG
129: TTAGCAATCA CAGAACTACA AGTTGGAACG GGGTGAAACT GTCCTTCCAG
C57: TTAGCAATCA CAGAACTACA AGTTGGAACG GGGTGAAACT GTCCTTCCAG
-829
LINE/L2
Balb⁄C: GAAATGAGTC ATACTAAGTC ATTCATGGGG CCCAGGTCTC GGAACACAGG
129: GAAATGAGTC ATACTAAGTC ATTCATGGGG CCCAGGTCTC GGAACACAGG
C57: GAAATGAGTC ATACTAAGTC ATTCATGGGG CCCAGGTCTC GGAACACAGG
-779
LINE/L2
Balb⁄C: TGTCCCTTCC TTCAGGAAGC CCGTCCTCAC ACCCCAGCTG GGTCAGGTGC
129: TGTCCCTTCC TTCAGGAAGC TCGTCCTCAC ACCCCAGCTG GGTCAGGTGC
C57: TGTCCCTTCC TTCAGGAAGC CCGTCCTCAC ACCCCAGCTG GGTCAGGTGC
-729
LINE/L2
Balb⁄C: --CCCCTAAC ACGGGCTCAA TGTCCTCTGG GCTCTCCCTT CCCGACCCTG
129: TCCCCCTAAC ACGGGCTCAA TGTCCTCTGG GCTCTCCCTT CCCGACCCTG
C57: --CCCCTAAC ACGGGCTCAA TGTCCTCTGG GCTCTCCCTT CCCGACCCTG
-679
LINE/L2
Balb⁄C: CCCGCTCTGG GTTGTCCCTG TCTGACTGTC CCACTGGACT TTAAGCCACA
129: CCCGCTCTGG GTTGTCCCTG TCTGACTGTC CCACTGGACT TTAAGCCACA
C57: CCCGCTCTGG GTTGTCCCTG TCTGACTGTC CCACTGGACT TTAAGCCACA
-629
Novel exon →→→
Balb⁄C: GCTGTCGGTA TCAGTCCCTG CTTGGGATGC AAGTGGGGAA TGGCTTAGAA
129: GCTGTCGGTA TCAGTCCCTG CTTGGGATGC AAGTGGGGAA TGGCTTAGAA
C57: GCTGTCGGTA TCAGTCCCTG CTTGGGATGC AAGTGGGGAA TGGCTTAGAA
-579
Splice donor
Balb⁄C: TGAGTGAGTC AATGTCTGTG GGCTGAGTCC ACCCACGCTT ACAGGGAGGG
129: TTAGTGAGTC AATGTCTGTG GGCTGAGTCC ACCCACGCTT ACAGGGAGGG
C57: TGAGTGAGTC AATGTCTGTG GGCTGAGTCC ACCCACGCTT ACAGGGAGGG
TSS
-529
Balb⁄C: CGTCCTCTGA AATCTCACCT CCCTCCTTTC TCTCTCTCTC TCTCTCTCTC
129: CGTCCTCTGA AATCTCACCT CCCTCCTCTC TCTCTCTCTC TCTCTCTCTC
C57: CGTCCTCTGA AATCTCACCT CCCTCCTCTC TCTCTCTCTC TCTCTCTCTC
CT repeats →→→


-479
Balb/C: TCTCTCTCTC TCTCTCTCTC TCTCTCTCTC TCTCTCTCTC TGTGTGTGTC
129: TCTCTCTCTC TCTCTCTCTC TCTCTCTCTC TCTCTCTC-- ----------
C57: TGTCTCTCTC TCTCTTCTC TCTCTCTCTC TCTCTCTCTC TGTGTGTGTC
-429
Balb/C: TCTCTCTCTC TCTCTCTGTC TCTCTCTCTG TCTCTCTCTC TCTCTGTCTC
129: ---------- ---------- ---------- ---------- ----------
C57: ---------- ---------- ---------- ---------- ----------
-379
Balb/C: TCTCTCTCTT TGTCTCTGTC TCTCTCTCCT TTCCTCCTTT CCCTCCCCCA
129: ---------- --TCTCTGTC TCTCTCTCCT TTCCTCCTTT CCCTCCCCCA
C57: ---------- -GTCTCTGTC TCTCTCTCCT TTCCTCCTTT CCCTCCCCCA
-329
Splice accepter
Balb/C: CCTCCTTTGA TCATCACTGA GCCGGATCTG GAGTCTGGGA AGCGCTCAAG
129: CCTCCTTTGA TCATCACTGA GCCGGATCTG GAGTCTGGGA AGCGCTCAAG
C57: CCTCCTTTGA TCATCACTGA GCCGGATCTG GAGTCTGGGA AGCGCTCAAG
-279
Balb/C: AGGGCCTTGG AACACAACTA CTTGAAGTCA AAGTCTCCCA GGTACCAAGA
129: AGGGCCTTGG AACACAACTA CTTGAAGTCA AAGTCTCCCA GGTACCAAGA
C57: AGGGCCTTGG AACACAACTA CTTGAAGTCA AAGTCTCCCA GGTACCAAGA
-229
Balb/C: TGCACAAGC TTCCATCCGC CCCAAACCAC AGCGGTCCTC CAGGACCATAG
129: TGCACAAGC TTCCATCCGC CCCAAACCAC AGCGGTCCTC CAGGACCATAG
C57: TGCACAAGC TTCCATCCGC CCCAAACCAC AGCGGTCCTC CAGGACCATAG
-179
Balb/C: AGAGCAGCG CGAATAGAGT TCCCCGCTCT AACTCCTCCG GGGAGCAGCGA
129: AGAGCAGCG CGAATAGAGT TCCCCGCTCT AACTCCTCCG GGGAGCAGCGA
C57: AGAGCAGCG CGAATAGAGT TCCCCGCTCT AACTCCTCCG GGGAGCAGCGA
TSS
-129
Balb/C: GACGAGCGA AGGGCCAGAG CGGCCGGAAG TGAGTCTAGC AGGAGTTGTGC
129: GACGAGCGA AGGGCCAGAG -GGCCGGAAG TGAGTCTAGC AGGAGTTGTGC
C57: GACGAGCGA AGGGCCAGAG CGGCCGGAAG TGAGTCTAGC AGGAGTTGTGC
-79
Ercc1 exon 1 →→→
Balb/C: TGGCTGTGC TGGCGTTGTG TCGCCTCTGT TTCCCCCCGT GGTATTTCCTT
129: TGGCTGTGC TGGCGTTGTG TCGCCTCTGT TTCCCCCCGT GGTATTTCCTT
C57: TGGCTGTGC TGGCGTTGTG TCGCCTCTGT TTCCCCCCGT GGTATTTCCTT
-29
+1
Balb/C: CTAGGCATC GGGAAAGACC AGGCCCCAGA TGGACCC
129: CTAGGCATC GGGAAAGACC AGGCCCCAGA TGGACCC
C57: CTAGGCATC GGGAAAGACC AGGCCCCAGA TGGACCC
Ercc1 exon 2 →→→

Sequence alignment of 129/Ola, C57BL/6 and Balb/C DNA for the Ercc1 flanking region. Identical sequence is indicated in black. Mismatched sequence is indicated in red. CT repeats are labelled with purple frame. Ercc1 exons are labelled with green frame with Ercc1 intron omitted. The end points of the 5'RACE are indicated by black arrows. Novel exon detected by RACE is labelled in blue frames. Potential transcriptional start site, normal transcriptional start site, splice donor and acceptor are all labelled above the sequence. The translational start site of mouse Ercc1 is considered as the "+1" base pair. Sequence elements: direct-repeat (dark underline), SINE/B2 (light blue boxes), LINE/L2 (light orange boxes), TATA signal (yellow box) and CAAT signal (red box) are indicated.

We further analyzed the 5' flanking sequence of the mouse Ercc1 gene. About 1.3kb of sequence from albino strain (Balb/C), the source of the keratinocytes used for the RACE determination, and pigmented strains (129/Ola and C57BL/6) were aligned together and properly labelled with the upstream and normal transcriptional start site, the 5'RACE end points and known exons (Figue 4.9). The translational start site (ATG) is numbered as +1.

There were two main differences between Balb/C and the pigmented strains. Firstly, the presence of an extra 185bp in Balb/C, around 1kb upstream of the normal Ercc1 transcriptional start site, that was not present in the pigmented strains. The sequence was analyzed using RepeatMasking (http://www.repeatmasker.org/) and this service indicated that the 185bp extra sequence in Balb/C was a SINE/B2 element. Secondly, a CT repeat region immediately downstream of the upstream transcriptional start site was longer in Balb/C (174bp) than in pigmented 129/Ola (78bp) and C57BL/6 (58bp) strains. A potential TATA box was found at the nt position -904, which was about 400bp 5' of the RACE end point. A potential CAAT box was found 52bp upstream of the TATA box. The LINE/L2 element was detected in all three tested strains and was located between the TATA box and CT repeats.

The potential promoter activity of this region in the three strains was analysed using the McPromoter programme, which is a program aiming at the exact localization of eukaryotic RNA polymerase II transcription start sites (http://tools.genome.duke.edu/generegulation/McPromoter/). To better understand how this programme worked, we first tested a well-studied promoter, the mouse ß-globin gene. The ß-globin gene has a classical promoter at the size of approximately 200bp located immediately upstream of its exon 1. Classical promoter elements like the CAAT box and TATA box were found within this region (Grosveld et al. 1981; Grosveld et al. 1982). Up to 800bp of 5'

sequence of the mouse ß-globin gene plus its exon 1 sequence was analysed by the McPromoter programme. The McPromoter promoter activity curve was then aligned with the ß-globin sequence (Figure 4.10.A). The promoter activity was generally less than 0 before the promoter region, but then peaked over the promoter region itself with the highest score of 0.02 at the TATA box.

After that we tested potential promoter activity of the Ercc1 gene in Balb/C, C57BL/6 and 129/Ola mouse strains (Figure 4.10.B, C and D). For Ercc1 in all three strains there were peaks at the normal transcriptional start site and the region immediately downstream of CT repeats. Troughs associated with the CT repeats themselves were detected in all three strains. There was no strong peak associated with CAAT/TATA or LINE/LE region in all three strains. However, in Balb/C there was a strong peak around the SINE/B2 element that was not present in the other two strains.

4.6 Discussion

To understand the mechanism of transcriptional regulation of Ercc1, it is essential to identify and characterize its promoter. The genomic structure of Ercc1 has been characterized in human and mouse and the promoter region, just at the 5' side of exon 1 is characterized by the absence of classical promoter elements, such as TATA and CAAT boxes (van Duin et al. 1987; van Duin et al. 1988). However, transcript analysis of human ERCC1 ESTs revealed a 5' variant containing a differentially spliced exon 1 (genebank association number: BG333187), which spans the entire previously characterized promoter region in human suggesting that at least some Ercc1 transcripts

may initiate further upstream (Wilson et al. 2001). Our group also identified a novel larger 1.5kb Ercc1 transcript in mouse skin, which is due to initiation of transcription upstream of the normal transcription start site (unpublished observations). These results suggest that there should be another Ercc1 promoter upstream of the normal promoter and additional upstream elements could play a key role in Ercc1 expression in both human and mouse.

We have investigated two computer predicted putative 11kb and 2.5kb upstream Ercc1 promoters in mouse but could not find any evidence to support their activity. RT-PCR assays were performed to detect activity from both putative promoters. We did not get any positive result but more primers should be tried. The splice pattern might be different from the computer prediction so the novel primers designed to be in the putative exons might actually be skipped by splicing. As our 5'RACE result is very close to the 5' end of the mouse Ercc1 transcript in skin as determined by northern analysis, if other further upstream novel exon(s) exist then their size should be very small. Thus it is very difficult to design new primers to identify such exon(s) because of the limited sequence. In addition, the putative promoters are in a highly GC-rich region that makes new primer design very difficult.

The 11kb upstream putative promoter has now been removed from the *Ensembl Genscan* website, which suggests a lower possibility of it being a real promoter. The 2.5kb upstream putative promoter, which is 5kb upstream in human, could still be interesting as it is highly conserved between mouse and human, as well as containing classical promoter elements (Wilson et al. 2001). It has been suggested that the lower than normal ERCC1 expression obtaining by placing the strong SV40 promoter in front of ERCC1 cDNA might indicate the synergistical regulation of ERCC1 expression by a combination of the 5kb upstream region and the normal ERCC1 promoter (van Duin et al. 1987; Wilson et al. 2001). Although there is no evidence for the activity of either of

Figure 4.10 Alignment of sequence elements and promoter activities in 129/Ola, C57BL/6 and Balb/C.

Promoter activities predicted by McPromoter are shown as a red curve. The McPromoter output is shown as the vertical axis. The McPromoter output is aligned with the DNA sequence elements which are shown underneath.

A. Alignment of sequence elements and promoter activities of the mouse ß-globin gene. The reported promoter is indicated as a bold blue arrow. TATA signal and CAAT signal are labelled with yellow and red squares. Exon 1 is indicated as a green box.

B, C, D. Alignment of sequence elements and promoter activities of mouse Ercc1 gene in 129/Ola, C57BL/6 and Balb/C. SINE/B2, LINE/L2, CTs and exons are indicated as blue, orange, purple and green boxes, respectively. The 5' end of the analyzed sequences are indicated in red pentagon boxes. TATA signal and CAAT signal are labelled with yellow and red squares.

A.

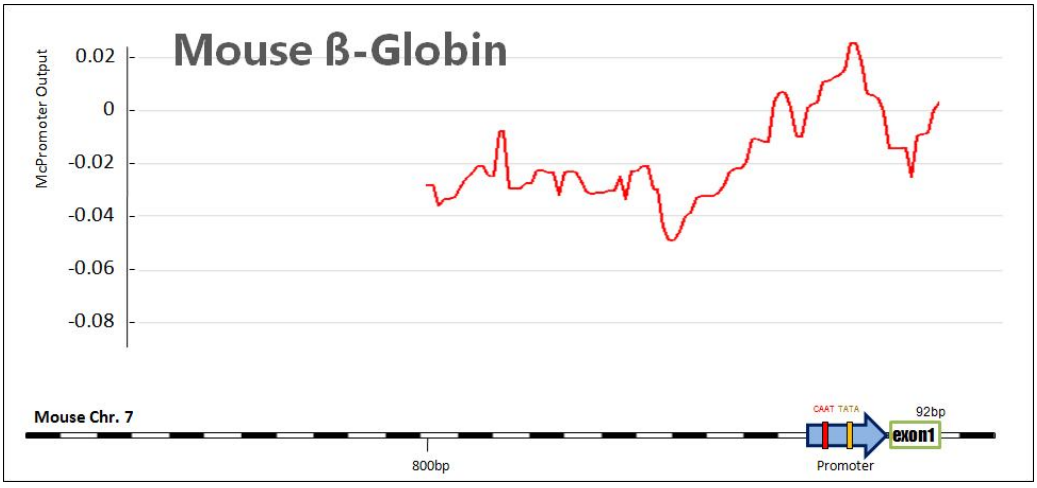

B.

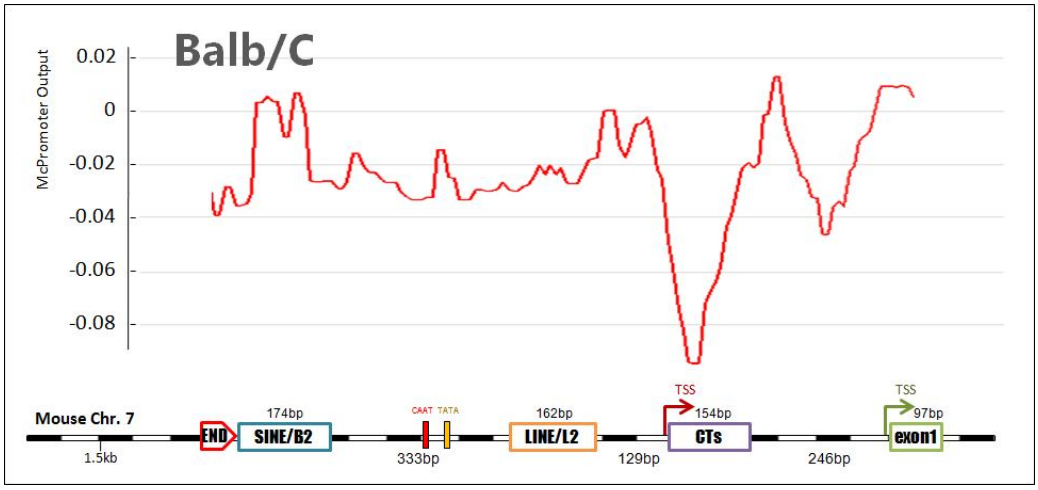
Balb/C
McPromoter Output
0.02
0
-0.02
-0.04
-0.06
-0.08
Mouse Chr. 7
1.5kb
END
174bp
SINE/B2
CAAT TATA
333bp
162bp
LINE/L2
TSS
154bp
129bp
CTs
TSS
97bp
246bp
exon1

C.

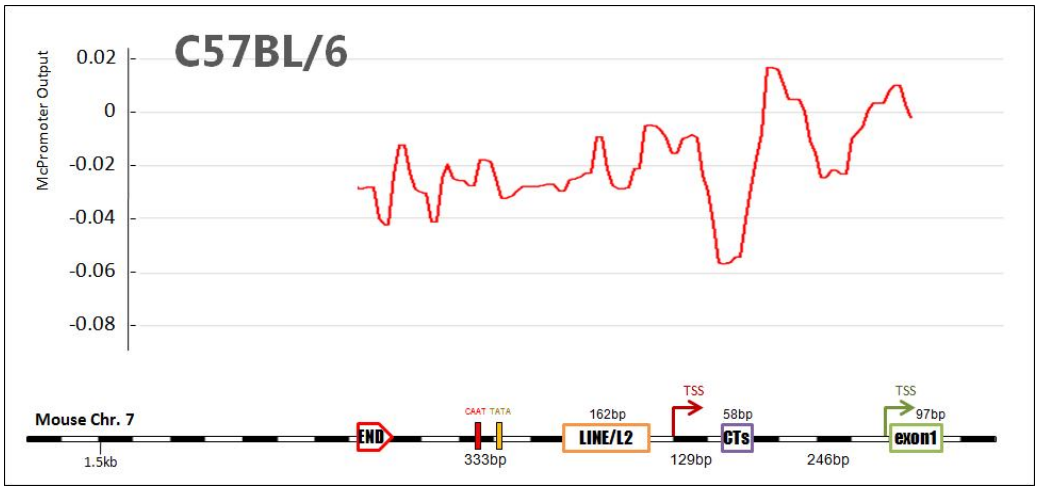
C57BL/6
McPromoter Output
0.02
0
-0.02
-0.04
-0.06
-0.08
Mouse Chr. 7
1.5kb
END
CAAT TATA
333bp
162bp
LINE/L2
TSS
58bp
129bp
CTs
TSS
97bp
246bp
exon1

D.

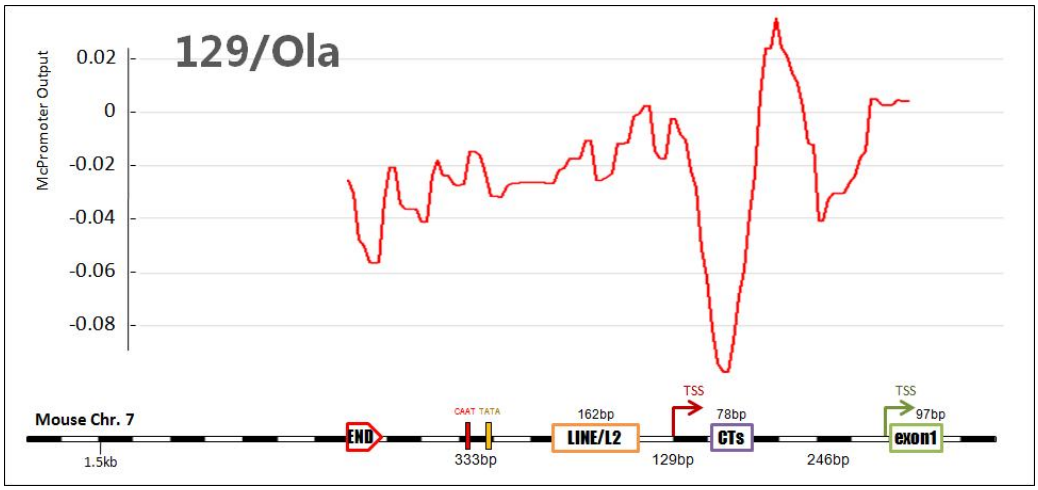
129/Ola
McPromoter Output
0.02
0
-0.02
-0.04
-0.06
-0.08
Mouse Chr. 7
1.5kb
END
CAAT TATA
333bp
162bp
LINE/L2
TSS
78bp
129bp
CTs
TSS
97bp
246bp
exon1

the upstream promoters in mouse from our study, further investigation of this putative promoter in human would be worthwhile.

A new genomic perspective of the Ercc1 gene reported that the region approximately 1kb to the 5' side of the known promoter was also conserved between human and mouse. This region contains transposable elements (TEs) LINE/L1 and LINE/L2, as well as the classical regulatory elements, CAAT and TATA boxes (Wilson et al. 2001). Transposable elements (TEs) are sequences of DNA that move from one location in the genome to another (Kidwell 2005). Recently these mobile elements were reported to be possibly involved in endogenous gene regulation, determining which genes are turned on and when this activation takes place (Pennisi 2007). The CAAT signal is considered to be the binding site for an RNA Pol II transcription factor and is normally located 75-80 bases upstream of the transcription initiation site. The TATA signal is normally bound by the TATA Binding Protein (TBP) in the process of transcription. Therefore this 1kb 5' region might play some kind of regulatory role in Ercc1 expression.

We investigated the sequence 5' of the normal Ercc1 promoter region between the albino and pigmented strains. The CAAT signal, TATA signal, LINE/L2 element and CT repeats were found from 264bp to 841bp upstream of the normal promoter in all investigated strains. The CAAT box was found 52bp upstream of the TATA box. Interestingly in the albino Balb/C strain only, beside these above regulatory elements, we found a SINE/B2 element 1023bp upstream of the normal promoter, which is about 300bp to the 5' side of the CAAT signal. The SINE/B2 element is reported to provide mobile RNA polymerase II promoters and is responsible for the production of the endogenous laminin alpha (Lama3) transcript in mouse (Ferrigno et al. 2001). Analysis among 20,193 gene promoter regions indicated that TEs have a big potential to influence gene regulation at the genomic scale by carrying potential transcription regulating

signals. When inserted in promoter regions, they can alter gene expression patterns by contributing transcription factor binding sites previously not present in promoters of specific genes (Thornburg et al. 2006). Therefore it is possible that the insertion of this SINE/B2 element could be involved in the altered Ercc1 gene expression between albino strains and pigmented strains. As the 1.5kb Ercc1 transcript is highly expressed in albino strains but not in pigmented strains, and the SINE/B2 element as well as the CT repeats are the only major differences in the 5' flanking sequence between the different mouse strains examined, it is proposed that the SINE/B2 element may interact with downstream elements to regulate the expression of this 1.5kb Ercc1 transcript synergistically. This hypothesis is also in agreement with the promoter activity prediction which shows an increased activity at the position of the SINE/B2 element in the Balb/C strain.

In previous experiments carried out after the skin-specific Ercc1 mRNA was discovered, but before the correlation between this transcript and mouse strain was understood, a previous postgraduate student, Yvonne Simpson (unpublished observations), had studied the expression of an Ercc1 minigene constructed by Dr Jim Selfridge (unpublished observations). This minigene, shown schematically in Figure 4.11.A, contained the normal Ercc1 promoter region and upstream sequence from strain 129Ola DNA shown in Figure 4.9. When transfected into Ercc1 deficient mouse keratinocytes it conferred UV resistance. RT-PCR analysis using primer pairs to detect skin-specific Ercc1 transcripts and all Ercc1 transcripts indicated that pooled keratinocyte clones containing the correcting Ercc1 minigene showed the same pattern of Ercc1 initiation as wild type keratinocytes (Figure 4.11.B). This suggests that this promoter region was capable of directing expression of the skin-specific Ercc1 transcript in this transfection assay in cultured keratinocytes despite lacking the SINE element that appears to be important for high level expression of this transcript in skin.

Figure 4.11: Structure and expression of an Ercc1 minigene

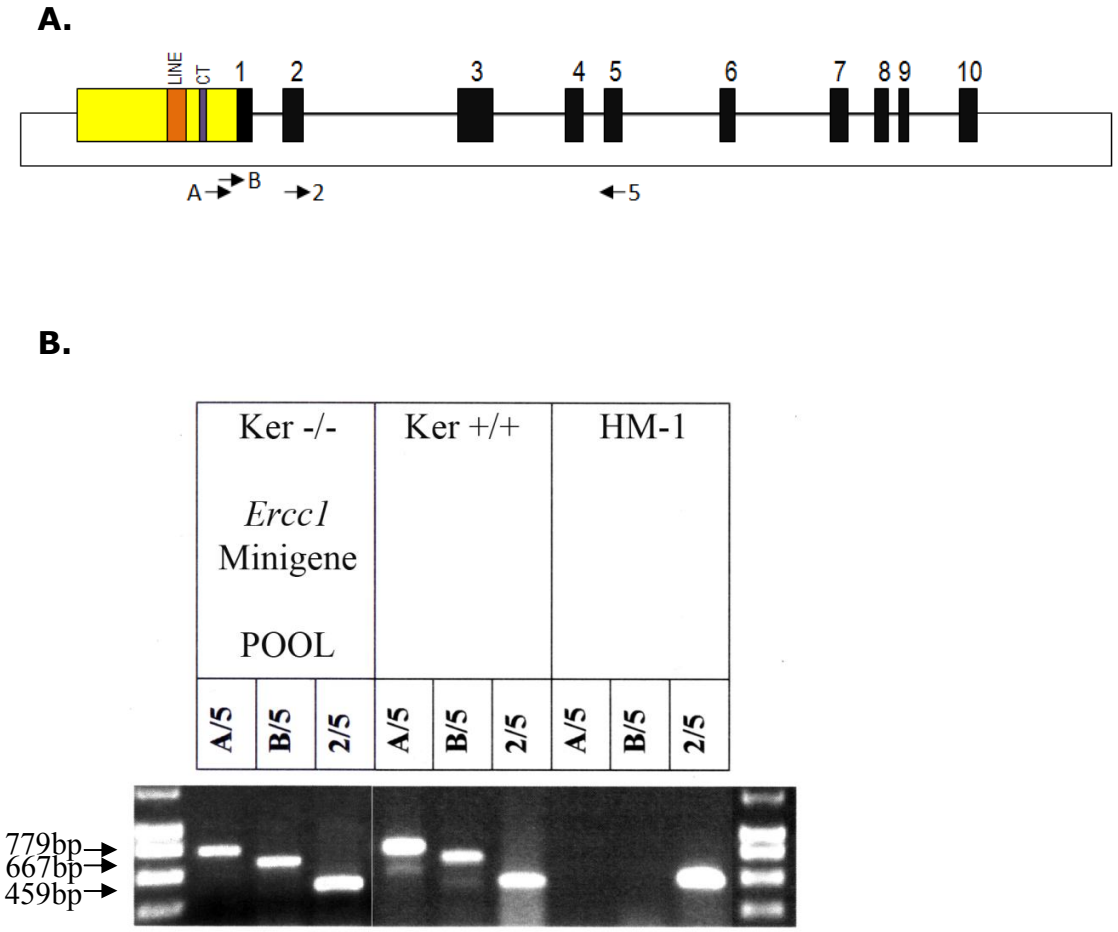

This experiment was carried out by Yvonne Simpson

A. The Ercc1 minigene used in our previous study is shown. The plasmid backbone is shown as a thin line. Ercc1 exons are shown in black. 1.2 kb of 5' flanking sequence of 129/Ola strain is shown in yellow. Regulatory elements LINE/L2 and CT repeats are shown in Orange and purple respectively. Primers are indicated by black arrows under the minigene.

B. RT-PCR analysis of RNA extracted from Ercc1-null keratinocytes pools transfected with Ercc1 minigene. Total RNA was prepared and reverse transcribed using oligo-dT primers. Three PCR reactions were performed on cDNA using the following forward primers; primer 'A' and primer 'B' are specific to a region upstream of the normal transcriptional start site and primer '2' is specific to exon2. Reverse primer '5' is specific to exon5.

In addition to our results, two mouse Ercc1 transcripts which contain the similar exon 1 as identified in the 1.5kb skin-specific transcript were published on a comprehensive cDNA-supported gene and transcripts annotation AceView, NCBI (Thierry-Mieg and Thierry-Mieg 2006). These two Ercc1 transcripts were reconstructed from cDNA clones of different mouse tissues and both have the exon 1 reconstructed from only a mouse visual cortex clone. The Ercc1 transcript variant cSep07 had a transcriptional start site just 18bp upstream of the end point of our 5'RACE result and had the same exon1 sequence as the 1.5kb Ercc1 transcript, except for the additional 18bp sequence at the 5' side. The cSep07 variant also has an alternative exon 8 which contains the known exon 8, intron 8 and exon 9 of Ercc1. An "opal" stop codon TGA was found in the intron 8, which might lead to a truncated ERCC1. Another Ercc1 transcript variant bSep07 had a slightly shorter exon 1 at the 5' side compared to the 1.5kb Ercc1 transcript and also had a 132bp longer exon 10. As both these transcript variants had the exon 1 reconstructed from the mouse brain tissue, we don't think these transcripts are as important as the 1.5kb Ercc1 transcript found in skin. Our northern blotting showed only a barely detectable hint of the 1.5kb Ercc1 transcript in tissues other than in skin. However, these two Ercc1 variant provide extra evidence that the 1.5kb Ercc1 transcript could be driven by the region just 5' of the normal Ercc1 promoter rather than by a promoter located much further upstream.

In conclusion, we believe that the source of the Ercc1 skin-specific transcript is most likely to be a promoter region adjacent to the RACE endpoints that we have mapped some 400bp upstream of the normal transcriptional start site, rather than at the more distal putative upstream promoter regions that we have investigated.

Chapter 5:

Role of ERCC1 and other DNA repair proteins in melanoma

5.1 Introduction

Melanoma is a malignant tumour of melanocytes that causes the majority of skin cancer related deaths. It is characterized by high resistance to chemotherapy and to date there is still no effective therapeutic regime. Cutaneous melanoma is the eighth most common cancer in the UK and the incidence is rising rapidly. Patients with early-stage melanoma have good long-term survival following simple surgical resection, but patients with metastatic disease, especially distant metastases, are generally considered incurable. The long-term survival rate for patients with metastatic melanoma is only 5% (Brown and Nelson 1999). Therefore, investigations are essential to improve and develop more effective prevention strategies and prognostic markers of melanoma.

As DNA repair deals with both environmental and anti-cancer drug induced DNA lesions, a better understanding of the functional role of DNA repair pathways could not only benefit the prevention but also the chemotherapy of melanomas. Analysis of differential gene expression was carried out to identify the gene-profile signature for human primary malignant melanoma associated with recurrence (ie. metastasis). 48 DNA repair genes, among a list of 234 genes, were found to be associated with metastatic progression, of which 44 genes were overexpressed (Kauffmann et al. 2008).This overexpression of DNA repair genes covers multiple repair pathways including BER, NER, MMR and HR and can potentially explain the cause of high resistance of metastatic melanoma to chemotherapy (Kauffmann et al. 2008). Our study with 596 Scottish melanoma patients and 441 population-based controls also found that polymorphisms in the NER genes ERCC1 and XPF were significantly associated with susceptibility to melanoma, especially for cases aged 50 and under (Povey et al. 2007).

The hypermethylation of the hMLH1 gene promoter could induce the loss of DNA mismatch repair which occurs at a high frequency in a number of human tumours. This loss of MMR is reported to be associated with resistance to a number of clinically important anticancer drugs, including the platinum-based chemotherapy drug cisplatin. It is reported that re-expression of the MLH1 gene in the MLH1 null mouse cells leads to sensitization to DNA damaging agents (Buermeyer et al. 1999).

In ovarian cancer, hMLH1 promoter methylation is observed at a higher frequency in tumours following chemotherapy treatment compared with tumours before treatment. The majority of cisplatin-resistant derivatives of ovarian tumour cell lines lacked MLH1 expression because of the methylation of its promoter (Strathdee et al. 1999). In vitro, the cisplatin-resistant variants became drug sensitive following re-expression of MLH1, or treatment with demethylating agents (Durant et al. 1999; Strathdee et al. 1999). In MMR-deficient human ovarian tumour xenografts, re-expression of MLH1 by prior demethylating agent treatment also resulted in sensitization to cisplatin (Plumb et al. 2000).

Therefore, the protein level of MLH1, as well as two other MMR proteins, MSH2 and MSH6, was investigated in this thesis.

In this investigation, levels of several different DNA repair proteins, including two NER proteins ERCC1 and XPF, three MMR proteins MSH2, MSH6 and MLH1, were quantitatively measured and compared using a panel of human melanoma, melanocyte and ovarian tumour cells in an attempt to identify any correlation between DNA repair capability and resistance to DNA damaging agents. Six melanoma cell cultures A375, C32, G361, WM115, HBL and EDMEL3, two immortalized melanocyte cell lines,

Hermes 1 and Hermes 4a and seven ovarian tumour cell lines were used in the investigation. PEO4 and PEO6 are cisplatin-resistant derivatives of PEO1, PEO23 and PEA2 are cisplatin-resistant derivatives of PEO14 and PEA1, respectively (Langdon et al. 1988).

5.2 Comparison of expression of NER proteins ERCC1, XPF and mismatch repair (MMR) proteins MSH2, MSH6, MLH1 in human melanoma cell lines, melanocytes and human ovarian tumour cell lines

Levels of two NER proteins, ERCC1 and XPF, and three MMR proteins, MSH2, MSH6 and MLH1, in human melanoma, melanocytes and ovarian tumour cells were determined by western blotting. Target protein bands were first detected using ECL-plus on high performance autoradiography film (Figure 5.1.A-5.5.A), and then immediately scanned with the phosphorimager STORM 840 system. Band densities, which correlate with the target protein level in cells, were quantified using the ImageQuant™ TL software. The levels of proteins were normalized to the loading control Tubulin or GAPDH. Experiments were repeated at least 3 times (MSH6 protein level in all cell lines and ERCC1 protein level in human melanocytes were tested twice only). The mean ratio of target protein against loading control in the melanoma group was set as 1, and then relative levels of proteins in each individual line were plotted (Figure 5.1B-5.5.B). Mean levels of protein in each cell type were also calculated and plotted (Figure 5.1C-5.5.C).

It was clear that the protein level of ERCC1 was significantly higher (>2-fold) in the melanoma group compared to the ovarian tumour group (P=0.004, Mann-Whitney U test)(Figure 5.1). In the melanoma group, the WM115 cell line showed the highest level of ERCC1, about two times higher than the C32 cell line, which has the lowest level of ERCC1. Interestingly, mean level of ERCC1 protein was also higher in melanocytes compared to ovarian tumours, though this was not statistically significant (p=0.380). This may be due to more DNA repair being required in skin to deal with UV-induced DNA damage. In the melanoma cell lines the level of ERCC1 was 60% higher than in non-transformed melanocytes (P=0.046). This could contribute to the extremely high resistance to chemotherapy of melanoma.

However, surprisingly there was no consistent correlation between ERCC1 protein levels and the chemotherapy resistance in ovarian tumour cultures. The cisplatin sensitive culture PEA1 has the lowest level, while the resistant culture PEO6 has the highest level of ERCC1. However, the cisplatin sensitive culture PEO14 showed a very similar high level of ERCC1 as PEO6. All other cultures generally showed similar protein level of ERCC1 irrespective of their cisplatin resistance or sensitivity.

ERCC1's partner, the XPF protein showed the same significant increased level in melanomas compared to the ovarian tumours and melanocytes (Figure 5.2). The level of XPF was 1.5 times higher in the melanoma group than the ovarian tumour group (P=0.022). However, different from ERCC1, XPF showed a lower protein level in human melanocytes, which is 31% compared to melanomas (p=0.046) and 44% compared to ovarian tumours (p=0.040), respectively. The trend of the XPF protein level in tested samples was very similar to the ERCC1 protein level. In melanomas, the C32 had the lowest level of both ERCC1 and XPF, while A375 and WM115 showed high levels of both proteins. In the ovarian tumour cells, PEA1 and PEA2 had low levels of

Figure 5.1 Expression pattern of NER protein ERCC1 in human melanoma, melanocytes and ovarian tumour cells.

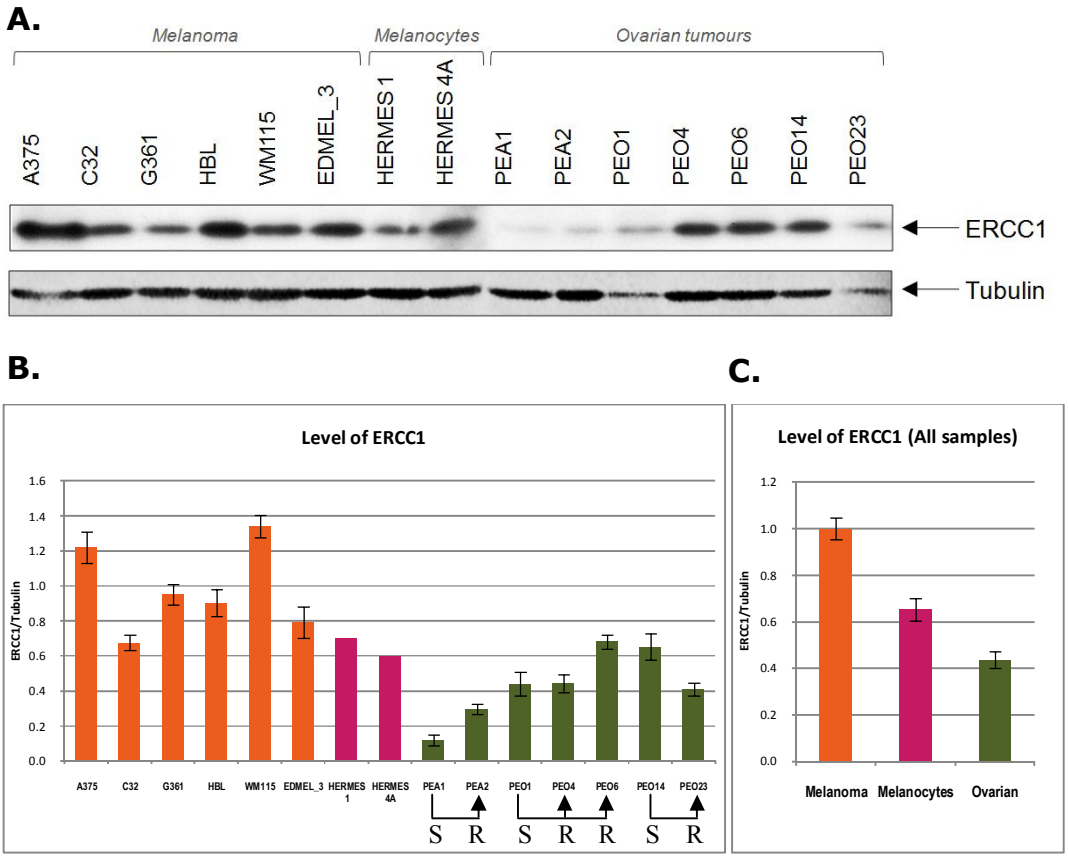

A. ERCC1 protein levels in human melanoma, melanocytes and ovarian tumour cells. Top panel shows bands of ERCC1, while the bottom panel shows bands of loading control tubulin. Figure is made from an autoradiograph.

B. Histogram showing mean level of ERCC1 in each individual cell line ±SEM standardized against the loading control tubulin. The ERCC1/Tubulin ratios are normalized to the mean level in all melanoma cell lines. Melanoma, melanocytes and ovarian tumour cultures are plotted in orange, purple and green columns, respectively. The cisplatin sensitive and resistant ovarian cell lines are indicated underneath, with black arrows showing original and daughter cell lines. There is no error bar for human melanocytes as they were tested only twice. Data from phosphorimager.

C. Histogram showing mean level of ERCC1 in each cell type ±SEM standardized against tubulin. Melanoma, melanocytes and ovarian tumour cultures are plotted in orange, purple and green columns, respectively. Data from phosphorimager.

Figure 5.2 Expression pattern of NER protein XPF in human melanoma, melanocytes and ovarian tumour cells.

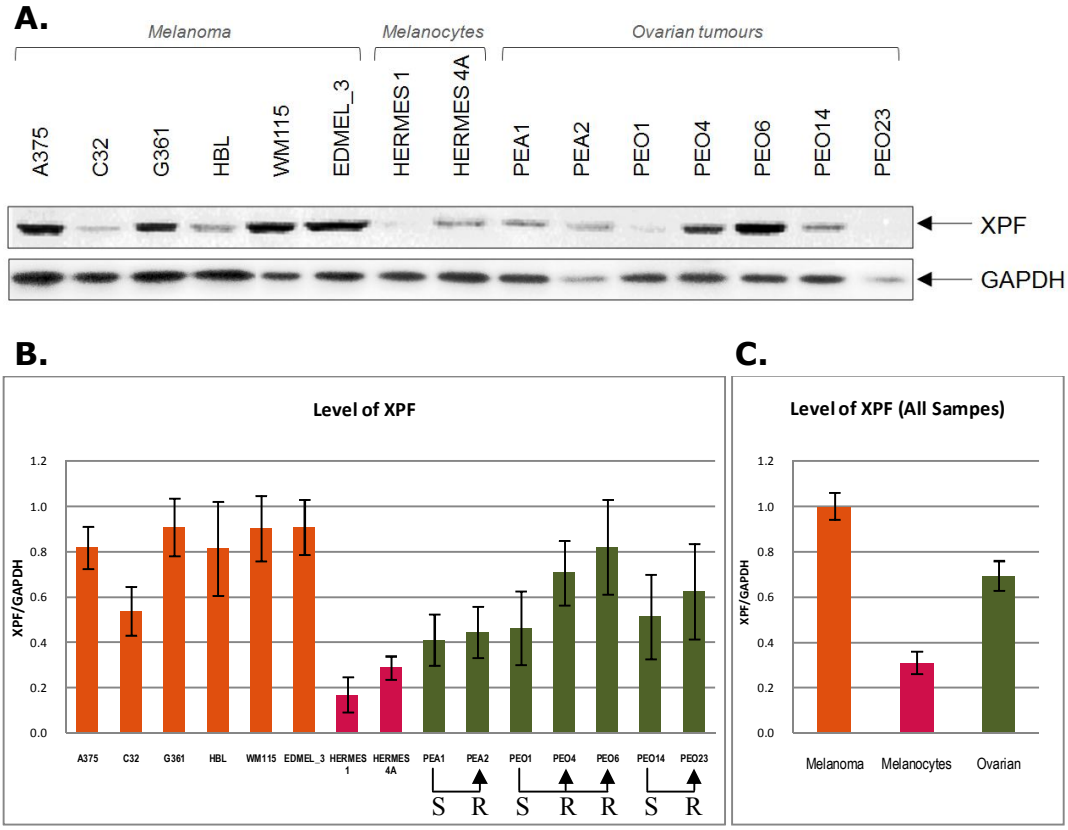

A. XPF protein levels in human melanoma, melanocytes and ovarian tumour cells. Top panel shows bands of XPF, while the bottom panel shows bands of loading control GAPDH. Figure is made from an autoradiograph.

B. Histogram showing mean level of XPF in each individual cell line ±SEM standardized against the loading control GAPDH. The XPF/GAPDH ratios are normalized to the mean level in all melanoma cell lines. Melanocytes and ovarian tumour cultures are plotted in orange, purple and green columns, respectively. The cisplatin sensitive and resistant ovarian cell lines are indicated underneath, with black arrows showing original and daughter cell lines. Data from phosphorimager.

C. Histogram showing mean level of XPF in each cell type ±SEM standardized against GAPDH. Melanoma, melanocytes and ovarian tumour cultures are plotted in orange, purple and green columns, respectively. Data from phosphorimager.

ERCC1 and XPF, while PEO6 had the highest levels of both two proteins.

We further tested three different MMR proteins MSH2, MSH6 and MLH1 using the same protocol as described above. There was no significant difference in MSH2 levels between the three cell types (Figure 5.3). As expected, there was no obvious correlation between cisplatin-resistance and MSH2 protein level, either.

The MSH6 protein showed a slightly higher level in the ovarian tumours cells compared to the melanoma lines, but this difference was not significant (Figure 5.4). Different from the MSH2, the level of MSH6 was much lower in melanocytes, about 40% of the level in melanomas and ovarian tumours. Within the cell types there was no obvious correlation between MSH2 and MSH6 protein levels.

Interestingly, another MMR protein, MLH1, showed an elevated level in melanomas compared to melanocytes (P=0.046) and ovarian tumour cells (P=0.003) (Figure 5.5). This is opposite to the previous investigations from the literature, which suggest that tumour cells with reduced MLH1 expression seem to have a survival advantage during combined chemotherapy and loss of MLH1 may relate to the drug resistance in breast and esophageal cancers (Mackay et al. 2000; Kishi et al. 2003). Melanoma is more resistant to chemotherapy compared to ovarian cancer, but the level of MLH1 in melanoma cell lines was nearly 1.5 times higher. The protein level of MLH1 was also higher in the cisplatin-resistant ovarian tumour cell lines compared to the sensitive ones. The mean MLH1 expression ratio was 0.74 and 0.57 in cisplatin-resistant and sensitive ovarian tumour cell lines, respectively, though this difference was not statistically significant (P=0.077).

Figure 5.3 Expression pattern of MMR protein MSH2 in human melanoma, melanocytes and ovarian tumour cells.

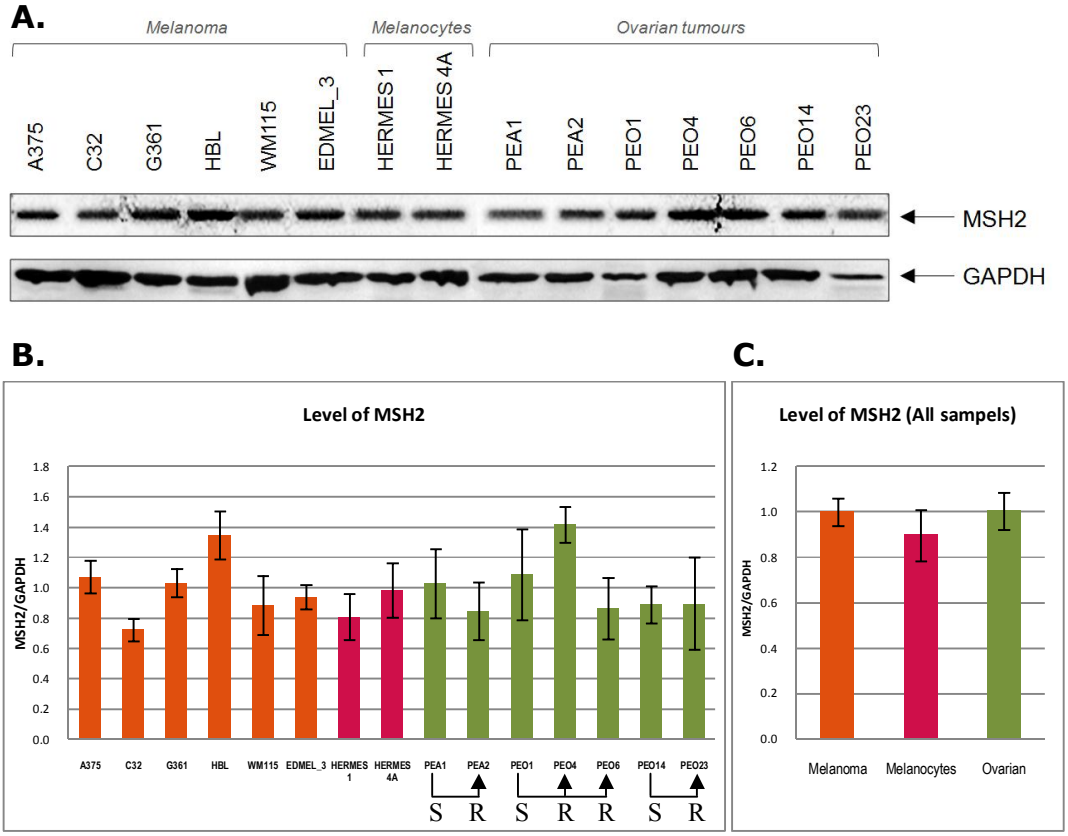

A. MSH2 protein levels in human melanoma, melanocytes and ovarian tumour cells. Top panel shows bands of MSH2, while the bottom panel shows bands of loading control GAPDH. Figure is made from an autoradiograph.

B. Histogram showing mean level of MSH2 in each individual cell line ±SEM standardized against the loading control GAPDH. The MSH2/GAPDH ratios are normalized to the mean level in all melanoma cell lines. Melanoma, melanocytes and ovarian tumour cultures are plotted in orange, purple and green columns, respectively. The cisplatin sensitive and resistant ovarian cell lines are indicated underneath, with black arrows showing original and daughter cell lines. Data from phosphorimager.

C. Histogram showing mean level of MSH2 in each cell type ±SEM standardized against GAPDH. Melanoma, melanocytes and ovarian tumour cultures are plotted in orange, purple and green columns, respectively. Data from phosphorimager.

Figure 5.4 Expression pattern of MMR protein MSH6 in human melanoma, melanocytes and ovarian tumour cells.

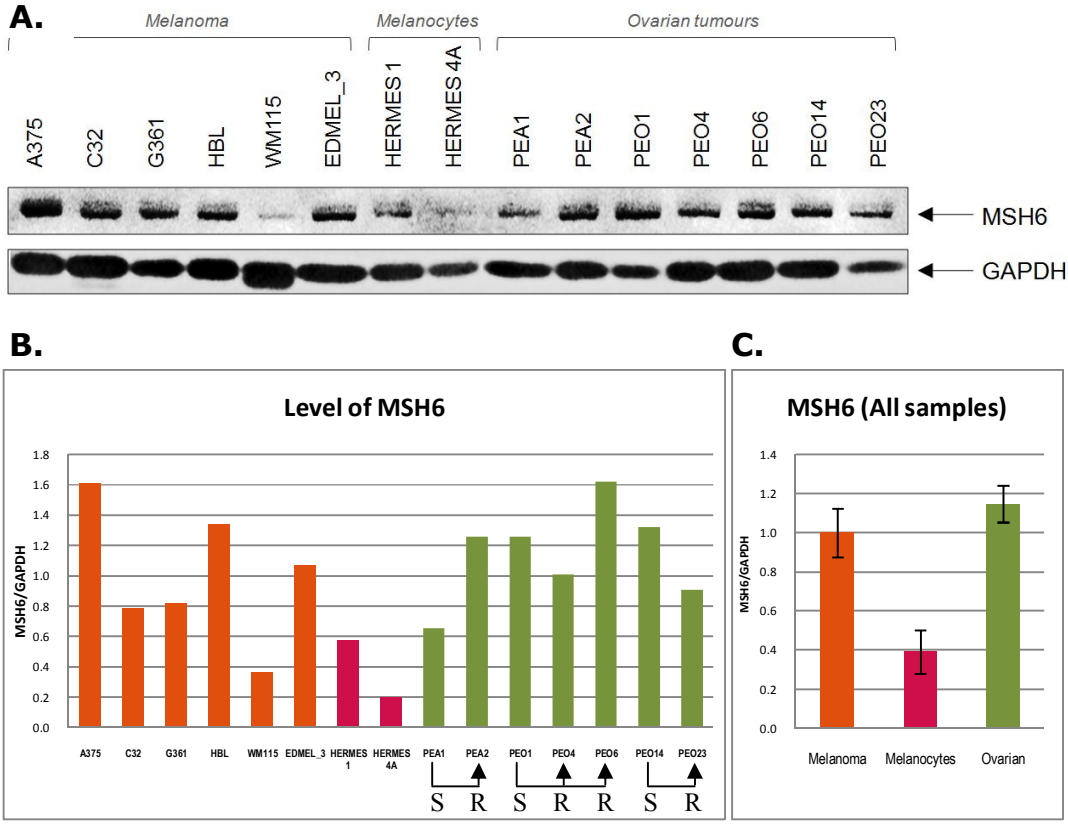

A. MSH6 protein levels in human melanoma, melanocytes and ovarian tumour cells. Top panel shows bands of MSH6, while the bottom panel shows bands of loading control GAPDH. Figure is made from an autoradiograph.

B. Histogram showing mean level of MSH6 in each individual cell line ±SEM standardized against the loading control GAPDH. The MSH6/GAPDH ratios are normalized to the mean level in all melanoma cell lines. Melanoma, melanocytes and ovarian tumour cultures are plotted in orange, purple and green columns, respectively. The cisplatin sensitive and resistant ovarian cell lines are indicated underneath, with black arrows showing original and daughter cell lines. There are no error bars for MSH6 proteins due to this test being repeated only twice. Data from phosphorimager.

C. Histogram showing mean level of MSH6 in each cell type ±SEM standardized against GAPDH. Melanoma, melanocytes and ovarian tumour cultures are plotted in orange, purple and green columns, respectively. Data from phosphorimager.

Figure 5.5 Expression pattern of MMR protein MLH1 in human melanoma, melanocytes and ovarian tumour cells.

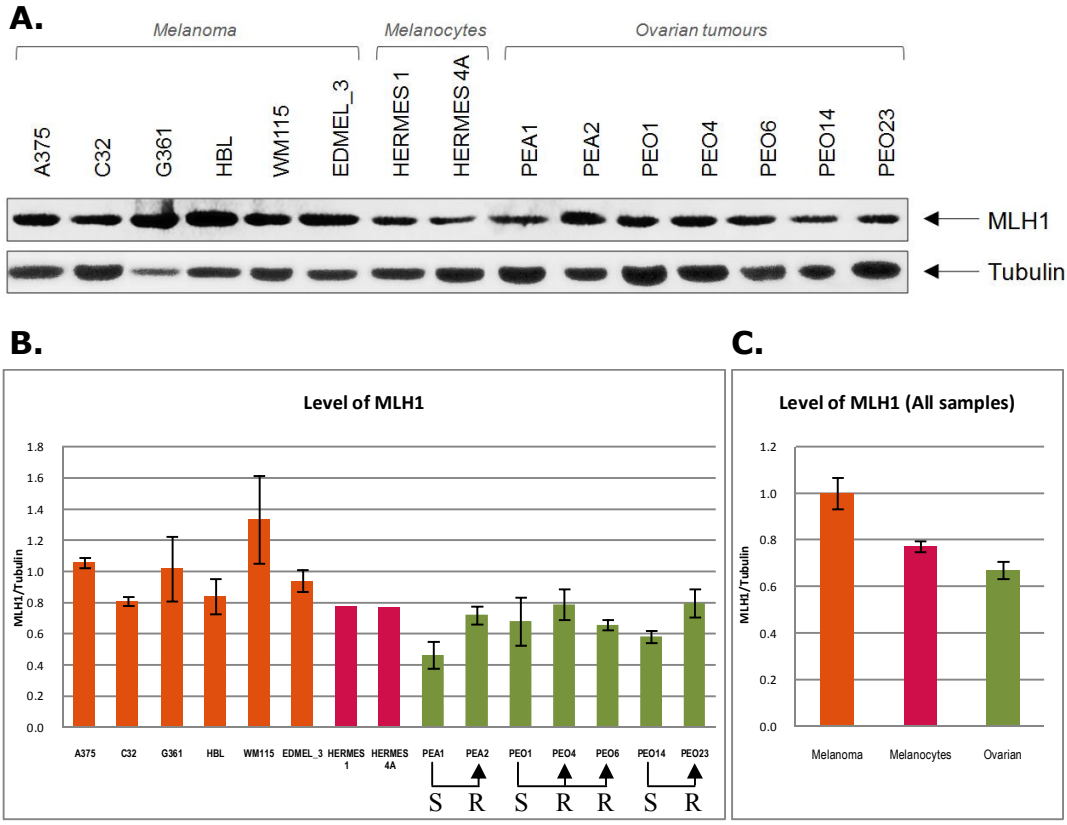

A. MLH1 protein levels in human melanoma, melanocytes and ovarian tumour cells. Top panel shows bands of MLH1, while the bottom panel shows bands of loading control Tubulin. Figure is made from an autoradiograph.

B. Histogram showing mean level of MLH1 in each individual cell line ±SEM standardized against the loading control Tubulin. The MLH1/Tubulin ratios are normalized to the mean level in all melanoma cell lines. The MLH1 protein level in melanomas is set to the ratio 1. Melanoma, melanocytes and ovarian tumour cultures are plotted in orange, purple and green columns, respectively. The cisplatin sensitive and resistant ovarian cell lines are indicated underneath, with black arrows showing original and daughter cell lines. There is no error bar for human melanocytes as they were tested only twice. Data from phosphorimager.

C. Histogram showing mean level of MLH1 in each cell type ±SEM standardized against Tubulin. Melanoma, melanocytes and ovarian tumour cultures are plotted in orange, purple and green columns, respectively. Data from phosphorimager.

5.3 Colony forming survival assay following UV-irradiation in human melanoma cell lines and human ovarian tumour cell lines.

To investigate whether the increased level of ERCC1 and XPF proteins relate to a higher DNA repair capability in melanomas, a colony forming assay was performed to study the long-term survival rate of different types of tumour cells following UV-induced DNA damage.

Preliminary studies were carried out on the majority of our melanoma and ovarian tumour cell lines to determine the appropriate cell densities for plating, the culture conditions and plating efficiency of each cell line. To avoid the subjective bias of manual enumeration of colonies, colonies were counted using the GEL-DOC 2000 system with proper parameters for enumeration of each cell line. From the preliminary results, cell lines that did not form clear visible colonies were excluded from this assay and finally 2 melanoma cell lines, A375 and G361, as well as 2 cisplatin resistant ovarian tumour cell lines, PEO4 and PEO6 were selected (Figure 5.6). Appropriate numbers of cells were plated in 60mm petri-dishes 24 hours before the UV irradiation at doses from $0Jm^{-2}$ (control) to $200Jm^{-2}$, dishes were then cultured until good and clear colonies were formed before being fixed and stained with crystal violet. Triplicate dishes of A375 and duplicate dishes of G361, PEO4 and PEO6 were set up in the assay. The A375 cell line grew rapidly and normally took about one week to finish a single assay. The G361, PEO4 and PEO6 grew much more slowly and took about 3 to 4 weeks to finish one single assay.

The D_{50} values (UV dose for 50% survival) for the melanoma cell lines were: A375, $15Jm^{-2}$, G361, $10Jm^{-2}$. The D_{50} values for the two cisplatin-resistant ovarian cell lines

Figure 5.6 Survival following UV-irradiation determined by colony forming assay.

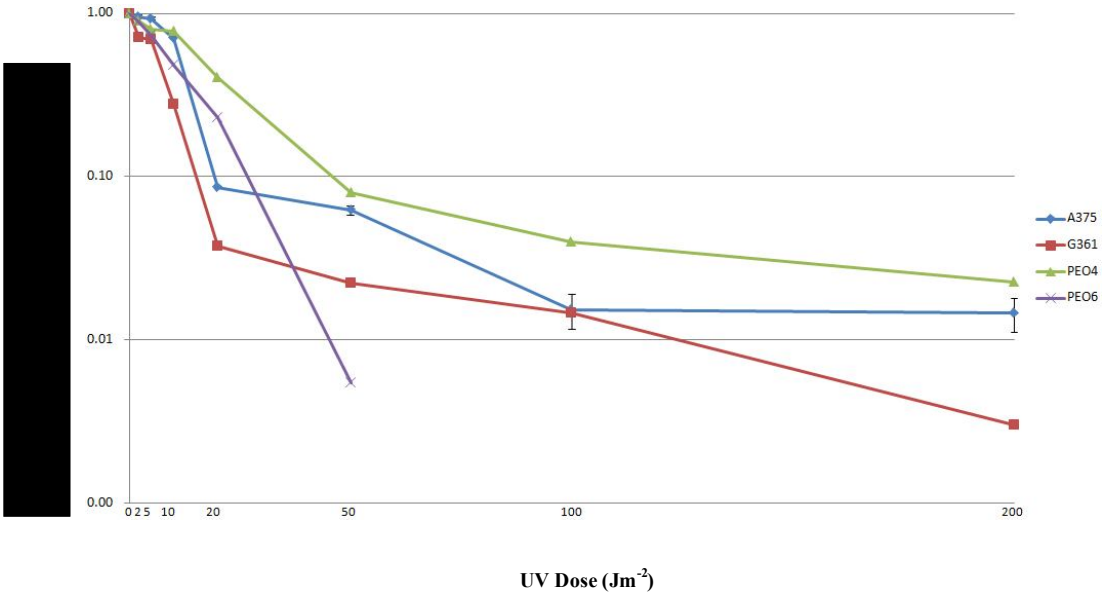

Relative plating efficiency is plotted on the Y-axis on a log scale. This is the plating efficiency at each UV dose, expressed as a percentage of the plating efficiency of control, non-irradiated cultures.

ERCC1 and XPF than the ovarian cell lines, but this did not correlate with increased UV survival.

5.4 Comparison of cisplatin resistance between human melanoma and ovarian tumour cells by Sulforhodamine B (SRB) assay.

Since some of the melanoma and ovarian cancer cell lines could not form good colonies we changed to using the SRB assay to test their resistance to the chemotherapy drug cisplatin. The SRB assay, based on the measurement of cellular protein content, is a widely used method for in vitro cytotoxicity screening (Skehan et al. 1990; Vichai and Kirtikara 2006). Generally, the SRB dye binds to protein components of trichloroacetic acid (TCA) fixed cells in a 96-well plate format, and then the amount of dye extracted from stained cells is measured at 510nm and the O.D value is directly proportional to the cell mass (Vichai and Kirtikara 2006). In our assay, 6 replicas of each cell line and cisplatin concentration were performed for each individual test to permit statistical analysis of the data.

Starting cell density is important for the SRB assay as an improper cell-seeding density will result in exceeding the linearity range of the absorbance reading and lead to spurious cytotoxicity effects of cisplatin. Therefore, pilot assays with a range of starting cell densities were performed using 4 cell lines of both human melanomas and ovarian tumour cells (Figure 5.7). The starting cell density that produced O.D.s in the exponential increase phase range, but not exceeding the linearity range of the absorbance reading, was selected for the final SRB assay with cisplatin treatment.

The day of setting up the plates was counted as day 0. Cells were harvested on day 4 to day 7. The A375 cell line grew very fast and achieved 100% confluence in the wells on day 6 using 1000 cells per well, though the O.D value was still within the linear range. Therefore 500 A375 cells per well was chosen for the cisplatin assay. For the rest of the cell lines, appropriate starting cell densities from 4K to 10K were chosen according to the pilot experiment (as shown in Figure 5.7 with the black arrow).

Following the pilot experiments, SRB assays with cisplatin treatment were carried out using optimal starting cell densities. The 96-well plates were set up with 150ul of appropriate media in each well on day 0. 24 hours (day 1) following the plating, the desired amount of cisplatin was mixed into 50ul of culture media and added to each well directly to make a total volume of 200ul of media with a final concentration of cisplatin ranging from 0.3uM to 10uM. For the controls, 50ul of culture media without cisplatin was added to each well. After that, plates were incubated for another 48 hours (day 2 and day 3) under the proper culture conditions. The first plate was harvested on day 4, which is 72 hours following the cisplatin treatment, and the last plate was harvested on day 7. Cisplatin was kept continuously in the media until the harvest of the plate.

For each individual cell line, the relative growth with different concentration of cisplatin treatment on each day was analyzed and plotted using a histogram. As cisplatin induces the ICL DNA lesions which interrupt the DNA replication and finally induce apoptosis (Pillaire et al. 1995), the long-term effect of its cytotoxicity should be obvious in this assay.

Figure 5.8 shows the relative growth on day 6 (the result on day 7 was very similar). In

Figure 5.7 Pilot experiments for SRB assay

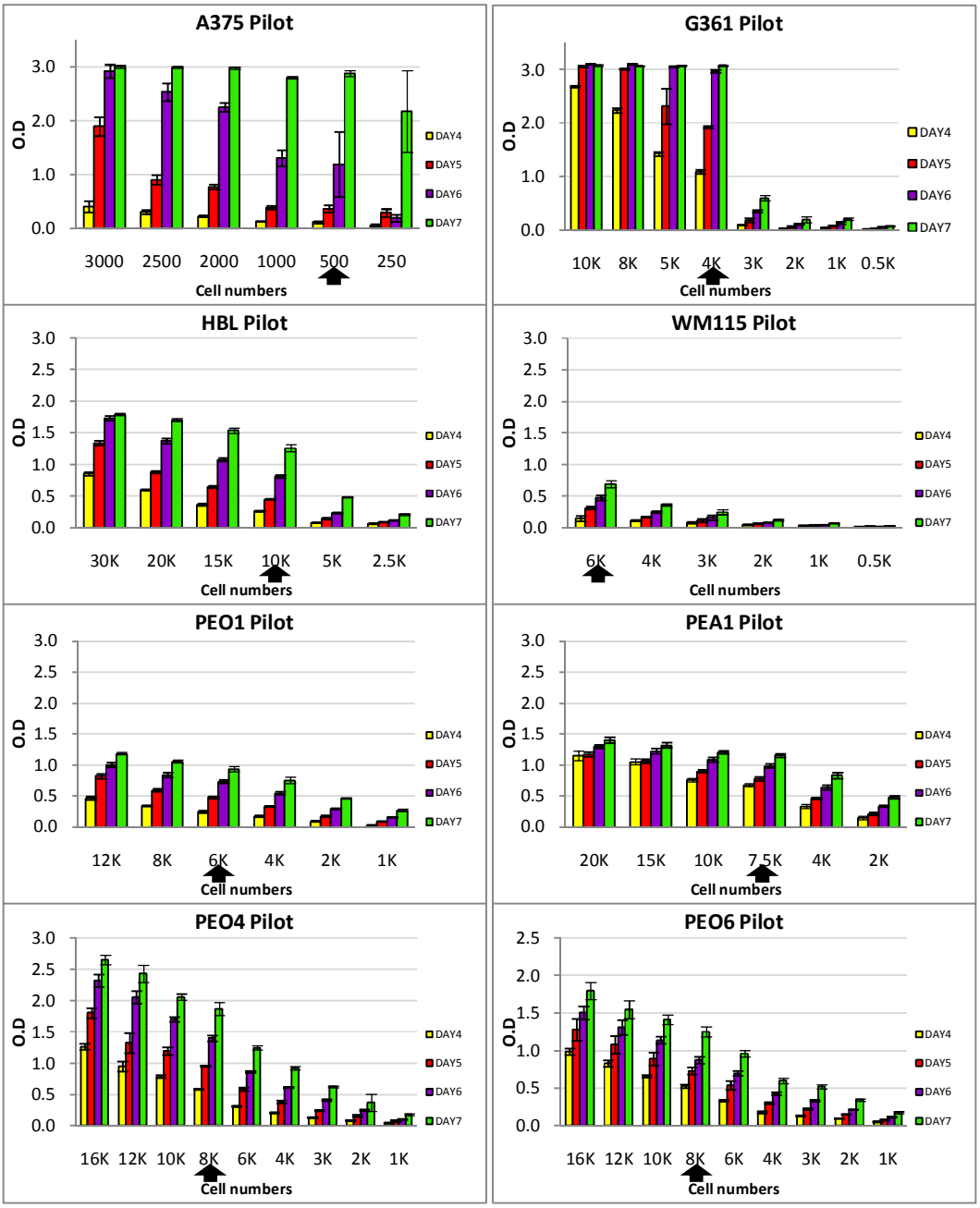

Histogram showing the O.D value at 510nm of pilot experiments for the SRB assay. Y-axis shows the O.D value while X-axis shows different starting cell densities used in the pilot assay for each individual cell line. Selected starting cell density for the following SRB assay with cisplatin treatment is indicated by a black arrow.

melanomas, HBL and WM115 were more sensitive to the cisplatin treatment compared to A375 and G361, as 0.3uM of cisplatin reduced growth by 30% for HBL and WM115 cells while the same concentration of cisplatin hardly had any effect on A375 and G361. In the ovarian tumour cells, the PEA1 and PEO1 cells were more sensitive to cisplatin compared to PEO4 and PEO6. 1uM of cisplatin reduced the growth to 70% in PEA1 and 40% in PEO1, while the same treatment has nearly no effect on PEO4 and PEO6. This result is reasonable because PEO4 and PEO6 are cisplatin-resistant derivatives of PEO1.

When compared to the melanoma cells, PEO4 and PEO6 cells showed a very similar cisplatin resistance to G361 cells, but they were more resistant than the other 3 melanoma cell lines tested. Therefore this suggests that there is no correlation between the level of NER protein ERCC1 and cisplatin resistance. For instance, A375 had a 2 times higher level of ERCC1 than PEO4 and PEO6 (Figure 5.2.B), but was less resistant to the cisplatin treatment. With 10uM of cisplatin, A375 cells showed a relative growth at less than 5% compared to 40% in PEO4 and PEO6 cells. The cisplatin resistance did not correlate with levels of other DNA repair proteins we tested either.

When all cell lines were combined together by tumour type, there was no statistical significance between the cisplatin resistance of the melanoma and ovarian tumour groups (Table 5.1.A). However, the in-group test showed that the cisplatin sensitive ovarian tumour cells had a significantly lower relative growth compared to the derivative cisplatin resistant cells (Table 5.1.B).

Figure 5.8 SRB assays of human melanoma and ovarian tumours cells following cisplatin treatment.

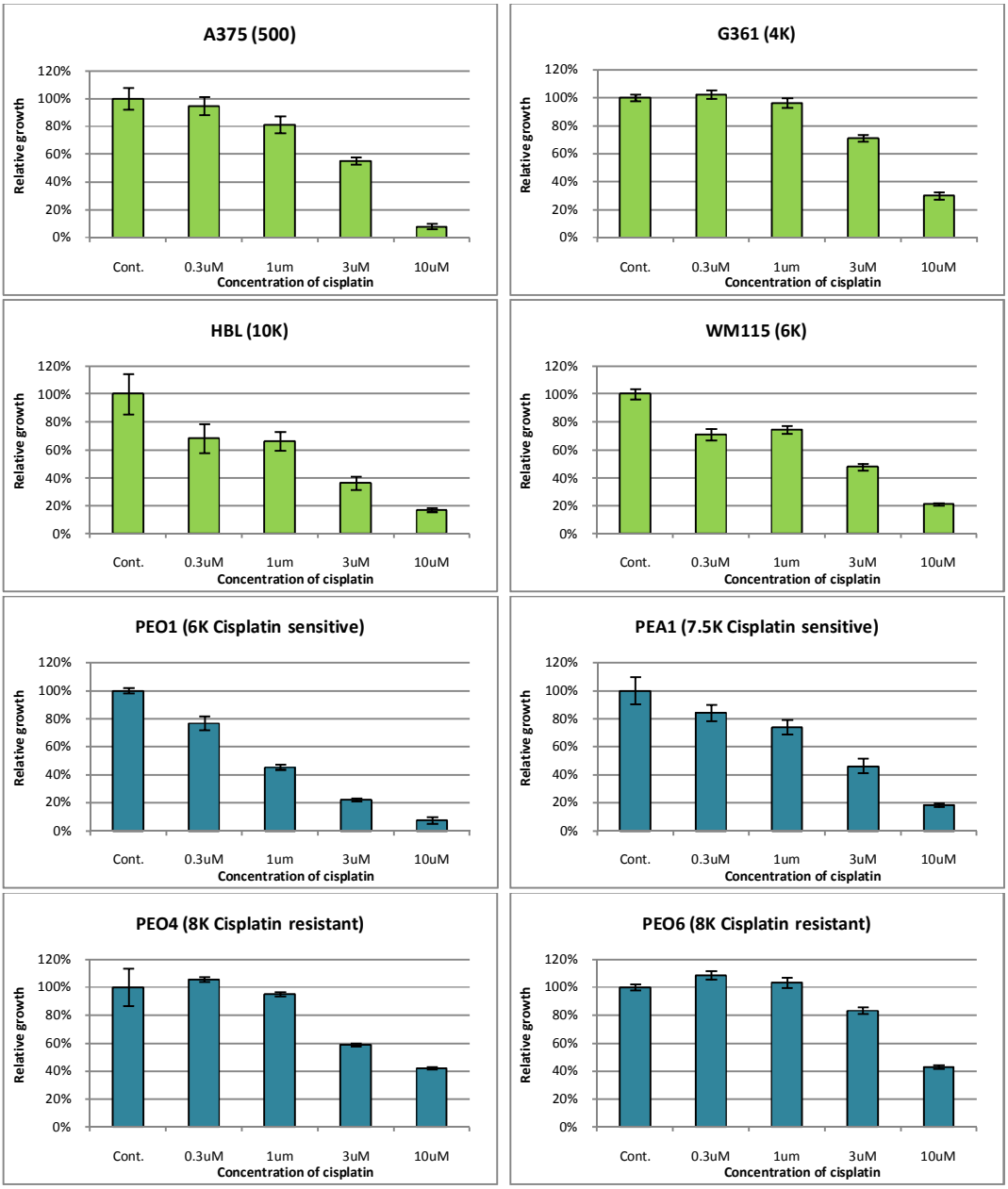

Histogram showing the relative growth following cisplatin treatment on day 6. Y-axis shows the relative growth while X-axis shows concentrations of cisplatin used on each individual cell line. Melanomas are shown in green histograms and ovarian tumours are shown in blue. Starting cell densities and the cisplatin sensitive and resistant ovarian tumour cell lines are shown in brackets.

5.5 A xenograft assay to investigate the importance of ERCC1 in melanoma.

The human melanoma cell lines had a higher level of ERCC1 and its partner, XPF, than the ovarian cancer cell lines we investigated, but they did not show the expected increased resistance to UV- and cisplatin-induced DNA damage. Although resistance to DNA damaging agents is only an indirect measure of DNA repair levels, we did not consider that our results justified measuring levels of DNA repair directly in the different cell lines. Instead, we turned to a system where we could manipulate the levels of ERCC1 directly and measure the consequences for melanoma growth and resistance to cisplatin. For this we used an immortalized mouse melanocyte cell line isolated from our mouse strain containing a floxed ERCC1 allele that was described in Chapter 1. This cell line grows as a xenograft in immunocompromised mice with the histological characteristics of malignant melanoma (D.Melton, unpublished observations).

Table 5.1 Statistical analysis of the cisplatin resistance between human melanoma and ovarian tumours cells

Table 5.1.A

	D4 0.3uM	D4 1uM	D4 3uM	D4 10uM	D5 0.3uM	D5 1uM	D5 3uM	D5 10uM
Mean of melanomas	84%	81%	59%	32%	84%	80%	53%	19%
Mean of ovarian tumours	98%	90%	73%	44%	94%	79%	53%	28%
Significance	0.468	0.149	0.149	0.564	0.248	1.000	1.000	0.564
	D6 0.3uM	**D6 1uM**	**D6 3uM**	**D6 10uM**	**D7 0.3uM**	**D7 1uM**	**D7 3uM**	**D7 10uM**
Mean of melanomas	85%	73%	47%	10%	91%	76%	49%	7%
Mean of ovarian tumours	95%	78%	43%	16%	97%	76%	37%	13%
Significance	0.309	0.773	0.773	0.309	0.564	0.885	0.564	0.309

Table 5.1.B

	D4 0.3uM	D4 1uM	D4 3uM	D4 10uM	D5 0.3uM	D5 1uM	D5 3uM	D5 10uM
Mean of cisplatin sensitive ovarian tumour cells	94%	79%	61%	22%	80%	60%	34%	13%
Mean of cisplatin resistant ovarian tumour cells	102%	102%	86%	66%	107%	99%	71%	43%
Significance	0.006	0.003	0.018	0.001	0.001	0.018	0.065	0.729
	D6 0.3uM	**D6 1uM**	**D6 3uM**	**D6 10uM**	**D7 0.3uM**	**D7 1uM**	**D7 3uM**	**D7 10uM**
Mean of cisplatin sensitive ovarian tumour cells	89%	59%	35%	7%	91%	57%	57%	7%
Mean of cisplatin resistant ovarian tumour cells	102%	96%	55%	24%	104%	96%	47%	19%
Significance	0.015	0.001	0.038	0.001	0.001	0.001	0.001	0.001

Significance (P value) by Mann Whitney U test using SPSS. D4, D5, D6 and D7 mean Day 4, Day 5, Day 6 and Day 7, respectively. **Table 5.1.A**: Mean relative growth of melanomas and ovarian tumour cell lines. **Table 5.1.B**: Mean relative growth of cisplatin sensitive and resistant ovarian tumour cell lines.

5.6 ERCC1-deficient melanoma xenografts are cured by cisplatin.

3-1-1 T1a is the immortalised mouse melanocyte cell line that contains an Ercc1 floxed allele (Figure 5.9) and grows as malignant melanoma when xenografted in nude mice. An Ercc1 deficient derivative was isolated by cotransforming 3-1-1 T1a cells with pBT/MTneo and pMCreN plasmids. Transfectant colonies were selected by resistance to G418, while cotransfection with pMCCreN should result in expression of Cre recombinase and deletion of the Ercc1 exon 3-5 region, resulting in an Ercc1 deficient 3-1-1 T1a melanocyte derivative. This experiment was carried out by Ann-Marie Ratchie.

G418-resistant colonies were picked, expanded and screened by PCR and western blotting. 8 out of 13 colonies screened were Ercc1-deficent. On such clone (Ercc1 3-1-1 T1a #5) is shown in Figure 5.9.B. The *in vitro* growth rates of both proficient and deficient mouse melanocytes were tested before the xenograft experiment (Figure 5.9.C). Both cell lines grew at the same rapid dividing speed approximately once per 24 hours.

The Ercc1 proficient and deficient melanocytes were then transplanted into nude mice. Each animal received 10^7 cells plus matrigel into each flank. The Ercc1 proficient xenografts grew very rapidly (Figure 5.10). The curve stops at day 24 because at this stage the tumours in some animals had reached the maximum permitted size ($1.44cm^2$) and the affected animals had to be culled. In comparison the Ercc1-deficient xenografts grew much more slowly taking 70 days before the largest tumours reached maximum permitted size. Thus although both cell lines grew equally well *in vitro*, Ercc1 was essential for good initial xenograft growth.

Figure 5.9 Generation of the ERCC1 deficient mouse melanocytes.

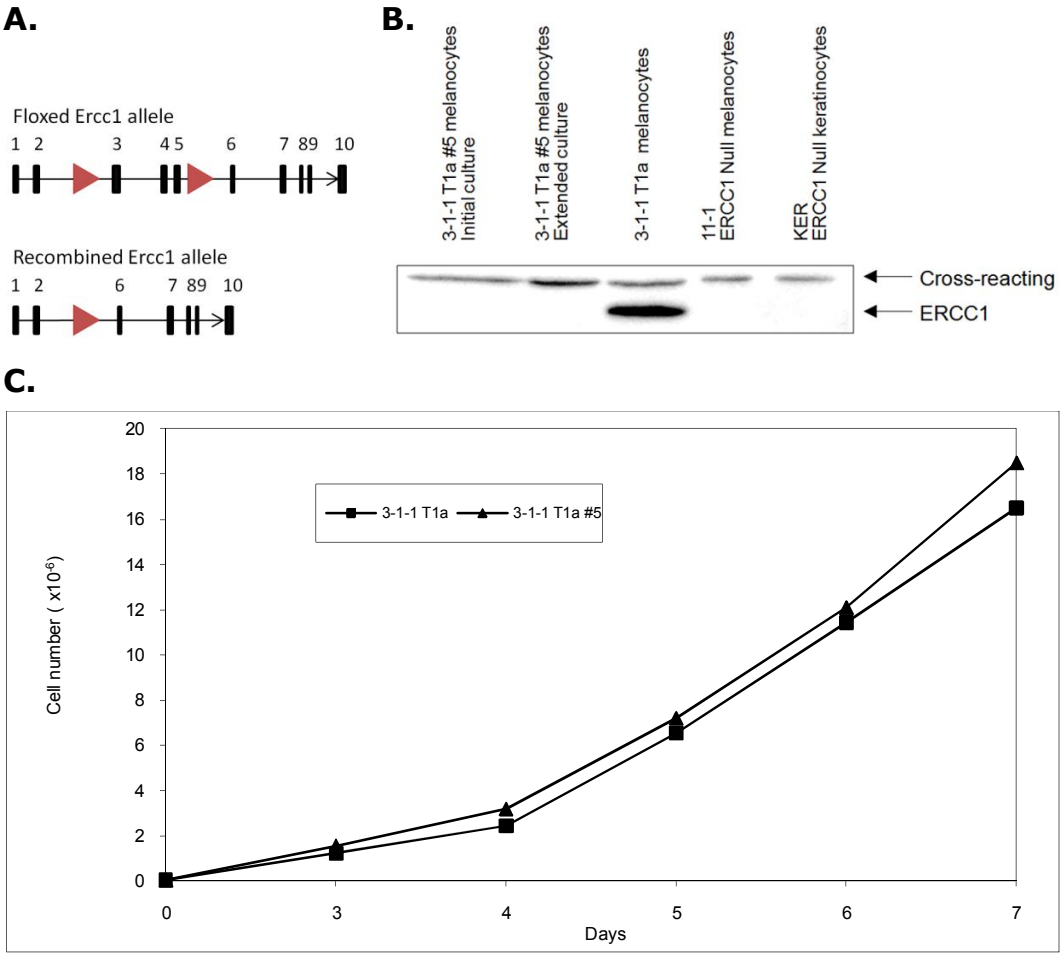

A. Schematic representation of floxed and recombined Ercc1 alleles. Ercc1 exons are numbered. Black squares indicate the Ercc1 exons. Red arrowheads represent loxP sites.

B. Screening using western blotting indicating the ERCC1 deficiency in the mouse melanocyte line 3-1-1T1a colony #5. Initial culture means the first culture from the colony. Extended culture indicates the same cells but with higher passage number. 11-1 and KER are ERCC1 deficient mouse melanocytes and keratinocytes, respectively. Cross-reacting bands and target ERCC1 bands are indicated by arrows on the right.

C. *In vitro* growth comparison between 3-1-1 T1a and its ERCC1-deficient derivative. For each cell line $5x10^4$ cells were plated in $25cm^2$ flasks. Each time point is the mean of duplicate flasks. Y-axis shows cell numbers at different harvest time points, while X-axis shows the time after plating.

Figure 5.10 Growth rates of ERCC1 proficient and deficient xenografts.

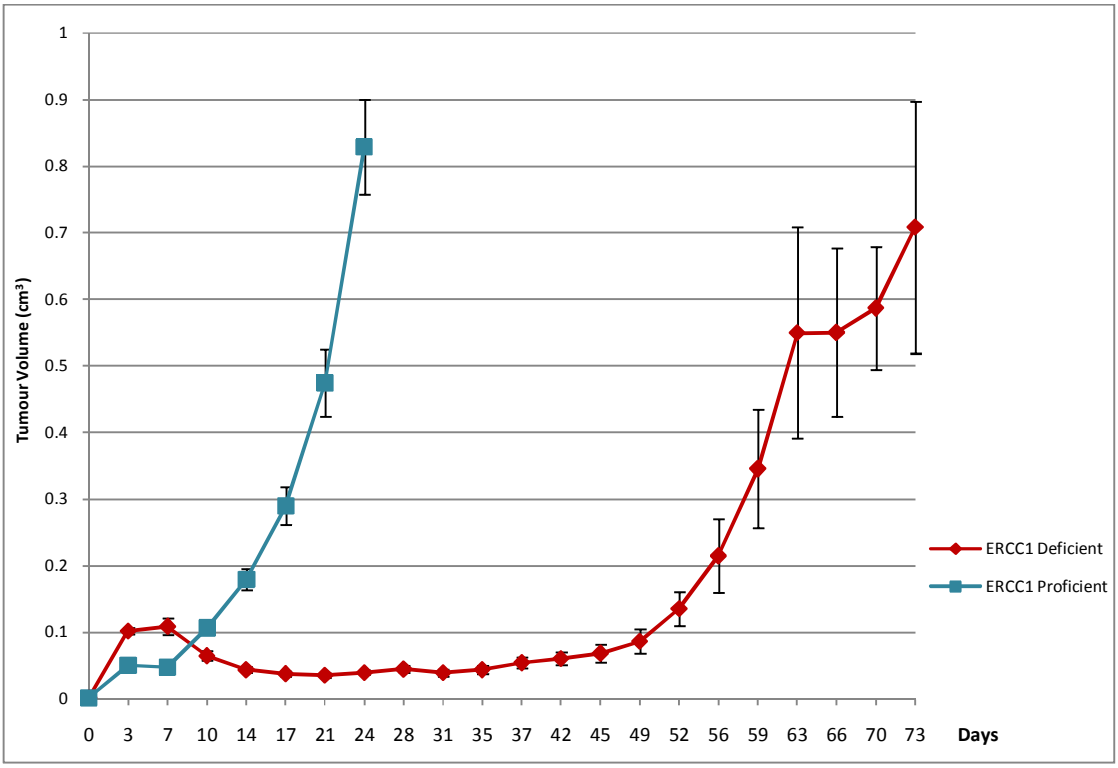

Growth of ERCC1 proficient and deficient xenografts in nude mice was measured. The red line represents the average of 5 mice with 2 ERCC1 proficient xenografts per mouse. The green line represents the average of 6 mice with 2 ERCC1 deficient xenografts per mouse.

Figure 5.11 Growth rates of ERCC1 proficient and deficient xenografts following cisplatin treatment.

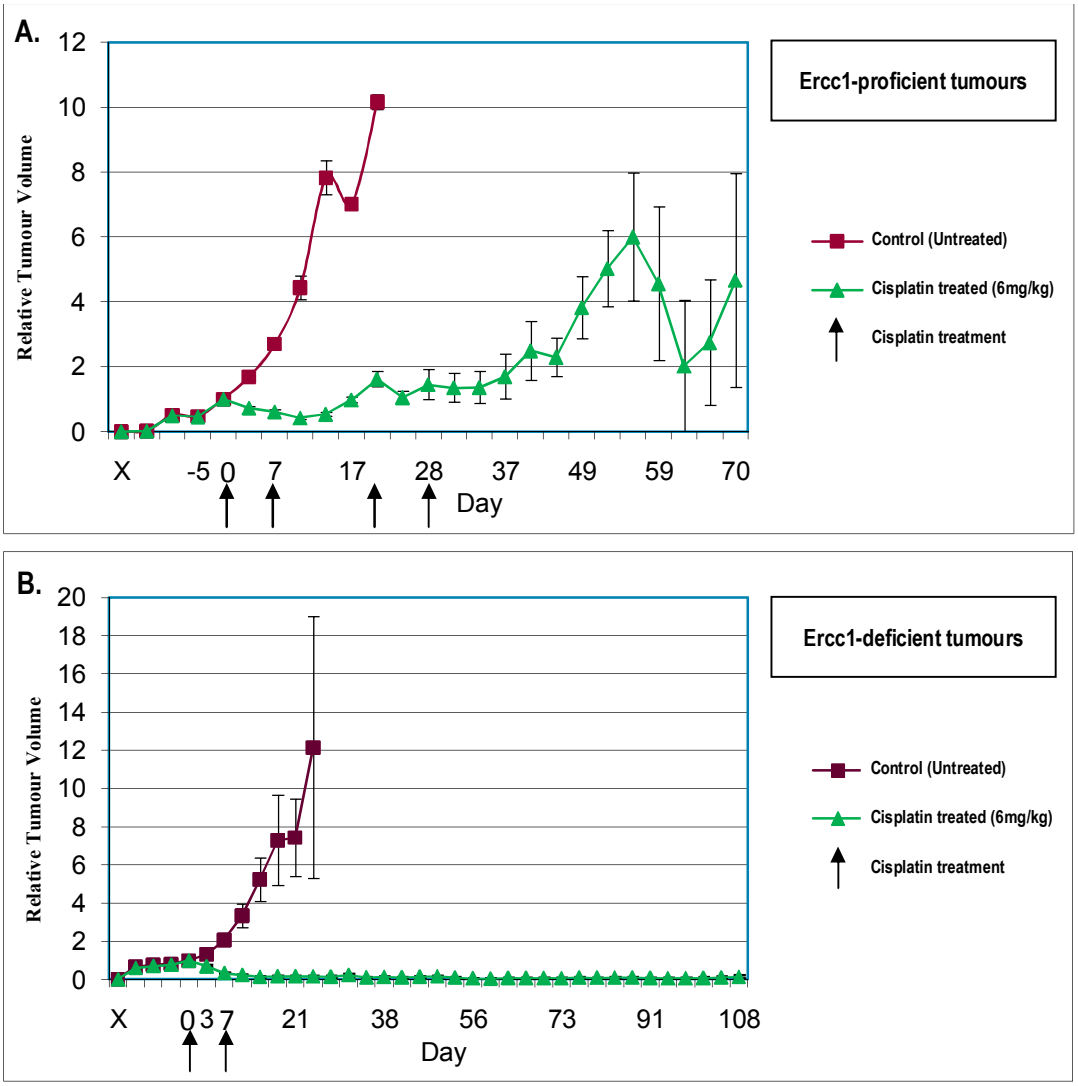

Growth of Ercc1-proficient and deficient xenografts in nude mice. The red line represents the average relative volume without cisplatin treatments. The green line represents the average relative volume with 6mg/kg cisplatin treatments. Volumes of all tested tumours are set to 1 on day 0. Y-axis indicates the relative tumour volume, which is calculated by dividing the measured tumour volume with the volume measured on day 0. X-axis indicates the time. It took X days before day 0 for xenografts to grow to the threshold volume for the treatment to start. Cisplatin treatments are indicated by black arrows under the X-axis **A.** Growth of Ercc1-proficient xenografts. Both control and treated groups have 5 mice with 2 xenografts per mouse. **B.** Growth of ERCC1 deficient xenografts. Both control and treated group have 4 mice with 2 xenografts per mouse.

Once the tumours had reached a threshold size of 0.1cm^3 mice with Ercc1 proficient and deficient xenografts were randomised into control and cisplatin groups and the mean tumour volume in each group was set at 1 and the day set at Day 0. In Figure 5.11, X is the number of day taken from injection to reach the starting size for cisplatin treatment at Day 0. X=12 for Ercc1 proficient and X=42 for Ercc1 deficient xenografts.

The Ercc1-proficient tumours grew rapidly in the absence of cisplatin, with the mean volume increasing 10-fold in 21 days before all animals had been culled because their tumours had reached the maximum size. Cisplatin injection (6mg/kg, intraperitoneally) on days 0 and 7 resulted in initial shrinkage of the Ercc1 proficient tumours, followed by regrowth that could not be prevented by two further cisplatin injections on day 21 and 29. The drop of the relative tumour volume curve around 55 days and increased error bars were due to the loss of some animals because their tumours had reached the maximum permitted size.

From day 0 in the ERCC1 deficient group, untreated control tumours grew as fast as the Ercc1-proficient group (Figure 5.11.B). The mean volume of tumours was 12 times bigger on day 24 and all animals had to be killed. However, very interestingly, the ERCC1 deficient tumours showed a hypersensitivity to the cisplatin treatment. Only two cisplatin treatments were performed on the ERCC1 deficient tumours, on days 0 and day 7. Tumours stopped growing and rapidly shrank following the treatment. No regrowth occurred up to day 108.

5.7 The level of ERCC1 protein was elevated in xenografts following cisplatin treatments

Cells were retrieved from the xenografts and cultured for further investigations. First of all, the status of ERCC1 was identified by western blotting. Figure 5.12.A shows some of the cells retrieved from xenografts. In the Ercc1-proficient group, the untreated control tumour cells 425R and 767L showed a very similar level of ERCC1 as the input cells (3-1-1 T1a) used to generate xenografts. Interestingly, in lines 764R2 and 769R1, derived from the cisplatin-treated group, the level of ERCC1 was increased compared to the input and control cells. No ERCC1 protein was detected in both input cells and control xenograft cells in the ERCC1 deficient group, as expected.

The ERCC1 protein was then detected in all retrieved cells and measured quantitatively. Level of ERCC1 was standardized by the loading control Tubulin (Figure 5.12.B). There were 5 samples in the input group (from independent 3-1-1 T1a cultures), 4 samples (from independent xenografts) in the control group and 8 samples (from independent xenografts) in the cisplatin group. The ratio of ERCC1/Tubulin in the control group was set to 1. There was no difference in ERCC1 levels between the input group and the control xenograft group, indicating that the transplanting of xenografts had no effect on ERCC1 expression. However, following the cisplatin treatment, the level of ERCC1 increased 2.1 times compared to the control group ($p=0.005$). Every individual cell line retrieved from the cisplatin treated xenografts showed a higher level of ERCC1 than the cell lines in the control group (data not shown).

Figure 5.12 Western blotting analysis of Ercc1-proficient and deficient cells used in the xenograft experiments.

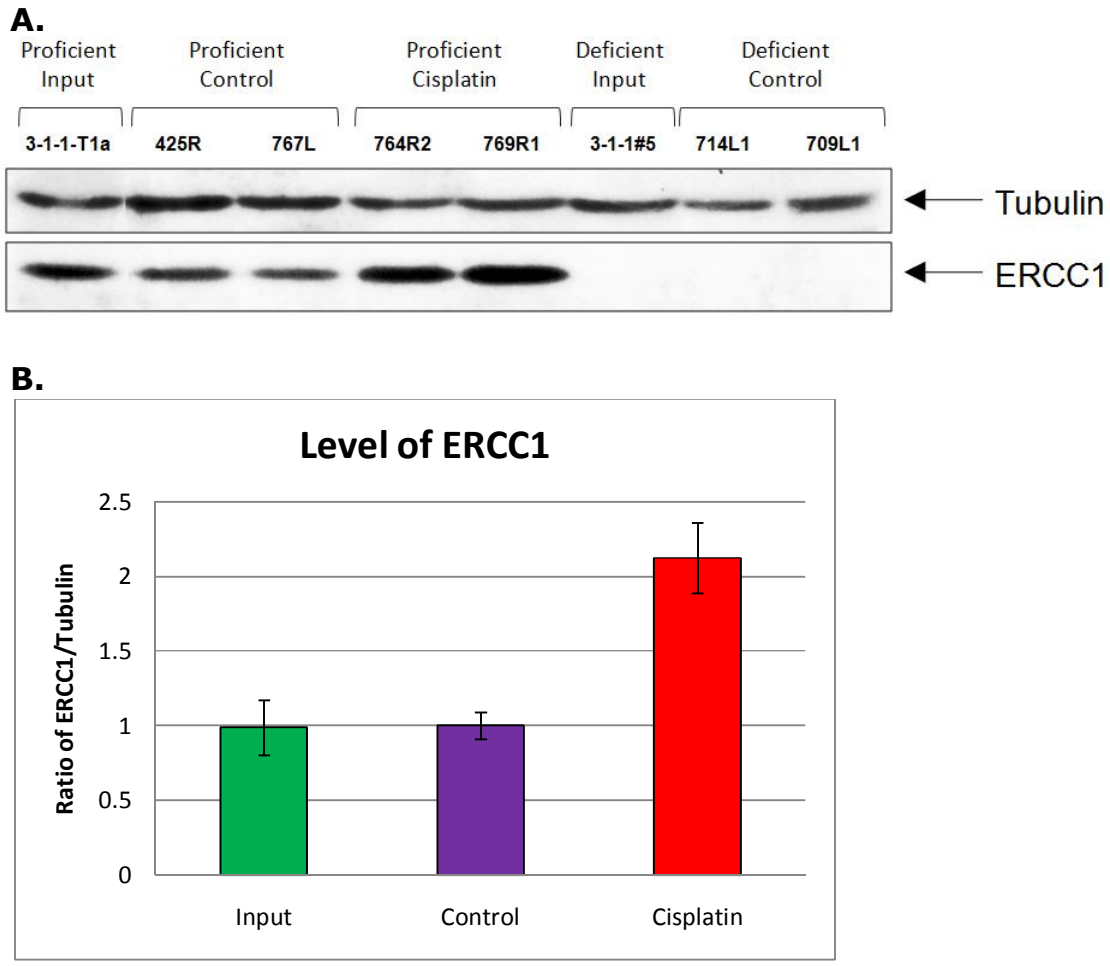

A. ERCC1 protein levels in cells retrieved from xenografts experiments. 3-1-1-T1a is the mouse melanocyte line used to generate the Ercc1-proficient xenografts. 425R and 767L are cells retrieved from the Ercc1-proficient control xenografts, mouse ID 425, right side tumour and 767 left side tumours. 764R2 and 769R1 are cells retrieved from the Ercc1-proficient cisplatin treated xenografts, mouse ID 764, right side tumour and 769 right side tumour. 3-1-1#5 is the Ercc1-deficient mouse melanocyte line used to generate the ERCC1 deficient xenografts. 714L1R and 709L1 are cells retrieved from the ERCC1 deficient xenografts, mouse ID 714, left side tumour and 709 left side tumours. Upper bands are loading control tubulin while lower bands are ERCC1.

B. Histogram showing the ERCC1 protein level in input Ercc1-proficient cells and cells retrieved from control and cisplatin xenografts, standardised against Tubulin and normalised for the mean ERCC1/Tubulin ratio in control xenografts.

5.8 Discussion

Treatment of cancer using chemotherapy often fails due to the resistance of tumours to drugs used. Thereby, better understanding the mechanisms of resistance may contribute to improved treatment. Generally, the resistance to the anti-cancer drug cisplatin can be catalogued into two types, acquired resistance and intrinsic resistance. Acquired resistance develops both in patients undergoing chemotherapy and in cell lines exposed to increasing concentrations of cisplatin until they have reached a high tolerance, while intrinsic resistance is described when patient tumours are naturally unaffected by platinum treatment (Zamble and Lippard 1995).

An increased level of DNA repair in tumour cells is suggested to be a main cause of resistance. The enhanced expression of proteins involved in repair is suggested to be associated with the elevation of DNA repair. However, other mechanisms, such as inhibition of drug uptake, enhanced replicative bypass of the cisplatin-DNA adducts and changes in the concentration of regulatory proteins may also contribute to the cisplatin resistance (Zamble and Lippard 1995).

ERCC1 is essential in the NER pathway that recognizes and removes cisplatin-induced DNA adducts (Zamble et al. 1996). ERCC1 also plays an important role in the repair of ICL in DNA and in recombination processes (Niedernhofer et al. 2004). It has been reported that the platinum resistance is linked with elevated expression of ERCC1 mRNA in cell lines from ovarian, cervical, testicular, bladder, and non–small-cell lung cancer (Altaha et al. 2004).

In this thesis, we have detected the level of five DNA repair proteins, including two NER proteins, ERCC1 and XPF, as well as 3 MMR proteins, MSH2, MSH6 and MLH1, in human melanomas, melanocytes and ovarian tumour cells. In our study, we noticed a higher level of ERCC1 protein, as well as its partner the XPF protein in melanoma cell lines compared to ovarian tumour cell lines. This might contribute to the high resistance to chemotherapy in melanoma. One MMR protein, MLH1, also showed a higher level in melanoma cell lines, while the other two MMR proteins, MSH2 and MSH6, showed a similar expression in all tested cell lines. However, we found that the elevated DNA repair protein level was not linked to an increased DNA repair capability for either UV or cisplatin induced DNA damage. The ovarian tumour cell line PEO4, which only has half the ERCC1 level compared to the melanoma cell line A375, showed the best survival rate following UV irradiation. In the SRB assay for detecting cisplatin cytotoxity and resistance, the ovarian tumour cell lines PEO4 and PEO6, which had a lower level of ERCC1 compared to all melanoma cell lines used in the assay, showed higher resistance to cisplatin.

Although only four cell lines were tested by colony forming assay, the result is in agreement with our previous data by short-term survival assay following UV irradiation (Ewan Brown, unpublished observations). The resistance to cisplatin in the ovarian tumours by SRB assay correlates with our previous IC_{50} data (Ewan Brown, unpublished observations). Combining all the data together, we found no evidence that the elevated level of DNA repair proteins in melanoma cell lines could be linked with increased DNA repair capabilities for UV or cisplatin induced damage. However, it is important to note that growth or survival assays give only an indirect measure of DNA repair capability.

Also, an investigation comparing DNA repair between totally different cell lines itself is problematic. More samples of each tumour type may be needed to achieve any solid conclusions. However, if we just focus on the ovarian tumour group, the result is still quite interesting.

As described before, PEO4 and PEO6 are cisplatin-resistant derivatives of PEO1, while PEO23 and PEA2 are cisplatin-resistant derivatives of PEO14 and PEA1, respectively (Langdon et al. 1988). According the western blotting analysis, a trend of slightly increased protein level was shown in three of five tested DNA repair proteins, ERCC1, XPF and MLH1, in derivative cisplatin-resistant cell lines. In terms of ERCC1 protein level, derivative PEA2 was 2 times higher than the original cell line PEA1, while derivatives PEO4 and PEO6 also showed an increased level of ERCC1. Only derivative PEO23 had a lower ERCC1 level than original cell line PEO14 (Figure 5.1). In terms of XPF, all derivatives showed an increased level compared to their original cell lines (Figure 5.2). In terms of MLH1, the majority of cisplatin-resistant derivatives had an increased protein level, except PEO6, which showed a slightly lower level of MLH1 than PEO1. However, although there is a trend for the cisplatin-resistant ovarian lines to have higher levels of these repair proteins, the differences are small and none are significant. For the other two MMR proteins MSH2 and MSH6, there was no correlation between protein levels and cisplatin resistance. There was no evidence that cisplatin resistant derivatives had decreased expression of MMR genes as previously reported (Strathdee et al. 1999).

In the colony forming assay, PEO6 showed an increased survival rate compared to PEO4. This could be due to the higher protein expression of both ERCC1 and XPF in PEO6 (Figure 5.6). In the SRB assay of cisplatin resistance (Figure 5.8), derivatives PEO4 and PEO6 showed a much higher resistance compared to the original cell line

PEO1. PEO6 was more resistant to cisplatin than PEO4, as with the treatment of 3uM cisplatin, PEO6 showed a survival rate at more than 80% compared to less than 60% for PEO4. Although PEO1 had higher DNA repair protein levels than PEA1 (both cisplatin sensitive), it was more sensitive to cisplatin than PEA1. This might suggest that in tested cell lines, the level of DNA repair proteins following the treatment, rather than before the treatment, is more meaningful to predicting chemotherapy resistance of the tumour. The elevated level of DNA repair proteins after the cisplatin treatment might be linked with higher tumour cell survival and higher resistance, representing some kind of acquired resistance.

As far as we are aware the melanoma cell lines we assayed had not been exposed to cisplatin previously, either *in vivo* or *in vitro*. The same applied to some of the ovarian tumour cell lines, while others had arisen as resistant derivatives following cisplatin treatment. Since the cisplatin resistant ovarian tumour cell lines were not maintained in cisplatin, any acquired resistance perhaps with associated increased levels of ERCC1 and XPF may have been lost during extensive in vitro culture in non-selective conditions. Thus, our approach to attempt to correlate DNA repair protein levels with resistance to DNA damaging agents by comparison between different tumour cell lines with different histories of exposure to DNA damaging agents was problematic. A better approach could be to measure levels of DNA repair proteins simultaneously on a large collection of tumour samples on a tissue microarray and correlate this directly with data on intrinsic or acquired resistance of individual tumours to chemotherapeutic agents.

Because of these limitations we switched to a different approach where we could study the consequence of altered levels of ERCC1 directly on melanoma growth in a series of isogenic immortalised mouse melanocyte cell lines. Xenografts of the Ercc1-proficient melanocyte line grew rapidly as malignant melanoma when xenografted into nude mice.

Cisplatin treatment caused an initial shrinkage of these tumours, but cisplatin resistance quickly appeared. Cell re-isolated from untreated xenografts had the same ERCC1 level as the input cell line, while cells from cisplatin-resistant tumours, had 2-fold elevated levels of ERCC1. This demonstrates in a direct functional assay that acquired resistance to cisplatin is associated with increased levels of ERCC1.

While the Ercc1-deficient derivative of the mouse melanocyte cell line grew as rapidly as the Ercc1-proficient partner *in vitro*, for the first seven weeks after being xenografted into mice it grew very slowly. During the first week after xenografting slow growing tumours often show some shrinkage as the supporting matrigel is resorbed and this was the case with both the Ercc1-proficient and Ercc1-deficient melanocytes. However, while the Ercc1-proficient melanocyte xenografts then grew rapidly resulting in tumour size end points being reached within 4 weeks, it took 7 weeks before the Ercc1-deficient melanocyte tumours began to grow rapidly.

It is very interesting to see that the lack of ERCC1 slowed the initial growth of xenografts in nude mice. Perhaps this results from greater exposure during the early stages of *in vivo* growth to endogenous DNA damage. During growth of tumours, a highly heterogeneous microenvironment, characterized by oxygen depletion, extracellular acidosis, elevated lactate levels, glucose deprivation, low energy status, and interstitial hypertension, can be developed (Vaupel et al. 1989). This hostile microenvironment could result in increased DNA damage that would normally be repaired by pathways requiring ERCC1. The physiological parameters of the microenvironment of tumours are mainly determined by the blood supply, which depends primarily on the vascular density (Vaupel 2004). At the initial growth stage of xenografts in mice, the vascular density will be very low, the blood supply of the tumour could be critical and the oxygen level could be low. With the establishment of the blood

supply, the oxygen level in the tumour cells could increase rapidly resulting in elevated level of oxidative DNA damage that would be growth inhibitory to the DNA repair deficient xenografts.

Another less likely possibility is that the Ercc1-deficient xenografts needed to acquire some new mutations before growth could commence *in vivo*. The Ercc1-deficient xenografts persisted in mice but only grew very slowly for a comparatively long period (more than 7 weeks) following the transplantation compared to the Ercc1-proficient xenografts. The Ercc1-deficient tumours then started to grow rapidly and this could potentially be linked to new mutations. This possibility could be investigated by performing microarray to identify gene expression changes between input Ercc1-deficient melanocytes and cells subsequently reisolated from rapidly growing tumours. Any changes could then be compared with any identified in a similar comparison of input Ercc1-proficient melanocytes with cells reisolated from tumours (Pardo et al. 2009).

Once the Ercc1-deficient xenografts had established themselves they grew as rapidly as Ercc1-proficient xenografts. However, they were cured by cisplatin treatment, while Ercc1-proficient xenografts rapidly became resistant. These results demonstrate that, in this mouse melanoma xenograft model, ERCC1 is important for melanoma growth and is essential for resistance to cisplatin. This raises the possibility that an ERCC1 inhibitor could be used to enhance the effectiveness of cisplatin treatment. The melanoma xenograft system that we have developed could be used to identify and test such inhibitors.

Chapter 6:

Conclusion

Maintaining genetic integrity is essential for proper cellular functioning because the accumulation of DNA mutations may activate proto-oncogenes and inactivate tumour suppressors, leading to an increased risk of tumourigenesis. The nucleotide excision repair (NER) pathway plays an important role in repairing various types of DNA damage, especially UV-induced DNA lesions. Studies have identified that defects in NER are linked with several diseases such as XP, TTD and CS. ERCC1 with its partner XPF plays an essential role in the NER pathway as an endonuclease to make the 5' incision around the DNA lesions. However, the consequences of ERCC1 deficiency in in human have not been studied in-depth due to its extreme rarity. The first reported case of human inherited ERCC1 deficiency was associated with Cerebro-Oculo-Facio-Skeletal (COFS) syndrome (Jaspers et al. 2007). The patient failed to pass any developmental milestones and died at the age of 14 months due to respiratory failure from bilateral pneumonia. Analysis on the patient is still going on but it is clear that in this case of ERCC1 deficiency in human there is a mild defect in NER and severe developmental failure.

Due to the limitation of using human subjects for disease pathogenesis studies, the availability of genetically-engineered mouse models becomes a powerful tool for investigating the molecular pathology of ERCC1 deficiency. Our group was the first to successfully generate the ERCC1 knockout mouse which was associated with severe runting and a very short lifespan due to liver failure (McWhir et al. 1993; Selfridge et al. 2001). We also created a mouse model with longer lifespan using a liver-specific transgene and a mouse model with tissue-specific ERCC1 knock out using an Ercc1 floxed allele. These made a good platform to perform further investigations of ERCC1 function and deficiency in mouse.

Previous group work has identified a 1.5kb skin-specific Ercc1 transcript which originates from an alternative upstream promoter in mouse skin (J.Selfridge, unpublished observations). In skin, the 1.5kb novel transcript was the major transcript compared to the normal 1.1kb Ercc1 transcript. This 1.5kb skin-specific transcript is more abundant in most albino mouse strains and is barely detectable in pigmented mouse strains.

Since NER has evolved to deal with UV-induced DNA damage and most UV damage in the body occurs in skin, we hypothesised that the novel transcript might be linked with increased DNA repair capability. Therefore we decided to investigate whether the high levels of novel Ercc1 transcript expression in skin was linked with any functional role, especially any link with repair of UV-induced DNA damage and protecting the skin from skin cancer.

It was important to find the source of the 1.5kb Ercc1 transcript as it is not possible for it to originate from the normal Ercc1 promoter. We found no evidence for the 11kb upstream and 2.5kb upstream potential promoter regions as the source of the 1.5kb skin-specific Ercc1 transcripts. Meanwhile, we investigated the region approximately 1kb to the 5' side of the known Ercc1 promoter and found an interesting different sequence pattern within this region among Balb/C (albino), C57BL/6 (pigmented) and 129/Ola (pigmented) mouse strains (Chapter 4). A CAAT signal, TATA signal, LINE/L2 transposable element and CT repeats were found in all investigated strains. However, in the albino Balb/C strain only, beside these above regulatory elements, we found a SINE/B2 element 1023bp upstream of the normal promoter. The CT repeats in the Balb/C strain were also longer than in the other two tested strains. As the insertion of a transposable element at the promoter region is known to be capable of altering gene expression patterns by contributing additional transcription factor binding sites

(Thornburg et al. 2006), it was possible that the insertion of this SINE/B2 element in albino strains could relate to the altered Ercc1 gene expression. CT repeats in a promoter region have also been reported to be linked with an alternative transcription start site (Xu and Goodridge 1998). It also has been reported that the CT repeats strongly regulate the human HMGA2 promoter with an activation pattern that correlates to its CT repeat length (Borrmann et al. 2003).

Our 5'RACE result and some confirmed Ercc1 transcripts in an online database, which contain the same exon 1 as our novel 1.5kb skin-specific Ercc1 transcript, mapped the transcription start site to the 5' region just upstream of the known Ercc1 promoter. In addition, the UV resistance of Ercc1 deficient mouse keratinocytes could be corrected by using a minigene which contains just the 1.03kb of sequence upstream of the known Ercc1 promoter and directs expression of the 1.5kb Ercc1 transcript. Thus, we believe that the high level of the novel 1.5kb skin-specific Ercc1 transcripts is driven by the region immediately upstream of the normal Ercc1 promoter.

The Ercc1 skin-specific transcript is expressed at a higher level in most albino strains analysed, but does it have a functional role? Firstly, we found that the size of the ERCC1 protein was the same in skin as in other tissues examined. This was in agreement with our previous studies on this 1.5kb Ercc1 transcript where we found no difference in the coding regions between the 1.1kb and 1.5kb Ercc1 transcripts. Secondly, we found that ERCC1 protein levels were generally consistent with Ercc1 mRNA levels in all mouse tissues examined except skin.

As the 1.5kb skin-specific transcript had a much higher level in most albino strains compared to pigmented strains, we further tested the ERCC1 protein level between

different mouse strains. As the 1.5kb Ercc1 transcript had a much higher level in albino mouse skin, we expected that this would produce higher protein expression of ERCC1 in albino skin. However, this was not what we found. Levels of this 1.5kb transcript were not increased in mouse skin and cultured mouse keratinocytes after UV irradiation. Perhaps this is because the level of the 1.5kb Ercc1 transcript mRNA is already high enough to maintain adequate level of ERCC1 protein to respond to UV-induced DNA damage.

Unrepaired UV-induced DNA damage blocks RNA Pol II transcription. This could lead to reduced levels of DNA repair proteins at precisely the time when they are most needed. Could the 1.5kb transcript be involved in maintaining adequate levels of ERCC1 in the presence of a UV-damaged template? Albino strains lacking pigment protection would be at a greater risk of UV-induced DNA damage than pigmented strains. The SINE/B2 elements could contribute additional transcription factor binding sites, while the longer CT repeats could contribute to a more stable level of transcription on a UV-damaged template (Borrmann et al. 2003). Both CPDs and 6-4PPs lead to altered helical structure. After UV irradiation the CT repeats could be expected to have a higher level of damage and the altered conformation might act as a local monitor of damage around the Ercc1 gene favouring adjacent initiation by RNA Pol II. To sum up, the role of the 1.5kb skin-specific Ercc1 transcript in albino strains may be to maintain Ercc1 transcription on a UV-damaged template rather than to boost expression. This hypothesis could be investigated by run on transcription assays from the normal and upstream Ercc1 promoter on UV-damaged and non-irradiated templates.

Chapter 5 investigated the functional role of ERCC1 in melanoma, especially its reported correlation with resistance to the widely used chemotherapy drug cisplatin. An increased level of Ercc1 mRNA is reported to be correlated with resistance and

prognosis in a number of different cancers, such as advanced colorectal cancer, non-small cell lung cancer and oesophageal cancer (Lord et al. 2002; Wei et al. 2008; Kim et al. 2009). We determined the level of NER proteins ERCC1 and its partner XPF between human melanoma and ovarian cancer cells. As melanoma is more resistance to cisplatin, we expected the level of the NER proteins to be higher in melanoma compared to ovarian cancer cell lines. Both ERCC1 and XPF showed an elevated level in melanoma. However, further investigations by proliferation assays didn't show any increased survival following UV-irradiation or cisplatin treatment in melanoma cell lines compared to ovarian cancer cell lines. The mechanism of the elevated level of NER proteins in cisplatin-resistant cells need to be investigated further. It is possible that the upstream promoter might be involved in this production of elevated level of ERCC1 mRNA in cancer. To investigate this, 5'RACE and northern blotting analysis should be carried out on RNAs from cisplatin sensitive and resistant tumours.

To investigate the role of ERCC1 in melanoma more directly, we turned to a system where we could manipulate the levels of ERCC1 directly and measure the consequences for melanoma growth and resistance to cisplatin. To achieve this, immortalized ERCC1 proficient and deficient mouse melanocyte cell lines isolated from our mouse strain and which grow as xenografts with the histological characteristics of malignant melanoma were transplanted into nude mice and some mice were treated with cisplatin. (D.Melton, unpublished observations).

Using this mouse model we noticed a very interesting result that the lack of ERCC1 slows down the xenograft growth rate significantly in nude mice. Although both cell lines grew at the same rate *in vitro*, the ERCC1 proficient xenografts grew very rapidly while the ERCC1 deficient xenografts showed nearly 3 times slower growth during the initial phase of xenograft growth.

Cisplatin treatments on ERCC1 proficient and deficient xenografts also showed a significant difference. ERCC1 proficient xenografts rapidly became cisplatin resistant, but the growth of ERCC1 deficient xenografts was completely inhibited. This raises the possibility that ERCC1 may be used to enhance the efficiency of cisplatin treatment. Moreover, this melanoma xenograft system could be ideal to identify and test possible ERCC1 inhibitors. Up to date, most of the reported ERCC1 inhibitors, such as UCN-01, actually do not inhibit ERCC1 directly but affect the interaction between ERCC1 and other NER proteins (Jiang and Yang 1999). We are screening the reported Ercc1 inhibitors, as well as searching for new potential drugs *in vitro* by proliferation assay now. Once some interesting drugs are found by *in vitro* assay, we can test them further using our xenograft model *in vivo*.

References

Adly Yacoub, R. M., Darin Hinman, Theodore Chung, Paul Dent, and Michael P. Hagan (2003). "Epidermal Growth Factor and Ionizing Radiation Up-regulate the DNA Repair Genes XRCC1 and ERCC1 in DU145 and LNCaP Prostate Carcinoma through MAPK Signaling." *Radiation Research* **159**(4): 439-452.

Al-Minawi, A. Z., N. Saleh-Gohari and T. Helleday (2008). "The ERCC1/XPF endonuclease is required for efficient single-strand annealing and gene conversion in mammalian cells." *Nucleic Acids Res* **36**(1): 1-9.

Altaha, R., X. Liang, J. J. Yu and E. Reed (2004). "Excision repair cross complementing-group 1: gene expression and platinum resistance." *Int J Mol Med* **14**(6): 959-970.

Andressoo, J. O., G. Weeda, J. de Wit, J. R. Mitchell, R. B. Beems, H. van Steeg, G. T. van der Horst and J. H. Hoeijmakers (2009). "An Xpb mouse model for combined xeroderma pigmentosum and cockayne syndrome reveals progeroid features upon further attenuation of DNA repair." *Mol Cell Biol* **29**(5): 1276-1290.

Andrieux, L. O., A. Fautrel, A. Bessard, A. Guillouzo, G. Baffet and S. Langouet (2007). "GATA-1 is essential in EGF-mediated induction of nucleotide excision repair activity and ERCC1 expression through ERK2 in human hepatoma cells." *Cancer Res* **67**(5): 2114-2123.

Anttinen, A., L. Koulu, E. Nikoskelainen, R. Portin, T. Kurki, M. Erkinjuntti, N. G. Jaspers, A. Raams, M. H. Green, A. R. Lehmann, J. F. Wing, C. F. Arlett and R. J. Marttila (2008). "Neurological symptoms and natural course of xeroderma pigmentosum." *Brain* **131**(Pt 8): 1979-1989.

Arnaudeau, C., C. Lundin and T. Helleday (2001). "DNA double-strand breaks associated with replication forks are predominantly repaired by homologous recombination involving an exchange mechanism in mammalian cells." *J Mol Biol* **307**(5): 1235-1245.

Baccarelli, A., D. Calista, P. Minghetti, B. Marinelli, B. Albetti, T. Tseng, M. Hedayati, L. Grossman, G. Landi, J. P. Struewing and M. T. Landi (2004). "XPD gene polymorphism and host characteristics in the association with cutaneous malignant melanoma risk." *Br J Cancer* **90**(2): 497-502.

Berg, R., A. d. Vries, H. v. Steeg and F. d. Gruijl (1997). "Relative susceptibilities of XPA knockout mice and their heterozygous and wild-type littermates to UVB-induced skin cancer." *Cancer Res*(57): 581-584.

Berg, R. J., H. Rebel, G. T. van der Horst, H. J. van Kranen, L. H. Mullenders, W. A. van Vloten and F. R. de Gruijl (2000). "Impact of global genome repair versus transcription-coupled repair on ultraviolet carcinogenesis in hairless mice." *Cancer Res* **60**(11): 2858-2863.

Bergink, S. and S. Jentsch (2009). "Principles of ubiquitin and SUMO modifications in DNA repair." *Nature* **458**(7237): 461-467.

Bertola, D. R., H. Cao, L. M. Albano, D. P. Oliveira, F. Kok, M. J. Marques-Dias, C. A. Kim and R. A. Hegele (2006). "Cockayne syndrome type A: novel mutations in eight typical patients." *J Hum Genet* **51**(8): 701-705.

Berwick, M. and A. Halpern (1997). "Melanoma epidemiology." *Curr Opin Oncol* **9**(2): 178-182.

Bishop, D. T., F. Demenais, A. M. Goldstein, W. Bergman, J. N. Bishop, B. Bressac-de Paillerets, A. Chompret, P. Ghiorzo, N. Gruis, J. Hansson, M. Harland, N. Hayward, E. A. Holland, G. J. Mann, M. Mantelli, D. Nancarrow, A. Platz and M. A. Tucker (2002). "Geographical variation in the penetrance of CDKN2A mutations for melanoma." *J Natl Cancer Inst* **94**(12): 894-903.

Blankenburg, S., I. R. Konig, R. Moessner, P. Laspe, K. M. Thoms, U. Krueger, S. G. Khan, G. Westphal, C. Berking, M. Volkenandt, K. Reich, C. Neumann, A. Ziegler, K. H. Kraemer and S. Emmert (2005). "Assessment of 3 xeroderma pigmentosum group C gene polymorphisms and risk of cutaneous melanoma: a case-control study." *Carcinogenesis* **26**(6): 1085-1090.

Blankenburg, S., I. R. Konig, R. Moessner, P. Laspe, K. M. Thoms, U. Krueger, S. G. Khan, G. Westphal, M. Volkenandt, C. Neumann, A. Ziegler, K. H. Kraemer, K. Reich

and S. Emmert (2005). "No association between three xeroderma pigmentosum group C and one group G gene polymorphisms and risk of cutaneous melanoma." *Eur J Hum Genet* **13**(2): 253-255.

Bliss, J. M., D. Ford, A. J. Swerdlow, B. K. Armstrong, M. Cristofolini, J. M. Elwood, A. Green, E. A. Holly, T. Mack and R. M. MacKie (1995). "Risk of cutaneous melanoma associated with pigmentation characteristics and freckling: systematic overview of 10 case-control studies. The International Melanoma Analysis Group (IMAGE)." *Int J Cancer* **62**(4): 367-376.

Bootsma, D., K. H. Kraemer, J. Cleaver and J. H. J. Hoeijmakers (2002). Nucleotide excision repair syndromes: xeroderma pigmentosum, Cockayne syndrome and trichothiodystrophy. New York, McGraw-Hill Professional; 2 edition.

Borrmann, L., B. Seebeck, P. Rogalla and J. Bullerdiek (2003). "Human HMGA2 promoter is coregulated by a polymorphic dinucleotide (TC)-repeat." *Oncogene* **22**(5): 756-760.

Branzei, D. and M. Foiani (2008). "Regulation of DNA repair throughout the cell cycle." *Nat Rev Mol Cell Biol* **9**(4): 297-308.

Brown, C. K. and J. M. Kirkwood (2003). "Medical management of melanoma." *Surg Clin North Am* **83**(2): 283-322, viii.

Brown, T. J. and B. R. Nelson (1999). "Malignant melanoma: a clinical review." *Cutis* **63**(5): 275-278, 281-274.

Buermeyer, A. B., C. Wilson-Van Patten, S. M. Baker and R. M. Liskay (1999). "The human MLH1 cDNA complements DNA mismatch repair defects in Mlh1-deficient mouse embryonic fibroblasts." *Cancer Res* **59**(3): 538-541.

Busch, D. B., H. van Vuuren, J. de Wit, A. Collins, M. Z. Zdzienicka, D. L. Mitchell, K. W. Brookman, M. Stefanini, R. Riboni, L. H. Thompson, R. B. Albert, A. J. van Gool and J. Hoeijmakers (1997). "Phenotypic heterogeneity in nucleotide excision repair mutants of rodent complementation groups 1 and 4." *Mutat Res* **383**(2): 91-106.

Cheo, D. L., D. K. Burns, L. B. Meira, J. F. Houle and E. C. Friedberg (1999). "Mutational inactivation of the xeroderma pigmentosum group C gene confers predisposition to 2-acetylaminofluorene-induced liver and lung cancer and to spontaneous testicular cancer in Trp53-/- mice." *Cancer Res* **59**(4): 771-775.

Cheo, D. L., H. J. Ruven, L. B. Meira, R. E. Hammer, D. K. Burns, N. J. Tappe, A. A. van Zeeland, L. H. Mullenders and E. C. Friedberg (1997). "Characterization of defective nucleotide excision repair in XPC mutant mice." *Mutat Res* **374**(1): 1-9.

Chin, L. (2003). "The genetics of malignant melanoma: lessons from mouse and man." *Nat Rev Cancer* **3**(8): 559-570.

Chipchase, M. D. and D. W. Melton (2002). "The formation of UV-induced chromosome aberrations involves ERCC1 and XPF but not other nucleotide excision repair genes." *DNA Repair (Amst)* **1**(4): 335-340.

Citterio, E., V. Van Den Boom, G. Schnitzler, R. Kanaar, E. Bonte, R. E. Kingston, J. H. Hoeijmakers and W. Vermeulen (2000). "ATP-dependent chromatin remodeling by the Cockayne syndrome B DNA repair-transcription-coupling factor." *Mol Cell Biol* **20**(20): 7643-7653.

Colella, S., T. Nardo, E. Botta, A. R. Lehmann and M. Stefanini (2000). "Identical mutations in the CSB gene associated with either Cockayne syndrome or the DeSanctis-cacchione variant of xeroderma pigmentosum." *Hum Mol Genet* **9**(8): 1171-1175.

Cone, R. D., D. Lu, S. Koppula, D. I. Vage, H. Klungland, B. Boston, W. Chen, D. N. Orth, C. Pouton and R. A. Kesterson (1996). "The melanocortin receptors: agonists, antagonists, and the hormonal control of pigmentation." *Recent Prog Horm Res* **51**: 287-317; discussion 318.

Darmstadt, G. L., P. Fleckman, M. Jonas, E. Chi and C. E. Rubens (1998). "Differentiation of cultured keratinocytes promotes the adherence of Streptococcus pyogenes." *J Clin Invest* **101**(1): 128-136.

David, S. S., V. L. O'Shea and S. Kundu (2007). "Base-excision repair of oxidative DNA damage." *Nature* **447**(7147): 941-950.

Davies, H., G. R. Bignell, C. Cox, P. Stephens, S. Edkins, S. Clegg, J. Teague, H. Woffendin, M. J. Garnett, W. Bottomley, N. Davis, E. Dicks, R. Ewing, Y. Floyd, K. Gray, S. Hall, R. Hawes, J. Hughes, V. Kosmidou, A. Menzies, C. Mould, A. Parker, C. Stevens, S. Watt, S. Hooper, R. Wilson, H. Jayatilake, B. A. Gusterson, C. Cooper, J. Shipley, D. Hargrave, K. Pritchard-Jones, N. Maitland, G. Chenevix-Trench, G. J. Riggins, D. D. Bigner, G. Palmieri, A. Cossu, A. Flanagan, A. Nicholson, J. W. Ho, S. Y. Leung, S. T. Yuen, B. L. Weber, H. F. Seigler, T. L. Darrow, H. Paterson, R. Marais, C. J. Marshall, R. Wooster, M. R. Stratton and P. A. Futreal (2002). "Mutations of the BRAF gene in human cancer." *Nature* **417**(6892): 949-954.

de Boer, J., J. de Wit, H. van Steeg, R. J. Berg, H. Morreau, P. Visser, A. R. Lehmann, M. Duran, J. H. Hoeijmakers and G. Weeda (1998). "A mouse model for the basal transcription/DNA repair syndrome trichothiodystrophy." *Mol Cell* **1**(7): 981-990.

de Boer, J., I. Donker, J. de Wit, J. H. Hoeijmakers and G. Weeda (1998). "Disruption of the mouse xeroderma pigmentosum group D DNA repair/basal transcription gene results in preimplantation lethality." *Cancer Res* **58**(1): 89-94.

de Boer, J. and J. H. Hoeijmakers (2000). "Nucleotide excision repair and human syndromes." *Carcinogenesis* **21**(3): 453-460.

de Boer, J., H. van Steeg, R. J. Berg, J. Garssen, J. de Wit, C. T. van Oostrum, R. B. Beems, G. T. van der Horst, C. F. van Kreijl, F. R. de Gruijl, D. Bootsma, J. H. Hoeijmakers and G. Weeda (1999). "Mouse model for the DNA repair/basal

transcription disorder trichothiodystrophy reveals cancer predisposition." *Cancer Res* **59**(14): 3489-3494.

de la Chapelle, A. (2004). "Genetic predisposition to colorectal cancer." *Nat Rev Cancer* **4**(10): 769-780.

de Laat, W. L., E. Appeldoorn, N. G. Jaspers and J. H. Hoeijmakers (1998). "DNA structural elements required for ERCC1-XPF endonuclease activity." *J Biol Chem* **273**(14): 7835-7842.

de Laat, W. L., N. G. Jaspers and J. H. Hoeijmakers (1999). "Molecular mechanism of nucleotide excision repair." *Genes Dev* **13**(7): 768-785.

de Laat, W. L., A. M. Sijbers, H. Odijk, N. G. Jaspers and J. H. Hoeijmakers (1998). "Mapping of interaction domains between human repair proteins ERCC1 and XPF." *Nucleic Acids Res* **26**(18): 4146–4152.

de Vries, A., R. J. Berg, S. Wijnhoven, A. Westerman, P. W. Wester, C. F. van Kreijl, P. J. Capel, F. R. de Gruijl, H. J. van Kranen and H. van Steeg (1998). "XPA-deficiency in hairless mice causes a shift in skin tumor types and mutational target genes after exposure to low doses of U.V.B." *Oncogene* **16**(17): 2205-2212.

de Vries, A., C. T. van Oostrom, F. M. Hofhuis, P. M. Dortant, R. J. Berg, F. R. de Gruijl, P. W. Wester, C. F. van Kreijl, P. J. Capel and H. van Steeg (1995). "Increased susceptibility to ultraviolet-B and carcinogens of mice lacking the DNA excision repair gene XPA." *Nature* **377**(6545): 169-173.

Doig, J., C. Anderson, N. J. Lawrence, J. Selfridge, D. G. Brownstein and D. W. Melton (2006). "Mice with skin-specific DNA repair gene (Ercc1) inactivation are hypersensitive to ultraviolet irradiation-induced skin cancer and show more rapid actinic progression." *Oncogene* **25**(47): 6229-6238.

Duncan, T., S. C. Trewick, P. Koivisto, P. A. Bates, T. Lindahl and B. Sedgwick (2002). "Reversal of DNA alkylation damage by two human dioxygenases." *Proc Natl Acad Sci U S A* **99**(26): 16660-16665.

Durant, S. T., M. M. Morris, M. Illand, H. J. McKay, C. McCormick, G. L. Hirst, R. H. Borts and R. Brown (1999). "Dependence on RAD52 and RAD1 for anticancer drug resistance mediated by inactivation of mismatch repair genes." *Curr Biol* **9**(1): 51-54.

Eggermont, A. M. and J. M. Kirkwood (2004). "Re-evaluating the role of dacarbazine in metastatic melanoma: what have we learned in 30 years?" *Eur J Cancer* **40**(12): 1825-1836.

Evans, E., J. G. Moggs, J. R. Hwang, J. M. Egly and R. D. Wood (1997). "Mechanism of open complex and dual incision formation by human nucleotide excision repair factors." *EMBO J* **16**(21): 6559-6573.

Ferrigno, O., T. Virolle, Z. Djabari, J. P. Ortonne, R. J. White and D. Aberdam (2001). "Transposable B2 SINE elements can provide mobile RNA polymerase II promoters." *Nat Genet* **28**(1): 77-81.

Florell, S. R., L. J. Meyer, K. M. Boucher, P. A. Porter-Gill, M. Hart, J. Erickson, L. A. Cannon-Albright, L. K. Pershing, R. M. Harris, W. E. Samlowski, J. J. Zone and S. A. Leachman (2004). "Longitudinal assessment of the nevus phenotype in a melanoma kindred." *J Invest Dermatol* **123**(3): 576-582.

Fousteri, M., W. Vermeulen, A. A. van Zeeland and L. H. Mullenders (2006). "Cockayne syndrome A and B proteins differentially regulate recruitment of chromatin remodeling and repair factors to stalled RNA polymerase II in vivo." *Mol Cell* **23**(4): 471-482.

Friedberg, E. C. (2003). "DNA damage and repair." *Nature* **421**(6921): 436-440.

Friedberg, E. C. and L. B. Meira (1999). "Database of mouse strains carrying targeted mutations in genes affecting cellular responses to DNA damage: version 3." *Mutat Res* **433**(2): 69-87.

Friedman, R. J., D. S. Rigel and A. W. Kopf (1985). "Early detection of malignant melanoma: the role of physician examination and self-examination of the skin." *CA Cancer J Clin* **35**(3): 130-151.

Garraway, L. A., H. R. Widlund, M. A. Rubin, G. Getz, A. J. Berger, S. Ramaswamy, R. Beroukhim, D. A. Milner, S. R. Granter, J. Du, C. Lee, S. N. Wagner, C. Li, T. R. Golub, D. L. Rimm, M. L. Meyerson, D. E. Fisher and W. R. Sellers (2005). "Integrative genomic analyses identify MITF as a lineage survival oncogene amplified in malignant melanoma." *Nature* **436**(7047): 117-122.

Giglia-Mari, G., F. Coin, J. A. Ranish, D. Hoogstraten, A. Theil, N. Wijgers, N. G. Jaspers, A. Raams, M. Argentini, P. J. van der Spek, E. Botta, M. Stefanini, J. M. Egly, R. Aebersold, J. H. Hoeijmakers and W. Vermeulen (2004). "A new, tenth subunit of TFIIH is responsible for the DNA repair syndrome trichothiodystrophy group A." *Nat Genet* **36**(7): 714-719.

Giglia-Mari, G., C. Miquel, A. F. Theil, P. O. Mari, D. Hoogstraten, J. M. Ng, C. Dinant, J. H. Hoeijmakers and W. Vermeulen (2006). "Dynamic interaction of TTDA with TFIIH is stabilized by nucleotide excision repair in living cells." *PLoS Biol* **4**(6): e156.

Gillespie, J. M. and R. C. Marshall (1983). "A comparison of the proteins of normal and trichothiodystrophic human hair." *J Invest Dermatol* **80**(3): 195-202.

Goldstein, A. M., M. T. Landi, S. Tsang, M. C. Fraser, D. J. Munroe and M. A. Tucker (2005). "Association of MC1R variants and risk of melanoma in melanoma-prone families with CDKN2A mutations." *Cancer Epidemiol Biomarkers Prev* **14**(9): 2208-2212.

Graham, J. M., Jr., K. Anyane-Yeboa, A. Raams, E. Appeldoorn, W. J. Kleijer, V. H. Garritsen, D. Busch, T. G. Edersheim and N. G. Jaspers (2001). "Cerebro-oculo-facio-skeletal syndrome with a nucleotide excision-repair defect and a mutated XPD gene, with prenatal diagnosis in a triplet pregnancy." *Am J Hum Genet* **69**(2): 291-300.

Gray-Schopfer, V., C. Wellbrock and R. Marais (2007). "Melanoma biology and new targeted therapy." *Nature* **445**(7130): 851-857.

Gray-Schopfer, V. C., S. C. Cheong, H. Chong, J. Chow, T. Moss, Z. A. Abdel-Malek, R. Marais, D. Wynford-Thomas and D. C. Bennett (2006). "Cellular senescence in naevi and immortalisation in melanoma: a role for p16?" *Br J Cancer* **95**(4): 496-505.

Groisman, R., J. Polanowska, I. Kuraoka, J. Sawada, M. Saijo, R. Drapkin, A. F. Kisselev, K. Tanaka and Y. Nakatani (2003). "The ubiquitin ligase activity in the DDB2 and CSA complexes is differentially regulated by the COP9 signalosome in response to DNA damage." *Cell* **113**(3): 357-367.

Grosveld, G. C., E. de Boer, C. K. Shewmaker and R. A. Flavell (1982). "DNA sequences necessary for transcription of the rabbit beta-globin gene in vivo." *Nature* **295**(5845): 120-126.

Grosveld, G. C., C. K. Shewmaker, P. Jat and R. A. Flavell (1981). "Localization of DNA sequences necessary for transcription of the rabbit beta-globin gene in vitro." *Cell* **25**(1): 215-226.

Haass, N. K., K. S. Smalley and M. Herlyn (2004). "The role of altered cell-cell communication in melanoma progression." *J Mol Histol* **35**(3): 309-318.

Han, J., G. A. Colditz, J. S. Liu and D. J. Hunter (2005). "Genetic variation in XPD, sun exposure, and risk of skin cancer." *Cancer Epidemiol Biomarkers Prev* **14**(6): 1539-1544.

Harada, Y. N., N. Shiomi, M. Koike, M. Ikawa, M. Okabe, S. Hirota, Y. Kitamura, M. Kitagawa, T. Matsunaga, O. Nikaido and T. Shiomi (1999). "Postnatal growth failure, short life span, and early onset of cellular senescence and subsequent immortalization in mice lacking the xeroderma pigmentosum group G gene." *Mol Cell Biol* **19**(3): 2366-2372.

Harrison, J. C. and J. E. Haber (2006). "Surviving the breakup: the DNA damage checkpoint." *Annu Rev Genet* **40**: 209-235.

Hayward, N. K. (2003). "Genetics of melanoma predisposition." *Oncogene* **22**(20): 3053-3062.

Hefferin, M. L. and A. E. Tomkinson (2005). "Mechanism of DNA double-strand break repair by non-homologous end joining." *DNA Repair (Amst)* **4**(6): 639-648.

Henning, K. A., L. Li, N. Iyer, L. D. McDaniel, M. S. Reagan, R. Legerski, R. A. Schultz, M. Stefanini, A. R. Lehmann, L. V. Mayne and E. C. Friedberg (1995). "The Cockayne syndrome group A gene encodes a WD repeat protein that interacts with CSB protein and a subunit of RNA polymerase II TFIIH." *Cell* **82**(4): 555-564.

Hennings, H., D. Michael, C. Cheng, P. Steinert, K. Holbrook and S. H. Yuspa (1980). "Calcium regulation of growth and differentiation of mouse epidermal cells in culture." *Cell* **19**(1): 245-254.

Hersey, P. (2003). "Adjuvant therapy for high-risk primary and resected metastatic melanoma." *Intern Med J* **33**(1-2): 33-43.

Hoeijmakers, J. H. (2001). "DNA repair mechanisms." *Maturitas* **38**(1): 17-22; discussion 22-13.

Itin, P. H., A. Sarasin and M. R. Pittelkow (2001). "Trichothiodystrophy: update on the sulfur-deficient brittle hair syndromes." *J Am Acad Dermatol* **44**(6): 891-920; quiz 921-894.

Jaspers, N. G., A. Raams, M. C. Silengo, N. Wijgers, L. J. Niedernhofer, A. R. Robinson, G. Giglia-Mari, D. Hoogstraten, W. J. Kleijer, J. H. Hoeijmakers and W. Vermeulen (2007). "First reported patient with human ERCC1 deficiency has cerebro-oculo-facio-skeletal syndrome with a mild defect in nucleotide excision repair and severe developmental failure." *Am J Hum Genet* **80**(3): 457-466.

Jiang, H. and L. Y. Yang (1999). "Cell cycle checkpoint abrogator UCN-01 inhibits DNA repair: association with attenuation of the interaction of XPA and ERCC1 nucleotide excision repair proteins." *Cancer Res* **59**(18): 4529-4534.

Kamb, A., D. Shattuck-Eidens, R. Eeles, Q. Liu, N. A. Gruis, W. Ding, C. Hussey, T. Tran, Y. Miki and J. Weaver-Feldhaus (1994). "Analysis of the p16 gene (CDKN2) as a candidate for the chromosome 9p melanoma susceptibility locus." *Nat Genet* **8**(1): 23-26.

Kapetanaki, M. G., J. Guerrero-Santoro, D. C. Bisi, C. L. Hsieh, V. Rapic-Otrin and A. S. Levine (2006). "The DDB1-CUL4ADDB2 ubiquitin ligase is deficient in xeroderma pigmentosum group E and targets histone H2A at UV-damaged DNA sites." *Proc Natl Acad Sci U S A* **103**(8): 2588-2593.

Karasarides, M., A. Chiloeches, R. Hayward, D. Niculescu-Duvaz, I. Scanlon, F. Friedlos, L. Ogilvie, D. Hedley, J. Martin, C. J. Marshall, C. J. Springer and R. Marais (2004). "B-RAF is a therapeutic target in melanoma." *Oncogene* **23**(37): 6292-6298.

Kauffmann, A., F. Rosselli, V. Lazar, V. Winnepenninckx, A. Mansuet-Lupo, P. Dessen, J. J. van den Oord, A. Spatz and A. Sarasin (2008). "High expression of DNA repair pathways is associated with metastasis in melanoma patients." *Oncogene* **27**(5): 565-573.

Kidwell, M. G. (2005). Transposable elements. San Diego, Elsevier.

Kim, S. H., H. C. Kwon, S. Y. Oh, D. M. Lee, S. Lee, J. H. Lee, M. S. Roh, D. C. Kim, K. J. Park, H. J. Choi and H. J. Kim (2009). "Prognostic value of ERCC1, thymidylate synthase, and glutathione S-transferase pi for 5-FU/oxaliplatin chemotherapy in advanced colorectal cancer." *Am J Clin Oncol* **32**(1): 38-43.

Kirkwood, J. M., J. Manola, J. Ibrahim, V. Sondak, M. S. Ernstoff and U. Rao (2004). "A pooled analysis of eastern cooperative oncology group and intergroup trials of adjuvant high-dose interferon for melanoma." *Clin Cancer Res* **10**(5): 1670-1677.

Kishi, K., Y. Doki, M. Yano, T. Yasuda, Y. Fujiwara, S. Takiguchi, S. Kim, I. Higuchi and M. Monden (2003). "Reduced MLH1 expression after chemotherapy is an indicator for poor prognosis in esophageal cancers." *Clin Cancer Res* **9**(12): 4368-4375.

Kolch, W. (2000). "Meaningful relationships: the regulation of the Ras/Raf/MEK/ERK pathway by protein interactions." *Biochem J* **351 Pt 2**: 289-305.

Kraemer, K. H. (1997). "Sunlight and skin cancer: another link revealed." *Proc Natl Acad Sci U S A* **94**(1): 11-14.

Kulaksiz, G., J. T. Reardon and A. Sancar (2005). "Xeroderma pigmentosum complementation group E protein (XPE/DDB2): purification of various complexes of XPE and analyses of their damaged DNA binding and putative DNA repair properties." *Mol Cell Biol* **25**(22): 9784-9792.

Kuraoka, I., W. R. Kobertz, R. R. Ariza, M. Biggerstaff, J. M. Essigmann and R. D. Wood (2000). "Repair of an interstrand DNA cross-link initiated by ERCC1-XPF repair/recombination nuclease." *J Biol Chem* **275**(34): 26632-26636.

Langdon, S. P., S. S. Lawrie, F. G. Hay, M. M. Hawkes, A. McDonald, I. P. Hayward, D. J. Schol, J. Hilgers, R. C. Leonard and J. F. Smyth (1988). "Characterization and properties of nine human ovarian adenocarcinoma cell lines." *Cancer Res* **48**(21): 6166-6172.

Lawrence, N. J., J. J. Sacco, D. G. Brownstein, T. H. Gillingwater and D. W. Melton (2008). "A neurological phenotype in mice with DNA repair gene Ercc1 deficiency." *DNA Repair (Amst)* **7**(2): 281-291.

Lawrence, N. J., L. Song, J. Doig, A. M. Ritchie, D. G. Brownstein and D. W. Melton (2009). "Topical thymidine dinucleotide application protects against UVB-induced skin cancer in mice with DNA repair gene (Ercc1)-deficient skin." *DNA Repair (Amst)* **8**(5): 664-671.

Leadon, S. A. and D. A. Lawrence (1991). "Preferential repair of DNA damage on the transcribed strand of the human metallothionein genes requires RNA polymerase II." *Mutat Res* **255**(1): 67-78.

Lehmann, A. R. (2001). "The xeroderma pigmentosum group D (XPD) gene: one gene, two functions, three diseases." *Genes Dev* **15**(1): 15-23.

Levy, C., M. Khaled and D. E. Fisher (2006). "MITF: master regulator of melanocyte development and melanoma oncogene." *Trends Mol Med* **12**(9): 406-414.

Li, G. M. (2008). "Mechanisms and functions of DNA mismatch repair." *Cell Res* **18**(1): 85-98.

Li, L. (2007). DNA REPAIR, GENETIC INSTABILITY, AND CANCER, World Scientific Publishing.

Lindahl, T., B. Demple and P. Robins (1982). "Suicide inactivation of the E. coli O6-methylguanine-DNA methyltransferase." *EMBO J* **1**(11): 1359-1363.

Lombard, D. B., K. F. Chua, R. Mostoslavsky, S. Franco, M. Gostissa and F. W. Alt (2005). "DNA repair, genome stability, and aging." *Cell* **120**(4): 497-512.

Lord, R. V., J. Brabender, D. Gandara, V. Alberola, C. Camps, M. Domine, F. Cardenal, J. M. Sanchez, P. H. Gumerlock, M. Taron, J. J. Sanchez, K. D. Danenberg, P. V. Danenberg and R. Rosell (2002). "Low ERCC1 expression correlates with prolonged survival after cisplatin plus gemcitabine chemotherapy in non-small cell lung cancer." *Clin Cancer Res* **8**(7): 2286-2291.

Mackay, H. J., D. Cameron, M. Rahilly, M. J. Mackean, J. Paul, S. B. Kaye and R. Brown (2000). "Reduced MLH1 expression in breast tumors after primary chemotherapy predicts disease-free survival." *J Clin Oncol* **18**(1): 87-93.

MacKie, R. M., C. A. Bray, D. J. Hole, A. Morris, M. Nicolson, A. Evans, V. Doherty and J. Vestey (2002). "Incidence of and survival from malignant melanoma in Scotland: an epidemiological study." *Lancet* **360**(9333): 587-591.

Magin, T. M., J. McWhir and D. W. Melton (1992). "A new mouse embryonic stem cell line with good germ line contribution and gene targeting frequency." *Nucleic Acids Res* **20**(14): 3795-3796.

Marrett, L. D., W. D. King, S. D. Walter and L. From (1992). "Use of host factors to identify people at high risk for cutaneous malignant melanoma." *CMAJ* **147**(4): 445-453.

Matsumura, Y. and H. N. Ananthaswamy (2002). "Proposed model for mammalian nucleotide excision repair (NER)." *Expert Reviews in Molecular Medicine*.

Matsunaga, T., C. H. Park, T. Bessho, D. Mu and A. Sancar (1996). "Replication protein A confers structure-specific endonuclease activities to the XPF-ERCC1 and XPG subunits of human DNA repair excision nuclease." *J Biol Chem* **271**(19): 11047-11050.

Maynard, S., S. H. Schurman, C. Harboe, N. C. de Souza-Pinto and V. A. Bohr (2009). "Base excision repair of oxidative DNA damage and association with cancer and aging." *Carcinogenesis* **30**(1): 2-10.

McCutchen-Maloney, S. L., C. A. Giannecchini, M. H. Hwang and M. P. Thelen (1999). "Domain mapping of the DNA binding, endonuclease, and ERCC1 binding properties of the human DNA repair protein XPF." *Biochemistry* **38**(29): 9417-9425.

McGurk, C. J., M. Cummings, B. Koberle, J. A. Hartley, R. T. Oliver and J. R. Masters (2006). "Regulation of DNA repair gene expression in human cancer cell lines." *J Cell Biochem* **97**(5): 1121-1136.

McWhir, J., J. Selfridge, D. J. Harrison, S. Squires and D. W. Melton (1993). "Mice with DNA repair gene (ERCC-1) deficiency have elevated levels of p53, liver nuclear abnormalities and die before weaning." *Nat Genet* **5**(3): 217-224.

Melton, D. W., A. M. Ketchen, F. Nunez, S. Bonatti-Abbondandolo, A. Abbondandolo, S. Squires and R. T. Johnson (1998). "Cells from ERCC1-deficient mice show increased genome instability and a reduced frequency of S-phase-dependent illegitimate chromosome exchange but a normal frequency of homologous recombination." *J Cell Sci* **111 (Pt 3)**: 395-404.

Miller, A. J. and M. C. Mihm, Jr. (2006). "Melanoma." *N Engl J Med* **355**(1): 51-65.

Millikan, R. C., A. Hummer, C. Begg, J. Player, A. R. de Cotret, S. Winkel, H. Mohrenweiser, N. Thomas, B. Armstrong, A. Kricker, L. D. Marrett, S. B. Gruber, H. A. Culver, R. Zanetti, R. P. Gallagher, T. Dwyer, T. R. Rebbeck, K. Busam, L. From, U. Mujumdar and M. Berwick (2006). "Polymorphisms in nucleotide excision repair genes and risk of multiple primary melanoma: the Genes Environment and Melanoma Study." *Carcinogenesis* **27**(3): 610-618.

Mu, D., D. S. Hsu and A. Sancar (1996). "Reaction mechanism of human DNA repair excision nuclease." *J Biol Chem* **271**(14): 8285-8294.

Mu, D., M. Wakasugi, D. S. Hsu and A. Sancar (1997). "Characterization of reaction intermediates of human excision repair nuclease." *J Biol Chem* **272**(46): 28971-28979.

Murakami, T., M. Fujimoto, M. Ohtsuki and H. Nakagawa (2001). "Expression profiling of cancer-related genes in human keratinocytes following non-lethal ultraviolet B irradiation." *J Dermatol Sci* **27**(2): 121-129.

Nakamura, M., J. P. Sundberg and R. Paus (2001). "Mutant laboratory mice with abnormalities in hair follicle morphogenesis, cycling, and/or structure: annotated tables." *Exp Dermatol* **10**(6): 369-390.

Nakane, H., S. Takeuchi, S. Yuba, M. Saijo, Y. Nakatsu, H. Murai, Y. Nakatsuru, T. Ishikawa, S. Hirota and Y. Kitamura (1995). "High incidence of ultraviolet-B-or chemical-carcinogen-induced skin tumours in mice lacking the xeroderma pigmentosum group A gene." *Nature* **377**(6545): 165-168.

Newman, M., J. Murray-Rust, J. Lally, J. Rudolf, A. Fadden, P. P. Knowles, M. F. White and N. Q. McDonald (2005). "Structure of an XPF endonuclease with and without DNA suggests a model for substrate recognition." *EMBO J* **24**(5): 895-905.

Nichols, A. F., T. Itoh, J. A. Graham, W. Liu, M. Yamaizumi and S. Linn (2000). "Human damage-specific DNA-binding protein p48. Characterization of XPE mutations and regulation following UV irradiation." *J Biol Chem* **275**(28): 21422-21428.

Niedernhofer, L. J., G. A. Garinis, A. Raams, A. S. Lalai, A. R. Robinson, E. Appeldoorn, H. Odijk, R. Oostendorp, A. Ahmad, W. van Leeuwen, A. F. Theil, W. Vermeulen, G. T. van der Horst, P. Meinecke, W. J. Kleijer, J. Vijg, N. G. Jaspers and J.

H. Hoeijmakers (2006). "A new progeroid syndrome reveals that genotoxic stress suppresses the somatotroph axis." *Nature* **444**(7122): 1038-1043.

Niedernhofer, L. J., H. Odijk, M. Budzowska, E. van Drunen, A. Maas, A. F. Theil, J. de Wit, N. G. Jaspers, H. B. Beverloo, J. H. Hoeijmakers and R. Kanaar (2004). "The structure-specific endonuclease Ercc1-Xpf is required to resolve DNA interstrand cross-link-induced double-strand breaks." *Mol Cell Biol* **24**(13): 5776-5787.

Nishino, T., K. Komori, Y. Ishino and K. Morikawa (2003). "X-ray and biochemical anatomy of an archaeal XPF/Rad1/Mus81 family nuclease: similarity between its endonuclease domain and restriction enzymes." *Structure* **11**(4): 445-457.

O'Donovan, A., A. A. Davies, J. G. Moggs, S. C. West and R. D. Wood (1994). "XPG endonuclease makes the 3' incision in human DNA nucleotide excision repair." *Nature* **371**(6496): 432-435.

Olaussen, K. A., A. Dunant, P. Fouret, E. Brambilla, F. Andre, V. Haddad, E. Taranchon, M. Filipits, R. Pirker, H. H. Popper, R. Stahel, L. Sabatier, J. P. Pignon, T. Tursz, T. Le Chevalier and J. C. Soria (2006). "DNA repair by ERCC1 in non-small-cell lung cancer and cisplatin-based adjuvant chemotherapy." *N Engl J Med* **355**(10): 983-991.

Pardo, B., B. Gomez-Gonzalez and A. Aguilera (2009). "DNA repair in mammalian cells: DNA double-strand break repair: how to fix a broken relationship." *Cell Mol Life Sci* **66**(6): 1039-1056.

Patrick, S. M., K. Tillison and J. M. Horn (2008). "Recognition of cisplatin-DNA interstrand cross-links by replication protein A." *Biochemistry* **47**(38): 10188-10196.

Pennisi, E. (2007). "EVOLUTION: Jumping Genes Hop Into the Evolutionary Limelight." *Science* **317**(5840): 894-895.

Pillaire, M. J., J. S. Hoffmann, M. Defais and G. Villani (1995). "Replication of DNA containing cisplatin lesions and its mutagenic consequences." *Biochimie* **77**(10): 803-807.

Plumb, J. A., G. Strathdee, J. Sludden, S. B. Kaye and R. Brown (2000). "Reversal of drug resistance in human tumor xenografts by 2'-deoxy-5-azacytidine-induced demethylation of the hMLH1 gene promoter." *Cancer Res* **60**(21): 6039-6044.

Pomerantz, J., N. Schreiber-Agus, N. J. Liegeois, A. Silverman, L. Alland, L. Chin, J. Potes, K. Chen, I. Orlow, H. W. Lee, C. Cordon-Cardo and R. A. DePinho (1998). "The Ink4a tumor suppressor gene product, p19Arf, interacts with MDM2 and neutralizes MDM2's inhibition of p53." *Cell* **92**(6): 713-723.

Povey, J. E., F. Darakhshan, K. Robertson, Y. Bisset, M. Mekky, J. Rees, V. Doherty, G. Kavanagh, N. Anderson, H. Campbell, R. M. MacKie and D. W. Melton (2007). "DNA repair gene polymorphisms and genetic predisposition to cutaneous melanoma." *Carcinogenesis* **28**(5): 1087-1093.

Prestridge, D. S. (1995). "Predicting Pol II promoter sequences using transcription factor binding sites." *J Mol Biol* **249**(5): 923-932.

Ramirez, A., A. Page, A. Gandarillas, J. Zanet, S. Pibre, M. Vidal, L. Tusell, A. Genesca, D. A. Whitaker, D. W. Melton and J. L. Jorcano (2004). "A keratin K5Cre transgenic line appropriate for tissue-specific or generalized Cre-mediated recombination." *Genesis* **39**(1): 52-57.

Rapic-Otrin, V., V. Navazza, T. Nardo, E. Botta, M. McLenigan, D. C. Bisi, A. S. Levine and M. Stefanini (2003). "True XP group E patients have a defective UV-damaged DNA binding protein complex and mutations in DDB2 which reveal the functional domains of its p48 product." *Hum Mol Genet* **12**(13): 1507-1522.

Reardon, J. T., T. Bessho, H. C. Kung, P. H. Bolton and A. Sancar (1997). "In vitro repair of oxidative DNA damage by human nucleotide excision repair system: possible explanation for neurodegeneration in xeroderma pigmentosum patients." *Proc Natl Acad Sci U S A* **94**(17): 9463-9468.

Rodel, C., S. Kirchhoff and H. Schmidt (1992). "The protein sequence and some intron positions are conserved between the switching gene swi10 of Schizosaccharomyces pombe and the human excision repair gene ERCC1." *Nucleic Acids Res* **20**(23): 6347-6353.

Sancar, A. (1996). "DNA excision repair." *Annu Rev Biochem* **65**: 43-81.

Sands, A. T., A. Abuin, A. Sanchez, C. J. Conti and A. Bradley (1995). "High susceptibility to ultraviolet-induced carcinogenesis in mice lacking XPC." *Nature* **377**(6545): 162-165.

Sargent, R. G., M. A. Brenneman and J. H. Wilson (1997). "Repair of site-specific double-strand breaks in a mammalian chromosome by homologous and illegitimate recombination." *Mol Cell Biol* **17**(1): 267-277.

Sedgwick, B., P. A. Bates, J. Paik, S. C. Jacobs and T. Lindahl (2007). "Repair of alkylated DNA: recent advances." *DNA Repair (Amst)* **6**(4): 429-442.

Selby, C. P. and A. Sancar (1997). "Human transcription-repair coupling factor CSB/ERCC6 is a DNA-stimulated ATPase but is not a helicase and does not disrupt the ternary transcription complex of stalled RNA polymerase II." *J Biol Chem* **272**(3): 1885-1890.

Selfridge, J., K. T. Hsia, N. J. Redhead and D. W. Melton (2001). "Correction of liver dysfunction in DNA repair-deficient mice with an ERCC1 transgene." *Nucleic Acids Res* **29**(22): 4541-4550.

Selfridge, J., A. M. Pow, J. McWhir, T. M. Magin and D. W. Melton (1992). "Gene targeting using a mouse HPRT minigene/HPRT-deficient embryonic stem cell system: inactivation of the mouse ERCC-1 gene." *Somat Cell Mol Genet* **18**(4): 325-336.

Selvakumaran, M., D. A. Pisarcik, R. Bao, A. T. Yeung and T. C. Hamilton (2003). "Enhanced cisplatin cytotoxicity by disturbing the nucleotide excision repair pathway in ovarian cancer cell lines." *Cancer Res* **63**(6): 1311-1316.

Serrano, M., G. J. Hannon and D. Beach (1993). "A new regulatory motif in cell-cycle control causing specific inhibition of cyclin D/CDK4." *Nature* **366**(6456): 704-707.

Shao, X. and N. V. Grishin (2000). "Common fold in helix-hairpin-helix proteins." *Nucleic Acids Res* **28**(14): 2643-2650.

Sharma, R. A. and G. L. Dianov (2007). "Targeting base excision repair to improve cancer therapies." *Mol Aspects Med* **28**(3-4): 345-374.

Sharpless, N. E., K. Kannan, J. Xu, M. W. Bosenberg and L. Chin (2003). "Both products of the mouse Ink4a/Arf locus suppress melanoma formation in vivo." *Oncogene* **22**(32): 5055-5059.

Shirota, Y., J. Stoehlmacher, J. Brabender, Y. P. Xiong, H. Uetake, K. D. Danenberg, S. Groshen, D. D. Tsao-Wei, P. V. Danenberg and H. J. Lenz (2001). "ERCC1 and thymidylate synthase mRNA levels predict survival for colorectal cancer patients receiving combination oxaliplatin and fluorouracil chemotherapy." *J Clin Oncol* **19**(23): 4298-4304.

Sijbers, A. M., P. J. van der Spek, H. Odijk, J. van den Berg, M. van Duin, A. Westerveld, N. G. Jaspers, D. Bootsma and J. H. Hoeijmakers (1996). "Mutational analysis of the human nucleotide excision repair gene ERCC1." *Nucleic Acids Res* **24**(17): 3370-3380.

Sinha, R. P. and D. P. Hader (2002). "UV-induced DNA damage and repair: a review." *Photochem Photobiol Sci* **1**(4): 225-236.

Skehan, P., R. Storeng, D. Scudiero, A. Monks, J. McMahon, D. Vistica, J. T. Warren, H. Bokesch, S. Kenney and M. R. Boyd (1990). "New colorimetric cytotoxicity assay for anticancer-drug screening." *J Natl Cancer Inst* **82**(13): 1107-1112.

Smalley, K. S., N. K. Haass, P. A. Brafford, M. Lioni, K. T. Flaherty and M. Herlyn (2006). "Multiple signaling pathways must be targeted to overcome drug resistance in cell lines derived from melanoma metastases." *Mol Cancer Ther* **5**(5): 1136-1144.

Soengas, M. S. and S. W. Lowe (2003). "Apoptosis and melanoma chemoresistance." *Oncogene* **22**(20): 3138-3151.

Sokhansanj, B. A. and D. M. Wilson, 3rd (2006). "Estimating the effect of human base excision repair protein variants on the repair of oxidative DNA base damage." *Cancer Epidemiol Biomarkers Prev* **15**(5): 1000-1008.

Strathdee, G., M. J. MacKean, M. Illand and R. Brown (1999). "A role for methylation of the hMLH1 promoter in loss of hMLH1 expression and drug resistance in ovarian cancer." *Oncogene* **18**(14): 2335-2341.

Sugasawa, K., T. Okamoto, Y. Shimizu, C. Masutani, S. Iwai and F. Hanaoka (2001). "A multistep damage recognition mechanism for global genomic nucleotide excision repair." *Genes Dev* **15**(5): 507-521.

Sugasawa, K., Y. Shimizu, S. Iwai and F. Hanaoka (2002). "A molecular mechanism for DNA damage recognition by the xeroderma pigmentosum group C protein complex." *DNA Repair (Amst)* **1**(1): 95-107.

Sun, X. Z., Y. N. Harada, S. Takahashi, N. Shiomi and T. Shiomi (2001). "Purkinje cell degeneration in mice lacking the xeroderma pigmentosum group G gene." *J Neurosci Res* **64**(4): 348-354.

Tani, M., A. Komura and T. Horikawa (1992). "1 alpha,25-dihydroxyvitamin D3 modulates Ia antigen expression induced by interferon-gamma and prostaglandin E2 production in Pam 212 cells." *Br J Dermatol* **126**(3): 266-274.

Thierry-Mieg, D. and J. Thierry-Mieg (2006). "AceView: a comprehensive cDNA-supported gene and transcripts annotation." *Genome Biol* **7 Suppl 1**: S12 11-14.

Thoma, B. S., M. Wakasugi, J. Christensen, M. C. Reddy and K. M. Vasquez (2005). "Human XPC-hHR23B interacts with XPA-RPA in the recognition of triplex-directed psoralen DNA interstrand crosslinks." *Nucleic Acids Res* **33**(9): 2993-3001.

Thomas, N. E., M. Berwick and M. Cordeiro-Stone (2006). "Could BRAF mutations in melanocytic lesions arise from DNA damage induced by ultraviolet radiation?" *J Invest Dermatol* **126**(8): 1693-1696.

Thornburg, B. G., V. Gotea and W. Makalowski (2006). "Transposable elements as a significant source of transcription regulating signals." *Gene* **365**: 104-110.

Tian, M., R. Shinkura, N. Shinkura and F. W. Alt (2004). "Growth retardation, early death, and DNA repair defects in mice deficient for the nucleotide excision repair enzyme XPF." *Mol Cell Biol* **24**(3): 1200-1205.

Towbin, H., T. Staehelin and J. Gordon (1979). "Electrophoretic transfer of proteins from polyacrylamide gels to nitrocellulose sheets: procedure and some applications." *Proc Natl Acad Sci U S A* **76**(9): 4350-4354.

Tripsianes, K., G. Folkers, E. Ab, D. Das, H. Odijk, N. G. Jaspers, J. H. Hoeijmakers, R. Kaptein and R. Boelens (2005). "The Structure of the Human ERCC1/XPF Interaction Domains Reveals a Complementary Role for the Two Proteins in Nucleotide Excision Repair." *Structure (Camb)* **13**(12): 1849-1858.

Tsao, H. (2000). "Update on familial cancer syndromes and the skin." *J Am Acad Dermatol* **42**(6): 939-969; quiz 970-932.

Tsao, H., M. B. Atkins and A. J. Sober (2004). "Management of cutaneous melanoma." *N Engl J Med* **351**(10): 998-1012.

Tsodikov, O. V., J. H. Enzlin, O. D. Scharer and T. Ellenberger (2005). "Crystal structure and DNA binding functions of ERCC1, a subunit of the DNA structure-specific endonuclease XPF-ERCC1." *Proc Natl Acad Sci U S A* **102**(32): 11236-11241.

van der Horst, G. T., L. Meira, T. G. Gorgels, J. de Wit, S. Velasco-Miguel, J. A. Richardson, Y. Kamp, M. P. Vreeswijk, B. Smit, D. Bootsma, J. H. Hoeijmakers and E. C. Friedberg (2002). "UVB radiation-induced cancer predisposition in Cockayne syndrome group A (Csa) mutant mice." *DNA Repair (Amst)* **1**(2): 143-157.

van der Horst, G. T., H. van Steeg, R. J. Berg, A. J. van Gool, J. de Wit, G. Weeda, H. Morreau, R. B. Beems, C. F. van Kreijl, F. R. de Gruijl, D. Bootsma and J. H. Hoeijmakers (1997). "Defective transcription-coupled repair in Cockayne syndrome B mice is associated with skin cancer predisposition." *Cell* **89**(3): 425-435.

van Duin, M., J. de Wit, H. Odijk, A. Westerveld, A. Yasui, H. M. Koken, J. H. Hoeijmakers and D. Bootsma (1986). "Molecular characterization of the human excision repair gene ERCC-1: cDNA cloning and amino acid homology with the yeast DNA repair gene RAD10." *Cell* **44**(6): 913-923.

van Duin, M., M. H. Koken, J. van den Tol, P. ten Dijke, H. Odijk, A. Westerveld, D. Bootsma and J. H. Hoeijmakers (1987). "Genomic characterization of the human DNA excision repair gene ERCC-1." *Nucleic Acids Res* **15**(22): 9195-9213.

van Duin, M., J. van den Tol, P. Warmerdam, H. Odijk, D. Meijer, A. Westerveld, D. Bootsma and J. H. Hoeijmakers (1988). "Evolution and mutagenesis of the mammalian excision repair gene ERCC-1." *Nucleic Acids Res* **16**(12): 5305-5322.

Vaupel, P. (2004). "Tumor microenvironmental physiology and its implications for radiation oncology." *Semin Radiat Oncol* **14**(3): 198-206.

Vaupel, P., F. Kallinowski and P. Okunieff (1989). "Blood flow, oxygen and nutrient supply, and metabolic microenvironment of human tumors: a review." *Cancer Res* **49**(23): 6449-6465.

Vichai, V. and K. Kirtikara (2006). "Sulforhodamine B colorimetric assay for cytotoxicity screening." *Nat Protoc* **1**(3): 1112-1116.

Volker, M., M. J. Mone, P. Karmakar, A. van Hoffen, W. Schul, W. Vermeulen, J. H. Hoeijmakers, R. van Driel, A. A. van Zeeland and L. H. Mullenders (2001). "Sequential assembly of the nucleotide excision repair factors in vivo." *Mol Cell* **8**(1): 213-224.

Wang, L., J. Wei, X. Qian, H. Yin, Y. Zhao, L. Yu, T. Wang and B. Liu (2008). "ERCC1 and BRCA1 mRNA expression levels in metastatic malignant effusions is associated with chemosensitivity to cisplatin and/or docetaxel." *BMC Cancer* **8**: 97.

Wang, Q. E., Q. Zhu, G. Wani, M. A. El-Mahdy, J. Li and A. A. Wani (2005). "DNA repair factor XPC is modified by SUMO-1 and ubiquitin following UV irradiation." *Nucleic Acids Res* **33**(13): 4023-4034.

Wang, X., C. A. Peterson, H. Zheng, R. S. Nairn, R. J. Legerski and L. Li (2001). "Involvement of nucleotide excision repair in a recombination-independent and error-prone pathway of DNA interstrand cross-link repair." *Mol Cell Biol* **21**(3): 713-720.

Weeda, G., I. Donker, J. de Wit, H. Morreau, R. Janssens, C. J. Vissers, A. Nigg, H. van Steeg, D. Bootsma and J. H. Hoeijmakers (1997). "Disruption of mouse ERCC1 results in a novel repair syndrome with growth failure, nuclear abnormalities and senescence." *Curr Biol* **7**(6): 427-439.

Wei, J., Z. Zou, X. Qian, Y. Ding, L. Xie, J. J. Sanchez, Y. Zhao, J. Feng, Y. Ling, Y. Liu, L. Yu, R. Rosell and B. Liu (2008). "ERCC1 mRNA levels and survival of advanced gastric cancer patients treated with a modified FOLFOX regimen." *Br J Cancer* **98**(8): 1398-1402.

Wellbrock, C. and R. Marais (2005). "Elevated expression of MITF counteracts B-RAF-stimulated melanocyte and melanoma cell proliferation." *J Cell Biol* **170**(5): 703-708.

Wijnhoven, S. W., R. B. Beems, M. Roodbergen, J. van den Berg, P. H. Lohman, K. Diderich, G. T. van der Horst, J. Vijg, J. H. Hoeijmakers and H. van Steeg (2005). "Accelerated aging pathology in ad libitum fed Xpd(TTD) mice is accompanied by features suggestive of caloric restriction." *DNA Repair (Amst)* **4**(11): 1314-1324.

Wilson, M. D., C. C. Ruttan, B. F. Koop and B. W. Glickman (2001). "ERCC1: a comparative genomic perspective." *Environ Mol Mutagen* **38**(2-3): 209-215.

Winsey, S. L., N. A. Haldar, H. P. Marsh, M. Bunce, S. E. Marshall, A. L. Harris, F. Wojnarowska and K. I. Welsh (2000). "A variant within the DNA repair gene XRCC3 is associated with the development of melanoma skin cancer." *Cancer Res* **60**(20): 5612-5616.

Wood, R. D. (1999). "DNA damage recognition during nucleotide excision repair in mammalian cells." *Biochimie* **81**(1-2): 39-44.

Xu, G. and A. G. Goodridge (1998). "A CT repeat in the promoter of the chicken malic enzyme gene is essential for function at an alternative transcription start site." *Arch Biochem Biophys* **358**(1): 83-91.

Ye, J., S. McGinnis and T. L. Madden (2006). "BLAST: improvements for better sequence analysis." *Nucleic Acids Res* **34**(Web Server issue): W6-9.

Yoon, T., A. Chakrabortty, R. Franks, T. Valli, H. Kiyokawa and P. Raychaudhuri (2005). "Tumor-prone phenotype of the DDB2-deficient mice." *Oncogene* **24**(3): 469-478.

Zamble, D. B. and S. J. Lippard (1995). "Cisplatin and DNA repair in cancer chemotherapy." *Trends Biochem Sci* **20**(10): 435-439.

Zamble, D. B., D. Mu, J. T. Reardon, A. Sancar and S. J. Lippard (1996). "Repair of cisplatin--DNA adducts by the mammalian excision nuclease." *Biochemistry* **35**(31): 10004-10013.

Zheng, H., X. Wang, A. J. Warren, R. J. Legerski, R. S. Nairn, J. W. Hamilton and L. Li (2003). "Nucleotide excision repair- and polymerase eta-mediated error-prone removal of mitomycin C interstrand cross-links." *Mol Cell Biol* **23**(2): 754-761.